CESifo WORKING PAPERS

10930
2024

January 2024

The Causal Effects of Global Supply Chain Disruptions on Macroeconomic Outcomes: Evidence and Theory

Xiwen Bai, Jesús Fernández-Villaverde, Yiliang Li, Francesco Zanetti

CESifo

Impressum:

CESifo Working Papers
ISSN 2364-1428 (electronic version)
Publisher and distributor: Munich Society for the Promotion of Economic Research - CESifo GmbH
The international platform of Ludwigs-Maximilians University's Center for Economic Studies and the ifo Institute
Poschingerstr. 5, 81679 Munich, Germany
Telephone +49 (0)89 2180-2740, Telefax +49 (0)89 2180-17845, email office@cesifo.de
Editor: Clemens Fuest
https://www.cesifo.org/en/wp
An electronic version of the paper may be downloaded
· from the SSRN website: www.SSRN.com
· from the RePEc website: www.RePEc.org
· from the CESifo website: https://www.cesifo.org/en/wp

CESifo *Working Paper No. 10930*

The Causal Effects of Global Supply Chain Disruptions on Macroeconomic Outcomes: Evidence and Theory

Abstract

We study the causal effects and policy implications of global supply chain disruptions. We construct a new index of supply chain disruptions from the mandatory automatic identification system data of container ships, developing a novel spatial clustering algorithm that determines real-time congestion from the position, speed, and heading of container ships in major ports around the globe. We develop a model with search frictions between producers and retailers that links spare productive capacity with congestion in the goods market and the responses of output and prices to supply chain shocks. The co-movements of output, prices, and spare capacity yield unique identifying restrictions for supply chain disturbances that allow us to study the causal effects of such disruptions. We document how supply chain shocks drove inflation during 2021 but that, in 2022, traditional demand and supply shocks also played an important role in explaining inflation. Finally, we show how monetary policy is more effective in taming inflation after a global supply chain shock than in regular circumstances.

JEL-Codes: E320, E580, J640.

Keywords: supply chain disruptions, search-and-matching in the goods market, SVAR, state-dependence of monetary policy.

Xiwen Bai
Tsinghua University, Beijing / China
xiwenbai@mail.tsinghua.edu.cn

Jesús Fernández-Villaverde
University of Pennsylvania
Philadelphia / PA / USA
jesusfv@econ.upenn.edu

Yiliang Li
University of International Business and Economics, Beijing / China
yiliang_li@uibe.edu.cn

Francesco Zanetti
University of Oxford / United Kingdom
francesco.zanetti@economics.ox.ac.uk

January 22, 2024

We are grateful to Klaus Adam, Fernando Álvarez, Hassan Afrouzi, Dennis Bonam, Bjoern Bruegemann, Elena María Díaz, Julian di Giovanni, Sebastian Heise, Bo Hu, Callum Jones, Nobuhiro Kiyotaki, Marco Lombardi, Emi Nakamura, George Nikolakoudis, Gauti Eggertsson, Ekaterina Peneva, Giorgio Primiceri, Omar Rachedi, Ricardo Reis, Karthik Sastry, Hyun Song Shin, Frank Smets, Bo Sun, Christian Wolf, Li Yu, Yang Yu, Charles Zhang, Yuan Zi, and participants at the NBU-EABCN Workshop on Monetary Policy in Emerging Markets 2023, NBER Workshop on Methods and Applications for DSGE Models Fall 2023, NBER Monetary Economics Meeting Fall 2023, the ECB-Cleveland Fed conference Inflation: Drivers and Dynamics 2023, EEA-ESEM Barcelona 2023, AMES Singapore 2023, 11th Shanghai Macroeconomics Workshop at SUFE, AMES China 2023, CEMA 2023, 26th T2M Conference, Leuven Summer Event 2023, 2nd Asia-Pacific SaM Online Workshop, 4th UIBE CCTER Workshop on Transportation Research, BIS, Boston Fed, Freie Universitat Berlin, Groningen University, Northwestern-Kellogg, Ohio State University, and the Tinbergen Institute for their comments and suggestions. Zhongjun Ma provided excellent research assistance. Francesco Zanetti gratefully acknowledges financial support from the British Academy.

1. Introduction

The world economy is organized around an intricate global supply chain. Any sudden and large shock to this global supply chain, such as those triggered by a war, a disruption of maritime trade, or the recent COVID-19 pandemic, might have large consequences for output, inflation, and unemployment. Furthermore, global supply chain shocks might also shift the trade-offs that policymakers face when stabilizing the economy.[1]

However, measuring the causal effect of a global supply chain shock and, hence, being able to design optimal policy responses to it, is challenging. First, researchers need to measure the size of the shock. Existing indices of supply chain disruptions are often inferred from changes in shipping prices or information from surveys on potential disruptions gleaned from the Purchasing Managers' Index (PMI). These measures are problematic. Shipping prices reflect endogenous movements in the demand for goods or expectations that might be unrelated to supply chain disruptions. Surveys of managers are subject to potentially large measurement errors arising from the subjective perceptions of interviewees. Instead, the ideal measurement requires data on the actual disruptions to the flow of goods around the globe.

Second, even after having measured the shock, researchers need a theoretical framework to derive the identification assumptions required for causality analysis. Given the endogeneity of fiscal and monetary policy responses to global supply chain shocks, research designs that rely less heavily on identification assumptions dictated by theory, such as quasi-natural experiments, are harder to implement. Unfortunately, there is no standard theory that encompasses the simultaneous rise in spare productive capacity – resulting from disruptions to the supply chain – along with the shortage of goods and the scarcity of supply in the retail market that exert upward pressure on prices.

Our paper addresses these issues by developing (i) a new index of global supply chain disruptions that tracks the congestion of container ships at major ports worldwide derived from high-frequency maritime satellite data and (ii) a novel theory that accounts for the coexistence of elevated spare capacity for producers and scarcity of supply in the retail market, and examines how these factors affect the responses of output and prices during a disruption to the supply

[1] Many articles in the popular press and policy institutions discuss the relevance of disruptions to the supply chain for economic performance and policy. See, for instance, Attinasi et al. (2021), Grimes and Edgecliffe-Johnson (2021), The White House (2021), Dempsey (2022), Lane (2022), and The World Bank (2022).

chain. Using our new data and the identification assumptions implied by theory, we cast new light on the causal effects of supply chain disruptions on aggregate outcomes and the implications for the effectiveness of monetary policy.

Relevance for the future. The importance of the answers to points (i) and (ii) above is that it is likely that the world economy might experience again large disruptions to the global supply chain, such as those caused by wars, geostrategic realignments, blockades, sanctions, or another pandemic. Far from being just a postmortem of what happened during COVID-19, our analysis distills important lessons for the future.

The measurement of supply chain disruptions. We follow maritime economics by studying disruptions to the supply chain through the degree of congestion at container ports around the globe. The concept of port congestion as a manifestation of global supply chain disruptions has gained widespread recognition. As early as 2006, the Transportation Research Board Executive Committee pinpointed congestion as a critical issue impacting all modes of transportation and logistical functions. This perspective was further corroborated by the influential work of Fan et al. (2012), who documented the impact of port congestion on the efficiency and reliability of global supply chains.

The reason is that container shipment plays a pivotal role in global trade. Around 60% of the total value of world seaborne trade passes through container ports (Coşar and Demir, 2018; UNCTAD, 2019; OECD and EUIPO, 2021), implying that even a mild increase in port congestion can generate large imbalances between the supply and demand for tradable goods. Importantly for us, the terms of shipping services for container ships – including itinerary, timing, and conditions of shipment – are typically fixed in advance. These service agreements often extend beyond a year and are rarely modified, as substantial penalties and high switching costs deter changes.

Furthermore, container ships operate on fixed routes that remain constant regardless of the general economic climate or changes in demand. Such a market structure ensures that congestion at a seaport is minimally influenced by the strategic decisions of shipping companies, prevailing economic conditions, or adjustments in capacity across routes to accommodate fluctuations in demand. The binding service agreements and fixed routes of container ships allow our measure of port congestion, based on the density of inactive vessels at ports, to be exogenous to the forces of demand that may otherwise skew measures of supply chain disruptions derived from shipment prices or the subjective judgment of managers on supply chain issues. In comparison, our index

also offers precise, real-time tracking of disruptions to the regular flow of goods worldwide.

We quantify port congestion around the globe from 2017 to 2023 using granular shipping data from the automatic identification system (AIS), the long-range identification and tracking system on container ships mandated by the International Maritime Organization (IMO), the specialized agency of the United Nations responsible for regulating the shipping industry worldwide. By developing a novel machine-learning clustering algorithm that utilizes the position, speed, and heading of container ships recorded in the AIS data, we construct a new dataset that provides a measure of port congestion at individual ports, which we then aggregate across ports to develop the first high-frequency index of the average congestion rate (ACR) worldwide. Our ACR index is the first measure of global supply chain disruptions obtained from maritime satellite data of container ships.[2] Unlike alternative metrics, our index indicates that supply chain disruptions and congestion in ports during the COVID-19 pandemic began in the second half of 2020 and remained elevated until the second half of 2022. It shows that the average proportion of container ships experiencing delays in their loading and unloading operations upon arrival at ports increased from 25% to 37%. At the same time, the average duration of such delays rose from 5.5 to 13.5 hours. Thus, our ACR index documents the large obstructions to the systematic flows of container ships around the globe during the COVID-19 pandemic.

Theoretical framework. Next, we develop a model that accounts for the imbalances between supply and demand for goods resulting from supply chain disturbances. Our model is built around the search and matching frictions between producers and retailers, each based in different locations. Also, the shipment of goods to retailers requires producers to pay transportation costs. Our model is inspired by the old literature on disequilibrium models from the 1970s (e.g., Barro and Grossman 1971), but recast in a microfounded framework with search and matching frictions by Michaillat and Saez (2015, 2022) and Ghassibe and Zanetti (2022). By separating producers and retailers and incorporating transportation costs, we can jointly generate spare capacity for producers, scarcity of supply, and increased congestion in the retail market.

The presence of search frictions introduces trading externalities that limit the allocation role of prices: retailers and producers of goods face a probability of failing to match with each other.

[2]The global nature and the construction of our ACR index account for any changes in port congestion that may result from adjustments in shipping routes, thus preserving the exogeneity of our ACR index when routes are altered. Additionally, since the AIS data have virtually no error in tracking the real-time movements of container ships across the globe, our ACR index is not subject to measurement error.

In other words, our framework accounts for rationing in the retail market that price adjustments cannot eliminate. Instead, trading is determined by the relative number of retailers and producers, which is influenced by supply chain disruptions. For instance, increased transportation costs hinder the free flow of goods between producers and retailers.

We assume that a supply chain shock can take two alternative forms. First is an increases in transportation costs, as evinced by the large empirical evidence linking supply chain disturbances to higher transportation costs (Alessandria et al., 2023; Dunn and Leibovici, 2023). The rise in transportation costs reduces the number of profitable shipments and curtails the volume of shipped goods, leading to a fall in the supply of goods available to retailers as well as increasing the spare capacity for producers. The shortage of supply to retailers increases the price.

Second, the supply chain disruption can also be modeled as a reduction in matching efficiency between producers and retailers. This modeling choice is consistent with the casual observations that producers and retailers faced increased difficulties in establishing effective partnerships during the COVID-19 pandemic. A reduction in matching efficiency decreases the probability of retailers meeting producers, thus imposing larger costs on retailers to form a match. We show that both alternative modelings of the supply chain disruption deliver the same set of predictions on the effects on consumption, price, and spare capacity.

Our model demonstrates that the responses of macro aggregates to a supply chain disruption shock differ from those of standard shocks to the demand and supply of goods. Unlike demand shocks, disruptions to the supply chain result in negative co-movements between output and the price of goods. Although traditional supply shocks are also characterized by negative co-movements between output and the price of goods, disruptions to the supply chain increase spare capacity for producers due to the reduction in the shipment of goods, whereas traditional supply shocks decrease it. Such a difference is intuitive: supply chain disruptions do not change the productive capacity in the goods market. Rather, they impede the flow of goods to retailers, giving rise to increased spare capacity and a deficient supply in the retail market. Hence, the increase in spare capacity, coupled with the rise in prices and the decline in output, enables the identification of supply chain disturbances.

The causal effects of supply chain disruptions. We apply our theoretical prediction on the responses of endogenous variables to identify a Bayesian structural vector autoregression (SVAR). Our main empirical results are as follows.

First, a disruption shock to the supply chain leads to a large and immediate drop in real GDP and a surge in unemployment. In addition, the supply chain disruption shock generates a persistent, positive response in inflation, an observation consistent with recent evidence (Bekaert et al., 2020; Gordon and Clark, 2023). As predicted by our model, the traditional supply shock and the supply chain shock differ in their effects on unemployment, which is our empirical proxy for spare productive capacity. For the supply shock, unemployment transiently falls for less than one quarter. At the same time, it persistently increases for the supply chain shock, with the median response reverting to zero slightly before the two-quarter mark.

Second, the historical decomposition shows that inflation since 2020 has gone through three phases. In the first phase (2020), the sharp fall in inflation was mainly driven by a significant contraction of aggregate demand that coincided with the first wave of the COVID-19 pandemic across the world. In the second phase (2021), inflation was largely caused by global supply chain disruptions. In the third phase (2022), inflation was driven to its peak by a combination of traditional demand and supply shocks, and supply chain shocks.

Policy implications. Our analysis shows that supply chain disruptions generate stagflation, accompanied by an increase in spare capacity for producers. This higher spare capacity curtails the supply of goods to retailers and results in a surge in prices, leading to a tighter retail market. We show that, in this situation, prices become highly sensitive to changes in demand, while output remains relatively inelastic. In other words, disruptions to the supply chain enhance the effectiveness of contractionary monetary policy in taming inflation while reducing the sensitivity of output to the policy. Our results reinforce the general findings on the state-dependence of the efficacy of monetary policy (Benigno and Ricci, 2011; Liu et al., 2019; Eichenbaum et al., 2022; Ikeda et al., 2024).

We test our theoretical prediction on the enhanced effectiveness of monetary policy during supply chain disruptions by developing a threshold vector autoregression (TVAR) model that estimates the statistical differences in the effects of a contractionary monetary policy shock at different levels of the ACR index. Consistent with the theory, we find that an exogenous tightening of monetary policy leads to a significantly larger and more persistent decline in inflation for a given decrease in output during periods of supply chain disruptions. Our results support a more aggressive, yet less contractionary, approach to tightening monetary policy in response to the elevated inflation consequent to supply chain disturbances. As a robustness analysis, we show

that we get similar results using linear projections.

As mentioned before, our policy results apply well beyond the COVID-19 recession: they suggest that central banks should respond vigorously to future global supply chain disruptions. In fact, our result resembles the celebrated analysis by Keynes (1940). Keynes argued that when output is constrained (in our case, because of supply chain disruptions, in Britain's case in 1940, because of resources employed in World War II), policymakers can lower aggregate demand aggressively to prevent inflation without much fear of lowering production.

Related literature. Our analysis is related to several realms of research. As mentioned above, our model builds on Barro and Grossman (1971), Michaillat and Saez (2015, 2022), and Ghassibe and Zanetti (2022). It is also related to studies that focus on the effects of supply chain disturbances on output and inflation, using the amount of spare-labor capacity (Benigno and Eggertsson, 2023), shortages in the goods market (Blanchard and Bernanke, 2023), capacity constraints (Comín et al., 2023), and a quasi-kinked demand curve for produced goods (Harding et al., 2023). The common finding across these studies is that the scarcity of goods during disturbances to the supply chain brings the economy close to its capacity constraint, thus generating a non-linear and strong increase in inflation with a limited effect on output.

Furthermore, our paper is related to studies showing that transportation costs are important for international trade and economic activity (Allen and Arkolakis, 2014; Brancaccio et al., 2020; Dunn and Leibovici, 2023), infrastructure investment (Fuchs and Wong, 2022), asset prices (Smirnyagin and Tsyvinski, 2022), working capital (Antràs, 2023; Kim and Shin, 2023), inflation expectations (Acharya et al., 2023), the design of new taxes and pricing rules to offset distortionary effects on the transportation network (Brancaccio et al., 2023), the interlinks between oil shocks and congestion in the supply chain (Bai and Li, 2022; Li et al., 2022), and the effects of supply chain disruptions during the COVID-19 pandemic (Brinca et al., 2021; Finck and Tillmann, 2022; Gordon and Clark, 2023).

The remainder of the paper is organized as follows. Section 2 constructs our ACR index of global supply chain disruptions. Section 3 develops our theoretical model and the identifying restrictions. Section 4 presents the estimation results. Section 5 studies the state-dependent effects of monetary policy shocks following supply chain disruptions. Section 6 concludes. An extensive appendix provides further details. Our data and additional results are available on our website: https://globalportcongestion.github.io/blog/intro.html.

2. Measuring Global Supply Chain Disruptions

In this section, we propose a novel index to track global supply chain disruptions through the lens of containerized trade. More concretely, we use satellite data on the positions, speeds, and headings of container ships to measure congestion in major ports around the world.

We will start by explaining why we look at containerized trade and highlighting key aspects of the industry. Next, we will introduce the satellite data we use. The core of the section is the motivation behind using port congestion as the measure of global supply chain disruptions and the presentation of the algorithm that accomplishes such a goal. We will close by reporting our ACR index, discussing several aspects of our measurement, including a comparison with alternative measures of global supply chain disruptions.

2.1. Containerized Seaborne Trade: Some Basic Facts

Containerized seaborne trade plays a prime role in the global supply chain, accounting for around 46% of all international trade (Notteboom et al., 2022).[3] Importantly, as Brancaccio et al. (2020, p. 2) explain "[t]he transportation sector … can be split into two categories: those that operate on fixed itineraries, much like buses, and those that operate on flexible routes, much like taxis. container ships … belong to the first group." These fixed itineraries are built around the seaports that serve as international hubs for freight collection and distribution. Even mild congestion at these ports can impair regular supply chains and trade flows, which run under tight schedules. Any disruption leads to elevated delay costs and far-reaching trickle-down consequences for international trade and macroeconomic outcomes.

Prior to 2020, waiting times at ports were just a few hours, reflecting the large investments worldwide in previous years to increase port capacity. However, general disruptions related to the COVID-19 pandemic led to extended delays, with waiting times reaching 2-3 days at several major ports, incurring substantial financial losses. Even if a wait of 2-3 days might not seem long, an analogy is a delay on a flight arriving at an airport hub just 60 minutes late: dozens of passengers will miss their connections, generating high levels of disruption. Similarly to stranded airline passengers, the buyers and sellers of goods encountered reduced transport efficiency and

[3]Most of the rest is either bulk cargo (e.g., oil) or specialized vessels (e.g., roll-on/roll-off vessels for wheeled cargo). Some high-value items, like chips, are often shipped by air. But chips are useless without other components, like motherboards or hard drives, that are shipped by containers.

heightened operational costs, demurrage and detention charges, and challenges in meeting contractual obligations and market demand. In the case of shippers and freight forwarders, the delays were compounded by surcharges like the port congestion surcharge (PCS), with fees escalating up to $1,250 per container. Given that the average value of goods in a 40-foot container (the most common container type) in 2020 was around $109,000, the PCS alone was a significant cost.

To frame how severe the disruptions can be, it is also important to notice that the industry is surprisingly concentrated. In 2022, there were only 5,589 container ships worldwide, of which around 500 or so belong to the larger classes in terms of size.[4] Therefore, the delay of even one large ship has significant consequences for global trade. For instance, the brand new MSC Loreto carries around 24,346 TEUs (a twenty-foot equivalent unit), each with a maximum amount of cargo of $21,600$ kilograms. The MSC Loreto can load up to 240 thousand tons of cargo at full capacity. A historical comparison puts this massive amount of cargo in perspective. Perhaps the most famous convoy of the Battle of the Atlantic during World War II was ONS 5, which sailed from Liverpool to Halifax from April 29 to May 6, 1943, and became the center of an epic battle against 43 German U-boats. ONS 5 involved 49 merchant ships with a combined cargo capacity of around 219 thousand tons, 10% less than the cargo capacity of the modern MSC Loreto.[5] Any delay in the loading and unloading operations of the MSC Loreto has ramifications for the operations of tens of thousands of different firms.[6]

Finally, recall that personnel restrictions did not cause port delays, as port workers were exempted from COVID-19 restrictions in the U.S., China, and Europe. For instance, the U.S. Department of Homeland Security identified workers within the transportation and logistics sector as "essential critical infrastructure workers." These workers were permitted to continue working despite lockdowns or stay-at-home orders, albeit under new safety guidelines. Instead, port delays were triggered by upstream and downstream problems, such as additional quarantine measures in ports that reduced port handling efficiency, trucks not arriving on time to pick up containers due to travel controls on the highways, or containers left unopened at inland factories because workers were not at hand to process the items inside them.[7]

[4]See https://unctad.org/rmt2022 (Accessed December 29, 2023).

[5]The official historian of the U.S. Navy, Samuel Eliot Morison, wrote: "The glorious battle of a British escort group under Commander P. W. Gretton to the Westbound convoy ONS 5 is regarded by both the Allies and the Germans as a turning point in the struggle for the North Atlantic" (Morison, 1954).

[6]In Appendix A, we provide further details on the containerized shipping industry.

[7]Furthermore, Appendix E.4 shows that our empirical results are robust to controlling for a stringency index in the COVID-19 restrictions imposed by the jurisdiction where the port is located.

2.2. AIS Data

We use satellite data from the AIS, a tracking system mandated by the IMO. International voyaging vessels larger than 300 gross tonnage must carry a transceiver that broadcasts information about the ship (Heiland et al., 2022). Each data entry includes the IMO number, timestamp, current draft, speed, heading, and geographical coordinates.[8] The AIS processes over 2,000 reports per minute and updates information as frequently as every two seconds, offering comprehensive coverage of the movements of container ships around the globe from January 2017 to September 2023.[9] The positioning, speed, and heading of ships allow us to monitor vessel movements within different port zones.

2.3. A Density-Based Spatial Clustering Algorithm

The literature on maritime economics has identified port congestion as a key measure of the state of the global supply chain (Talley and Ng, 2016; Karimi-Mamaghan et al., 2020; Bai et al., 2023). Furthermore, the literature has suggested measuring port congestion by estimating the likelihood that a vessel will first moor in an anchorage area within the port before docking at a berth. An anchorage is a location within a port where ships can lower anchors, while a berth is a designated spot within a port where vessels moor to load and unload cargo. If port congestion were not a concern, a ship would dock at a berth immediately upon its arrival in the port to begin loading or unloading cargo. Hence, measuring port congestion requires the identification of berth and anchorage areas, a task for which practitioners before us have largely relied on navigational charts and individual knowledge of ports, making it labor-intensive and challenging to generalize to ports with varying internal arrangements. Hence, we develop an iterative, multi-attribute, density-based machine-learning spatial clustering algorithm that is both accurate in identifying different areas within ports and applicable to ports with different morphologies.

The algorithm identifies different port areas by focusing on the density of container ships' mooring points recorded in the AIS data. Our algorithm operates in two layers of clustering. The

[8]The draft measures the vertical distance from the bottom of a vessel's keel to the water's surface, indicating how deeply the ship is submerged. While the draft reflects a vessel's cargo load (Bai and Li, 2022; Li et al., 2022), this measurement is less useful for container ships since loading and unloading operations often occur concurrently.

[9]Over 99% of international container shipments are transported by container ships that exceed 500 gross tonnage. Even vessels smaller than 300 gross tonnage commonly carry an AIS transponder because of the high safety bonus it brings at a low cost (around $1000 for a basic unit). Thus, our coverage is nearly universal.

first layer identifies high-density areas, i.e., locations where we record many AIS observations, which are considered potential berth and anchorage areas. The second layer determines whether these high-density areas are berths or anchorages using domain knowledge about ports. For example, if we observe all the headings in an orderly and close fashion, we identify the area as a berth. If, instead, the headings are more random, we identify the area as an anchorage.

(a) Headings at a Berth **(b)** Headings at an Anchorage

Figure 1: Information on Headings: Two Examples

Figure 1 illustrates this point. The left panel shows two clusters, one in orange and one in green. Both include many AIS observations, with bows (the tips of the white signs) closely aligned (to the left in the orange cluster and to the right in the green cluster), representing the two different headings of a mooring. If we superimpose a satellite photograph over the clusters, we can check that this is indeed a berth. The right panel shows several clusters of AIS data points, where the headings are random, with some of them appearing in a ring shape.[10]

Our algorithm is designed to address two challenges that existing clustering algorithms struggle with. First is the variability in the density of ships' mooring points *across* ports due to differences in trade volume handled, frequency of vessel visits, and geographical morphologies and boundaries. Our algorithm automatically iterates and refines its clustering parameters for each port, accommodating varied port environments. Second, thanks to its two layers, our algo-

[10] Appendix B provides details on our clustering algorithm, including pseudo-codes and a case study involving the Port of Ningbo-Zhoushan (to the south of Shanghai), which illustrates the effectiveness of our methodology compared to alternative approaches in identifying berth and anchorage areas in ports with different morphologies.

rithm accurately distinguishes between berth and anchorage areas *within* ports despite the high density of ships' mooring points. Importantly, our algorithm is readily adaptable to other applications, such as port handling efficiency and waiting time, canal traffic, or stress at maritime choke points (e.g., piracy at straits). More in general, the algorithm's core mechanism – transforming domain knowledge into non-spatial attributes and using them as additional metrics between data points in an iterative clustering process – offers a versatile framework for classifying clusters of varying densities with specific labels in other contexts as well (e.g., identifying disease hotspots, urban planning, and environmental monitoring).

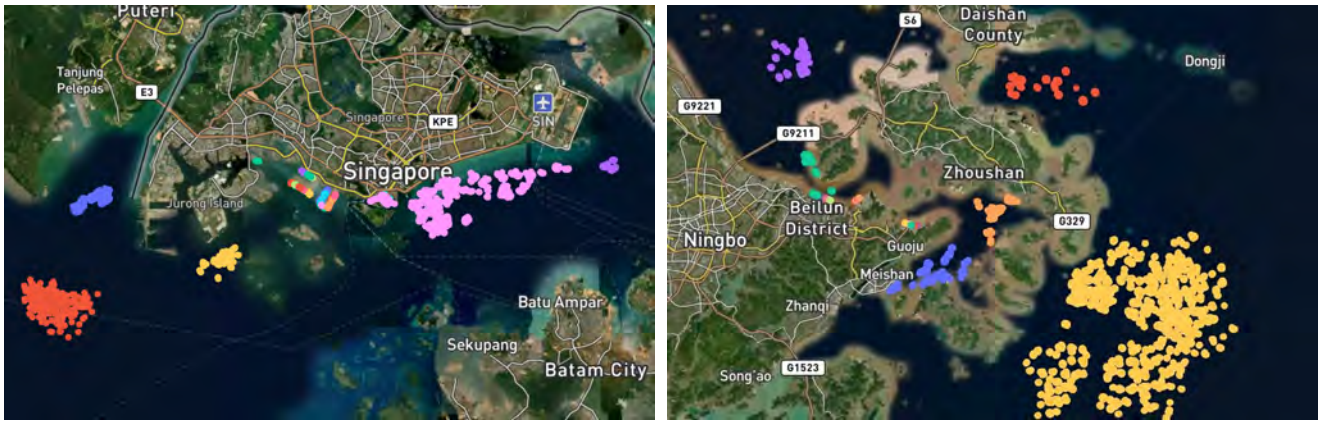

(a) Singapore

(b) Ningbo-Zhoushan, China

(c) Rotterdam, Netherlands

(d) Los Angeles and Long Beach, U.S.

Figure 2: Identification of Anchorage and Berth Areas of a Port Using Machine Learning

Note. The underlying sample for each figure incorporates the first 50,000 AIS observations of container ships entering each port since January 1, 2020.

Figure 2 reports the results of our algorithm. In each panel, we superimpose the anchorage (colors including red, yellow, blue, purple, pink, cyan, and orange) and berth areas (markers

of other colors) on satellite photographs of four major container ports: Singapore (Panel a), Ningbo-Zhoushan (Panel b), Rotterdam (Panel c), and Los Angeles and Long Beach (Panel d). Our algorithm accurately identifies the anchorage and berth areas in each port despite a broad range of geographical and operational port conditions.

2.4. The ACR Index

Port congestion arises when ships cannot immediately load and unload cargo upon arrival at ports. This delay results in vessels waiting in an anchorage area until a berth is free. For the top 50 container ports worldwide, denoted as $\mathscr{P}$, we count the number of delayed ship visits to each port p where the ship first moors in an anchorage before docking at a berth.[11] We then calculate the congestion rate for each port p by dividing the number of delayed ship visits by the total number of ship visits:

$$Congestion_{pt} \equiv \frac{Delayed_{pt}}{Delayed_{pt} + Undelayed_{pt}}, \ \forall p \in \mathscr{P}, \tag{1}$$

where $Delayed_{pt}$ and $Undelayed_{pt}$ represent the number of delayed and undelayed ship visits at port p in month t, respectively. We calculate the congestion rate for each port on a monthly basis throughout the sample period.

Figure 3 displays the monthly congestion rates for the top ten container ports worldwide, along with the Ports of Los Angeles and Long Beach, from January 2017 to September 2023, the period for which AIS data are available. While below we will utilize data from the top 50 ports worldwide, the ports in Figure 3 represent more than 30% of the total volume of containerized seaborne trade globally and summarize our main findings.

Our data indicate that the onset of the COVID-19 pandemic in March 2020 had few early effects. The congestion rates of ports such as Singapore and Rotterdam remained largely stable for several months. The situation changed in the fall of 2020 (notice the rise in chromatic intensity in Figure 3 after October 2020). By our calculations, approximately 80% of inbound ships at the Port of Los Angeles were unable to dock at a berth immediately upon arrival in late 2020.[12] Our

[11] A ship visit, or port call, refers to the arrival of a ship at a port where it docks to load and unload cargo.

[12] This measurement aligns with official statistics. According to the Pacific Merchant Shipping Association, the percentage of container ships in Los Angeles waiting five or more days for unloading surged from 10% in August to 26% in December 2020. Additionally, the Marine Exchange of Southern California reported that the number of vessels anchored in Los Angeles waters rose from fewer than 20 in August to more than 35 in December 2020.

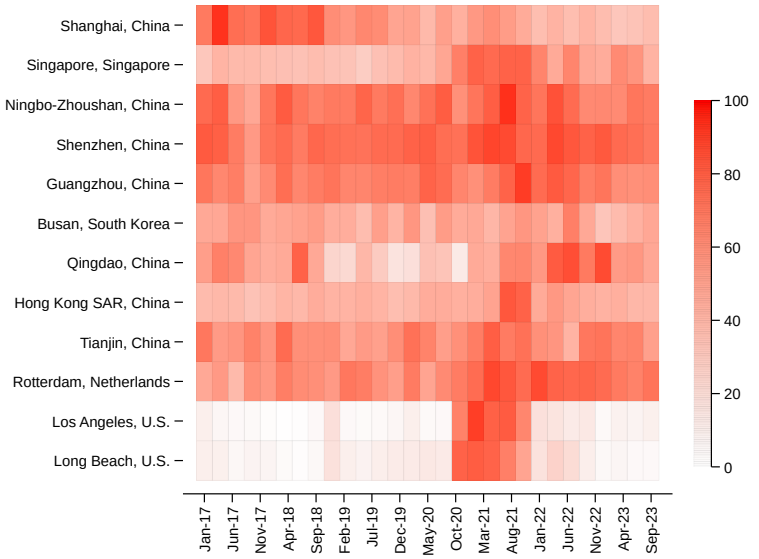

Figure 3: Congestion Rates for the Major Container Ports Worldwide

Notes. Heatmap of the monthly congestion rates for the top ten global container ports plus the Ports of Los Angeles and Long Beach from January 2017 to September 2023. The congestion rate for each port is normalized and expressed as a percentage of its peak value observed within the sample period. Cells in darker shades indicate higher congestion levels as defined in Equation (1) for the respective port during the specified month.

analysis reveals that global supply disruptions became acute in 2020:Q4.

To construct a time series of global supply chain disruptions, we define the average congestion rate (ACR) by computing the weighted average of the congestion rates for the top 50 container ports worldwide, using as weights the relative number of ship visits to each port:

$$ACR_t = \sum_{p \in \mathcal{P}} \left[\frac{Delayed_{pt} + Undelayed_{pt}}{\sum_{p \in \mathcal{P}} (Delayed_{pt} + Undelayed_{pt})} \cdot Congestion_{pt} \right]. \tag{2}$$

Figure 4 displays our ACR index. Prior to 2018, the index followed a declining trend, stabilizing around 28% before dropping to a sample minimum of 25% from early 2019 to mid-2020. Subsequently, the index consistently rose, peaking at 37% in June 2021, indicative of significant supply chain disruptions related to the COVID-19 pandemic. The ACR index remained elevated until mid-2022, then began to decline, returning to the sample median (29.1%) by the end of the sample period. By then, port congestion had returned to normal levels, and global supply chain disruptions had largely subsided, despite remaining above the average of the pre-COVID period.

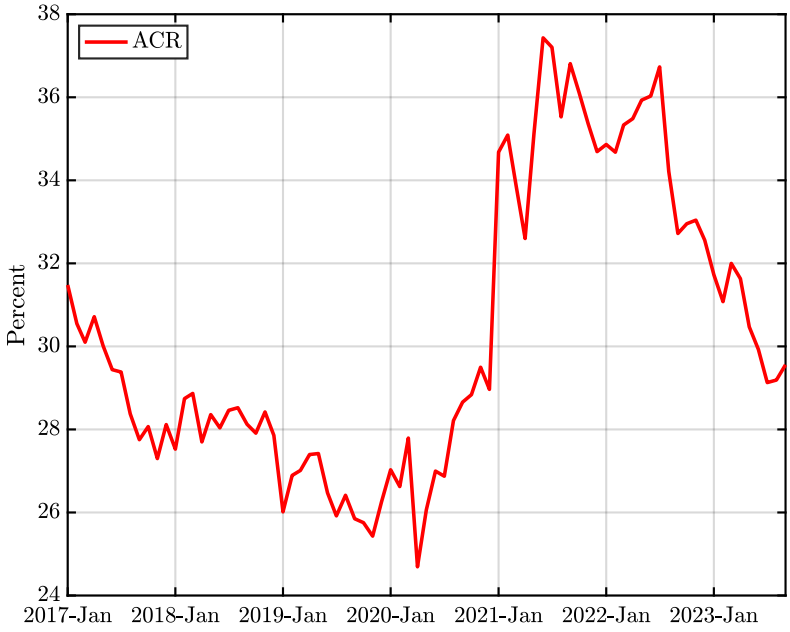

Figure 4: ACR Index of Global Supply Chain Disruptions

Note. The ACR index of global supply chain disruptions is derived by taking a weighted average of the congestion rates for the top 50 global container ports, with the relative number of ship visits used as the weight for each port. The index is presented in percentage terms and has been seasonally adjusted. For the complete ranking of container ports, see https://www.worldshipping.org/top-50-ports (Accessed June 15, 2022).

2.5. Discussion

Several aspects of our index deserve further discussion. First, we use the relative number of ship visits to each port as weights because they reflect the importance of different ports within the global supply chain. A slight increase in the congestion rate for the Port of Hong Kong would likely have triggered a more pronounced global supply chain disruption than a significant increase for the Port of Manila. Nonetheless, we could build regional or national indices; our methodology would remain unchanged.

Second, the normalization of the congestion rate ($Congestion_{pt}$) by the number of ship visits ($Delayed_{pt} + Undelayed_{pt}$) nets out variations in the level of congestion resulting from infrequent but significant changes in demand. The stringent terms of shipping services for container ships usually render our congestion tracking at seaports independent of general economic conditions and demand fluctuations. As we have emphasized, container ships operate on fixed itineraries, largely independent of the current level of demand.

Third, any infrequent adjustments in shipping capacity across routes (and the subsequent changes in congestion at different ports) are canceled out when we aggregate the congestion

rates. For example, a high level of congestion in port A might lead to lower congestion in port B, as the ships destined for this second port have not left port A.

Fourth, notice that the industry follows a practice known as "hurry up and wait": despite forewarnings of potential delays at the destination port, container ships often do not alter their route or speed, as doing so would necessitate changing many contractual arrangements. Therefore, even if ports started to become congested in the fall of 2020, we can consider the routes and speeds of vessels as largely fixed (this observation will be important for our SVAR identification). Furthermore, Appendix A documents the unimportance of oil prices for ship speeds (corroborating a well-known result in the literature).

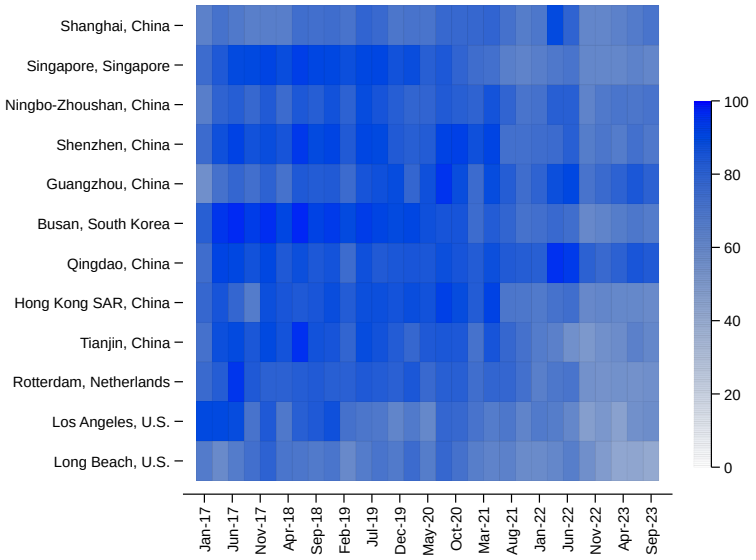

Figure 5: Ship Visits to the Major Container Ports Worldwide

Note. The heatmap displays the number of ship visits to each of the top ten global container ports, as well as the Ports of Los Angeles and Long Beach, covering the period from January 2017 to September 2023. Collectively, these ports represent over 30% of the total volume of containerized seaborne trade worldwide. The number of ship visits to each port is normalized and expressed as a percentage of its peak value observed within the sample period. Cells in darker shades denote a greater number of ship visits during the specified month.

However, our sample includes the exceptional period of COVID-19, during which service agreements might have been canceled, and container ship itineraries could have been temporarily modified or suspended, affecting port congestion. For instance, at the pandemic's onset, shipping companies engaged in capacity management in response to significant declines in demand (Notteboom et al., 2021).[13] Similarly, when the demand for goods surged toward the end of 2021,

[13]In April-May 2020, as lockdowns led to unprecedented declines in consumer and business demand, shipping carriers reduced their network capacity on primary trade routes by up to 20% and sidelined over 2.7 million TEUs

carriers struggled to maintain weekly sailing schedules due to overwhelmed ports and ensuing congestion, leading to many blank sailings (Sea-Intelligence, 2021).[14] These adjustments caused significant variations in the number of ship visits to each port, potentially influencing congestion levels. As shown in Figure 5, the number of ship visits to major container ports globally remained relatively stable until mid-2021, followed by a notable decrease for several local ports, including Singapore, Shenzhen, and Los Angeles. Given these factors' joint effect in lowering port congestion, our index might underestimate the true extent of disruption in the global supply chain. We will return to this point in the SVAR analysis later in the paper. Appendix A discusses additional issues in more detail, such as the rate of ship idleness.

2.6. Alternative Indices

Appendix F compares our ACR index to other indices of supply chain disruptions in the literature, notably the Harper Peterson Time Charter Rates Index (HARPEX), New York Fed's Global Supply Chain Pressure Index (GSCPI), and the Supply Disruptions Index (SDI) compiled by Smirnyagin and Tsyvinski (2022). We show that there are significant differences between the indices that influence the interpretations of supply chain disruptions and their causal effects on the macro aggregates of interest, such as inflation. Additionally, Appendix F.4 also constructs an alternative measure of port congestion – the average congestion time (ACT) – using AIS data and our spatial clustering algorithm. The ACT index measures the average number of hours a container ship waits in an anchorage area of a port before docking at a berth, weighted by the number of ship visits. We show that using the ACT index in the causality assessment delivers results quantitatively similar to those obtained with the ACR index.

The integration of high-frequency AIS data with our spatial clustering algorithm also enables the construction of port congestion indices at higher frequencies than monthly updates. Appendix B.3 reconstructs the ACR and ACT indices using weekly updates of the AIS data and highlights that, despite heightened volatility, the weekly indices of port congestion exhibit the same patterns as their monthly counterparts.

of fleet capacity, equivalent to over 11% of the global container fleet.

[14] Blank sailing, or void sailing, refers to situations where a scheduled ship does not sail, occurring when a carrier cancels a vessel's journey, causing it to miss specific ports or its entire intended route.

3. A Model of Congestion and Spare Capacity

Next, we develop a model of congestion and spare capacity that will provide us with identification restrictions for our causality analysis. Without theoretical guidance, it is hard to find a research design that allows us to ascertain causality given that monetary and fiscal policy respond endogenously to the global supply shocks.

We develop a search and matching model because it highlights what was, to us, the fundamental issue during COVID-19: the inability of prices to play a fully allocative role. Nonetheless, our model will impose identification restrictions that could also be derived from a New Keynesian model. In such a framework, nominal rigidities replace search and matching frictions as impediments to the smooth working of prices. Readers who prefer New Keynesian thinking shall not find it too difficult to jump to Table 1, where we summarize the identification restrictions derived from theory, and see how those restrictions would also come from many New Keynesian models.

Our economy comprises producers, retailers, and households. Producers manufacture goods using a fixed amount of labor supplied by households and incur transportation costs when selling the goods to retailers. Retailers purchase goods from producers but face search frictions that make it difficult to meet with the former. Retailers then sell the goods to households. Households own the producers and retailers, accruing all the profits in the economy.

We distinguish between producers and retailers to capture the idea that firms must trade in a global supply chain. Search and matching frictions make this trade non-trivial.[15] Transportation costs and search frictions hinder the allocative role of prices in clearing the quantity of goods sold by producers to retailers.[16] Thus, we introduce disruptions to the global supply chain either as higher transportation costs or lower efficiency of the matching function.

Our model will allow us to study three standard shocks: an aggregate demand shock (i.e., a change in the money held by households due to a change in monetary policy), a productive capacity shock (i.e., a change in labor supply), and a supply chain shock (i.e., an increase in transportation costs or lower matching efficiency). Our model has distinctive predictions regarding the co-movements of spare capacity with prices and output in response to each of these shocks that

[15] Our approach is similar to the case where firms require intermediate goods for the production of final goods. See, for instance, Costinot et al. (2013), Kasahara and Lapham (2013), and Ramondo and Rodríguez-Clare (2013).

[16] Appendix C discusses the evidence of search and matching frictions in the goods market and the relevance of transportation costs for the severance of commercial trade.

will let us identify the causal effects of supply chain disruptions (Section 4) and connect these disruptions to the effectiveness of monetary policy (Section 5).

3.1. Producers and Retailers

There is an exogenous unit mass of producers and an endogenous measure of retailers. When matched with a retailer, a producer manufactures $y = l$ final goods using labor. Given that l is supplied inelastically by the household and that the household is the owner of all the firms in the economy, we normalize the wage to zero, i.e., the household receives the income from the match entirely as profits and not as a combination of profits and wages. In this way, we avoid adding an extra layer of complexity to the model in terms of an explicit labor market and the income flows it generates.[17]

Producers sell the goods to retailers in a frictional goods market that prevents the sale of the full capacity. Each unmatched retailer (identified by the subscript U) makes one visit per period to unmatched producers, with each visit entailing a fixed cost per unit of the final good $\rho > 0$. Upon a meeting of producers and retailers that results in a trade (we will discuss below when this happens), the retailer resells the purchased goods to the household at a retail price p.

Matching process. In each period, the number of meetings ($\mathscr{M}$) between unmatched producers, x_U, and retailers, i_U, is governed by a constant-returns-to-scale matching function:

$$\mathscr{M} = A(x_U^{-\xi} + i_U^{-\xi})^{-\frac{1}{\xi}}, \tag{3}$$

where A is the efficiency of the matching function and ξ is the elasticity of substitution between x_U and i_U. We assume $\xi > 0$, such that $\mathscr{M} \leq A \cdot \min\{x_U, i_U\}$. For the moment, we parameterize $A = 1$. Later, we will explore a supply chain shock that yields $0 < A < 1$.

Product market tightness $\theta \equiv i_U/x_U$ is the ratio between the number of visits by the unmatched retailers and the number of unmatched producers. Product market tightness is taken as given by individual firms. Specifically, the probability for a producer to meet a retailer is:

$$f(\theta) = \frac{\mathscr{M}}{x_U} = A(1 + \theta^{-\xi})^{-\frac{1}{\xi}}, \tag{4}$$

[17] While this normalization increases the surplus of a match (since the producer does not have to subtract wage costs from its profits), it does not have any effect on the identification restrictions we derive from the model.

and the probability for a retailer to meet a producer is:

$$q(\theta) = \frac{\mathscr{M}}{i_U} = A(1+\theta^{\xi})^{-\frac{1}{\xi}}. \tag{5}$$

The function $f(\theta)$ satisfies that $f(0) = 0$, $\lim_{\theta\to+\infty} f(\theta) = A$, and $f'(\theta) > 0$, whereas $q(\theta)$ satisfies that $q(0) = A$, $\lim_{\theta\to+\infty} q(\theta) = 0$, and $q'(\theta) < 0$. Two additional properties that will be useful later are that $f(\theta)/q(\theta) = \theta$ and $f'(\theta) = A^{-\xi}q(\theta)^{1+\xi}$.

Transportation cost. Producers pay a per-unit idiosyncratic transportation cost to ship their goods to retailers.[18] In each period, producers draw a per-unit transportation cost z from the log-normal distribution $G(z)$ with the scale parameter γ and the shape parameter σ, i.e., $G(z) \equiv \Phi\left[(\log z - \gamma)/\sigma\right]$, where $\Phi(\cdot)$ is the standard normal cumulative density function.[19] As we discuss later, there exists a reservation level of transportation cost $\bar{z}$, above which matches ($z > \bar{z}$) are unprofitable and, hence, severed, whereas they continue otherwise ($z \leq \bar{z}$).

Value functions. At the beginning of each period, the matched producers sell the manufactured goods to retailers and pay the transportation costs. In contrast, the matched retailers sell their purchased goods to households and pay the wholesale price of goods to the producers. The unmatched producers and retailers search to form a match with each other. At the beginning of the next period, each producer draws a new transportation cost, and the match continues if the new cost is sufficiently low, such that there is a positive surplus from trade.

Four value functions describe the return for the different statuses of producers and retailers. The value for a matched producer (identified by the subscript M), $X_M(z)$, is equal to:

$$X_M(z) = (r(z) - z)\, l + \beta \mathbb{E}_{z'}\left[\max\left(X_M(z'), X_U\right)\right], \tag{6}$$

where $r(z)$ is the (endogenous) wholesale price per unit of the final good, β is the discount factor, and z' is the draw of transportation cost at the beginning of the next period. Equation (6) shows that the present value of being a matched producer is the profit margin $(r(z) - z)\, l$, plus the continuation value, which depends on whether the producer separates from the match.

[18] Our results hold if the transportation cost is borne by retailers instead because the match separation condition (14) is invariant to this modeling choice. For simplicity, we also assume that the household receives this shipping cost as a payment for its work in moving the goods.

[19] We could consider a more general setup where each producer maintains its previous draw of transportation cost with probability $1 - \varphi$, and with probability φ, the producer draws a new transportation cost from $G(z)$. This setup is often found in models that study the labor market outcomes following a rise in economic turbulence (den Haan et al., 2005; Thomas and Zanetti, 2009; Fujita, 2018; Pizzinelli et al., 2020). Despite more involved algebra, our main results still hold in this more general setup.

Separation is determined by the transportation cost next period, z', and the max operator picks the optimal continuation/separation decision.

The value for an unmatched producer, X_U, is:

$$X_U = \beta f(\theta) \mathbb{E}_{z'} \left[\max \left(X_M(z'), X_U \right) \right] + \beta \left(1 - f(\theta) \right) X_U. \tag{7}$$

With probability $f(\theta)$, the unmatched producer meets a retailer and then decides whether to separate if the draw of transportation cost makes the match unprofitable. With probability $1 - f(\theta)$, the producer forgoes a successful match with a retailer and remains unmatched at the beginning of the next period.

The value for a matched retailer, $I_M(z)$, is:

$$I_M(z) = \left(p - r(z) \right) l + \beta \mathbb{E}_{z'} \left[\max \left(I_M(z'), I_U \right) \right]. \tag{8}$$

The retailer earns the price p by reselling each unit of the purchased goods to the households and pays the corresponding wholesale price $r(z)$ to the producer. As before, the max operator picks the optimal continuation/separation decision conditional on z'.

If the drawn transportation cost makes the match unprofitable, the retailer separates from the match and starts the next period with a return:

$$I_U = -\rho l + \beta q(\theta) \mathbb{E}_{z'} \left[\max \left(I_M(z'), I_U \right) \right] + \beta \left(1 - q(\theta) \right) I_U, \tag{9}$$

where ρ is a fixed cost per unit of the final good that the retailer pays to the producer during the visit. Free entry into the product market drives the value for an unmatched retailer to zero in equilibrium, i.e., $I_U = 0$.

Nash bargaining. The total surplus from matching is equal to:

$$S(z) = X_M(z) - X_U + I_M(z) - I_U, \tag{10}$$

and it is split through Nash bargaining. The producer earns a constant share η of the total surplus, and the retailer earns the remaining share $1 - \eta$, which in equilibrium yields:

$$\eta \left(I_M(z) - I_U \right) = (1 - \eta) \left(X_M(z) - X_U \right). \tag{11}$$

Given the Nash bargaining sharing rule (11), the value functions (6), (7), (8), and the free-entry

condition $I_U = 0$, the wholesale price that splits the surplus is equal to:

$$r(z) = \eta(p + \rho\theta) + (1 - \eta)z. \tag{12}$$

When the bargaining power of the producer is low ($\eta \to 0$), the wholesale price is close to the cost of transportation (z). Congestion in the matching process, captured by tightness in the product market, worsens the bargaining position of retailers by lowering their matching probability. Thus, higher tightness increases the wholesale price retailers pay to the producers.

Match separation. Since the total value for a matched producer and a matched retailer, i.e., $X_M(z) + I_M(z)$, strictly decreases with the cost of transportation z, there exists a cut-off transportation cost $\bar{z}$, above which the costs are too high, making the matches unprofitable and consequently severed. This cut-off makes the total surplus in Equation (10) equal to zero:

$$S(\bar{z}) = 0. \tag{13}$$

By substituting the value functions (6), (7), (8), and the free-entry condition $I_U = 0$ into Equation (13), we can express the match separation condition as a function of p, $\bar{z}$, and θ satisfying:

$$\mathbb{F}(p, \bar{z}, \theta) = (p - \bar{z})\, l + (1 - \eta f(\theta))\, \beta \mathbb{E}_{z'} S(z') = 0, \tag{14}$$

where $\mathbb{E}_{z'} S(z') = \int_0^{\bar{z}} S(z') dG(z')$ is the expected surplus.

Match creation. Using the value function for an unmatched retailer (9) and the free-entry condition $I_U = 0$, we define the match creation condition as a function of $\bar{z}$ and θ satisfying:

$$\mathbb{H}(\bar{z}, \theta) = \frac{\rho l}{q(\theta)} - (1 - \eta)\beta \mathbb{E}_{z'} S(z') = 0. \tag{15}$$

Aggregate supply. The aggregate supply in the economy results from the equilibrium in the product market, defined as:

Definition 1. *The equilibrium in the product market consists of a price p, a reservation transportation cost $\bar{z}$, and a product market tightness θ such that the conditions for match separation (14) and match creation (15) simultaneously hold: $\mathbb{F}(p, \bar{z}, \theta) = \mathbb{H}(\bar{z}, \theta) = 0$.*

Definition 1 tells us that the equilibrium product market tightness can be expressed as a function of the price and the reservation transportation cost. Next, we characterize this relationship.

Proposition 1. *In equilibrium, the price p, reservation transportation cost $\bar{z}$, and product market tightness θ satisfy:*

$$\theta(p, \bar{z}) = \frac{1-\eta}{\eta\rho}\left(p - \bar{z} + \beta \int_0^{\bar{z}} G(z')dz'\right), \tag{16}$$

where $G(\cdot)$ is the log-normal cumulative density function. Hence, product market tightness θ has the following properties:

1. *$\theta(p^{min}, \bar{z}) = 0$ and $\lim_{p\to+\infty} \theta(p, \bar{z}) = +\infty$, where p^{min} satisfies:*

$$p^{min} - \bar{z} + \beta \int_0^{\bar{z}} G(z')dz' = 0;$$

2. *$\theta(p, \bar{z})$ is strictly increasing on $[p^{min}, +\infty)$;*

3. *$\theta(p, \bar{z})$ is linear on $[p^{min}, +\infty)$;*

4. *$\lim_{\bar{z}\to 0^+} \theta(p, \bar{z}) = (1-\eta)p/(\eta\rho)$ and $\theta(p, \bar{z}^{max}) = 0$, where $\bar{z}^{max}$ satisfies:*

$$p - \bar{z}^{max} + \beta \int_0^{\bar{z}^{max}} G(z')dz' = 0;$$

5. *$\theta(p, \bar{z})$ is strictly decreasing on $(0, \bar{z}^{max}]$; and*

6. *$\theta(p, \bar{z})$ is convex on $(0, \bar{z}^{max}]$.*

Proof. See Appendix D.1. ■

Proposition 1 establishes that product market tightness strictly increases with the price of goods and decreases with the reservation transportation cost. These properties are intuitive. When the total surplus rises due to a higher price, retailers visit more producers, leading to increased tightness. Conversely, a rise in the reservation transportation cost diminishes the total surplus shared between producers and retailers at the margin. As a result, the incentives for retailers to visit producers are dampened, causing a more slack product market.[20]

Next, the aggregate supply comprises the quantity of goods traded by the retailers and producers that survive separation for a given productive capacity, equal to the total labor supply l. To determine the equilibrium number of matched producers, we consider the law of motion for

[20] An increase in the reservation transportation cost raises the expected total surplus, $\beta\mathbb{E}_{z'}S(z')$, since matches are less likely to dissolve in the subsequent period. However, this positive effect is outweighed by the decrease in the profit margin $p - \bar{z}$, resulting in a net negative impact on the total surplus.

the number of matched producers at the beginning of the next period:

$$x'_M = G(\bar{z})x_M + f(\theta)G(\bar{z})x_U, \tag{17}$$

and that for the number of unmatched producers at the beginning of the next period:

$$x'_U = \left[1 - f(\theta) + f(\theta)\left(1 - G(\bar{z})\right)\right] x_U + \left(1 - G(\bar{z})\right) x_M. \tag{18}$$

Instead of examining the full transition dynamics of the model (a discussion we relegate to Appendix D.10), we focus on the steady state. As shown in Section 3.4, using comparative statics suffices to derive a set of identifying restrictions for each shock of interest in our causality analysis.

Setting $x'_M = x_M$ in Equation (17) and recalling that $x_M + x_U = 1$, we derive the steady state number of matched producers:

$$x_M^{ss}(\bar{z}, \theta) = \frac{f(\theta)G(\bar{z})}{1 - G(\bar{z}) + f(\theta)G(\bar{z})},$$

where the product market tightness θ, as determined in Equation (16), will be solved as a (steady state) constant once we impose the goods market clearing condition. The (steady state) aggregate supply is thus equal to the quantity of goods supplied by matched producers given l:

$$c_s(\bar{z}, \theta) = x_M^{ss}(\bar{z}, \theta)l = \frac{f(\theta)G(\bar{z})}{1 - G(\bar{z}) + f(\theta)G(\bar{z})}l. \tag{19}$$

By substituting the expressions for $f(\theta)$ and θ from Equations (4) and (16) into Equation (19), we express aggregate supply as a function of price and reservation transportation cost.

Definition 2. *The aggregate supply c_s, expressed as a function of p and $\bar{z}$, is equal to:*

$$c_s(p, \bar{z}) = \frac{A\left\{1 + \left[\frac{1-\eta}{\eta\rho}\left(p - \bar{z} + \beta\int_0^{\bar{z}} G(z')dz'\right)\right]^{-\xi}\right\}^{-\frac{1}{\xi}} G(\bar{z})}{1 - G(\bar{z}) + A\left\{1 + \left[\frac{1-\eta}{\eta\rho}\left(p - \bar{z} + \beta\int_0^{\bar{z}} G(z')dz'\right)\right]^{-\xi}\right\}^{-\frac{1}{\xi}} G(\bar{z})} l, \tag{20}$$

for all $(p, \bar{z})$ satisfying:

$$p - \bar{z} + \beta\int_0^{\bar{z}} G(z')dz' \geq 0. \tag{21}$$

Since $c_s(p, \bar{z})$ is determined by two endogenous variables, there exist infinite combinations of p and $\bar{z}$'s that yield the same aggregate supply, as long as they satisfy the constraint (21). The reason is that each producer-retailer pair decides the price in a situation of bilateral monopoly, a problem with indeterminate solution (Howitt and McAfee, 1987; Hall, 2005). This indeterminacy

is common in related search models (e.g., Michaillat and Saez 2015).

We resolve the indeterminacy by selecting the equilibrium (and its associated steady state) where the reservation transportation cost remains fixed at an arbitrary level τ, and the price moves to satisfy the aggregate supply condition. Selecting one equilibrium (at least implicitly) by determining one variable from outside the model is standard in the search literature. For example, in Mortensen and Pissarides (1994), the price of the final good is assumed to follow an exogenous stochastic process.[21]

By considering the equilibrium (and its associated steady state) with freely adjusting prices, we can study the responses of prices to the distinct disturbances to aggregate demand, productive capacity, and the supply chain, respectively, and then use their co-movements with other endogenous variables to formulate unique identifying restrictions to estimate the causal effects of supply chain disturbances in our SVAR model in Section 4, as well as the state-dependent effects of monetary tightening in our TVAR model in Section 5. Hence, Definition 2′ recasts the original Definition 2 of the aggregate supply as a function of price p for an arbitrary τ.[22]

Definition 2′. *For an arbitrary reservation transportation cost $\tau \in (0, +\infty)$, the flexible price aggregate supply c_s^{flex} is the function of price p defined by:*

$$c_s^{flex}(p) = \frac{A\left\{1 + \left[\frac{1-\eta}{\eta\rho}\left(p - \tau + \beta\int_0^\tau G(z')dz'\right)\right]^{-\xi}\right\}^{-\frac{1}{\xi}} G(\tau)}{1 - G(\tau) + A\left\{1 + \left[\frac{1-\eta}{\eta\rho}\left(p - \tau + \beta\int_0^\tau G(z')dz'\right)\right]^{-\xi}\right\}^{-\frac{1}{\xi}} G(\tau)} l, \tag{22}$$

for all $p \in [p^{min}, +\infty)$, where p^{min} satisfies:

$$p^{min} - \tau + \beta\int_0^\tau G(z')dz' = 0.$$

The next proposition outlines the properties of the aggregate supply when the price adjusts to satisfy the aggregate supply condition.

Proposition 2. *The flexible price aggregate supply c_s^{flex} has the following properties:*

1. *$c_s^{flex}(p^{min}) = 0$ and $\lim_{p\to+\infty} c_s^{flex}(p) = G(\tau)l$;*

[21] Another possibility is to pick the price of the final good as the numeraire in the economy. We do not follow this route here because we want to build a theory of aggregate demand where the monetary unit is the numeraire.

[22] Appendix D.8 discusses the alternative equilibrium selection mechanism in which p remains fixed while τ can vary. In addition to deriving its key analytical properties, we use numerical methods to approximate this fixed price aggregate supply and illustrate its properties across different values of the reservation transportation cost.

2. $c_s^{flex}(p)$ *is strictly increasing in* p *on* $[p^{min}, +\infty)$*; and*

3. $c_s^{flex}(p)$ *is concave on* $[p^{min}, +\infty)$.

Proof. See Appendix D.2. ■

The aggregate supply $c_s^{flex}(p)$ in Equation (22) represents the quantity of goods traded that satisfies Equation (20) for a given reservation transportation cost τ. That is, the interaction between the price and tightness in the product market determines the aggregate supply. A higher price leads to a greater total surplus by increasing the value for the matched retailer. This, in turn, enhances the incentives for retailers to visit producers, resulting in increased product market tightness and a higher probability for a producer to match with a retailer. More matches are created, resulting in a higher aggregate supply. While transportation costs and matching frictions reduce the aggregate supply of goods to retailers and create spare capacity, the model retains the standard positive relationship between the price and the aggregate supply.

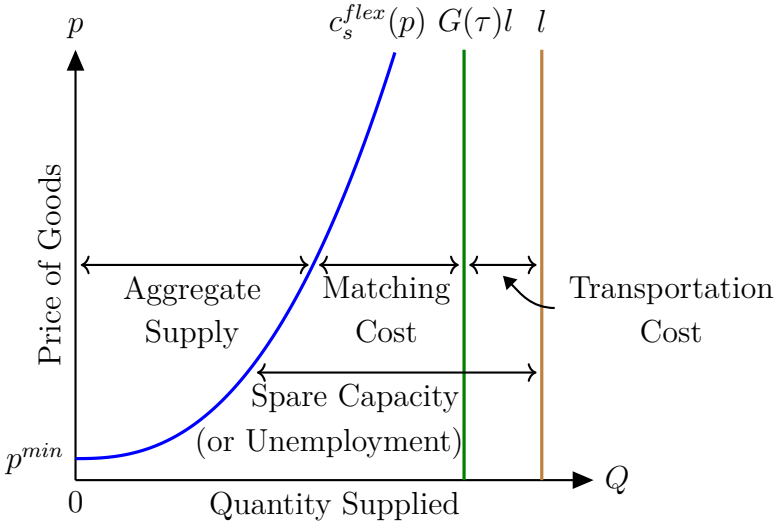

Figure 6: Supply Side of the Economy with Flexible Prices

Figure 6 shows the aggregate supply in the quantity-price (Q,p) plane. For a given productive capacity of the economy l (brown line), transportation costs limit the production to $G(\tau)l$ (green line).[23] Search frictions further reduce the aggregate supply to the level $c_s^{flex}(p)$ (blue line), which, as in standard models, increases with the price. The spare capacity, represented by the difference between the productive capacity of the economy and the actual production (i.e., $l - c_s^{flex}(p)$),

[23] Setting $A = 1$ in Equation (22) and assuming the absence of search frictions yield such a boundary.

arises from both the transportation and matching costs. The spare capacity is equivalent to unemployment in the labor market, as it represents the difference between the total labor supply and the demand for labor.

3.2. The Representative Household

The representative household derives utility from consuming goods and holding real money balances:

$$u\left(c, \frac{m}{p}\right) = \frac{\chi}{1+\chi} c^{\frac{\varepsilon-1}{\varepsilon}} + \frac{1}{1+\chi}\left(\frac{m}{p}\right)^{\frac{\varepsilon-1}{\varepsilon}},$$

where c denotes consumption, m is the nominal money balance, p is the price level, the parameter $\chi > 0$ represents the taste for consumption relative to holding money, and the parameter $\varepsilon > 1$ is the elasticity of substitution between consumption and real money balances. We borrow this utility function from Michaillat and Saez (2015) to ensure that aggregate demand is instrumental to the changes in macro aggregates.

Taking the price as given, the household chooses consumption and nominal money balances to maximize utility, subject to the budget constraint:

$$\begin{aligned} pc + m &\leq \mu + \underbrace{pc_s^{flex}(p) - \int_0^{\tau} z' c_s^{flex}(p) dG(z')}_{\text{Profits of Producers \& Retailers}} + \underbrace{\int_0^{\tau} z' c_s^{flex}(p) dG(z')}_{\text{Transportation Costs}} \\ &= \mu + p\left[\frac{f\left(\theta(p)\right) G(\tau)}{1 - G(\tau) + f\left(\theta(p)\right) G(\tau)} l\right], \end{aligned} \tag{23}$$

where $\mu > 0$ is the household's endowment of nominal money.

Solving the household's problem yields the optimal condition:

$$\frac{\chi}{1+\chi} c^{-\frac{1}{\varepsilon}} = \frac{1}{1+\chi}\left(\frac{m}{p}\right)^{-\frac{1}{\varepsilon}}. \tag{24}$$

Aggregate demand. The aggregate demand in the economy is equal to the level of consumption that maximizes utility at a given price when the money market clears (this condition holds in and outside the steady state). By replacing m with μ in Equation (24) and rearranging, we derive the aggregate demand in the economy.

Definition 3. *The aggregate demand c_d for a given price $p \in (0, +\infty)$ equals:*

$$c_d(p) = \chi^{\varepsilon} \frac{\mu}{p}. \tag{25}$$

Proposition 3. *$c_d(p)$ is strictly decreasing and convex on $(0, +\infty)$.*

Proof. Direct proof from Equation (25). ■

Figure 7 below shows the aggregate demand, which is downward sloping in the (Q, p) plane. Since a higher price leads to lower real money balances, the household's indifference between consumption and holding money implies that it desires lower consumption when the price is higher. Hence, the aggregate demand in the economy decreases with the price.

3.3. The Flexible Price Steady State

For a given reservation transportation cost τ, the flexible price steady state is presented in Definition 4, and its existence is demonstrated in Proposition 4.

Definition 4. *Fixing the reservation transportation cost $\bar{z}$ to an arbitrary value $\tau > 0$, the flexible price steady state consists of a price p that equates aggregate supply and aggregate demand, $c_s^{flex}(p) = c_d(p)$, yielding:*

$$\frac{f\left(\theta(p)\right) G(\tau)}{1 - G(\tau) + f\left(\theta(p)\right) G(\tau)} l = \chi^{\varepsilon} \frac{\mu}{p}, \tag{26}$$

where the product market tightness θ is given by:

$$\theta(p) = \frac{1 - \eta}{\eta \rho} \left(p - \tau + \beta \int_0^{\tau} G(z') dz' \right). \tag{27}$$

In addition, the household's budget constraint (23) also holds with equality.

Proposition 4. *For any $\tau > 0$, there exists a unique flexible price steady state that features positive price and consumption.*

Proof. See Appendix D.3. ■

Figure 7 shows the aggregate supply, aggregate demand, and the steady-state price, p_0, where the aggregate supply and demand intersect on the (Q, p) plane. The maximum quantity of goods that could be supplied when the matching process between producers and retailers becomes frictionless and the productive capacity of the economy are also plotted on the figure for comparison.

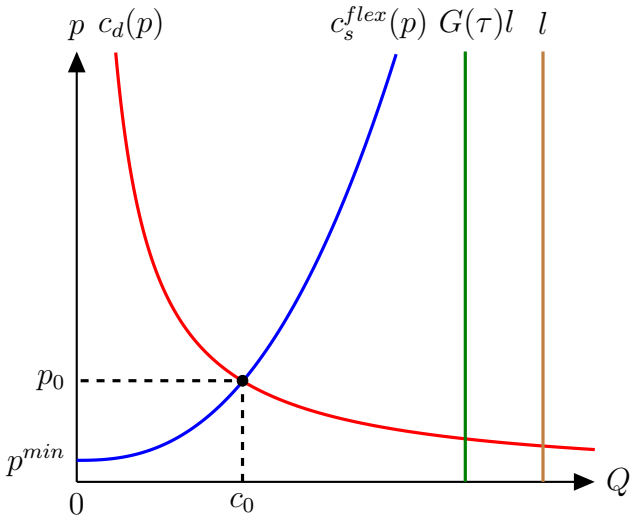

Figure 7: Aggregate Demand and Supply

3.4. Comparative Statics

We use comparative statics to study the responses of the macro aggregates to (unanticipated) adverse shocks to aggregate demand, productive capacity, and the supply chain, respectively, when the economy is at the steady state. These responses provide unique identifying restrictions for studying the causal effects of supply chain disturbances in the SVAR model in the subsequent section, as well as the state-dependent effects of monetary tightening in the TVAR model in Section 5. Appendix D.10 shows (numerically) the complete dynamics of the model after each shock. Suffice it to say here that the transition dynamics are fully consistent with our discussion below and the implied identification assumptions.

An adverse shock to aggregate demand can manifest as either a decrease in the money supply, μ, or a decline in the preference for consuming goods, χ. An adverse shock to productive capacity corresponds to a negative disturbance to the inelastic labor supply, l. An adverse shock to the supply chain involves an increase in the distribution of transportation costs (characterized by a rise in γ, the scale parameter of the log-normal distribution of transportation costs) or a lower matching efficiency (characterized by a fall in A such that $0 < A < 1$).

Proposition 5 summarizes the responses of aggregate variables to each shock.

Proposition 5. *At the steady state:*

- ***An adverse shock to aggregate demand*** *increases matching cost and spare capacity (or, equivalently, unemployment) while it decreases consumption (or, equivalently, output),*

price, product market tightness, and wholesale price.

- ***An adverse shock to productive capacity*** *increases price, product market tightness, and wholesale price. At the same time, it decreases consumption (or, equivalently, output), matching cost, and spare capacity (or equivalently, unemployment).*

- ***An adverse shock to the supply chain*** *increases price and spare capacity (or, equivalently, unemployment) while it decreases consumption (or, equivalently, output). The responses of product market tightness, wholesale price, and matching cost are undetermined after an increase in transportation costs. In comparison, product market tightness and wholesale price increase while matching cost remains undetermined after a fall in matching efficiency.*

Proof. See Appendices D.4 and D.9. ■

Table 1 summarizes the signs of the responses of the endogenous variables to each shock. Figure 8 plots the comparative statics (left panels) for the aggregate demand, productive capacity, and supply chain shocks (represented by an increase in γ) alongside the corresponding equilibrium conditions between product market tightness and price (right panels) from Equation (27), which describes the optimal response of product market tightness to a change in price.[24]

Table 1: Comparative Statics for Adverse Shocks to Aggregate Demand, Productive Capacity, and the Supply Chain

Adverse Shock To:	**Effects On:**					
	Consumption (or Output) c	Price p	Product Market Tightness θ	Wholesale Price r	Matching Cost $\frac{AG(\tau)}{1-(1-A)G(\tau)}l-c$	Spare Capacity (or Unemployment) $l-c$
Aggregate Demand ($\mu\downarrow$ or $\chi\downarrow$)	$-$	$-$	$-$	$-$	$+$	$+$
Productive Capacity ($l\downarrow$)	$-$	$+$	$+$	$+$	$-$	$-$
Supply Chain ($\gamma\uparrow$)	$-$	$+$	Undetermined	Undetermined	Undetermined	$+$
Supply Chain ($A\downarrow$)	$-$	$+$	$+$	$+$	Undetermined	$+$

Panel (a) in Figure 8 shows the comparative statics of a decline in aggregate demand. The aggregate demand curve shifts inward from c_d to c_d', driven by the preference for lower consumption by households, either because they hold less money or prefer to decrease consumption. Thus, the price decreases to clear the market. As the price decreases and the profits from sales to the

[24] To save space, we relegate the discussion of the case with a lower matching efficiency to Appendix D.9, since the reasoning closely aligns with the scenario involving higher transportation costs.

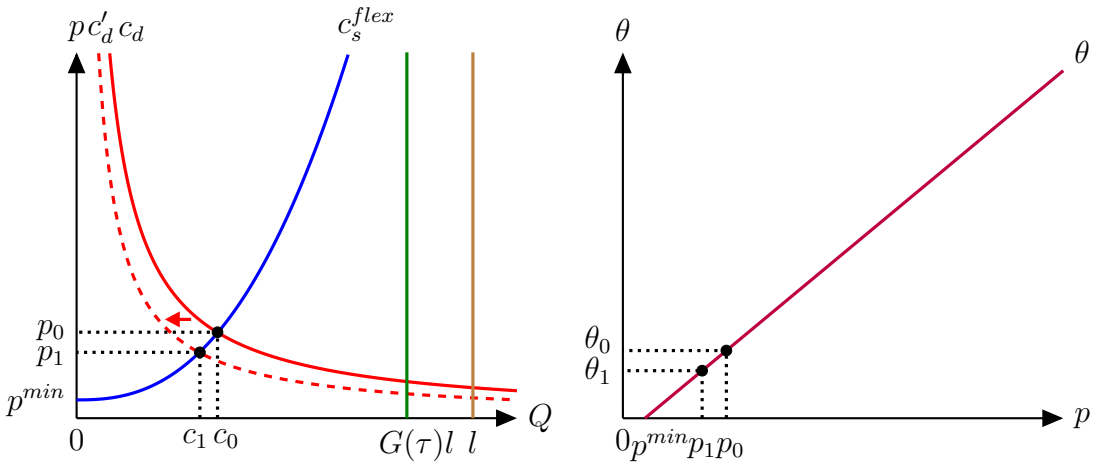

(a) An Adverse Shock to Aggregate Demand, i.e., $\mu \downarrow$ or $\chi \downarrow$

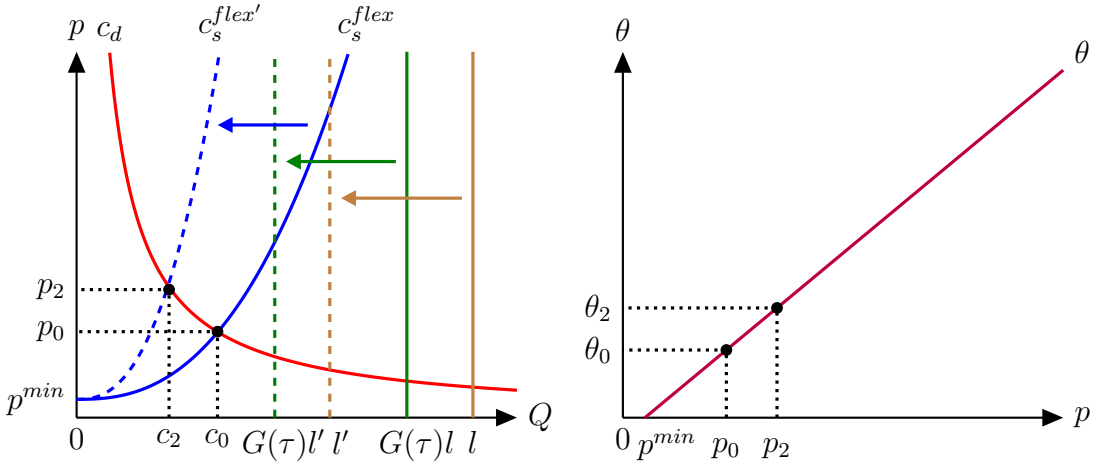

(b) An Adverse Shock to Productive Capacity, i.e., $l \downarrow$

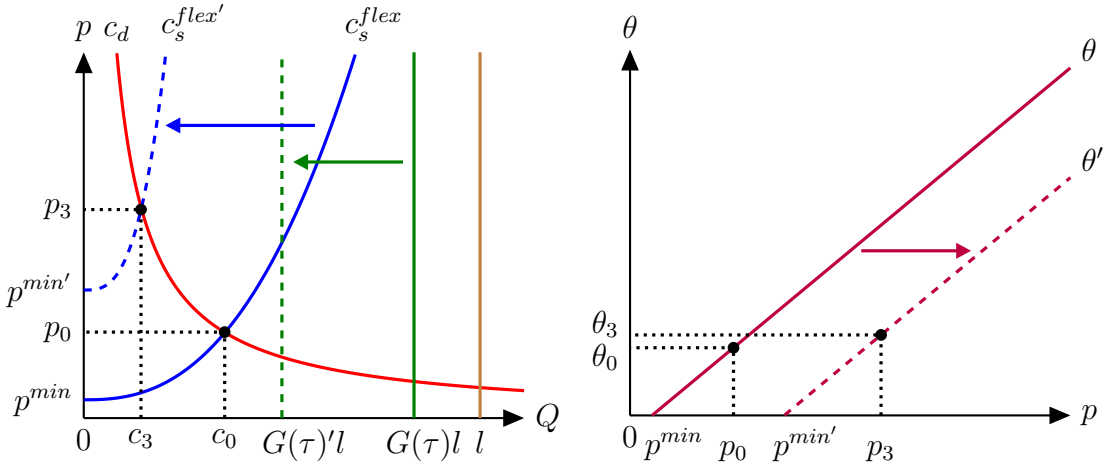

(c) An Adverse Shock to Supply Chain, i.e., $\gamma \uparrow$

Figure 8: Graphical Representation of Comparative Statics

households fall, retailers visit fewer producers to participate in trade, hence lowering product market tightness. The declines in price and product market tightness lead to a lower wholesale price, since not only the sale of goods is less profitable, but also the probability of establishing a match with producers increases. Consequently, producers sell a lower fraction of their productive capacity, resulting in lower consumption (or, equivalently, output) and higher spare capacity (or, equivalently, unemployment) and matching costs.

Panel (b) in Figure 8 shows the response to a negative supply shock that decreases productive capacity from l to l'. This shock causes the aggregate supply curve to rotate inward while leaving p^{min} unchanged (since the distribution of transportation costs remains the same, and thus the minimum price for profitable transactions is unchanged). The price increases to clear the market and consumption falls. The higher price attracts more retailers to enter the market, which raises product market tightness. The simultaneous rise in price and θ leads to a higher wholesale price. Matching costs and spare capacity (or, equivalently, unemployment) also fall.

Panel (c) in Figure 8 shows the comparative statics of an increase in the scale parameter γ of the log-normal distribution of transportation costs $G(\cdot)$. Higher mean transportation costs increase the likelihood that producers will draw a transportation cost above the fixed reservation threshold. As a result, the fraction of shipped output from producers decreases, curtailing the supply of goods available to households, and the price of goods increases to clear the market. Thus, the price rises while consumption falls. Graphically, this process is represented by an inward shift of the aggregate supply curve from c_s^{flex} to $c_s^{flex'}$, together with an increase in p^{min}. Since the productive capacity (or, equivalently, labor supply) remains unchanged while the number of successful trades falls, spare capacity (or, equivalently, unemployment) increases.

The disturbance to the supply chain can either tighten or loosen product market tightness, depending on the extent to which the price rise compares to the fall in expected profits due to higher transportation costs. To consider these countervailing forces more explicitly, we revisit the equilibrium condition for product market tightness in Equation (27):

$$\theta(\gamma) = \frac{1-\eta}{\eta\rho}\left[\underbrace{p(\gamma)-\tau}_{\text{Profit Margin }\uparrow} + \underbrace{\beta\int_0^{\tau}\Phi\left(\frac{\log z'-\gamma}{\sigma}\right)dz'}_{\text{Expected Total Surplus }\downarrow}\right],$$

where $\Phi(\cdot)$ is the standard normal cumulative density function. This equation illustrates how

the sensitivity of price to transportation costs determines the "profit margin," which incentivizes retailers to search for producers, thereby increasing tightness in the product market. Conversely, higher transportation costs decrease the "expected total surplus" from trading, which deters retailers from searching for producers. The net change in product market tightness resulting from a supply chain disruption is determined by the interplay of these two opposing forces.[25]

Important to our analysis in Section 5 on the effectiveness of monetary policy in controlling inflation and output, changes in product market tightness also have implications for the sensitivity of goods supply to price variations following an adverse shock to the supply chain. Suppose the price increase is sufficiently large that the rise in visits made by unmatched retailers significantly outpaces the increase in the number of unmatched producers (i.e., the goods market is congested on the retailers' side). While this imbalance leads to a tighter product market and increases the likelihood of a producer participating in trade, an additional retailer has only a limited impact on the producer's probability of forming a match. To see even a slight further increase in such a probability, prices would need to rise considerably more due to the diminishing returns to searching inherent in the constant-returns-to-scale matching function (see Equation (3)). Consequently, the number of matches and the supply of goods become less sensitive to price changes resulting from supply chain disruptions when the goods market is tight. Graphically, this change in the sensitivity of output to price fluctuations is represented by a steeper slope of the aggregate supply curve, as depicted in Panel (c) of Figure 8.[26]

4. The Causal Effects of Supply Chain Disruptions

We are now ready to study the causal effects of supply chain disruptions by developing an SVAR model that utilizes our ACR index and constrains the responses of the macro aggregates to the three distinct shocks in line with our theoretical results from the model.[27]

[25] The simulation results in Appendix D.10 corroborate this point. Specifically, as illustrated in Table D.5, in the scenario of a 10% increase in γ, the resulting price increase is sufficient to raise product market tightness in the new steady state. However, in an alternative scenario with only a 1% increase in γ, as shown in Table D.7, the resulting price increase does not lead to greater tightness in the product market.

[26] Appendix D.4 demonstrates that the changes in the wholesale price and matching cost depend on the responses of product market tightness and price to the supply chain shock. Lastly, in Appendix D.5, we show that the slope of the aggregate supply curve is inversely related to product market tightness. Specifically, the aggregate supply curve becomes steeper in the (Q, p) plane as product market tightness increases. Figure D.1 illustrates the alternative scenario where the price increase is insufficient to raise product market tightness.

[27] In principle, we could also undertake a full structural estimation of our model. However, that strategy would force us to buy into too many ancillary assumptions (e.g., parametric forms, persistence of shocks, etc.) that can

Our empirical specification is based on Rubio-Ramírez et al. (2010) and Arias et al. (2018):

$$\boldsymbol{y}_t'\boldsymbol{A}_0 = \sum_{l=1}^{L} \boldsymbol{y}_{t-l}'\boldsymbol{A}_l + \boldsymbol{\omega}_t'\boldsymbol{C} + \boldsymbol{\varepsilon}_t', \quad 1 \leq t \leq T, \tag{28}$$

where $\boldsymbol{y}_t$ is an $n \times 1$ vector of endogenous variables, $\boldsymbol{\omega}_t = [1, t]'$ is a 2×1 vector of a constant and a linear trend, $\boldsymbol{\varepsilon}_t$ is an $n \times 1$ vector of structural shocks, $\boldsymbol{A}_l$ is an $n \times n$ matrix of structural parameters for $0 \leq l \leq L$ with $\boldsymbol{A}_0$ invertible, $\boldsymbol{C}$ is a $2 \times n$ matrix of parameters, L is the lag length, and T is the sample size. The vector $\boldsymbol{\varepsilon}_t$, conditional on past information and the initial conditions $\boldsymbol{y}_0, \ldots, \boldsymbol{y}_{1-L}$, is Gaussian with mean zero and covariance matrix $\mathbf{1}_{n\times n}$, i.e., the $n \times n$ identity matrix. The SVAR model described in Equation (28) can be written compactly as:

$$\boldsymbol{y}_t'\boldsymbol{A}_0 = \boldsymbol{x}_t'\boldsymbol{A}_+ + \boldsymbol{\varepsilon}_t', \quad 1 \leq t \leq T, \tag{29}$$

where $\boldsymbol{A}_+' = [\boldsymbol{A}_1' \ \ldots \ \boldsymbol{A}_L' \ \boldsymbol{C}']$ and $\boldsymbol{x}_t' = [\boldsymbol{y}_{t-1}' \ \ldots \ \boldsymbol{y}_{t-L}' \ \boldsymbol{\omega}_t']$ for $1 \leq t \leq T$. The dimension of $\boldsymbol{A}_+$ is $m \times n$, where $m = nL + 2$. The reduced-form representation implied by Equation (29) is given by:

$$\boldsymbol{y}_t' = \boldsymbol{x}_t'\boldsymbol{B} + \boldsymbol{u}_t', \quad 1 \leq t \leq T,$$

where $\boldsymbol{B} = \boldsymbol{A}_+\boldsymbol{A}_0^{-1}, \boldsymbol{u}_t' = \boldsymbol{\varepsilon}_t'\boldsymbol{A}_0^{-1}$, and $\mathbb{E}(\boldsymbol{u}_t\boldsymbol{u}_t') = \boldsymbol{\Sigma} = (\boldsymbol{A}_0\boldsymbol{A}_0')^{-1}$.

Motivated by the variables present in our theoretical model, we estimate our SVAR model using the monthly U.S. series for real GDP, personal consumption expenditures (PCE) goods price, unemployment, retail market tightness, import price as well as our ACR index over the sample period from January 2017 to September 2023, with all series being seasonally adjusted. The import price is used as a proxy for the wholesale price in order to capture the international sourcing strategies of U.S. retailers, particularly during the COVID-19 pandemic. All variables are retrieved directly or constructed using available data from the Federal Reserve Economic Data (FRED), maintained by the Federal Reserve Bank of St. Louis.[28] Real GDP, PCE goods

be problematic given the current state of knowledge about models of the global supply chain. While we used some of those assumptions to derive our identification restrictions, we are cautiously optimistic that the restrictions will hold for more general specifications (even if we can only show it numerically). Thus, this seems to be a situation where the additional flexibility offered by SVARs is most convenient.

[28] The mnemonics of the variables that we use in the SVAR estimation are: `GDPC1` (real GDP), `INDPRO` (industrial production), `DGDSRG3M086SBEA` (PCE goods price), `UNRATE` (unemployment), `RETAILIMSA` (retailers' inventories), `RETAILIRSA` (retailers' inventories to sales ratio), `MNFCTRIMSA` (manufacturers' inventories), and `IR` (import price). The monthly time series for real GDP is constructed using interpolation of the corresponding quarterly series, as in Bernanke and Mihov (1998) and Arias et al. (2019). Specifically, we apply the Chow-Lin method for temporal disaggregation (Chow and Lin, 1971) to interpolate real GDP based on the industrial production index. The monthly time series for retail market tightness is constructed by dividing the new orders made by retailers by the

price, retail market tightness, and import price enter the SVAR model in log percent, while unemployment and the ACR index enter in percent. We set the number of lags to two in the baseline specification, but the results are robust to considering longer lags.[29]

Our identification scheme applies the sign restrictions derived from our theoretical model, as summarized in Table 1, as well as the zero restrictions on the contemporary responses of the ACR index to adverse shocks to aggregate demand and productive capacity. We impose these zero restrictions to sharpen our identification of the supply chain disturbance and more importantly, because they are motivated by our domain knowledge of the shipping industry: container ships will not alter their routes or ports without at least several weeks' notice in response to shocks to aggregate demand or capacity. Nonetheless, we verify the robustness of our results by testing them without these restrictions in the estimation, as detailed in Appendix E.1.[30]

We estimate the SVAR using the Bayesian approach as in Arias et al. (2018, 2019, 2023) with restrictions only on the first period of response (i.e., horizon $k = 1$), thus imposing a minimal structure as in Mumtaz and Zanetti (2012, 2015).[31] Furthermore, as illustrated in Appendix D.10,

inventories held by manufacturers, where the retailers' new orders ($Order_t$) are approximated as:

$$Order_t = (Inventory_t - Inventory_{t-1}) + Sale_t,$$

where $Inventory_t$ and $Sale_t$ represent U.S. retailers' inventories and sales in month t. The monthly series for the PCE goods price and unemployment are raw series directly taken from FRED, while the series for import price is seasonally adjusted using the X-13ARIMA-SEATS algorithm.

[29] Appendix E.2 demonstrates the robustness of our results when considering various lag structures, specifically one, three, or four lags. Additionally, we make several substitutions: the real GDP is replaced with the real PCE of goods; the PCE goods price is substituted with the GDP deflator; the import price with the producer price; the unemployment rate with spare capacity; and manufacturers' inventories with merchant wholesalers' inventories for the construction of retail market tightness. The monthly time series for the GDP deflator is derived by interpolating its corresponding quarterly series using the Chow-Lin method, which incorporates both the consumer price index and the producer price index. The monthly time series for spare capacity is constructed by subtracting the capacity utilization rate from 100. As shown in Appendix E.3, despite these substitutions, the results remain consistent. Also, we conduct a robustness check by applying a fitted ACR index in our estimation after regressing the port-specific congestion rate on the Oxford Stringency (OS) Index (Mathieu et al., 2020) and extracting the fitted values. As shown in Appendix E.4, the results are quantitatively similar to those obtained using the ACR index directly.

[30] A more radical alternative would be to estimate an SVAR where we interpret the ACR as a noisy signal of a latent variable "state of the global supply chain." This could be done with a state space representation where an SVAR that includes the "state of the global supply chain" as an (unobserved) variable is the transition equation, and the measurement equation links the "state of the global supply chain" with our measurement ACR. While this seems a worthwhile exercise, we leave it for future research, as it would require a more thorough treatment than what we can give it in this already lengthy study.

[31] We use a Normal-Generalized-Normal (NGN) prior distribution over $\boldsymbol{A}_0$ and $\boldsymbol{A}_+$. The NGN prior is a conjugate prior characterized by four parameters $(\nu, \boldsymbol{\Phi}, \boldsymbol{\Psi}, \boldsymbol{\Omega})$. The parameters ν and $\boldsymbol{\Phi}$ govern the marginal prior distribution of $vec(\boldsymbol{A}_0)$, while $\boldsymbol{\Psi}$ and $\boldsymbol{\Omega}$ govern the prior distribution of $vec(\boldsymbol{A}_+)$, conditional on $\boldsymbol{A}_0$. We pick $\nu = 0, \boldsymbol{\Phi} = \boldsymbol{0}_{n\times n}, \boldsymbol{\Psi} = \boldsymbol{0}_{m\times n}$, and $\boldsymbol{\Omega}^{-1} = \boldsymbol{0}_{m\times m}$. This parameterization generates prior densities that are equivalent to those in Uhlig (2005). Appendix E.5 ascertains that our results are robust to using the prior robust approach in Giacomini and Kitagawa (2021).

the convergence of the dynamic version of our theoretical model from one steady state to another following each shock of interest occurs almost instantaneously, and the process is monotonic. This justifies our decision to impose identifying restrictions only at $k = 1$. More concretely, we impose the following restrictions:

Restriction 1. ***An adverse shock to aggregate demand*** *leads to a negative response of real GDP, PCE goods price, retail market tightness, and import price, as well as to a positive response of unemployment at $k = 1$. The ACR does not respond at $k = 1$.*

Restriction 2. ***An adverse shock to the productive capacity*** *leads to a negative response of real GDP and unemployment, as well as to a positive response of PCE goods price, retail market tightness, and import price at $k = 1$. The ACR does not respond at $k = 1$.*

Restriction 3. ***An adverse shock to the supply chain*** *leads to a negative response of real GDP, as well as to a positive response of PCE goods price, unemployment, and the ACR at $k = 1$.*

When estimating the causal effects of a supply chain disruption shock, we leave the responses of retail market tightness and import price unrestricted since those responses depend on the type of supply chain disruption shock (i.e., higher transportation cost vs. lower matching efficiency).[32]

Figures 9, 10, and 11 show our baseline results for the responses of the endogenous variables to an adverse shock to aggregate demand, productive capacity, and the supply chain, respectively. The solid lines show the point-wise posterior median impulse response functions (IRFs) of the endogenous variables to each structural shock, and the gray-shaded areas represent the corresponding 68% and 90% posterior probability bands.[33] The shape and size of our estimated IRFs to demand and capacity shocks are comparable to those found in classic papers that estimate the responses of macroeconomic aggregates to traditional demand and supply shocks (Christiano et al., 1999; Peersman, 2005; Smets and Wouters, 2007; Fry and Pagan, 2011).

We begin by discussing the IRFs to an adverse shock to aggregate demand in Figure 9. On impact, real GDP declines significantly by approximately 0.8%, and unemployment rises sharply

[32]For robustness, in an alternative SVAR estimation, we also apply additional positive sign restrictions on the contemporary responses of retail market tightness and import price to an adverse shock to the supply chain. This robustness check follows our theoretical prediction in Proposition 5 for a supply chain disturbance represented by a lower matching efficiency. As shown in Appendix E.6, the results are quantitatively similar to those obtained without imposing such restrictions.

[33]These results are based on 100,000 independent draws from the posterior distribution of the structural parameters, with the structural shocks normalized to one standard deviation.

by more than 0.5%. Such responses persist with a high posterior probability for the first six months following the shock. Retail market tightness also falls substantially by approximately 1.5% on impact, then rebounds to 0.5%, and gradually reverts to zero. In contrast, the response of the PCE goods price is muted, with an initial drop of about 0.2% before gradually reverting to zero after one year. The import price exhibits a similar pattern, albeit returning quicker at the three-quarter mark. Lastly, the ACR index's response is less precisely estimated, with a large posterior probability mass centered around zero.

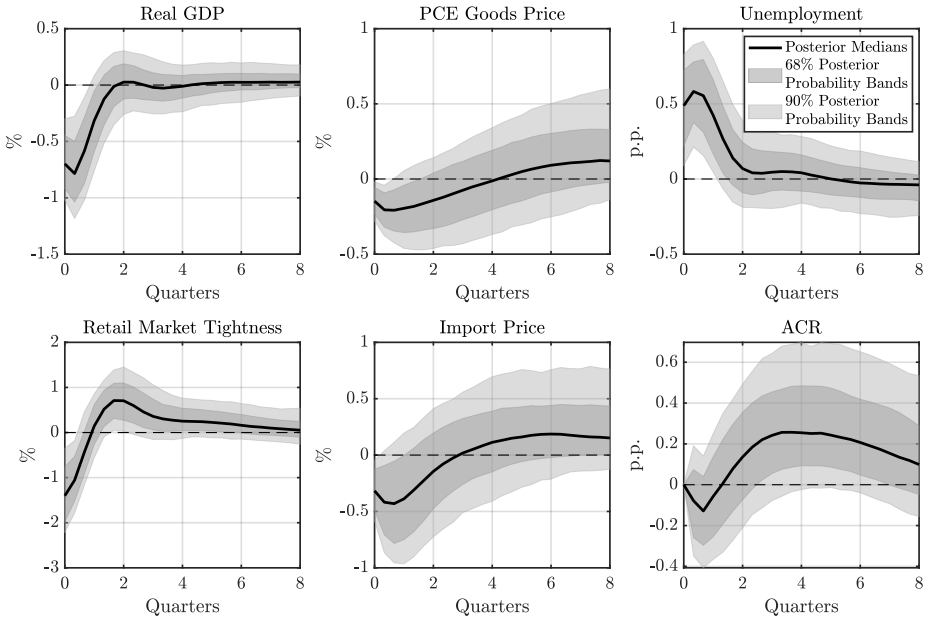

Figure 9: IRFs to an Adverse Shock to Aggregate Demand

Notes. The IRFs to a one standard deviation adverse shock to aggregate demand are identified using the ACR index and Restrictions 1, 2, and 3. The solid line shows the point-wise posterior medians and the shaded bands represent the 68% and 90% equal-tailed point-wise posterior probability bands. The figure is based on 100,000 independent importance sampling draws.

Figure 10 shows the IRFs to an adverse shock to productive capacity. On impact, the responses of real GDP and unemployment are negative, whereas the response of retail market tightness is positive, in accordance with Restriction 2. Subsequently, real GDP continues to decline, reaching a trough of approximately 0.2%, which occurs about one quarter after the shock. Largely due to the fall in real GDP, the initial decrease in unemployment quickly reverses, turning positive within one quarter of the shock and peaking at around 0.1% before returning to zero. The post-impact response of retail market tightness initially approaches zero, then increases again. The PCE goods price rises and remains high for about two years, reflecting the lagged effects of

supply-side disruptions. The import price exhibits a similar pattern, although it reaches its peak earlier. Lastly, the median response of the ACR index is zero on impact but remains consistently above zero for approximately six quarters after that.

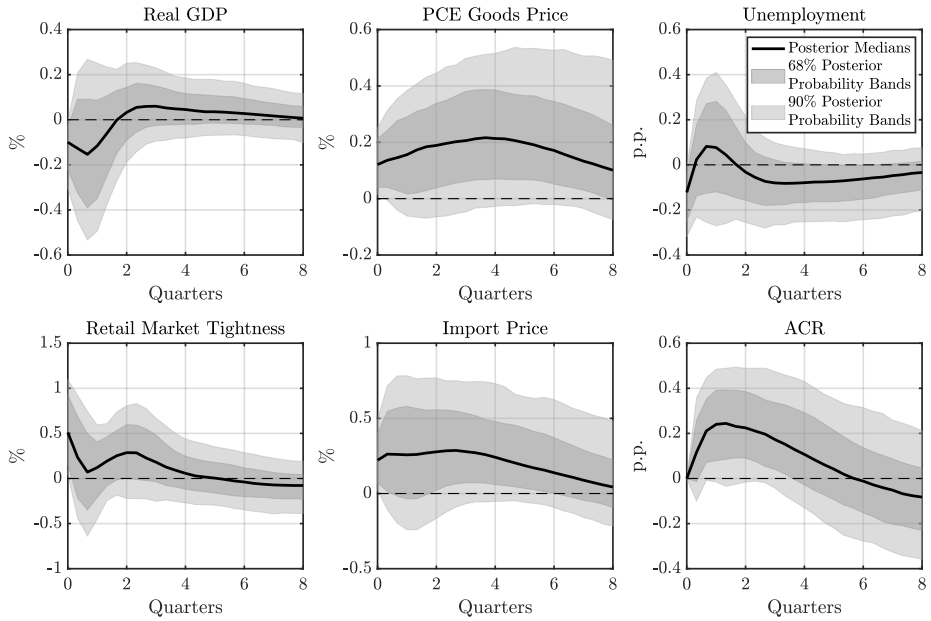

Figure 10: IRFs to an Adverse Shock to Productive Capacity

Notes. The IRFs to a one standard deviation adverse shock to productive capacity are identified using the ACR index and Restrictions 1, 2, and 3. The solid line shows the point-wise posterior medians and the shaded bands represent the 68% and 90% equal-tailed point-wise posterior probability bands. The figure is based on 100,000 independent importance sampling draws.

Figure 11 shows the IRFs following a negative shock to the supply chain. The median response of real GDP is negative on impact and stays below zero for over a quarter after the shock. While real GDP decreases, unemployment increases by roughly the same magnitude and remains elevated for one quarter. In terms of the response of retail market tightness, which is unrestricted, it initially decreases before sharply increasing to peak at 0.5% after one quarter.[34] The surges in both the PCE goods price and the import price are consistent with the magnitudes observed following the negative capacity shock, highlighting the substantial impact of supply chain disruptions on price inflation. Despite the uncertainty around our estimates, as indicated by the wide posterior probability bands, the positive responses of both the PCE goods price and the import price stay within the 68% probability band. Furthermore, for both series, the lower boundary of

[34] In line with our theoretical prediction in Section 3.4, the initial decrease in tightness can be largely attributed to the rise in spare capacity following the supply chain disruption when prices have not adjusted. Subsequently, as prices continue to rise, more retailers are drawn into the product market, resulting in elevated tightness.

the 90% probability approaches the zero response line when the corresponding median response hits the peak at approximately the one-year mark. Lastly, the ACR index remains elevated for five quarters after the shock.

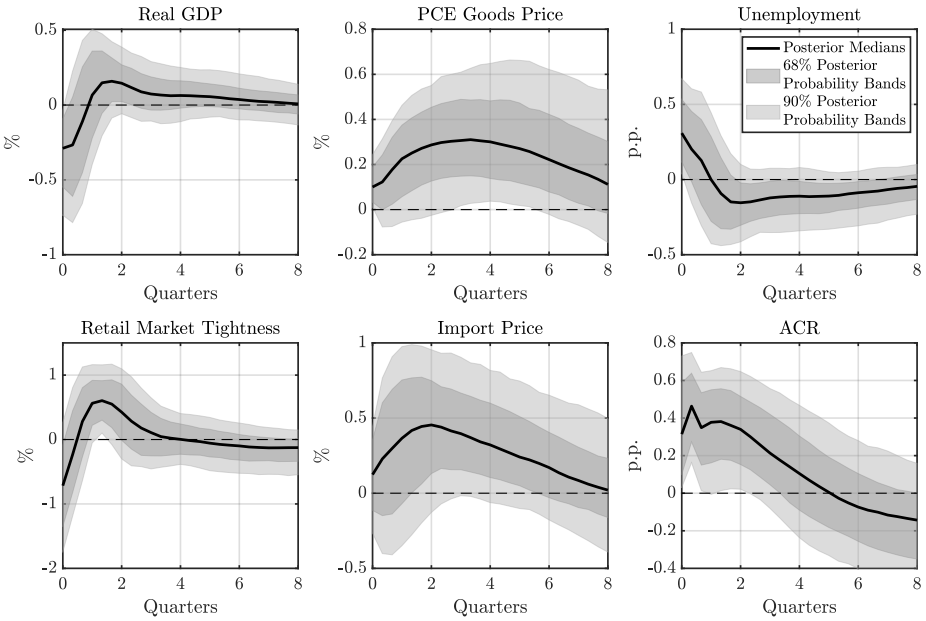

Figure 11: IRFs to an Adverse Shock to Supply Chain

Notes. The IRFs to a one standard deviation adverse shock to the supply chain are identified using the ACR index and Restrictions 1, 2, and 3. The solid line shows the point-wise posterior medians and the shaded bands represent the 68% and 90% equal-tailed point-wise posterior probability bands. The figure is based on 100,000 independent importance sampling draws.

Figure 12 shows the proportions of forecast error variance explained by each of the three structural shocks. The aggregate demand shock accounts for the largest share of unexpected fluctuations in real GDP, unemployment, and retail market tightness across all horizons. Conversely, although the demand shock explains the majority of unexpected variations in the PCE goods and import prices at shorter horizons, supply chain disturbances become the dominant factor accounting for the largest portion of these unexpected fluctuations in both price indicators over longer horizons, suggesting that disruptions to the supply chain have enduring effects on price increases. Capacity shocks also contribute to the price movements but are less influential than supply chain shocks. Moreover, supply chain shocks are more potent in explaining the unexpected variations in real GDP, unemployment, and retail market tightness than capacity shocks.

Figure 13 displays the key empirical finding of our analysis. It shows the cumulative historical contribution of each of the three structural shocks to U.S. quarter-on-quarter goods inflation for

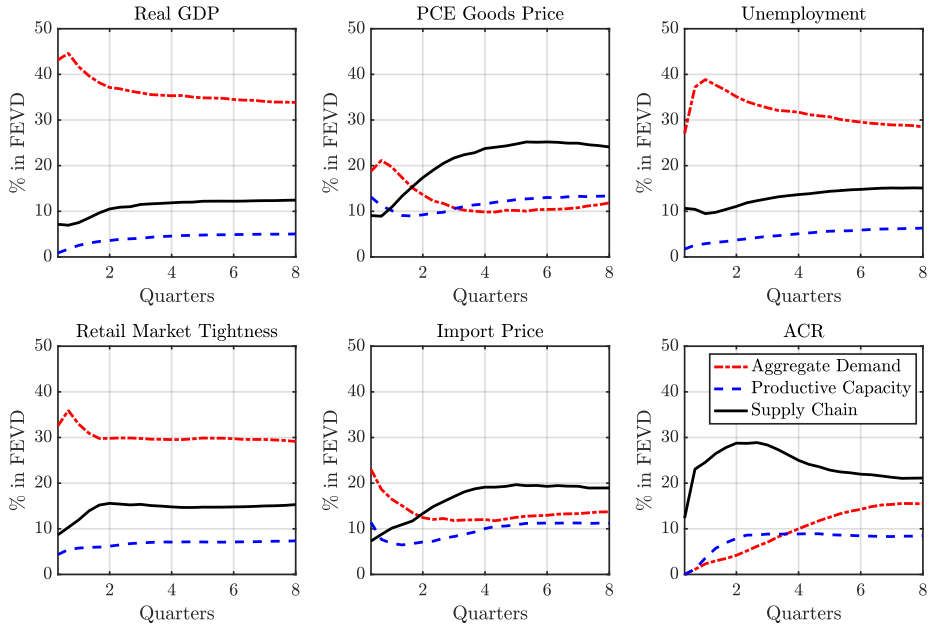

Figure 12: Forecast Error Variance Decomposition (FEVD) from the SVAR

Notes. Each line presents the median fraction of the forecast error variance for each endogenous variable, explained by each of the three identified structural shocks at various time horizons. The FEVD is estimated using the ACR index and Restrictions 1, 2, and 3, and based on 100,000 independent importance sampling draws.

the sample period from January 2017 to September 2023.[35] Using our ACR index and the theory-predicted identifying restrictions, our estimation can be summarized in five findings.

First, supply chain disturbances consistently generated a negative contribution to inflation prior to the start of the COVID-19 pandemic.[36] Second, the initial drop in inflation at the onset of the COVID-19 pandemic in early 2020 was largely attributed to a substantial decrease in aggregate demand, likely linked with mobility restrictions (which lowered the desire to consume) and elevated uncertainty. Third, the subsequent rises in inflation, especially those during 2021, were mainly due to adverse shocks to the supply chain. Fourth, the landscape changed in the first half of 2022: adverse shocks to productive capacity kept inflation elevated. Recent evidence from the U.S. labor market, drawn from Goda and Soltas (2022), Hobijn and Şahin (2022), and Lee et al. (2023), supports our findings. This evidence highlights that the large decline in the U.S. labor supply during the first half of 2022 was driven by a combination of decreased

[35] To facilitate the comparison of series across different scales, we have applied Z-score standardization, which rescales data to have a mean of zero and a standard deviation of one.

[36] This finding supports the notion of strategic enhancements to supply chain operations to alleviate inflationary pressures. For instance, several U.S. ports (e.g., Port of Los Angeles) underwent considerable infrastructure upgrades between 2017 and 2019, aiming to increase their capacity, efficiency, and resilience against potential systemic disruptions.

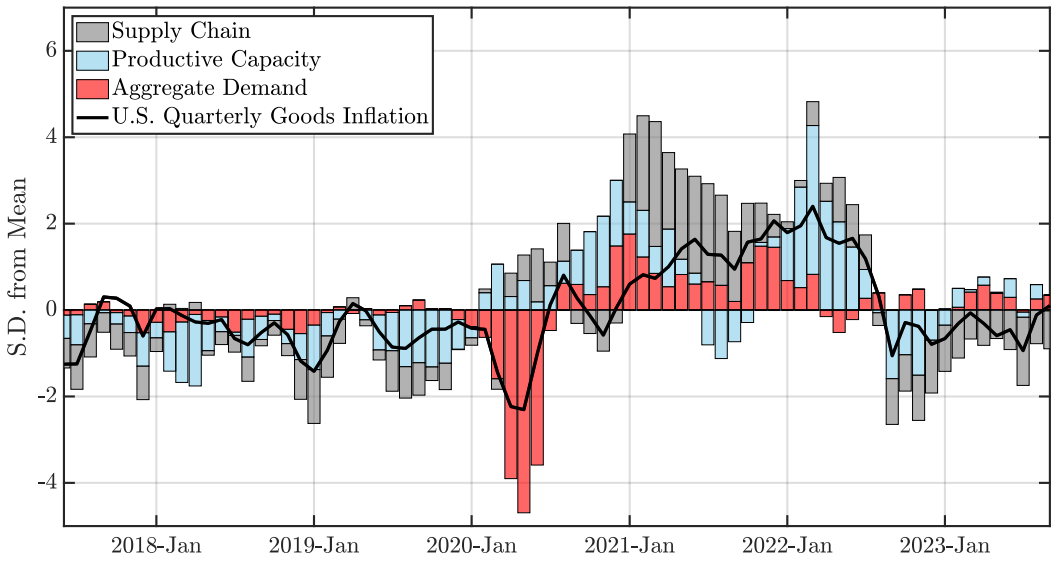

Figure 13: Historical Decomposition (HD) of U.S. Quarter-on-Quarter Goods Inflation

Notes. The solid line represents the standardized goods inflation rate in the U.S., i.e., the quarter-on-quarter growth of the PCE goods price index. The shaded bars represent the corresponding standardized cumulative historical contribution of shocks to aggregate demand, productive capacity, and the supply chain to goods inflation. The shocks are identified using the SVAR specification in Equation (28), with the ACR index included as the measure of global supply chain disruptions, and Restrictions 1, 2, and 3 imposed on the IRFs of each endogenous variable. The figure is derived from the posterior medians, based on 100,000 independent importance sampling draws.

labor force participation and a substantial reduction in work hours. These changes, influenced by factors like higher unemployment benefits post-pandemic and a shift in worker preferences toward more flexible work arrangements, have played a pivotal role in reshaping the labor market and, according to our estimates, in keeping inflation elevated during this period. Interestingly, aggregate demand played a small role in inflation, suggesting that monetary and fiscal policy might not have been excessively expansionary. Fifth, from the second half of 2022 onward, a combination of weakened demand, strengthened capacity, and supply chain recovery has driven down inflation.

Table 2 also reports the cumulative historical contribution of each shock to U.S. year-on-year goods inflation, highlighting that aggregate demand shocks were the main driving force behind the dynamics of inflation in 2020, supply chain shocks in 2021, and the convolution of all three shocks in driving inflation from 2022 onward.[37]

[37]In Appendix F, we present the estimation results using alternative indices of supply chain disruptions found in the literature, including the HARPEX, the New York Fed's GSCPI, and the SDI by Smirnyagin and Tsyvinski (2022), among others. These results show significant variations among the indices in terms of the estimated impacts of aggregate demand, productive capacity, and supply chain shocks on U.S. goods inflation.

Table 2: Cumulative Historical Contribution of Each Shock to U.S. Year-On-Year Goods Inflation

Date	U.S. Goods Inflation (Y-O-Y, Percent)	Cumulative Historical Contribution		
		Aggregate Demand (%)	Productive Capacity (%)	Supply Chain (%)
2018-Jun	1.4	-16.6	-47.1	-23.1
2019-Jun	-0.6	35.2	95.9	68.7
2020-Jun	-1.8	85.2	15.7	-0.4
2021-Jun	5.7	17.8	14.8	18.6
2022-Jun	10.8	6.8	9.7	8.8
2023-Jun	1.1	31.2	-17.7	-62.4

Notes. U.S. goods inflation rate, calculated as the year-on-year growth of the PCE goods price index, along with the cumulative historical contribution of shocks to aggregate demand, productive capacity, and the supply chain to goods inflation, measured as a percentage of the corresponding year-on-year goods inflation rate for each sampling year from 2018 to 2023. For interpretation, if the goods inflation rate is positive (negative), a positive cumulative historical contribution implies that the shock is contributing to the rise (fall) in inflation, and *vice versa*. The shocks are identified using the SVAR specification in Equation (28), with the ACR index included as the measure of global supply chain disruptions, and Restrictions 1, 2, and 3 imposed on the IRFs of each endogenous variable. The numbers reported for the cumulative historical contribution are the posterior medians, based on 100,000 independent importance sampling draws.

5. The Effectiveness of Monetary Policy

Our next task is to study the interplay between supply chain disruptions and the effectiveness of monetary policy in controlling inflation and output. First, we show through our theoretical model that a disruption to the supply chain increases the sensitivity of inflation and reduces the sensitivity of output to a contractionary monetary policy shock, generating state-dependence in the trade-off for monetary policy. Then, we will test and empirically corroborate our theoretical prediction using a threshold vector autoregression (TVAR) model.

5.1. Theoretical Prediction

We derive the theoretical prediction for the state-dependence of monetary policy by returning to our model in Section 3. The money supply parameter μ encapsulates the action of monetary policy, and the scale parameter of the distribution of transportation costs γ captures the disruption to the supply chain (in the interest of space, the case where the matching efficiency falls is relegated to Appendix D.9; suffice it to say that we get the same results). We study the compar-

ative statics of the impacts of a tightening in monetary policy, focusing on whether the effects of the policy intervention on inflation and output are different amid the supply chain disruption.[38] Proposition 6 summarizes our results.

Proposition 6. *For any given threshold of reservation transportation cost $\tau > 0$ and parameter values relevant for monetary policy $\mu \in \mathbb{R}^+$ and transportation costs $\gamma \in \mathbb{R}$, when product market tightness is sufficiently elevated to allow producers to recoup the increase in transportation costs due to the supply chain disruption, as represented by the following constraint:*

$$\frac{\partial \theta(\mu,\gamma)}{\partial \gamma} > \frac{\theta(1+\theta^{\xi})}{(1-G(\tau))\,G(\tau)} \frac{1}{\sigma\sqrt{2\pi}} \exp\left[-\frac{(\log\tau-\gamma)^2}{2\sigma^2}\right], \tag{30}$$

where $G(\tau) \equiv \Phi[(\log\tau-\gamma)/\sigma]$, $\Phi(.)$ is the standard normal cumulative density function, the responses of the endogenous variables to a change in monetary policy are described by the partial derivatives:

$$\frac{\partial c(\mu,\gamma)}{\partial \mu} > 0,\ \frac{\partial p(\mu,\gamma)}{\partial \mu} > 0,\ \frac{\partial \theta(\mu,\gamma)}{\partial \mu} > 0,\ \frac{\partial r(\mu,\gamma)}{\partial \mu} > 0,$$
$$\frac{\partial}{\partial \mu}\left[G(\tau)l - c(\mu,\gamma)\right] < 0,\ \frac{\partial}{\partial \mu}\left[l - c(\mu,\gamma)\right] < 0.$$

The cross derivatives of the endogenous variables that describe the optimal interplay between a change in monetary policy and the supply chain disruption are given by:

$$\frac{\partial^2 c(\mu,\gamma)}{\partial \mu \partial \gamma} < 0,\ \frac{\partial^2 p(\mu,\gamma)}{\partial \mu \partial \gamma} > 0,\ \frac{\partial^2 \theta(\mu,\gamma)}{\partial \mu \partial \gamma} > 0,\ \frac{\partial^2 r(\mu,\gamma)}{\partial \mu \partial \gamma} > 0,$$
$$\frac{\partial^2}{\partial \mu \partial \gamma}\left[G(\tau)l - c(\mu,\gamma)\right] > 0,\ \frac{\partial^2}{\partial \mu \partial \gamma}\left[l - c(\mu,\gamma)\right] > 0,$$

where $c, p, \theta, r, G(\tau)l - c$, and $l - c$ represent consumption (or, equivalently, output), price, product market tightness, wholesale price, matching cost, and spare capacity (or, equivalently, unemployment), respectively.

Proof. See Appendix D.6. ■

The partial and cross derivatives in Proposition 6 imply that when the increase in product market tightness is sufficiently large during the supply chain disruption, and therefore producers

[38] In Appendix D.7, we derive the theoretical prediction for the effectiveness of monetary policy, depending on whether the productive capacity of the economy is constrained or not. Similar to the scenario in which the supply chain is disrupted, contractionary monetary policy is more effective at taming inflation and reducing the sensitivity of output when the productive capacity is constrained. The only difference is that the state-dependent effects of monetary policy are unconditional.

have greater incentives to trade with retailers (as stated in Equation (30)), the supply chain disruption intensifies the fall in inflation while dampening the fall in consumption (or, equivalently, output) that is associated with a contractionary monetary policy shock.[39]

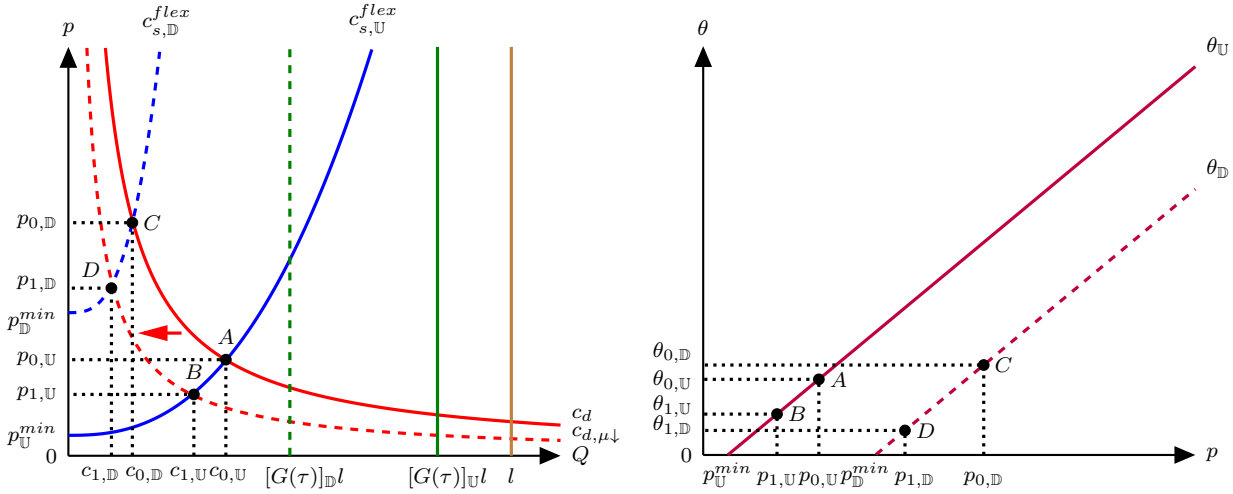

Figure 14: State-Dependent Effects of a Contractionary Monetary Policy Shock: Theoretical Prediction

Notes. The panels illustrate the adjustment of the economy to a contractionary monetary policy shock and to what extent the adjustment depends on disruptions to the supply chain. The two respective states – i.e., supply chain disrupted ($\mathbb{D}$) versus undisrupted ($\mathbb{U}$) – are plotted against each other. $c_{s,\mathbb{D}}^{flex}$ and $c_{s,\mathbb{U}}^{flex}$ represent the aggregate supply curves in the two states, while $\theta_{\mathbb{D}}$ and $\theta_{\mathbb{U}}$ represent the schedules of product market tightness in the two states. c_d and $c_{d,\mu\downarrow}$ denote the aggregate demand curves before and after the contractionary monetary policy shock, respectively. The labels on the axes corresponding to each state are differentiated by their subscripts, and the capital letters ($A \to B, C \to D$) indicate the dynamics of the economy in the two states.

Figure 14 provides the graphical representation of our theoretical prediction. In response to a contractionary monetary policy shock, households reduce consumption due to decreased money holdings. This reduction causes the aggregate demand curve to shift inward, leading to lower prices and reduced consumption of goods. Consequently, product market tightness decreases as retailers visit fewer producers to purchase goods. This reduction in demand and product market tightness leads to a lower wholesale price. Facing diminished demand, producers sell a smaller fraction of their productive capacity to retailers, which results in decreased output. Consequently, matching costs and spare capacity (or, equivalently, unemployment) increase.

Recall from our discussion in Section 3.4 that the aggregate supply curve becomes steeper when the increase in product market tightness during the supply chain disruption is sufficiently

[39] Proposition 6 also shows that during the supply chain disruption, the responses of product market tightness and wholesale price are more pronounced, while the responses of matching cost and spare capacity (or, equivalently, unemployment) are less pronounced.

large, as described in Equation (30). This steepening occurs because the probability of producers engaging in trade becomes less sensitive to price changes when the market is already tight. In such scenarios, the number of matches is constrained by the shorter side, namely, the number of unmatched producers. As a result, the supply of goods becomes less responsive to price changes during the supply chain disruption. Consequently, a contractionary monetary policy shock significantly reduces inflation with only a relatively modest decrease in output.

5.2. Empirical Validation

We test our theoretical prediction for the state-dependence of monetary policy by developing a structural TVAR model – building on Chen and Lee (1995) – that allows for endogenous variations in the parameters based on the estimated threshold of our ACR index. The reduced-form TVAR model is:

$$\boldsymbol{y}_t = I_t \left[\sum_{l=1}^{L} \boldsymbol{B}'_{\mathbb{D},l} \boldsymbol{y}_{t-l} + \boldsymbol{C}'_{\mathbb{D}} \boldsymbol{\omega}_t + \boldsymbol{\Sigma}_{\mathbb{D}}^{1/2} \boldsymbol{\varepsilon}_t \right] + (1 - I_t) \left[\sum_{l=1}^{L} \boldsymbol{B}'_{\mathbb{U},l} \boldsymbol{y}_{t-l} + \boldsymbol{C}'_{\mathbb{U}} \boldsymbol{\omega}_t + \boldsymbol{\Sigma}_{\mathbb{U}}^{1/2} \boldsymbol{\varepsilon}_t \right], \tag{31}$$

where $1 \leq t \leq T$, $\boldsymbol{y}_t$ is an $n \times 1$ vector of endogenous variables, $\boldsymbol{\omega}_t = [1, t]'$ is a 2×1 vector of a constant and a linear trend, $\boldsymbol{\varepsilon}_t$ is an $n \times 1$ vector of structural shocks, $\boldsymbol{B}_{\mathbb{D},l}$ and $\boldsymbol{B}_{\mathbb{U},l}$ are two $n \times n$ matrices of coefficients for the lagged endogenous variables $\boldsymbol{y}_{t-l}$, $\boldsymbol{C}_{\mathbb{D}}$ and $\boldsymbol{C}_{\mathbb{U}}$ are two $2 \times n$ matrices of coefficients for the constant and linear trend, $\boldsymbol{\Sigma}_{\mathbb{D}}$ and $\boldsymbol{\Sigma}_{\mathbb{U}}$ are the covariance matrices, L is the lag length, and T is the sample size (we allow the covariance matrix to be regime-specific). The vector $\boldsymbol{\varepsilon}_t$, conditional on past information and the initial conditions $\boldsymbol{y}_0, \ldots, \boldsymbol{y}_{1-L}$, is Gaussian with mean zero and covariance matrix $\mathbf{1}_{n \times n}$, i.e., an $n \times n$ identity matrix. Switches between the two regimes – i.e., supply chain disrupted ($\mathbb{D}$) vs. undisrupted ($\mathbb{U}$) – are governed by the indicator variable $I_t \in \{0, 1\}$, which is equal to one if the ACR index in period $t-1$, ACR_{t-1}, is above the threshold $\overline{ACR}$, and equal to zero otherwise:[40]

$$I_t = \begin{cases} 1, & \text{if } ACR_{t-1} > \overline{ACR}; \\ 0, & \text{if } ACR_{t-1} \leq \overline{ACR}. \end{cases} \tag{32}$$

Under the Normal-Inverse-Wishart conjugate prior for the TVAR parameters and conditional on the value of the threshold $\overline{ACR}$, the posterior distribution of the TVAR parameter vector is

[40] In principle, we could have different threshold levels, but two regimes are sufficient to document the argument we are making.

a conditional Normal-Inverse-Wishart distribution, and we use the Gibbs sampler to draw from the distribution. We use a Metropolis-Hastings algorithm to obtain the posterior distribution of the threshold $\overline{ACR}$ conditional on the TVAR parameters, similar to Chen and Lee (1995), Lopes and Salazar (2006), and Pizzinelli et al. (2020). Appendix G.1 provides the details on the Normal-Inverse-Wishart prior.

To retain comparability with our previous empirical results, we include the same variables used in our SVAR model in Section 4, with the addition of the federal funds rate to reflect changes in the stance of U.S. monetary policy. For consistency, we also retain the same sampling period from January 2017 to September 2023.[41]

To identify the contractionary monetary policy shock, we follow the theoretical prediction presented in Proposition 6 and impose the following standard restriction on the IRFs:

Restriction 4. ***A contractionary monetary policy shock*** *leads to a negative response of real GDP, PCE goods price, retail market tightness, and import price, as well as to a positive response of unemployment and the federal funds rate at* $k = 1$*. The ACR does not respond at* $k = 1$.[42]

We compute the identified set of IRFs using the Bayesian approach similar to that in Pizzinelli et al. (2020) and Bratsiotis and Theodoridis (2022).[43] We use one lag in the baseline estimation and select the one-month lag of the ACR index as the variable that determines the state I_t.[44]

Figure 15 plots the IRFs to a contractionary monetary policy shock for both the supply chain disrupted (black) and undisrupted (red) regimes, reporting both the point-wise posterior medians (solid lines) and the 68% equal-tailed point-wise posterior probability bands (shaded area and dotted lines) from horizon $k = 0$ up to horizon $k = 12$ (i.e., four quarters). The figure shows significant differences in the responses of the endogenous variables to the contractionary monetary

[41] All the series have been seasonally adjusted, except the federal funds rate. Real GDP, PCE goods price, retail market tightness, and import price enter the TVAR in log percent, whereas the federal funds rate, unemployment, and the ACR index enter the TVAR in percent.

[42] Restriction 4 enriches Restriction 1, which is intended for the identification of an adverse shock to aggregate demand, by including the positive response of the federal funds rate on impact, which is the main instrument to control monetary policy.

[43] To implement the sign and zero restrictions on the IRFs, we use the penalty function approach (PFA) developed in Uhlig (2005) and Mountford and Uhlig (2009). The PFA consists of using a loss function to find an orthogonal matrix that satisfies the zero restrictions and that satisfies or comes close to satisfying the sign restrictions. Appendix G.2 provides the details on the PFA.

[44] Appendix G.3 plots the posterior distribution of the threshold $\overline{ACR}$, together with the time series of the identified regimes using the median of the posterior $\overline{ACR}$.

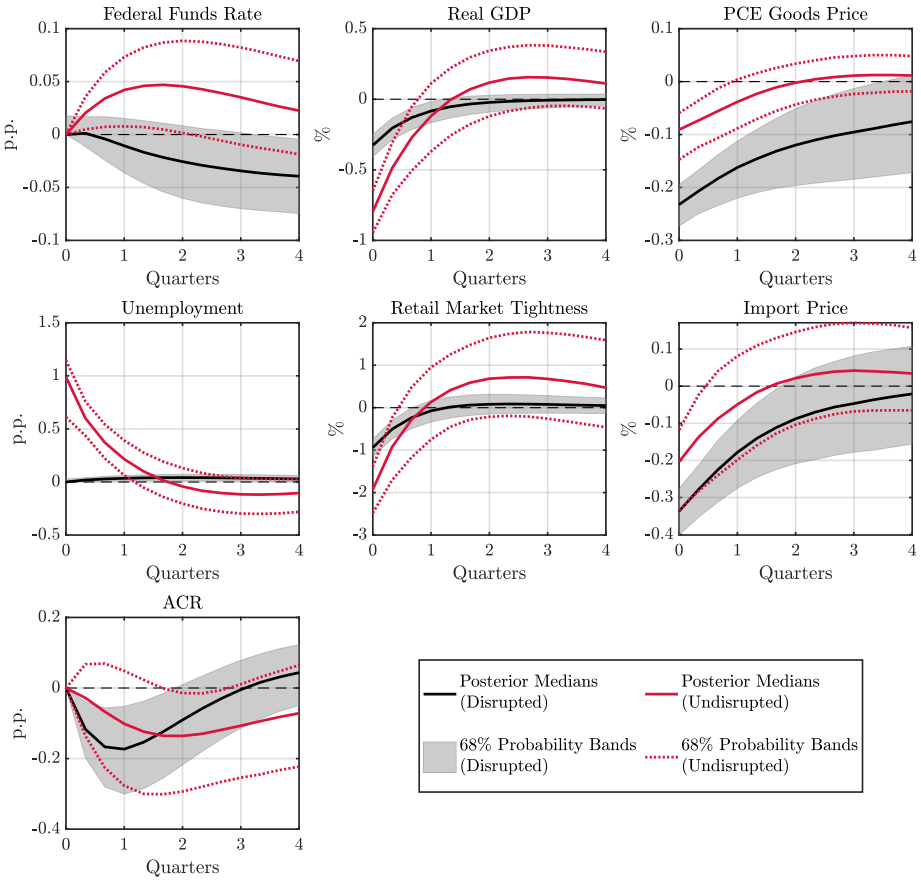

Figure 15: State-Dependent Effects of a Contractionary Monetary Policy Shock: Empirical Validation

Notes. The figure shows the IRFs to a one standard deviation contractionary monetary policy shock identified using Restriction 4 for both the supply chain disrupted and undisrupted regimes. The solid black (solid red) line shows the point-wise posterior medians, and the shaded black area (dotted red lines) depicts the 68% equal-tailed point-wise posterior probability bands for the supply chain disrupted (undisrupted) regime. The figure is based on 10,000 independent draws from the posterior.

policy shock between the two regimes. In accordance with Proposition 6, the PCE goods price and import price are more responsive. At the same time, real GDP and unemployment are less responsive in the regime where the supply chain is disrupted, and the differences in the responses are statistically significant. The responses of the federal funds rate in the two regimes also align with the observed patterns for prices and output, as the federal funds rate remains elevated throughout the horizons in the undisrupted regime while dipping below zero in the disrupted regime. The responses of retail market tightness and the ACR index between the two regimes, however, cannot be disentangled from each other.

Appendix H shows that our results hold across several variations to the benchmark model: (i) using the Wu-Xia shadow federal funds rate (Wu and Xia, 2016) to reflect the stance of U.S.

monetary policy; (ii) dropping the zero restriction imposed on the on-impact response of the ACR index; (iii) employing different lag structures; and (iv) adopting a looser prior (i.e., $\lambda = 0.5$ instead of 0.25; see Appendix G.1 for details on the tightness of the prior). Appendix I also shows that our results continue to hold when we use local projections with interaction terms, as in Ramey and Zubairy (2018), Ghassibe and Zanetti (2022), and Arias et al. (2023), to estimate the state-dependent effects of a contractionary monetary policy shock.

6. Conclusion

Our study constructs the first index of global supply chain disruptions using data from the AIS whose records have been publicly available since 2017. We quantify supply chain disruptions by developing a novel spatial clustering algorithm to estimate congestion in 50 major ports around the world. This algorithm identifies port zones and distinguishes between berth and anchorage areas within ports of different geographical morphologies, utilizing the precise locations, speeds, and headings of container ships. By aggregating congestion rates across ports, we build the first high-frequency index of the ACR worldwide.

We develop a new theoretical framework that includes separate production and retailing processes, search frictions in the exchange between producers and retailers, and transportation costs. The model simultaneously generates spare capacity for producers and a scarcity of supply for retailers, leading to sharp price increases and heightened search frictions that curtail output in response to disruptions to the supply chain. Our framework demonstrates that disturbances to the supply chain reduce output and increase prices, as in standard models, *and importantly*, they also increase the spare productive capacity. The co-movements of spare productive capacity, prices, and output allow us to uniquely identify supply chain shocks and study their causal effects on macroeconomic outcomes through an SVAR model with sign and zero restrictions derived from our theory. The empirical model establishes that supply chain shocks lead to an immediate, large increase in prices and a simultaneous detrimental effect on real GDP and unemployment.

We show, both theoretically and empirically, that monetary policy exerts a stronger influence on inflation, albeit with a diminished effect on output, amid supply chain disruptions. Thus, disruptions to the supply chain enhance the effectiveness of contractionary monetary policy in taming inflation while simultaneously reducing the sensitivity of output to the policy.

Our study opens several important avenues for future research. First, our new index reveals significant heterogeneity in the congestion of ports around the world. It would be interesting to study whether the spillovers between ports are primarily driven by geographical proximity or the production synergies that Fernández-Villaverde et al. (2021, 2023, 2024) find critical for the matching between producers and retailers. The presence of heterogeneity raises the possibility of reducing congestion from supply chain disturbances by strategically re-organizing the location of producers and retailers across ports in accordance with their production synergies. Second, our results show that spare productive capacity is central to the ramifications of supply chain disturbances in the economy. Thus, enriching the analysis by endogenizing the adjustment of spare capacity and studying its persistence might be important.[45] Third, it would be worthwhile to consider input-output networks and explore the role of spare capacity in the transmission of supply chain disruptions across firms in the network. The structure of the production network could potentially magnify or dampen the disturbances to the supply chain, which may trigger endogenous changes in the structure of the network, as documented in Ghassibe (2023). Fourth, the incorporation of predictive analytics into our spatial clustering algorithm will enable the algorithm to anticipate supply chain disruptions by identifying changes and systematic patterns in the shipments using real-time positions, speeds, and weights of container ships. The enriched algorithm could prove a powerful tool to design preemptive policy actions to offset or minimize the disruptions to the supply chain. We plan to pursue some of these extensions in our future work.

[45]Seminal studies by Ramey (1989), Burnside et al. (1995), and Basu (1996) suggest an important role for inventories and spare capacity in business cycle fluctuations.

References

Acharya, V. V., Crosignani, M., Eisert, T., and Eufinger, C. (2023). How Do Supply Shocks to Inflation Generalize? Evidence From the Pandemic Era in Europe. *NBER Working Paper 31790*.

Alessandria, G., Khan, S. Y., Khederlarian, A., Mix, C., and Ruhl, K. J. (2023). The Aggregate Effects of Global and Local Supply Chain Disruptions: 2020–2022. *Journal of International Economics*, page 103788.

Allen, T. and Arkolakis, C. (2014). Trade and the Topography of the Spatial Economy. *Quarterly Journal of Economics*, 129(3):1085–1140.

Antràs, P. (2023). An 'Austrian' Model of Global Value Chains. *NBER Working Paper 30901*.

Arias, J. E., Caldara, D., and Rubio-Ramírez, J. F. (2019). The Systematic Component of Monetary Policy in SVARs: An Agnostic Identification Procedure. *Journal of Monetary Economics*, 101:1–13.

Arias, J. E., Fernández-Villaverde, J., Rubio-Ramírez, J. F., and Shin, M. (2023). The Causal Effects of Lockdown Policies on Health and Macroeconomic Outcomes. *American Economic Journal: Macroeconomics*, 15(3):287–319.

Arias, J. E., Rubio-Ramírez, J. F., and Waggoner, D. F. (2018). Inference Based on Structural Vector Autoregressions Identified With Sign and Zero Restrictions: Theory and Applications. *Econometrica*, 86:685–720.

Attinasi, M. G., Balatti, M., Mancini, M., and Metelli, L. (2021). Supply Chain Disruptions and the Effects on the Global Economy. *ECB Economic Bulletin Issue 8*.

Bai, X. and Li, Y. (2022). The Congestion Effect of Oil Transportation and Its Trade Implications. *Working Paper*.

Bai, X., Ma, Z., Hou, Y., Li, Y., and Yang, D. (2023). A Data-Driven Iterative Multi-Attribute Clustering Algorithm and Its Application in Port Congestion Estimation. *IEEE Transactions on Intelligent Transportation Systems*, 24:12026–12037.

Barro, R. J. and Grossman, H. I. (1971). A General Disequilibrium Model of Income and Employment. *American Economic Review*, 61(1):82–93.

Basu, S. (1996). Procyclical Productivity: Increasing Returns or Cyclical Utilization? *Quarterly Journal of Economics*, 111(3):719–751.

Bekaert, G., Engstrom, E., and Ermolov, A. (2020). Aggregate Demand and Aggregate Supply Effects of COVID-19: A Real-Time Analysis. *Finance and Economic Discussion Series 2020-049*.

Benigno, P. and Eggertsson, G. B. (2023). It's Baaack: The Surge in Inflation in the 2020s and the Return of the Non-Linear Phillips Curve. *NBER Working Paper 31197*.

Benigno, P. and Ricci, L. A. (2011). The Inflation-Output Trade-off With Downward Wage Rigidities. *American Economic Review*, 101(4):1436–66.

Bernanke, B. S. and Mihov, I. (1998). Measuring Monetary Policy. *Quarterly Journal of Economics*, 113:869–902.

Blanchard, O. J. and Bernanke, B. S. (2023). What Caused the US Pandemic-Era Inflation? *NBER Working Paper 31417*.

Brancaccio, G., Kalouptsidi, M., and Papageorgiou, T. (2020). Geography, Transportation, and Endogenous Trade Costs. *Econometrica*, 88(2):657–691.

Brancaccio, G., Kalouptsidi, M., Papageorgiou, T., and Rosaia, N. (2023). Search Frictions and Efficiency in Decentralized Transport Markets. *Quarterly Journal of Economics*, pages 2451–2503.

Bratsiotis, G. J. and Theodoridis, K. (2022). Precautionary Liquidity Shocks, Excess Reserves and Business Cycles. *Journal of International Financial Markets, Institutions and Money*, 77:101518.

Brinca, P., Duarte, J. B., and e Castro, M. F. (2021). Measuring Labor Supply and Demand Shocks During COVID-19. *European Economic Review*, 139:103901.

Burnside, C., Eichenbaum, M., and Rebelo, S. (1995). Capital Utilization and Returns to Scale. *NBER Macroeconomics Annual*, 10:67–110.

Chen, C. W. and Lee, J. C. (1995). Bayesian Inference of Threshold Autoregressive Models. *Journal of Time Series Analysis*, 16:483–492.

Chow, G. C. and Lin, A.-l. (1971). Best Linear Unbiased Interpolation, Distribution, and Extrapolation of Time Series by Related Series. *Review of Economics and Statistics*, 53:372–375.

Christiano, L. J., Eichenbaum, M., and Evans, C. L. (1999). Chapter 2 Monetary Policy Shocks: What Have We Learned and to What End? In *Handbook of Macroeconomics*, volume 1, pages 65–148. Elsevier.

Comín, D. A., Johnson, R. C., and Jones, C. J. (2023). Supply Chain Constraints and Inflation. *NBER Working Paper 31179*.

Costinot, A., Vogel, J., and Wang, S. (2013). An Elementary Theory of Global Supply Chains. *Review of Economic Studies*, 80:109–144.

Coşar, A. K. and Demir, B. (2018). Shipping Inside the Box: Containerization and Trade. *Journal of International Economics*, 114:331–345.

Dempsey, H. (2022). Is There an End in Sight to Supply Chain Disruption? Financial Times. Available at: https://www.ft.com/content/21242e3b-298b-4a6f-a35f-32fdde905952 (Accessed: January 9, 2022).

den Haan, W. J., Ramey, G., and Haefke, C. (2005). Turbulence and Unemployment in a Job Matching Model. *Journal of the European Economic Association*, 3:1360–1385.

Dunn, J. and Leibovici, F. (2023). Navigating the Waves of Global Shipping: Drivers and Aggregate Implications. *Federal Reserve Bank of St. Louis Working Paper 2023-002*.

Eichenbaum, M., Rebelo, S., and Wong, A. (2022). State-Dependent Effects of Monetary Policy: The Refinancing Channel. *American Economic Review*, 112(3):721–61.

Fan, L., Wilson, W. W., and Dahl, B. (2012). Congestion, Port Expansion and Spatial Competition for US Container Imports. *Transportation Research Part E: Logistics and Transportation Review*, 48(6):1121–1136.

Fernández-Villaverde, J., Mandelman, F., Yu, Y., and Zanetti, F. (2021). The "Matthew Effect" and Market Concentration: Search Complementarities and Monopsony Power. *Journal of Monetary Economics*, 121:62–90.

Fernández-Villaverde, J., Mandelman, F., Yu, Y., and Zanetti, F. (2024). Search Complementarities, Aggregate Fluctuations, and Fiscal Policy. *Review of Economic Studies*. forthcoming.

Fernández-Villaverde, J., Yu, Y., and Zanetti, F. (2023). Technological Synergies, Heterogenous Firms, and Idiosyncratic Volatility. *Working Paper*.

Finck, D. and Tillmann, P. (2022). The Macroeconomic Effects of Global Supply Chain Disruptions. *BOFIT Discussion Paper 14/2022*.

Fry, R. and Pagan, A. (2011). Sign Restrictions in Structural Vector Autoregressions: A Critical Review. *Journal of Economic Literature*, 49(4):938–60.

Fuchs, S. and Wong, W. F. (2022). Multimodal Transport Networks. *Federal Reserve Bank of Atlanta Working Paper 2022-13*.

Fujita, S. (2018). Declining Labor Turnover and Turbulence. *Journal of Monetary Economics*, 99:1–19.

Ghassibe, M. (2023). Endogenous Production Networks and Non-Linear Monetary Transmission. *CREi Working Paper Series*.

Ghassibe, M. and Zanetti, F. (2022). State Dependence of Fiscal Multipliers: The Source of Fluctuations Matters. *Journal of Monetary Economics*, 132:1–23.

Giacomini, R. and Kitagawa, T. (2021). Robust Bayesian Inference for Set-Identified Models. *Econometrica*, 89:1519–1556.

Goda, G. S. and Soltas, E. J. (2022). The Impacts of COVID-19 Illnesses on Workers. *NBER Working Paper 30435*.

Gordon, M. V. and Clark, T. E. (2023). The Impacts of Supply Chain Disruptions on Inflation. *Federal Reserve Bank of Cleveland Economic Commentary 2023-08*.

Grimes, C. and Edgecliffe-Johnson, A. (2021). The Supply Chain Crisis and US Ports: 'Disruption on Top of Disruption'. Financial Times. Available at: https://www.ft.com/content/aa24d82e-16c7-4e3e-868e-42bd32f593be (Accessed: October 14, 2021).

Hall, R. E. (2005). Employment Fluctuations With Equilibrium Wage Stickiness. *American Economic Review*, 95(1):50–65.

Harding, M., Lindé, J., and Trabandt, M. (2023). Understanding Post-COVID Inflation Dynamics. *Journal of Monetary Economics*.

Heiland, I., Moxnes, A., Ulltveit-Moe, K. H., and Zi, Y. (2022). Trade From Space: Shipping Networks and the Global Implications of Local Shocks. *CEPR Discussion Paper 14193*.

Hobijn, B. and Şahin, A. (2022). Missing Workers and Missing Jobs Since the Pandemic. *NBER Working Paper 30717*.

Howitt, P. and McAfee, R. P. (1987). Costly Search and Recruiting. *International Economic Review*, 28(1):89–107.

Ikeda, D., Li, S., Mavroeidis, S., and Zanetti, F. (2024). Testing the Effectiveness of Unconventional Monetary Policy in Japan and the United States. *American Economic Journal: Macroeconomics*. forthcoming.

Karimi-Mamaghan, M., Mohammadi, M., Pirayesh, A., Karimi-Mamaghan, A. M., and Irani, H. (2020). Hub-And-Spoke Network Design Under Congestion: A Learning Based Metaheuristic. *Transportation Research Part E: Logistics and Transportation Review*, 142:102069.

Kasahara, H. and Lapham, B. (2013). Productivity and the Decision to Import and Export: Theory and Evidence. *Journal of International Economics*, 89:297–316.

Keynes, J. M. (1940). *How to Pay for the War*. Macmillan and Co.

Kim, S.-J. and Shin, H. S. (2023). Theory of Supply Chains: A Working Capital Approach. *BIS Working Paper 1070*.

Lane, P. R. (2022). Bottlenecks and Monetary Policy. ECB Blog. Available at: https://www.ecb.europa.eu/press/blog/date/2022/html/ecb.blog220210~1590dd90d6.en.html (Accessed: February 10, 2022).

Lee, D., Park, J., , and Shin, Y. (2023). Where Are the Workers? From Great Resignation to Quiet Quitting. *NBER Working Paper 30833*.

Li, Y., Bai, X., Wang, Q., and Ma, Z. (2022). A Big Data Approach to Cargo Type Prediction and Its Implications for Oil Trade Estimation. *Transportation Research Part E: Logistics and Transportation Review*, 165:102831.

Liu, P., Theodoridis, K., Mumtaz, H., and Zanetti, F. (2019). Changing Macroeconomic Dynamics at the Zero Lower Bound. *Journal of Business & Economic Statistics*, 37(3):391–404.

Lopes, H. F. and Salazar, E. (2006). Bayesian Model Uncertainty in Smooth Transition Autoregressions. *Journal of Time Series Analysis*, 27:99–117.

Mathieu, E., Ritchie, H., Rodés-Guirao, L., Appel, C., Giattino, C., Hasell, J., Macdonald, B., Dattani, S., Beltekian, D., Ortiz-Ospina, E., and Roser, M. (2020). Coronavirus Pandemic (COVID-19). Our World in Data. Available at: https://ourworldindata.org/coronavirus (Accessed: August 17, 2022).

Michaillat, P. and Saez, E. (2015). Aggregate Demand, Idle Time, and Unemployment. *Quarterly Journal of Economics*, 130:507–569.

Michaillat, P. and Saez, E. (2022). An Economical Business-Cycle Model. *Oxford Economic Papers*, 74:382–411.

Morison, S. E. (1954). *The Atlantic Battle Won: May 1943-May 1945*. Little, Brown and Company.

Mortensen, D. T. and Pissarides, C. A. (1994). Job creation and job destruction in the theory of unemployment. *Review of Economic Studies*, 61(3):397–415.

Mountford, A. and Uhlig, H. (2009). What Are the Effects of Fiscal Policy Shocks? *Journal of Applied Econometrics*, 24:960–992.

Mumtaz, H. and Zanetti, F. (2012). Neutral Technology Shocks and the Dynamics of Labor Input: Results From an Agnostic Identification. *International Economic Review*, 53:235–254.

Mumtaz, H. and Zanetti, F. (2015). Labor Market Dynamics: A Time-Varying Analysis. *Oxford Bulletin of Economics and Statistics*, 77:319–338.

Notteboom, T., Pallis, A., and Rodrigue, J.-P. (2022). *Port Economics, Management and Policy*. Routledge, 1 edition.

Notteboom, T., Pallis, T., and Rodrigue, J. (2021). Disruptions and Resilience in Global Container Shipping and Ports: The COVID-19 Pandemic Versus the 2008–2009 Financial Crisis. *Maritime Economics & Logistics*, 23:179–210.

OECD and EUIPO (2021). *Misuse of Containerized Maritime Shipping in the Global Trade of Counterfeits*. OECD.

Peersman, G. (2005). What Caused the Early Millennium Slowdown? Evidence Based on Vector Autoregressions. *Journal of Applied Econometrics*, 20(2):185–207.

Pizzinelli, C., Theodoridis, K., and Zanetti, F. (2020). State Dependence in Labor Market Fluctuations. *International Economic Review*, 61:1027–1072.

Ramey, V. A. (1989). Inventories as Factors of Production and Economic Fluctuations. *American Economic Review*, 79(3):338–354.

Ramey, V. A. and Zubairy, S. (2018). Government Spending Multipliers in Good Times and in Bad: Evidence From US Historical Data. *Journal of Political Economy*, 126:850–901.

Ramondo, N. and Rodríguez-Clare, A. (2013). Trade, Multinational Production, and the Gains From Openness. *Journal of Political Economy*, 121:273–322.

Rubio-Ramírez, J. F., Waggoner, D. F., and Zha, T. (2010). Structural Vector Autoregressions: Theory of Identification and Algorithms for Inference. *Review of Economic Studies*, 77:665–696.

Sea-Intelligence (2021). 20%–25% Weekly Capacity Blanked on Asia-NAWC. Sea-Intelligence. Available at: https://sea-intelligence.com/press-room/111-20-25-weekly-capacity-blanked-on-asia-nawc (Accessed: December 15, 2021).

Smets, F. and Wouters, R. (2007). Shocks and Frictions in US Business Cycles: A Bayesian DSGE Approach. *American Economic Review*, 97(3):586–606.

Smirnyagin, V. and Tsyvinski, A. (2022). Macroeconomic and Asset Pricing Effects of Supply Chain Disasters. *NBER Working Paper 30503*.

Talley, W. K. and Ng, M. W. (2016). Port Multi-Service Congestion. *Transportation Research Part E: Logistics and Transportation Review*, 94:66–70.

The White House (2021). Fact Sheet: Biden Administration Efforts to Address Bottlenecks at Ports of Los Angeles and Long Beach: Moving Goods from Ship to Shelf. The White House. Available at: https://www.whitehouse.gov/briefing-room/statements-releases/2021/10/13/fact-sheet-biden-administration-efforts-to-address-bottlenecks-at-ports-of-los-angeles-and-long-beach-moving-goods-from-ship-to-shelf/ (Accessed: October 13, 2021).

The World Bank (2022). *Global Economic Prospects, June 2022*. Washington, DC: World Bank.

Thomas, C. and Zanetti, F. (2009). Labor Market Reform and Price Stability: An Application to the Euro Area. *Journal of Monetary Economics*, 56(6):885–899.

Transportation Research Board Executive Committee (2006). *Critical Issues in Transportation*. The National Academies Press, Washington, DC.

Uhlig, H. (2005). What Are the Effects of Monetary Policy on Output? Results From an Agnostic Identification Procedure. *Journal of Monetary Economics*, 52:381–419.

UNCTAD (2019). Review of Maritime Transport 2019. UNCTAD. Available at: https://unctad.org/webflyer/review-maritime-transport-2019 (Accessed: November 1, 2021).

Wu, J. C. and Xia, F. D. (2016). Measuring the Macroeconomic Impact of Monetary Policy at the Zero Lower Bound. *Journal of Money, Credit and Banking*, 48(2-3):253–291.

Online Appendices

The Causal Effects of Global Supply Chain Disruptions on Macroeconomic Outcomes: Evidence and Theory

Xiwen Bai, Jesús Fernández-Villaverde, Yiliang Li, Francesco Zanetti

Contents

A. Background on the Containerized Shipping Industry

In the appendix, we provide some further background on the containerized shipping industry.

Port congestion and speed adjustment. As mentioned in the main text, the shipping industry generally adopts a "hurry up and wait" practice regarding the port call process (Du et al., 2015). For instance, a vessel departs the loading port at full speed, aiming to meet the original requested time of arrival at the pilot boarding place (RTA PBP) scheduled for day 14. However, if three days into the voyage, the port encounters delays altering the RTA PBP to day 17, the ship may not receive this updated information in time to adjust its speed. Even if the ship does receive the forewarnings, it often chooses not to alter its speed, as such a speed adjustment might violate contractual obligations. Consequently, even if a port is experiencing congestion, vessels will still "hurry" to arrive and then "wait" at anchorage.

Oil price, speed adjustment, and congestion. Fuel costs account for approximately 50% to 60% of a vessel's operating costs for a liner shipping company (Notteboom, 2006). Moreover, the fuel consumption of a vessel is roughly a cubic function of the sailing speed (Li et al., 2016). Hence, vessel sailing speed significantly impacts operating costs. In principle, shipping companies would dynamically adjust sailing speeds based on current bunker oil prices. However, based on AIS data, researchers have found that this relationship between speed and oil prices is not apparent in practice (Adland and Jia, 2016). Furthermore, by regressing the monthly average speed of container ships on the West Texas Intermediate (WTI) crude oil futures price after taking the natural logarithm of both series, we find that the two series are statistically uncorrelated, with an estimated coefficient of -0.0035 and a p-value of 0.619. The corresponding R^2 stands at 0.0031. This has been attributed to the rigidity of contractual structures and the lack of coordination between ports and vessels or, simply, that ships are optimized for operating at one particular speed (with changes in oil prices affecting the design of the next generation of ships, e.g., fuel-efficient cargo vessels). Consequently, the observed impact of oil prices on vessel speed, and thus on port congestion, is limited.

Idle ships. According to the Clarksons Shipping Intelligence Network, idle container ships are defined as vessels not recorded with an average speed greater than one knot for seven days or more, not identified as subject to another status (e.g., laid-up, under repair, in storage, or similar), and not subsequently recorded with an average speed greater than one knot for two or

more consecutive days or not having moved more than 20 km.

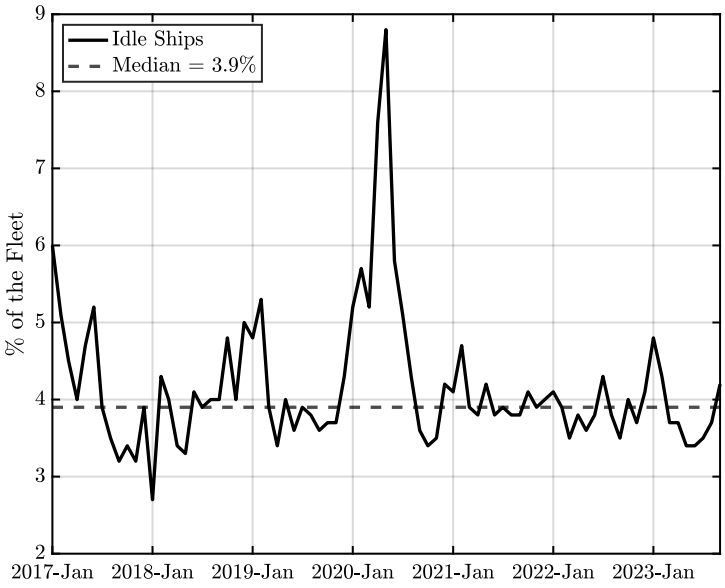

Figure A.1: Idle Ships

Notes. Proportion of container ships with an idle status in the global fleet. Idle status applies to ships not recorded with an average speed greater than one knot for seven days or more, not identified as subject to another status (e.g., laid-up, under repair, in storage, or similar), and either not subsequently recorded with an average speed greater than one knot for two or more consecutive days or not having moved more than 20 km.

Figure A.1 plots the series of idle ships expressed as a percentage of the entire global fleet. This proportion declined from 6% to approximately 3% during 2017, then hovered around 4% through 2018–2019 before soaring to slightly below 9% at the onset of the COVID-19 pandemic in early 2020. Subsequently, it dived back down and stabilized at 4% thereafter. As illustrated in Section 2.5, the spike in the proportion of idle ships at the onset of the pandemic is closely related to the active capacity management by shipping companies, which set aside capacity in response to the unprecedented declines in consumer and business demand. To minimize the effect of such an abrupt change in the occurrence of idling on the estimation of port congestion, we exclude idle ships in the construction of the congestion indices (see Appendix B.1.1).

B. A Density-Based Spatial Clustering Algorithm

In this appendix, we provide the technical details of our density-based spatial clustering algorithm, namely the iterative, multi-attribute, density-based spatial clustering of applications with noise (IMA-DBSCAN). Most of the technical details provided in this appendix can also be found in

the companion paper, Bai et al. (2023).

This algorithm is used to estimate port congestion for the top 50 container ports worldwide.[1] In subsequent sections, we first delve into the methodology underpinning our algorithm. We then present an illustrative case where we apply the algorithm to the Port of Ningbo-Zhoushan, demonstrating its capability to identify both anchorage and berth areas of a port, where other methods fall short. Lastly, we present the weekly congestion indices – namely, the ACR and the ACT – to highlight that our estimation of port congestion is robust to using different time frequencies.

B.1. Methodology

As depicted in Figure B.1, the proposed IMA-DBSCAN algorithm has several distinct features. Foremost among these is its two-tiered iterative structure. At the first level, we extract the trajectory of each container ship at each of our 50 ports from the AIS data. For each ship, a traditional DBSCAN (Ester et al., 1996) is employed to filter out noise and cluster all its mooring points. While this level can pinpoint mooring areas, it does not adequately differentiate between anchorage and berth areas of a port. The second level addresses this limitation. Here, we apply a spatial-temporal-DBSCAN (ST-DBSCAN; see Birant and Kut, 2007) to the clustering. During this phase, we employ an iterative method to determine a generalized and optimal parameter setting for the clustering algorithm. Another hallmark of IMA-DBSCAN is its integration of multiple attributes at the second level. Beyond spatial data (like coordinates), we also weave in non-spatial information (such as headings and timestamps) to enhance clustering accuracy. Next, we elaborate on the specifics of each level of IMA-DBSCAN.

B.1.1. The First Level – Data Pre-Processing

While AIS data provide detailed information on the positions of each ship, directly clustering these positions to determine the anchorage and berth areas of a port presents several challenges. First, even if we restrict the data to a specific port area within a certain time frame, the sheer volume of records means that inputting them directly into DBSCAN would result in extended processing times. Second, a high incidence of incorrect AIS signal assignments could lead to

[1] See https://www.worldshipping.org/top-50-ports (accessed June 15, 2022) for the full list of ports.

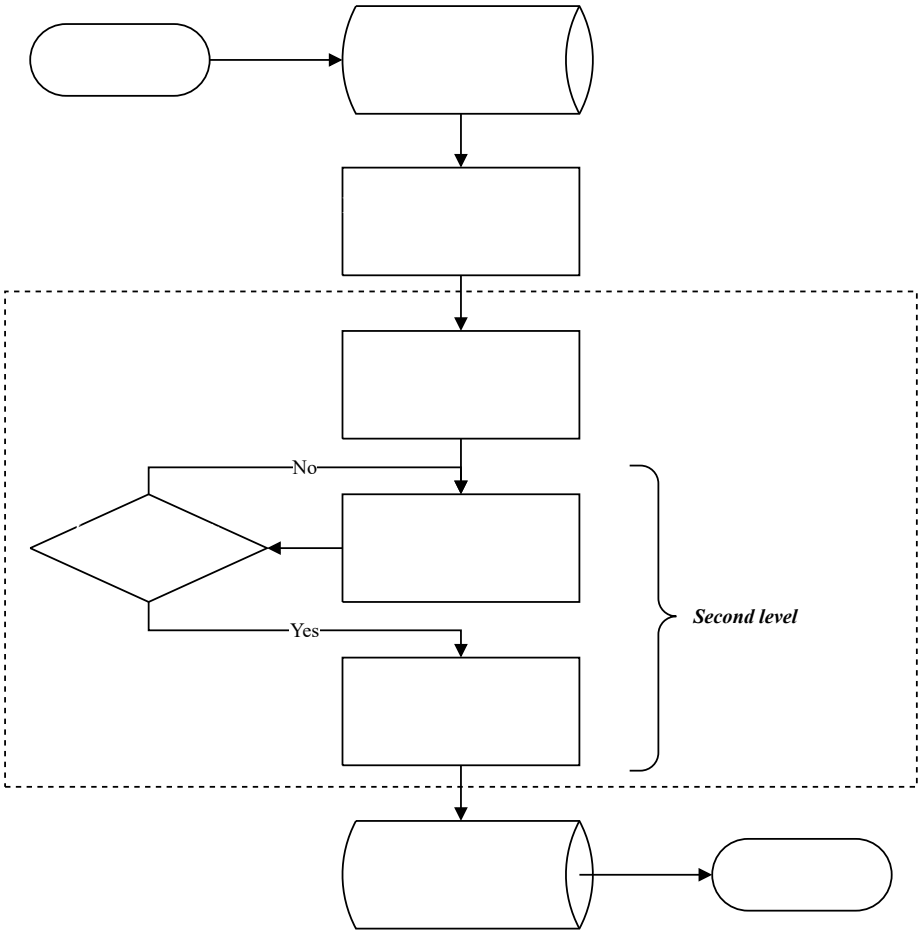

Figure B.1: Methodology Framework of IMA-DBSCAN

inaccurate clustering outcomes, such as identifying a cluster that is not an actual berth or one that covers an unusually large geographical area. Third, if a ship stays in a port area for an extended period, the dense AIS data could cause DBSCAN to mistakenly identify it as a cluster. Given these challenges, we must preprocess the AIS data.

In the first level of IMA-DBSCAN, we begin by filtering the AIS data for each ship in the port area, focusing on records indicating speeds of less than one knot. Such positions suggest that a ship is either berthed, anchored, or in an unusual situation (e.g., idle, laid-up, under repair, in storage, or similar). We then tally these positions; if their number falls outside an acceptable range (e.g., less than 100 or more than 100,000), we deem the ship's data to be abnormal and exclude it from further analysis. Since a ship might dock at a port multiple times, we establish a period, Δt (e.g., 12 hours), as the cut-off between two consecutive arrivals. If the gap between two arrivals exceeds Δt, we treat them as separate port calls. To streamline the data while maintaining consistency, we retain only the first data point for each hour. For every port call

of a ship, its positions are clustered using the traditional DBSCAN with parameters Eps and $MinPts$. We choose an Eps value small enough to identify the ship's mooring areas and an appropriate $MinPts$ value to ensure transient stops are classified as noise. At this stage, the AIS data pre-processing is complete. The refined samples are then used to identify the anchorage and berth areas of a port in the second level of IMA-DBSCAN. For reference, the pseudo-code for the first level of IMA-DBSCAN is detailed in Algorithm 1.

B.1.2. The Second Level – Multiple Attributes and Iteration

Information on headings. As highlighted in the main text, AIS data integrate both spatial (i.e., geographical coordinates) and non-spatial (i.e., headings) information. In Figure 1 in the main text, we illustrate the positions of a ship in a port alongside its headings. We observe that the headings of a ship at a berth are either aligned in the same direction or are exact opposites. In contrast, headings in an anchorage area appear to be random, with no discernible pattern. This observation aligns with real-world scenarios, where ships in anchorage areas often struggle to maintain consistent headings over time due to significant wind and wave variations.

Consequently, in the second level of IMA-DBSCAN, we leverage this heading information to enhance estimation accuracy.[2] Specifically, IMA-DBSCAN incorporates three parameters: $Eps1$, $Eps2$, and $MinPts$. Here, $Eps1$ denotes the maximum geographical coordinate (spatial) distance, $Eps2$ represents the maximum non-spatial distance between two headings, and $MinPts$ is the minimum number of points within the distances defined by $Eps1$ and $Eps2$. The geographical coordinate (spatial) distance, D, is calculated using the Haversine formula:

$$D\left[(x_1, x_2), (y_1, y_2)\right] = 2 \cdot R \cdot \arcsin\left[\sqrt{\sin^2\left(\frac{x_1 - y_1}{2}\right) + \cos x_1 \cos y_1 \sin^2\left(\frac{x_2 - y_2}{2}\right)}\right], \quad \text{(B.1)}$$

where the geographical coordinates are measured in radians and $R = 6,371$ is the mean radius of Earth in kilometers. On the other hand, the non-spatial distance Δh between two headings is

[2]Such non-spatial information is also useful when distinguishing between different berths (see Algorithm 2). In our initial experiment, the coordinates could only help us identify the approximate locations of anchorage and berth areas of a port, not the exact number of berths.

calculated as follows:

$$\Delta h(h_1, h_2) = \begin{cases} |h_1 - h_2|\,, & \text{if } |h_1 - h_2| \leq 180°; \\ 360° - |h_1 - h_2|\,, & \text{otherwise.} \end{cases} \tag{B.2}$$

With the two measures of distance defined above, the neighbors of a point are those with a geographical coordinate (spatial) distance less than $Eps1$ and a non-spatial distance less than $Eps2$. A core is defined as a point with a number of neighbors greater than or equal to $MinPts$. The clusters in IMA-DBSCAN consist only of these core points.

Iteration process. Given that the geographical shapes of anchorage and berth areas vary significantly across ports, the values of these three parameters in IMA-DBSCAN should ideally differ to achieve optimal estimation results. Hence, we propose an iterative method to determine these parameter values. Specifically, while we fix $Eps2$ at 1°, our method allows the values of $Eps1$ and $MinPts$ to vary between different ports. During the iteration process, we define four intermediate variables: $Dist$, m, m', and $NumC$. Here, $Dist$ represents the average distance between a point in a cluster and the center of that cluster, m denotes the number of points, and m' represents the number of noisy points, which is initialized to zero. Lastly, $NumC$ indicates the number of clusters.[3] Using these intermediate variables, $MinPts$, and $Eps1$ are:

$$Eps1 = \alpha \cdot Dist,$$
$$MinPts = \beta \cdot \frac{m - m'}{NumC}.$$

Regarding α and β, even though there is no explicit constraint on their values, they should fall within a reasonable range to ensure both the algorithm's convergence and the validity of the identification results. After evaluating the performance of IMA-DBSCAN under various parameter settings, we find that an admissible range of $0.4 \leq \alpha \leq 0.6$ and $0.06 \leq \beta \leq 0.1$ is appropriate. We also introduce an intermediate variable, $Dist_0$, which records the value of $Dist$ from the previous iteration and is initialized to zero.

Following this, we execute ST-DBSCAN iteratively. In each iteration, ST-DBSCAN operates with $Eps1$ and $MinPts$ set to their current values, and $Eps2$ set to 1°. The outputs classify each point either into a cluster or as noise. Based on these outputs, the values of the intermediate

[3]Since there are no clusters at initialization, we treat all points as if they were part of the same cluster. Additionally, if all points are classified as noise, we set $NumC = 1$.

variables, as well as those for $Eps1$ and $MinPts$, are updated. These updated values are then reapplied in ST-DBSCAN for the subsequent iteration. The entire process concludes when the difference, $Dist - Dist_0$, is less than or equal to $\Delta Dist$ (e.g., 100 m). Consequently, each point is either assigned to a cluster or labeled as noise. We then interpret the areas of clusters as berths and the areas with noisy points as anchorages.

Information on timestamps. After running ST-DBSCAN, we find that a large proportion of clusters should be merged, as they essentially represent the same berth in reality. To achieve a more accurate identification of berth areas, we merge certain clusters by taking advantage of the time information (i.e., timestamps) in the AIS data. See Figure B.2 for an illustration. More precisely, we first calculate the start and end times of each port call in each cluster. Subsequently, since only one ship can dock at a berth at any given moment, for each cluster under consideration, we identify the cluster closest to it and check whether there is any overlap in the docking times. If there is (at least) one overlap, the two clusters are considered to represent two different berths. If there is no overlap, the two clusters are merged to represent one berth.

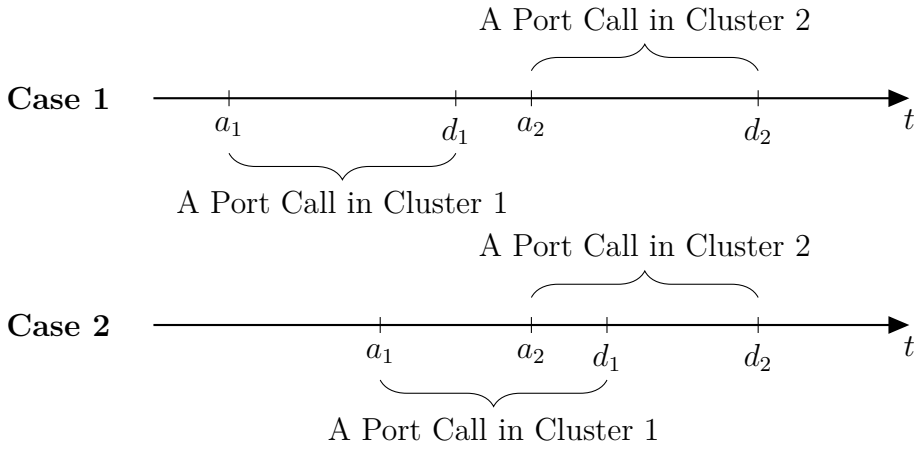

Figure B.2: Merging Clusters

Notes. The figure illustrates two scenarios and discusses the criteria for merging clusters after executing ST-DBSCAN at the second level. Here, a_1 and d_1 represent the arrival and departure times of a ship during a port call assigned to cluster 1. Similarly, a_2 and d_2 correspond to the times for a port call assigned to cluster 2, which is geographically the closest to cluster 1. In the first scenario, there is no overlap in the docking times, so clusters 1 and 2 are merged. In contrast, the second scenario shows an overlap in the docking times. As a result, clusters 1 and 2 are kept separate since two ships cannot occupy a single berth simultaneously.

Furthermore, to differentiate between anchorage areas, we perform another DBSCAN on those points classified as noise. In this process, the two parameters associated with DBSCAN, i.e., Eps' and $MinPts'$, are set according to our domain knowledge. Finally, we remove clusters with fewer

than N port calls, with N set based on our domain knowledge. For reference, the pseudo-codes for the second level of IMA-DBSCAN can be found in Algorithms 2, 3, and 4.

Lastly, in estimating port congestion for the top 50 container ports worldwide, the parameter values set for IMA-DBSCAN are provided in Table B.1.

Table B.1: Parameter Values for IMA-DBSCAN

	Parameter					
First Level	Δt	Eps	$MinPts$			
Value	12 hours	50 m	10			
Second Level	α	β	$\Delta Dist$	Eps'	$MinPts'$	N
Value	0.5	0.08	100 m	1,000 m	50	5

Algorithm 1 Level 1 IMA-DBSCAN

Inputs:

$A_l = \{a_{1,l}, \ldots, a_{n,l}\}$: the set of coordinates recorded in the AIS data for a ship l
$S_l = \{s_{1,l}, \ldots, s_{n,l}\}$: the set of speeds recorded in the AIS data for a ship l
$T_l = \{t_{1,l}, \ldots, t_{n,l}\}$: the set of timestamps recorded in the AIS data for a ship l

Outputs:

$D_l = \{d_{1,l}, \ldots, d_{m,l}\}$: the coordinates of the first observation for each hour in B_l
$H_l = \{h_{1,l}, \ldots, h_{m,l}\}$: the headings of the first observation for each hour in B_l

/ Data Pre-Processing */*
$B_l = \{b_{1,l} \ldots b_{k,l}\} \leftarrow$ the set of coordinates in A_l that indicate a speed less than 1 knot
/ Exception Identification */*
if $|B_l| < 100$ **or** $|B_l| > 100,000$ **then**
    Remove the data and stop ▷ *The ship has an abnormal port call*
else
    Continue
end if
/ DBSCAN Clustering */*
$X \leftarrow b_{1,l}$
for $i \leftarrow 2 : k$ **do**
    if $t_i - t_{i-1} \leq \Delta t$ **then**
        Append $b_{i,l}$ to X
    else
        $DBSCAN(X, Eps, MinPts)$
        $X \leftarrow \emptyset$
        Append $b_{i,l}$ to X
    end if
end for
Remove the observations labeled as noise from B_l
Keep only the first observation for each hour in B_l ▷ *Note that only m observations remain in B_l at this stage*
$D_l = \{d_{1,l}, \ldots, d_{m,l}\} \leftarrow$ the coordinates of the first observation for each hour in B_l
$H_l = \{h_{1,l}, \ldots, h_{m,l}\} \leftarrow$ the headings of the first observation for each hour in B_l

Algorithm 2 Level 2 IMA-DBSCAN

Inputs:

$\boldsymbol{D} = \{D_1, \ldots, D_L\}$: the set of coordinates for all ships after Level 1 IMA-DBSCAN
$\boldsymbol{H} = \{H_1, \ldots, H_L\}$: the set of headings for all ships after Level 1 IMA-DBSCAN
$\boldsymbol{O} = \{\boldsymbol{D}, \boldsymbol{H}\} = \{o_1, \ldots, o_M\}$: the combined set of coordinates and headings

Outputs:

C_{berth}: the set of clusters marked as berths
$C_{anchorage}$: the set of clusters marked as anchorages

/ Parameter Initialization */*
$Dist \leftarrow$ the average distance between a point in $\boldsymbol{D}$ and the center of the mass of $\boldsymbol{D}$
$m \leftarrow |\boldsymbol{D}|$
$Eps1 \leftarrow \alpha \cdot Dist$
$MinPts \leftarrow \beta \cdot m$
/ Iteration Process */*
$Dist_0 \leftarrow 0$
while $Dist - Dist_0 > \Delta Dist$ km **do**
    $ST - DBSCAN(\boldsymbol{O}, Eps1, Eps2 = 1°, MinPts)$ ▷ *See function ST-DBSCAN*
    $Dist_0 \leftarrow Dist$
    $Dist \leftarrow$ the average distance between a non-noisy point in $\boldsymbol{D}$ and the center of the mass of its assigned cluster
    $m' \leftarrow$ |noisy points in $\boldsymbol{O}$|
    $NumC \leftarrow$ |clusters in $\boldsymbol{O}$|
    $Eps1 \leftarrow \alpha \cdot Dist$
    $MinPts \leftarrow \beta \cdot (m - m') / NumC$
end while
/ Merging Clusters */*
Use the center of the mass of each cluster to calculate the distance in between
for all clusters c in $\boldsymbol{O}$ **do**
    $c' \leftarrow$ the nearest cluster less than 500 m away from c
    if the docking times of c' and c do not overlap **then**
        Replace the cluster label of c' with that of c
    end if
end for
/ Berth and Anchorage Detection */*
$C_{berth} \leftarrow$ clusters in $\boldsymbol{O}$
$C_{anchorage} \leftarrow DBSCAN$(Noisy points in $\boldsymbol{O}, Eps', MinPts'$)
/ Exception Removal */*
for all clusters c **in** C_{berth} **and** $C_{anchorage}$ **do**
    $NumP \leftarrow$ the number of port calls in cluster c
    if $NumP < N$ **then**
        Remove c
    end if
end for

Algorithm 3 ST-DBSCAN

Inputs:

$\boldsymbol{O} = \{o_1, \ldots, o_M\}$: the combined set of coordinates and headings
$Eps1$: maximum geographical coordinate (spatial) distance
$Eps2$: maximum non-spatial distance
$MinPts$: minimum number of points within the distance of $Eps1$ and $Eps2$

Outputs:

$C = \{c_1, \ldots, c_M\}$: the set of clusters in $\boldsymbol{O}$

```
/* The codes are adapted from those in Birant and Kut (2007).                    */
function ST − DBSCAN(D, Eps1, Eps2, MinPts)
    ClusterLabel = 0
    for i ← 1 : m do
        if o_i is not in a cluster then
            Y ← RetrieveNeighbors(o_i, Eps1, Eps2)        ▷ See function RetrieveNeighbors
            if |Y| < MinPts then
                Mark o_i as noise
            else                                          ▷ Construct a new cluster
                ClusterLabel ← ClusterLabel + 1
                for j ← 1 : |Y| do
                    Mark all objects in Y with current ClusterLabel
                end for
                Push(all objects in Y)
                while not IsEmpty() do
                    CurrentObj = Pop()
                    Z ← RetrieveNeighbors(CurrentObj, Eps1, Eps2)
                    if |Z| ≥ MinPts then
                        for all objects o in Z do
                            if o is not marked as noise or it is not in a cluster then
                                Mark o with current ClusterLabel
                                Push(o)
                            end if
                        end for
                    end if
                end while
            end if
        end if
    end for
    C = {c_1, ..., c_M} ← the set of clusters in O
end function
```

Algorithm 4 RetrieveNeighbors

Inputs:

o: an observation in $\boldsymbol{O}$

$Eps1$: maximum geographical coordinate (spatial) distance

$Eps2$: maximum non-spatial distance

Outputs:

$Neighbors$: the set of neighbors for o

function $RetrieveNeighbors(o, Eps1, Eps2)$
    $Neighbors \leftarrow \emptyset$
    for all observations o' **in** O **do**
        $Dist1 \leftarrow D(o, o')$ ▷ *See Equation* (B.1)
        $Dist2 \leftarrow \Delta h(o, o')$ ▷ *See Equation* (B.2)
        if $Dist1 \leq Eps1$ **and** $Dist2 \leq Eps2$ **then**
            Append o' to $Neighbors$
        end if
    end for
    return $Neighbors$
end function

B.2. Illustrative Case: Port of Ningbo-Zhoushan

To demonstrate the capability of IMA-DBSCAN in accurately identifying anchorage and berth areas of a port, which other methods might fail to achieve, we apply the algorithm to the Port of Ningbo-Zhoushan in China. We chose this specific port due to its intricate layout.[4] Figure B.3a showcases the first 50,000 AIS observations from January 2020 within the Port of Ningbo-Zhoushan.[5] The observations are represented by blue dots on the map, with each dot indicating the position of a low-speed container ship. Before applying IMA-DBSCAN to the AIS data, we mark the approximate locations of anchorages and berths using satellite images and nautical charts as benchmarks. The red polygons on the map indicate the anchorage areas, while the yellow rectangles denote the berth locations.

Figure B.3b presents the clustering results of IMA-DBSCAN for the Port of Ningbo-Zhoushan, which mirrors the map in Figure B.3a for a direct comparison between our algorithm's outcomes and the actual observations. The clusters in Figure B.3b (colored in red, yellow, blue, purple, cyan, and orange) correspond closely with the anchorage areas in Figure B.3a.[6] Additionally, in Figure B.3e, we spotlight the locations of four terminals within Ningbo-Zhoushan: Beilun, Daxie, Pukou, and Yuandong. Using satellite maps as a reference, we confirm the accuracy of these identifications; each berth in the terminals is pinpointed precisely, and the delineated areas align closely with reality.[7]

To assess the performance of IMA-DBSCAN against that of other spatial clustering algorithms, we contrast it with the outcomes from ST-DBSCAN.[8] Given that ST-DBSCAN is capable of processing spatial-temporal databases and is recognized as one of the most prominent spatial clustering algorithms in the literature, this comparison is relevant. Figure B.3c illustrates the results derived from ST-DBSCAN, underscoring its lesser precision in comparison to

[4]We also apply the same exercise to the Ports of Singapore, Rotterdam, Los Angeles and Long Beach. We confirm that our IMA-DBSCAN algorithm delivers more accurate identification results than the traditional ST-DBSCAN algorithm across all these ports. The comparison results are available upon request.

[5]This example focuses on a one-month snapshot. It is reasonable to assume that the identification results would be indicative of anchorage and berth areas in subsequent months, given that we do not expect significant short-term changes in the port areas. In real-world applications of IMA-DBSCAN, periodic identification can be conducted to monitor potential changes in port anchorages and berths.

[6]For clarity, we also display the convex hulls formed by these clusters in Figure B.3d.

[7]Furthermore, some of the blue dots in Figure B.3a do not correspond to any anchorage or berth in Figure B.3b, indicating that ships anchored in these areas for only a short duration.

[8]For this comparison, the input parameters of ST-DBSCAN are set to $Eps1 = 2500$ m, $Eps2 = 1°$, and $MinPts = 100$, as recommended by Ester et al. (1996).

IMA-DBSCAN. Notably, while ST-DBSCAN can generally detect points within the anchorages that are highlighted in blue in Figure B.3c, it mistakenly identifies several high-density regions as berths, even though they are not genuine berths. For example, within the blue rectangle in Figure B.3f, points that ought to be categorized as noise are incorrectly marked as berths, given that ships stayed in these locations for extended periods (potentially for maintenance tasks). Additionally, in the black rectangle, ST-DBSCAN mislabels several points as berths when they should be designated as mooring areas. Consequently, while employing ST-DBSCAN on the sample data offers insights into the arrangement of anchorage areas, it does not succeed in precisely pinpointing berth locations.

Furthermore, in Figure B.4, we present the detailed results of berth identification for each of the four terminals within the Port of Ningbo-Zhoushan: Beilun, Daxie, Pukou, and Yuandong. The outcomes from ST-DBSCAN are ambiguous and feature overlapping sections, which are proximate in position but with significant differences in heading. Although the general range of these terminals can be discerned, individual berths are scarcely distinguishable. In contrast, our IMA-DBSCAN method produces clusters that align precisely with each berth within a terminal. Admittedly, increasing the $MinPts$ value or reducing the $Eps1$ value could enhance the ST-DBSCAN results. However, this would necessitate constant parameter adjustments, which are challenging to execute consistently for each port. Conversely, our IMA-DBSCAN algorithm operates iteratively to automatically determine a set of parameters that can accurately identify both berths and anchorages.

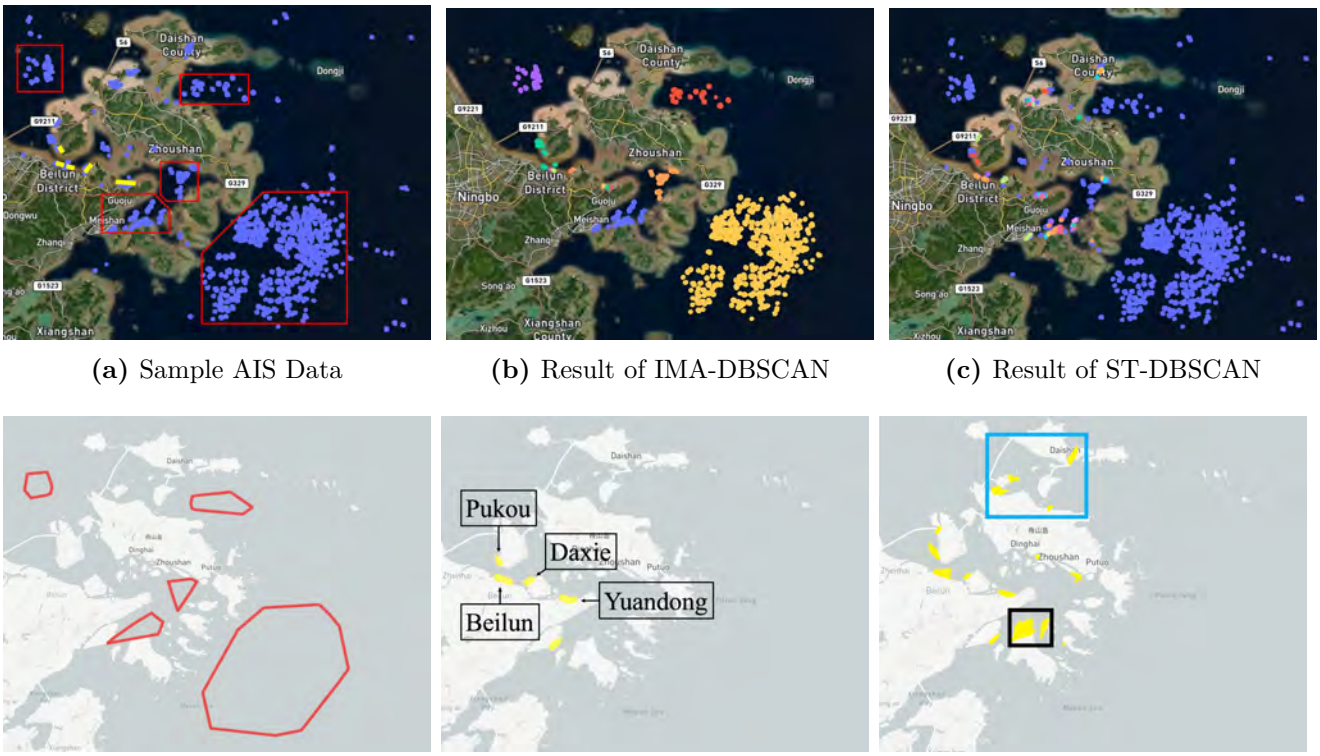

(a) Sample AIS Data **(b)** Result of IMA-DBSCAN **(c)** Result of ST-DBSCAN

(d) Anchorages (IMA-DBSCAN) **(e)** Berths (IMA-DBSCAN) **(f)** Berths (ST-DBSCAN)

Figure B.3: Identification of Anchorage and Berth Areas in the Port of Ningbo-Zhoushan

Notes. In Figure (a), the sample data comprise the first 50,000 AIS observations taken in January 2020 within the Port of Ningbo-Zhoushan. These observations are represented by blue dots on the map, corresponding to coordinates ranging from 121.60°E to 123.00°E and from 29.50°N to 30.35°N. As a benchmark, using satellite maps and nautical charts, we identify the approximate areas of the anchorages with red polygons and the approximate locations of the berths with yellow rectangles. We apply two clustering algorithms, IMA-DBSCAN and ST-DBSCAN, to the sample data. The resulting clusters are depicted in Figures (b) and (c) respectively. Notably, blue dots in Figure (b) represent the identified anchorage areas, while those in Figure (c) represent noise, which outlines the general layout of anchorage areas but does not distinctly identify each one. In Figure (d), the anchorages from Figure (b) are shown separately in red. In Figure (e), the berths from Figure (b) are displayed separately in yellow. The four terminals are identified as Pukou, Daxie, Beilun, and Yuandong. Lastly, in Figure (f), the yellow areas depict the approximate positions of the berths as identified by ST-DBSCAN. The blue and black rectangles indicate misidentifications of noise as berths and confusion between anchorages and berths, respectively.

(a) Terminal Beilun **(b)** Terminal Daxie **(c)** Terminal Pukou **(d)** Terminal Yuandong

Figure B.4: Detailed Results of Berth Identification: IMA-DBSCAN (Top Row) vs. ST-DBSCAN (Bottom Row)

Notes. Detailed results of berth identification for each of the four terminals: Beilun, Daxie, Pukou, and Yuandong, within the Port of Ningbo-Zhoushan. The berths identified by IMA-DBSCAN are presented in yellow on the top row, while those pinpointed by ST-DBSCAN are depicted in brown on the bottom row.

B.3. Weekly Indices of Port Congestion

The integration of high-frequency AIS data with our IMA-DBSCAN algorithm enables the construction of port congestion indices at even higher frequencies than monthly updates. The AIS system processes over 2,000 reports per minute, with the capacity to update information as frequently as every two seconds. This remarkable rate of data collection allows for the capture of detailed, real-time movements of vessels. Furthermore, unlike many traditional algorithms that require data at specific time intervals to function effectively, IMA-DBSCAN is uniquely flexible. Its streamlined design allows it to operate independently of a fixed time frequency, making it particularly suitable for working with the variable and high-speed data provided by AIS.

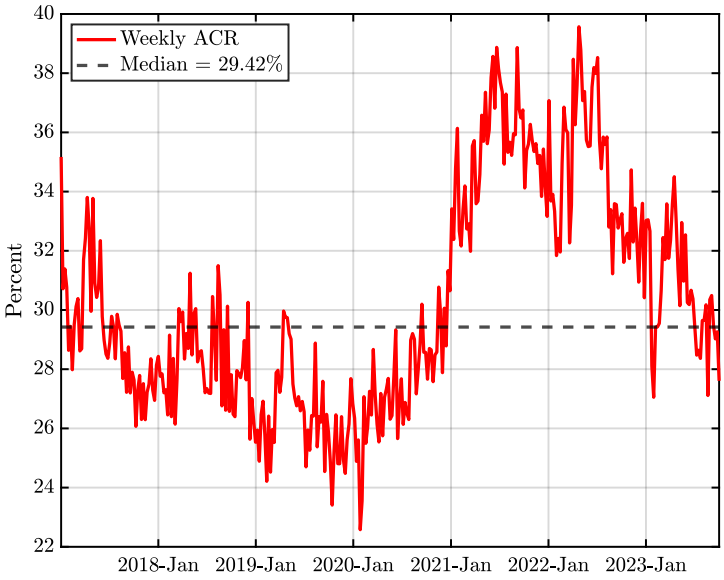

Figure B.5: Weekly ACR Index of Global Supply Chain Disruptions

Notes. The weekly ACR index of global supply chain disruptions is derived in the same way as the monthly ACR index, except that the construction process – i.e., counting the number of delayed ships, normalizing using the number of ship visits, and aggregating into a time series measure – is now based on weekly updates of the AIS data. The index is presented in percentage terms.

Figure B.5 presents our ACR index at a weekly frequency. Compared to the monthly frequency ACR index in Figure 4, we can see that the general trends between the two series are essentially the same. However, the weekly series is significantly more volatile than the monthly series, as the number of ship visits to each port might vary considerably during each week.[9]

[9]Technically, we could also construct the ACR index based on daily or even hourly updates of the AIS data. However, since there are only a few ship visits to a port each day or hour, the constructed ACR index would become extremely volatile, with 0% and 100% occurring frequently.

In addition to the ACR index, we also introduce an alternative high-frequency congestion metric for ports, namely, the Average Congestion Time (ACT). Unlike the ACR index, the ACT index measures the average number of hours a container ship waits in an anchorage area of a port before docking at a berth, weighted by the relative number of ship visits to each of the top 50 container ports worldwide:

$$ACT_t = \sum_{p \in \mathcal{P}} \left[\frac{Delayed_{pt} + Undelayed_{pt}}{\sum_{p \in \mathcal{P}} (Delayed_{pt} + Undelayed_{pt})} \cdot \frac{DelayHours_{pt}}{Delayed_{pt} + Undelayed_{pt}} \right],$$

where $Delayed_{pt}$, $Undelayed_{pt}$, and $DelayHours_{pt}$ represent the number of delayed and undelayed ship visits, and the total number of hours that container ships spend in the anchorage areas of port p in week t, respectively. Figure B.6 plots the ACT index at a weekly frequency, which is observed to closely co-move with the ACR index during the sample period. In Appendix F.4, we also reduce the time dimension of our ACT index to a monthly frequency and use the resulting series in the causality assessment. We show that our identification results are robust when using the ACT index as the measure of global supply chain disruptions.

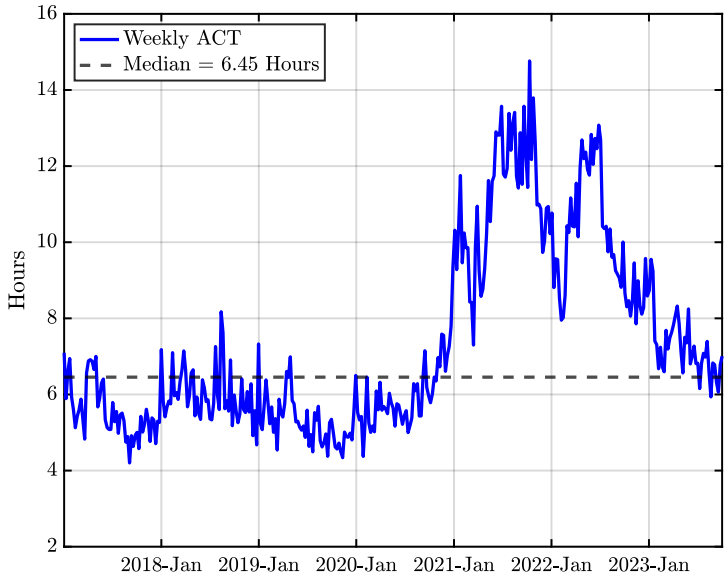

Figure B.6: Weekly ACT Index of Global Supply Chain Disruptions

Notes. The ACT index of global supply chain disruptions is derived by taking a weighted average of the number of hours a container ship waits in an anchorage area of a port before docking at a berth, with the weights based on the relative number of ship visits to each port. The ACT index is measured in hours and updated at a weekly frequency.

C. Discussion on the Assumptions in the Model

In this appendix, we discuss two critical assumptions in our theoretical model: search and matching frictions in the product market and endogenous separation of producer-retailer matches due to transportation costs. First, to represent the search and matching frictions in an analytically tractable manner, we assume that a matching function governs the number of trades between producers and retailers. Second, to succinctly capture the decision-making process between a producer and a retailer when their trade is subject to a transportation cost, we assume that upon meeting, both parties choose to endogenously separate from each other once the idiosyncratic transportation cost lies above a reservation threshold. We discuss each of these two assumptions in turn.

The matching function. There is ample literature studying the origins of matching frictions in the product market, including but not limited to locating and building connections with buyers in different locations (Benguria, 2021; Krolikowski and McCallum, 2021; Lenoir et al., 2022), the costly acquisition of information about market conditions elsewhere (Allen, 2014; Chaney, 2014), and informal trade barriers such as common language (Melitz and Toubal, 2014) and geography (Eaton and Kortum, 2002). Common across all these theories is the presence of prevalent trade barriers between producers and retailers, implying that not all unmatched producers engage in trade and not all sourcing visits by retailers are successful. Consistent with these theories, we assume a constant-returns-to-scale matching function that summarizes how unmatched producers and visits by retailers are transformed into trades through the matching process. Thus, we abstract from modeling the complex matching process while still preserving its main implication: the unmatched producers only engage in trade with probability $f(\theta)G(\tau) < 1$, and the visits of retailers to producers are only successful with probability $q(\theta)G(\tau) < 1$.

Endogenous separation on transportation cost. In much the same way as the separation margin in the labor market can be modeled endogenously when workers face productivity shocks to their employment matches, and bad draws possibly lead to separations (Bils et al., 2011; Menzio and Shi, 2011; Fujita and Ramey, 2012), the separation margin in the product market can also be modeled endogenously. This occurs when producers face idiosyncratic transportation costs to their trading relationships with retailers, and bad draws possibly lead to the termination of such relationships. Such a modeling assumption is reasonable only if we find convincing evidence that

(i) transportation costs are taken into account when trading partners decide on a potential trade and (ii) there exists a threshold of transportation costs above which trading partners choose to sever their relationship.

The prediction that transportation cost affects the probability of trade has been empirically examined in the trade literature. To name a few examples, evidence in Rodrigue (2020) underlines that across all modes, increasing transportation costs by 10% reduces trade volumes by more than 20%. In the context of maritime transportation, Brancaccio et al. (2020) exploit changes in tariffs across the trade network to estimate the elasticity of world trade value with respect to shipping costs. They estimate that a 1% change in shipping costs leads to approximately a 1% change in world trade value. Similarly, Wong (2022) estimates the containerized trade elasticity with respect to freight rates using the round-trip effect as an instrument. In particular, for route i, j, she uses a Bartik-style instrument to proxy for the predicted trade value on route j, i. Wong (2022) reports that a 1% increase in per-unit container freight rates decreases containerized trade value by 2.8% when dyad-by-product controls are included in the regression. Together, these estimated elasticities emphasize that transportation costs are indeed taken into account when trading partners choose to form a relationship and that a rise in transportation costs deters trade substantially.

Both theory and casual observation also suggest the presence of a reservation transportation cost, which trading partners often consider when assessing the profitability of potential trades in the product market. Notably, to reconcile the empirical evidence that export and import intensities vary across plants, Kasahara and Lapham (2013) extend the model in Melitz (2003) by allowing for heterogeneity in transportation costs. Incorporating heterogeneous transportation costs provides a plausible self-selection mechanism for trade decisions, as plants with low transportation costs self-select into exporting and importing. Consequently, there must exist a threshold value of transportation cost below which plants choose to engage in trade.[10] Furthermore, the reservation transportation cost is likely to be largely fixed in the short run, as in our equilibrium selection mechanism, given that transportation technology and the price outlook for

[10] A similar argument is found in the discussion of transport infrastructure and its effects on a firm's exporting decision. For instance, Naudé and Matthee (2011)argue that the availability of transport infrastructure will have a threshold effect – a certain minimum level of infrastructure is required for a firm to start exporting. However, once this threshold is reached, improved infrastructure will not necessarily have a large impact on the extent of an individual firm's exports. Since the availability of transport infrastructure (at least partially) determines the transportation cost, this argument is consistent with the presence of a reservation transportation cost that firms take into account when making exporting decisions.

shipping fuel are unlikely to vary in a few years' time.

Lastly, the modeling assumption that transportation cost follows a log-normal distribution is borrowed from Kasahara and Lapham (2013). A random distribution of transportation costs captures the idea that, in the real world, there is a wide range of transportation costs that vary across countries, routes, directions, and commodities (Brown et al., 2021). This is more appealing than a fixed transportation cost (for instance, the "iceberg" formulation of trade costs as in Samuelson, 1954). A log-normal distribution gives one scale parameter that serves as a possible theoretical counterpart to our ACR index. Indeed, Figure F.1 shows the positive empirical relationship between the ACR index and shipping costs.

Alternatively, we could augment the current model with a full-fledged transportation sector, where the interactions between producers and shipowners determine the transportation cost. Such an endogenous setting can be found in Brancaccio et al. (2020), Bai and Li (2022), and Dunn and Leibovici (2023). Nonetheless, we maintain the current setting for its tractability.

D. Long Proofs and Model Dynamics

The following appendices include all long proofs that are omitted from the main text, as well as several important discussions on model dynamics. For simplicity, in the proofs presented from Appendix D.1 to D.8, we omit the matching efficiency parameter A, since it is parameterized to one. In Appendix D.9, where the supply chain disruption is modeled as a reduction in matching efficiency, and in Appendix D.10, where we examine the convergence dynamics of the model from one steady state to another following each shock of interest, A is explicitly incorporated in all derivations.

D.1. Proof of Proposition 1

We first rewrite $\mathbb{E}_{z'}S(z')$. Using the definition of $S(z)$ in Equation (10), we have:

$$S(z) = (p - z)l + (1 - \eta f(\theta))\,\beta \mathbb{E}_{z'}S(z').$$

Subtracting Equation (14) from the above equation yields $S(z) = (\bar{z} - z)l$. Replacing $S(z')$ in $\mathbb{E}_{z'}S(z')$ with $(\bar{z} - z')l$, we derive that:

$$\begin{aligned}
\mathbb{E}_{z'}S(z') &= l\int_0^{\bar{z}} (\bar{z} - z')dG(z') \\
&= l\left[(\bar{z} - z')G(z')\Big|_0^{\bar{z}} + \int_0^{\bar{z}} G(z')dz'\right] \\
&= l\int_0^{\bar{z}} G(z')dz'.
\end{aligned}$$

Subsequently, by replacing $\mathbb{E}_{z'}S(z')$ in Equations (14) and (15) with $l\int_0^{\bar{z}} G(z')dz'$, the match separation condition can be re-written as:

$$\mathbb{F}(p, \bar{z}, \theta) = p - \bar{z} + (1 - \eta f(\theta))\,\beta \int_0^{\bar{z}} G(z')dz' = 0,$$

and the match creation condition is given by:

$$\mathbb{H}(\bar{z}, \theta) = \frac{\rho}{q(\theta)} - (1 - \eta)\beta \int_0^{\bar{z}} G(z')dz' = 0.$$

Combining the two conditions yields Equation (16):

$$
\begin{aligned}
0 &= p - \bar{z} + (1 - \eta f(\theta))\,\beta \int_0^{\bar{z}} G(z')dz' + \frac{\rho}{q(\theta)} - (1-\eta)\beta \int_0^{\bar{z}} G(z')dz' \\
0 &= p - \bar{z} - \eta f(\theta)\beta \int_0^{\bar{z}} G(z')dz' + \frac{\rho}{q(\theta)} + \eta\beta \int_0^{\bar{z}} G(z')dz' \\
0 &= p - \bar{z} - \eta f(\theta)\frac{\rho}{q(\theta)(1-\eta)} + \beta \int_0^{\bar{z}} G(z')dz' \\
\theta &= \frac{1-\eta}{\eta\rho}\left(p - \bar{z} + \beta \int_0^{\bar{z}} G(z')dz'\right),
\end{aligned}
$$

where the last step is obtained using the property $\theta = f(\theta)/q(\theta)$.

The first property is obvious. Since θ cannot be negative, for a given $\bar{z}$, p is bounded on $[p^{min}, +\infty)$, where p^{min} is such that it solves $p^{min} - \bar{z} + \beta \int_0^{\bar{z}} G(z')dz' = 0$ for any $\bar{z} > 0$. As for the second and third properties, we get that:

$$
\frac{\partial \theta(p, \bar{z})}{\partial p} = \frac{1-\eta}{\eta\rho} > 0.
$$

Therefore, product market tightness $\theta(p, \bar{z})$ is strictly increasing and linear on $[p^{min}, +\infty)$.

The fourth property is also obvious from the definition of $\bar{z}^{max}$, as θ cannot be negative. In terms of the fifth and last properties, we derive that:

$$
\frac{\partial \theta(p, \bar{z})}{\partial \bar{z}} = \frac{1-\eta}{\eta\rho}\left(-1 + \beta G(\bar{z})\right) < 0,
$$

$$
\frac{\partial^2 \theta(p, \bar{z})}{\partial \bar{z}^2} = \frac{(1-\eta)\beta}{\eta\rho}\frac{1}{\bar{z}\sigma}\phi\left(\frac{\log \bar{z} - \gamma}{\sigma}\right) > 0,
$$

where $\phi(.)$ is the standard normal probability density function. Hence, product market tightness $\theta(p, \bar{z})$ is strictly decreasing and convex on $(0, \bar{z}^{max}]$.

D.2. Proof of Proposition 2

The first property is obvious. When $p = p^{min}$, we have $\theta(p^{min}) = 0$, $f\left(\theta(p^{min})\right) = 0$, and $c_s^{flex}(p^{min}) = 0$. When $p \to +\infty$, since A is parameterized to one, we have $\lim_{p\to+\infty} \theta(p) = +\infty$, $\lim_{p\to+\infty} f\left(\theta(p)\right) = 1$, and hence $\lim_{p\to+\infty} c_s^{flex}(p) = G(\tau)l$. In terms of the second and third properties, we derive that:

$$
\frac{dc_s^{flex}(p)}{dp} = \frac{1-\eta}{\eta\rho}\frac{\left(1 - G(\tau)\right) q(\theta)^{1+\xi} G(\tau) l}{\left(1 - G(\tau) + f(\theta)G(\tau)\right)^2} > 0,
$$

$$\frac{d^2 c_s^{flex}(p)}{dp^2} = -\left(\frac{1-\eta}{\eta\rho}\right)^2 (1-G(\tau))\, G(\tau) l \cdot \frac{(1-G(\tau)+f(\theta)G(\tau))\,\theta^{\xi-1}(1+\xi)(1+\theta^{\xi})^{-\frac{1+\xi}{\xi}-1} + 2G(\tau)q(\theta)^{2(1+\xi)}}{(1-G(\tau)+f(\theta)G(\tau))^3} < 0.$$

Therefore, the flexible price aggregate supply c_s^{flex} is strictly increasing and concave on $[p^{min}, +\infty)$.

D.3. Proof of Proposition 4

Since we look for a flexible price equilibrium with positive consumption, we restrict our search of price p within the range $[p^{min}, +\infty)$. The equilibrium condition (26) can be re-written as:

$$\frac{f(\theta(p))\, p}{1-G(\tau)+f(\theta(p))\, G(\tau)} = \chi^{\varepsilon}\frac{\mu}{G(\tau)l}. \tag{D.1}$$

For any $\tau > 0$, the right-hand side is a strictly positive constant. For the left-hand side, when $p = p^{min}$, $\theta(p^{min}) = 0$, and $f(\theta(p^{min})) = 0$, it has a limit of zero; when $p \to +\infty$, $\lim_{p\to+\infty}\theta(p) = +\infty$, and $\lim_{p\to+\infty} f(\theta(p)) = 1$, it has a limit of positive infinity. For $p \in [p^{min}, +\infty)$, the derivative of the left-hand side with respect to p is given by:

$$\frac{d}{dp}\left[\frac{f(\theta(p))\, p}{1-G(\tau)+f(\theta(p))\, G(\tau)}\right] = \frac{(1-G(\tau))\,\frac{1-\eta}{\eta\rho}q(\theta)^{1+\xi}p + f(\theta)\,(1-G(\tau)+f(\theta)G(\tau))}{(1-G(\tau)+f(\theta)G(\tau))^2} > 0.$$

Therefore, the left-hand side is strictly increasing from zero to positive infinity on $[p^{min}, +\infty)$ and there is a unique $p \in [p^{min}, +\infty)$ that solves Equation (D.1).

D.4. Proof of Proposition 5

We first consider an adverse shock to aggregate demand. No matter whether the negative aggregate demand shock is represented by a decrease in the money supply μ or in the taste for consumption of goods χ, the right-hand side of Equation (D.1) will decrease. To balance both sides of Equation (D.1), price p will decrease since the derivative of the left-hand side with respect to p is positive (see the proof for Proposition 4). As p decreases, by the second property in Proposition 1 and the second property in Proposition 2, product market tightness θ and consumption (or, equivalently, output) c will decrease. Since both p and θ decrease, according to Equation (12), wholesale price r will decline as well. For the matching cost, $G(\tau)l - c$, and spare capacity (or, equivalently, unemployment), $l - c$, since both are strictly decreasing in c, they will increase following an adverse shock to aggregate demand.

Next, we consider an adverse shock to productive capacity, which is parameterized by a decrease in l. On impact, the right-hand side of Equation (D.1) increases. Similar to the above reasoning, price p will increase. As p increases, by the second property in Proposition 1 and Proposition 3, product market tightness θ will increase while consumption (or, equivalently, output) c will fall. Again, since both p and θ increase, according to Equation (12), wholesale price r will rise. In terms of the matching cost and spare capacity (or, equivalently, unemployment), they can be alternatively expressed as:

$$matching\ cost = G(\tau)l - c = \frac{(1-G(\tau))\,(1-f(\theta))}{1-(1-f(\theta))\,G(\tau)}G(\tau)l,$$

$$spare\ capacity = l - c = \frac{1-G(\tau)}{1-G(\tau)+f(\theta)G(\tau)}l,$$

respectively. With θ increasing and l decreasing following the capacity shock, it is easy to verify that both the matching cost and spare capacity will decrease.

Lastly, we consider an adverse shock to the supply chain, which is represented by an increase in γ, i.e., the scale parameter of the log-normal distribution of transportation costs $G(.)$. We first look at the effect on price. Using the re-arranged equilibrium condition (D.1), we define a function $\mathbb{T} : [p^{min}, +\infty) \times \mathbb{R} \to \mathbb{R}$:

$$\begin{aligned}\mathbb{T}(p,\gamma) &= \chi^{\varepsilon}\frac{\mu}{G(\tau)l} - \frac{f(\theta)p}{1-G(\tau)+f(\theta)G(\tau)} \\ &= \chi^{\varepsilon}\frac{\mu}{\Phi(\frac{\log\tau-\gamma}{\sigma})l} - \frac{\left\{1+\left[\frac{1-\eta}{\eta\rho}\left(p-\tau+\beta\int_0^{\tau}\Phi(\frac{\log z'-\gamma}{\sigma})dz'\right)\right]^{-\xi}\right\}^{-\frac{1}{\xi}}p}{1-\Phi(\frac{\log\tau-\gamma}{\sigma})+\left\{1+\left[\frac{1-\eta}{\eta\rho}\left(p-\tau+\beta\int_0^{\tau}\Phi(\frac{\log z'-\gamma}{\sigma})dz'\right)\right]^{-\xi}\right\}^{-\frac{1}{\xi}}\Phi(\frac{\log\tau-\gamma}{\sigma})},\end{aligned}$$

where $\Phi(.)$ is the standard normal cumulative density function. Assuming the existence of a tuple $(p_0, \gamma_0) \in [p^{min}, +\infty) \times \mathbb{R}$ such that $\mathbb{T}(p_0, \gamma_0) = 0$ and $\partial\mathbb{T}(p,\gamma)/\partial p|_{p=p_0,\gamma=\gamma_0} \neq 0$, by the implicit function theorem, there is a neighborhood of (p_0, γ_0) such that whenever γ is sufficiently close to γ_0, there is a unique p so that $\mathbb{T}(p, \gamma) = 0$. This assignment makes p a continuous function of γ. Applying implicit differentiation to $\mathbb{T}(p, \gamma)$ around (p_0, γ_0) yields:

$$\frac{dp(\gamma)}{d\gamma} = -\frac{\partial\mathbb{T}(p,\gamma)/\partial\gamma}{\partial\mathbb{T}(p,\gamma)/\partial p}.$$

In terms of $\partial\mathbb{T}(p,\gamma)/\partial\gamma$, we derive that:

$$\begin{aligned}\frac{\partial\mathbb{T}(p,\gamma)}{\partial\gamma} =&\chi^{\varepsilon}\frac{\mu}{l}\frac{\frac{1}{\sigma}g(\tau)}{G(\tau)^2}+\frac{(1-G(\tau))\,\frac{(1-\eta)\beta}{\eta\rho}\left[\int_0^{\tau}\frac{1}{\sigma}g(z')dz'\right]q(\theta)^{1+\xi}p}{\left(1-G(\tau)+f(\theta)G(\tau)\right)^2}\\&+\frac{\left(1-f(\theta)\right)f(\theta)p\frac{1}{\sigma}g(\tau)}{\left(1-G(\tau)+f(\theta)G(\tau)\right)^2}>0,\end{aligned}$$

where $g(\tau)\equiv\phi[(\log\tau-\gamma)/\sigma]$, $g(z')\equiv\phi[(\log z'-\gamma)/\sigma]$, while $\phi(.)$ is the standard normal probability density function. In terms of $\partial\mathbb{T}(p,\gamma)/\partial p$, it can be written as follows:

$$\frac{\partial\mathbb{T}(p,\gamma)}{\partial p}=-\frac{(1-G(\tau))\,\frac{1-\eta}{\eta\rho}q(\theta)^{1+\xi}p+f(\theta)\left(1-G(\tau)+f(\theta)G(\tau)\right)}{\left(1-G(\tau)+f(\theta)G(\tau)\right)^2}<0.$$

By combining $\partial\mathbb{T}(p,\gamma)/\partial\gamma$ with $\partial\mathbb{T}(p,\gamma)/\partial p$ and collecting terms, we have:

$$\begin{aligned}\frac{dp(\gamma)}{d\gamma}=&\left[(1-G(\tau))\,\frac{1-\eta}{\eta\rho}q(\theta)^{1+\xi}p+f(\theta)\left(1-G(\tau)+f(\theta)G(\tau)\right)\right]^{-1}\\&\cdot\Big\{\left(1-G(\tau)+f(\theta)G(\tau)\right)f(\theta)\frac{1}{\sigma}g(\tau)\frac{p}{G(\tau)}\\&+(1-G(\tau))\,\frac{(1-\eta)\beta}{\eta\rho}\left[\int_0^{\tau}\frac{1}{\sigma}g(z')dz'\right]q(\theta)^{1+\xi}p\\&+\left(1-f(\theta)\right)f(\theta)p\frac{1}{\sigma}g(\tau)\Big\}>0.\end{aligned}\tag{D.2}$$

Hence, price p will increase on impact after an adverse shock to the supply chain. In terms of consumption (or, equivalently, output), it is written as:

$$c(\gamma)=\chi^{\varepsilon}\frac{\mu}{p(\gamma)},$$

where p is an implicit function of γ. Therefore, the derivative of c with respect to γ is:

$$\begin{aligned}\frac{dc(\gamma)}{d\gamma}=&-\chi^{\varepsilon}\frac{\mu}{p}\left[(1-G(\tau))\,\frac{1-\eta}{\eta\rho}q(\theta)^{1+\xi}p+f(\theta)\left(1-G(\tau)+f(\theta)G(\tau)\right)\right]^{-1}\\&\cdot\Big\{\left(1-G(\tau)+f(\theta)G(\tau)\right)f(\theta)\frac{1}{\sigma}g(\tau)\frac{1}{G(\tau)}\\&+(1-G(\tau))\,\frac{(1-\eta)\beta}{\eta\rho}\left[\int_0^{\tau}\frac{1}{\sigma}g(z')dz'\right]q(\theta)^{1+\xi}\\&+\left(1-f(\theta)\right)f(\theta)\frac{1}{\sigma}g(\tau)\Big\}<0.\end{aligned}$$

Hence, consumption (or, equivalently, output) c will fall. Next, in terms of product market

tightness, it is given by:

$$\theta(\gamma) = \frac{1-\eta}{\eta\rho}\left(p(\gamma) - \tau + \beta\int_0^{\tau}\Phi(\frac{\log z' - \gamma}{\sigma})dz'\right). \tag{D.3}$$

Accordingly, the derivative of θ with respect to γ is:

$$\begin{aligned}\frac{d\theta(\gamma)}{d\gamma} =& \frac{1-\eta}{\eta\rho}\left[(1-G(\tau))\,\frac{1-\eta}{\eta\rho}q(\theta)^{1+\xi}p + f(\theta)\,(1-G(\tau)+f(\theta)G(\tau))\right]^{-1} \\ &\cdot\Big\{(1-G(\tau)+f(\theta)G(\tau))\,f(\theta)\frac{1}{\sigma}g(\tau)\frac{p}{G(\tau)} + (1-f(\theta))\,f(\theta)p\frac{1}{\sigma}g(\tau) \\ &-(1-G(\tau)+f(\theta)G(\tau))\,f(\theta)\beta\left[\int_0^{\tau}\frac{1}{\sigma}g(z')dz'\right]\Big\},\end{aligned} \tag{D.4}$$

whose value depends on the values of θ and p. As we will discuss later in Appendix D.6, this dependence is crucial for our discussion on the effectiveness of a contractionary monetary policy shock in controlling inflation and output. Similarly, by substituting Equation (D.3) into Equation (12), we can express the wholesale price as follows:

$$r(\gamma) = p(\gamma) + (1-\eta)\beta\int_0^{\tau}\Phi(\frac{\log z' - \gamma}{\sigma})dz' + (1-\eta)(z-\tau).$$

Differentiating $r(\gamma)$ with respect to γ yields:

$$\begin{aligned}\frac{dr(\gamma)}{d\gamma} =& \left[(1-G(\tau))\,\frac{1-\eta}{\eta\rho}q(\theta)^{1+\xi}p + f(\theta)\,(1-G(\tau)+f(\theta)G(\tau))\right]^{-1} \\ &\cdot\Big\{(1-G(\tau)+f(\theta)G(\tau))\,f(\theta)\frac{1}{\sigma}g(\tau)\frac{p}{G(\tau)} \\ &+(1-G(\tau))\,\frac{(1-\eta)\beta}{\rho}\left[\int_0^{\tau}\frac{1}{\sigma}g(z')dz'\right]q(\theta)^{1+\xi}p \\ &+(1-f(\theta))\,f(\theta)p\frac{1}{\sigma}g(\tau) \\ &-(1-G(\tau)+f(\theta)G(\tau))\,f(\theta)(1-\eta)\beta\left[\int_0^{\tau}\frac{1}{\sigma}g(z')dz'\right]\Big\},\end{aligned}$$

whose value is also dependent on the values of θ and p. As for the matching cost, given that it is measured by the difference between $G(\tau)l$ and c, its derivative with respect to γ can be written as follows:

$$\begin{aligned}\frac{d}{d\gamma}\left[matching\ cost(\gamma)\right] =& \left[(1-G(\tau))\,\frac{1-\eta}{\eta\rho}q(\theta)^{1+\xi}p + f(\theta)\,(1-G(\tau)+f(\theta)G(\tau))\right]^{-1} \\ &\cdot\Big(\chi^{\varepsilon}\frac{\mu}{p}\Big\{(1-G(\tau)+f(\theta)G(\tau))\,f(\theta)\frac{1}{\sigma}g(\tau)\frac{1}{G(\tau)}\end{aligned}$$

$$
\begin{aligned}
&+ (1 - G(\tau))\, \frac{(1-\eta)\beta}{\eta\rho} \left[\int_0^\tau \frac{1}{\sigma} g(z')dz'\right] q(\theta)^{1+\xi} \\
&+ (1 - f(\theta))\, f(\theta) \frac{1}{\sigma} g(\tau) \Big\} \\
&- (1 - G(\tau))\, \frac{1-\eta}{\eta\rho} q(\theta)^{1+\xi} p \frac{1}{\sigma} g(\tau) l \\
&- f(\theta)\, (1 - G(\tau) + f(\theta) G(\tau))\, \frac{1}{\sigma} g(\tau) l \Big),
\end{aligned}
$$

whose value is again dependent on the values of θ and p. On the contrary, since the spare capacity (or, equivalently, unemployment) is measured by the difference between l and c, its derivative with respect to γ is positive, i.e.,

$$
\begin{aligned}
\frac{d}{d\gamma}\left[spare\ capacity(\gamma)\right] =& \chi^{\varepsilon} \frac{\mu}{p} \left[(1 - G(\tau))\, \frac{1-\eta}{\eta\rho} q(\theta)^{1+\xi} p + f(\theta)\, (1 - G(\tau) + f(\theta) G(\tau))\right]^{-1} \\
&\cdot \Big\{ (1 - G(\tau) + f(\theta) G(\tau))\, f(\theta) \frac{1}{\sigma} g(\tau) \frac{1}{G(\tau)} \\
&+ (1 - G(\tau))\, \frac{(1-\eta)\beta}{\eta\rho} \left[\int_0^\tau \frac{1}{\sigma} g(z')dz'\right] q(\theta)^{1+\xi} \\
&+ (1 - f(\theta))\, f(\theta) \frac{1}{\sigma} g(\tau) \Big\} > 0.
\end{aligned}
$$

D.5. Slope of the Aggregate Supply Curve and Its Dependence on Product Market Tightness

Given Equation (22), the slope of the aggregate supply curve is determined by the following:

$$
\frac{dc_s^{flex}}{dp} = \frac{(1-\eta) l}{\eta\rho} \frac{(1 - G(\tau))\, G(\tau) \left(1 + \theta^{\xi}\right)^{-\frac{1+\xi}{\xi}}}{\left[1 - G(\tau) + (1 + \theta^{-\xi})^{-\frac{1}{\xi}} G(\tau)\right]^2}.
$$

Differentiating it with respect to product market tightness θ yields:

$$
\begin{aligned}
\frac{d^2 c_s^{flex}}{dp d\theta} =& - \frac{(1-\eta) l}{\eta\rho} \frac{1}{\left[1 - G(\tau) + (1 + \theta^{-\xi})^{-\frac{1}{\xi}} G(\tau)\right]^3} \\
&\cdot \Big\{ \left[1 - G(\tau) + \left(1 + \theta^{-\xi}\right)^{-\frac{1}{\xi}} G(\tau)\right] (1 - G(\tau))\, G(\tau) \theta^{\xi-1} (1 + \xi) \left(1 + \theta^{\xi}\right)^{-\frac{1+\xi}{\xi}-1} \\
&+ 2\, (1 - G(\tau))\, G(\tau)^2 \left(1 + \theta^{\xi}\right)^{-\frac{2(1+\xi)}{\xi}} \Big\} < 0.
\end{aligned}
$$

Therefore, the aggregate supply curve becomes steeper in the (Q, p) plane as product market tightness increases.

Furthermore, to complement our discussion in Section 3.4 regarding the response of the system

to an adverse supply chain disturbance, we depict an alternative scenario in which the resulting price increase fails to elevate product market tightness at the new equilibrium in the following figure.

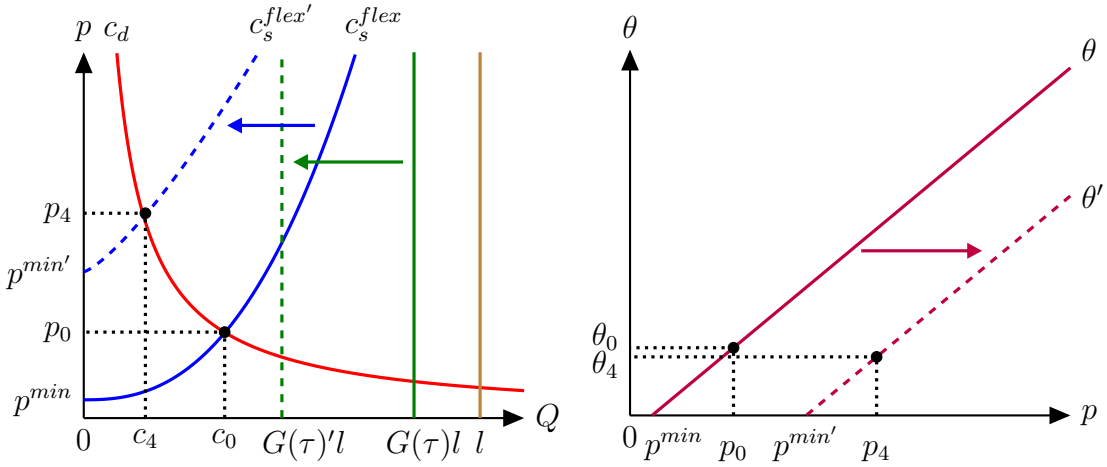

Figure D.1: Alternative Scenario When There Is an Adverse Shock to the Supply Chain

D.6. Proof of Proposition 6

We start the proof by re-visiting the function $\mathbb{T} : [p^{min}, +\infty) \times \mathbb{R}^+ \times \mathbb{R} \to \mathbb{R}$:

$$\mathbb{T}(p,\mu,\gamma) = \chi^{\varepsilon}\frac{\mu}{G(\tau)l} - \frac{f(\theta)p}{1-G(\tau)+f(\theta)G(\tau)}$$
$$= \chi^{\varepsilon}\frac{\mu}{\Phi(\frac{\log\tau-\gamma}{\sigma})l} - \frac{\left\{1+\left[\frac{1-\eta}{\eta\rho}\left(p-\tau+\beta\int_0^{\tau}\Phi(\frac{\log z'-\gamma}{\sigma})dz'\right)\right]^{-\xi}\right\}^{-\frac{1}{\xi}}p}{1-\Phi(\frac{\log\tau-\gamma}{\sigma})+\left\{1+\left[\frac{1-\eta}{\eta\rho}\left(p-\tau+\beta\int_0^{\tau}\Phi(\frac{\log z'-\gamma}{\sigma})dz'\right)\right]^{-\xi}\right\}^{-\frac{1}{\xi}}\Phi(\frac{\log\tau-\gamma}{\sigma})},$$

where $\Phi(.)$ is the standard normal cumulative density function. Assuming the existence of a tuple $(p_0,\mu_0,\gamma_0) \in [p^{min},+\infty)\times\mathbb{R}^+\times\mathbb{R}$ such that $\mathbb{T}(p_0,\mu_0,\gamma_0)=0$ and $\partial\mathbb{T}(p,\mu,\gamma)/\partial p|_{p=p_0,\mu=\mu_0,\gamma=\gamma_0} \neq 0$, by the implicit function theorem, there is a neighborhood of (p_0,μ_0,γ_0) such that whenever (μ,γ) is sufficiently close to (μ_0,γ_0), there is a unique p so that $\mathbb{T}(p,\mu,\gamma)=0$. This assignment makes p a continuous function of μ and γ. Applying implicit differentiation to $\mathbb{T}(p,\mu,\gamma)$ around (p_0,μ_0,γ_0) yields:

$$\frac{\partial p(\mu,\gamma)}{\partial\mu} = -\frac{\partial\mathbb{T}(p,\mu,\gamma)/\partial\mu}{\partial\mathbb{T}(p,\mu,\gamma)/\partial p}.$$

The numerator can be written as:

$$\frac{\partial\mathbb{T}(p,\mu,\gamma)}{\partial\mu} = \chi^{\varepsilon}\frac{1}{G(\tau)l} > 0,$$

whereas the denominator is given by:

$$\frac{\partial \mathbb{T}(p,\mu,\gamma)}{\partial p} = -\frac{(1-G(\tau))\,\frac{1-\eta}{\eta\rho}q(\theta)^{1+\xi}p + f(\theta)\,(1-G(\tau)+f(\theta)G(\tau))}{(1-G(\tau)+f(\theta)G(\tau))^2} < 0.$$

By combining $\partial\mathbb{T}(p,\mu,\gamma)/\partial\mu$ with $\partial\mathbb{T}(p,\mu,\gamma)/\partial p$, we derive that:

$$\begin{aligned}\frac{\partial p(\mu,\gamma)}{\partial \mu} &= \chi^{\varepsilon}\frac{1}{G(\tau)l}\frac{(1-G(\tau)+f(\theta)G(\tau))^2}{(1-G(\tau))\,\frac{1-\eta}{\eta\rho}q(\theta)^{1+\xi}p + f(\theta)\,(1-G(\tau)+f(\theta)G(\tau))}\\ &= \frac{1}{\mu}\left[\frac{(1-G(\tau))\,\frac{1-\eta}{\eta\rho}q(\theta)^{1+\xi}}{f(\theta)\,(1-G(\tau)+f(\theta)G(\tau))}+\frac{1}{p}\right]^{-1} > 0,\end{aligned}$$

where the last step is obtained because:

$$\mathbb{T}(p,\mu,\gamma)=0 \;\Rightarrow\; \chi^{\varepsilon}\frac{1}{G(\tau)l} = \frac{f(\theta)p}{\mu\,(1-G(\tau)+f(\theta)G(\tau))}.$$

In terms of the partial derivative of consumption (or, equivalently, output) with respect to μ, using the expression for the aggregate demand in Equation (25), we can derive that:

$$\begin{aligned}\frac{\partial c(\mu,\gamma)}{\partial \mu} &= \chi^{\varepsilon}\frac{(1-G(\tau))\,\frac{1-\eta}{\eta\rho}q(\theta)^{1+\xi}}{(1-G(\tau))\,\frac{1-\eta}{\eta\rho}q(\theta)^{1+\xi}p + f(\theta)\,(1-G(\tau)+f(\theta)G(\tau))}\\ &= \chi^{\varepsilon}\left[p+\frac{f(\theta)\,(1-G(\tau)+f(\theta)G(\tau))}{(1-G(\tau))\,\frac{1-\eta}{\eta\rho}q(\theta)^{1+\xi}}\right]^{-1} > 0.\end{aligned}$$

Consequently, the partial derivatives $\partial p(\mu,\gamma)/\partial\mu$ and $\partial c(\mu,\gamma)/\partial\mu$ both depend on the following fraction:

$$\frac{(1-G(\tau))\,\frac{1-\eta}{\eta\rho}q(\theta)^{1+\xi}}{f(\theta)\,(1-G(\tau)+f(\theta)G(\tau))}. \tag{D.5}$$

Next, we study the dependence of the fraction (D.5) on γ, as it directly determines the signs of the cross derivatives $\partial^2 p(\mu,\gamma)/\partial\mu\partial\gamma$ and $\partial^2 c(\mu,\gamma)/\partial\mu\partial\gamma$. It is given by:

$$\begin{aligned}\frac{\partial}{\partial\gamma}\left[\frac{(1-G(\tau))\,\frac{1-\eta}{\eta\rho}q(\theta)^{1+\xi}}{f(\theta)\,(1-G(\tau)+f(\theta)G(\tau))}\right] &= \frac{f(\theta)\,(1-G(\tau)+f(\theta)G(\tau))\left[\frac{1}{\sigma}g(\tau)\frac{1-\eta}{\eta\rho}q(\theta)^{1+\xi}\right]}{[f(\theta)\,(1-G(\tau)+f(\theta)G(\tau))]^2}\\ &- \frac{f(\theta)\,(1-G(\tau)+f(\theta)G(\tau))\left[(1-G(\tau))\,\frac{1-\eta}{\eta\rho}\frac{\partial\theta(\mu,\gamma)}{\partial\gamma}(1+\xi)\theta^{\xi-1}(1+\theta^{\xi})^{-\frac{1+\xi}{\xi}-1}\right]}{[f(\theta)\,(1-G(\tau)+f(\theta)G(\tau))]^2}\\ &- \frac{(1-G(\tau))\,\frac{1-\eta}{\eta\rho}q(\theta)^{1+\xi}\left[\frac{\partial\theta(\mu,\gamma)}{\partial\gamma}q(\theta)^{1+\xi}\,(1-G(\tau)+f(\theta)G(\tau))\right]}{[f(\theta)\,(1-G(\tau)+f(\theta)G(\tau))]^2}\\ &- \frac{(1-G(\tau))\,\frac{1-\eta}{\eta\rho}q(\theta)^{1+\xi}\left[f(\theta)\left(\frac{1}{\sigma}g(\tau)+\frac{\partial\theta(\mu,\gamma)}{\partial\gamma}q(\theta)^{1+\xi}G(\tau)-f(\theta)\frac{1}{\sigma}g(\tau)\right)\right]}{[f(\theta)\,(1-G(\tau)+f(\theta)G(\tau))]^2},\end{aligned}$$

and is proportional to:

$$\begin{aligned}
&\frac{\partial}{\partial\gamma}\left[\frac{(1-G(\tau))^{\frac{1-\eta}{\eta\rho}}q(\theta)^{1+\xi}}{f(\theta)\left(1-G(\tau)+f(\theta)G(\tau)\right)}\right] \\
&\propto f(\theta)^2\frac{1}{\sigma}g(\tau)-f(\theta)\left(1-G(\tau)+f(\theta)G(\tau)\right)\left(1-G(\tau)\right)\frac{\partial\theta(\mu,\gamma)}{\partial\gamma}(1+\xi)\frac{\theta^{\xi-1}}{1+\theta^{\xi}} \\
&\quad-\left(1-G(\tau)\right)\frac{\partial\theta(\mu,\gamma)}{\partial\gamma}q(\theta)^{1+\xi}\left(1-G(\tau)+f(\theta)G(\tau)\right) \\
&\quad-\left(1-G(\tau)\right)f(\theta)\frac{\partial\theta(\mu,\gamma)}{\partial\gamma}q(\theta)^{1+\xi}G(\tau),
\end{aligned}$$

where $g(\tau)\equiv\phi[(\log\tau-\gamma)/\sigma]$ and $\phi(.)$ is the standard normal probability density function. When the partial derivative of θ with respect to γ satisfies:

$$\frac{\partial\theta(\mu,\gamma)}{\partial\gamma}>\frac{f(\theta)^2\frac{1}{\sigma}g(\tau)}{\left(1-G(\tau)\right)f(\theta)q(\theta)^{1+\xi}G(\tau)}=\frac{\theta(1+\theta^{\xi})\frac{1}{\sigma}g(\tau)}{\left(1-G(\tau)\right)G(\tau)}>0,$$

it is straightforward to verify that:

$$\frac{\partial}{\partial\gamma}\left[\frac{(1-G(\tau))^{\frac{1-\eta}{\eta\rho}}q(\theta)^{1+\xi}}{f(\theta)\left(1-G(\tau)+f(\theta)G(\tau)\right)}\right]<0,$$

and the values of the cross derivatives can thus be determined:

$$\begin{aligned}
\frac{\partial^2 p(\mu,\gamma)}{\partial\mu\partial\gamma}=&-\left\{\frac{\partial}{\partial\gamma}\left[\frac{(1-G(\tau))^{\frac{1-\eta}{\eta\rho}}q(\theta)^{1+\xi}}{f(\theta)\left(1-G(\tau)+f(\theta)G(\tau)\right)}\right]-\frac{\partial p(\mu,\gamma)}{\partial\gamma}\frac{1}{p^2}\right\} \\
&\cdot\left[\frac{(1-G(\tau))^{\frac{1-\eta}{\eta\rho}}q(\theta)^{1+\xi}}{f(\theta)\left(1-G(\tau)+f(\theta)G(\tau)\right)}+\frac{1}{p}\right]^{-2}\frac{1}{\mu}>0,
\end{aligned}$$

$$\begin{aligned}
\frac{\partial^2 c(\mu,\gamma)}{\partial\mu\partial\gamma}=&-\left\{\frac{\partial p(\mu,\gamma)}{\partial\gamma}-\frac{\partial}{\partial\gamma}\left[\frac{(1-G(\tau))^{\frac{1-\eta}{\eta\rho}}q(\theta)^{1+\xi}}{f(\theta)\left(1-G(\tau)+f(\theta)G(\tau)\right)}\right]\left[\frac{(1-G(\tau))^{\frac{1-\eta}{\eta\rho}}q(\theta)^{1+\xi}}{f(\theta)\left(1-G(\tau)+f(\theta)G(\tau)\right)}\right]^{-2}\right\} \\
&\cdot\left[p+\frac{f(\theta)\left(1-G(\tau)+f(\theta)G(\tau)\right)}{(1-G(\tau))^{\frac{1-\eta}{\eta\rho}}q(\theta)^{1+\xi}}\right]^{-2}\chi^{\varepsilon}<0,
\end{aligned}$$

where $\partial p(\mu,\gamma)/\partial\gamma>0$ according to Equation (D.2). With the derivatives of p and c determined, deriving the rest of the derivatives in Proposition 6 becomes straightforward. First, concerning product market tightness, its partial and cross derivatives are given by:

$$\frac{\partial\theta(\mu,\gamma)}{\partial\mu}=\frac{1-\eta}{\eta\rho}\frac{\partial p(\mu,\gamma)}{\partial\mu}>0,\ \frac{\partial^2\theta(\mu,\gamma)}{\partial\mu\partial\gamma}=\frac{1-\eta}{\eta\rho}\frac{\partial^2 p(\mu,\gamma)}{\partial\mu\partial\gamma}>0.$$

Those corresponding to the wholesale price are:

$$\frac{\partial r(\mu,\gamma)}{\partial \mu} = \frac{\partial p(\mu,\gamma)}{\partial \mu} > 0, \ \frac{\partial^2 r(\mu,\gamma)}{\partial \mu \partial \gamma} = \frac{\partial^2 p(\mu,\gamma)}{\partial \mu \partial \gamma} > 0.$$

Lastly, regarding the matching cost and spare capacity (or, equivalently, unemployment), their derivatives are expressed as follows:

$$\frac{\partial}{\partial \mu}\left[G(\tau)l - c(\mu,l)\right] = -\frac{\partial c(\mu,\gamma)}{\partial \mu} < 0, \ \frac{\partial^2}{\partial \mu \partial \gamma}\left[G(\tau)l - c(\mu,l)\right] = -\frac{\partial^2 c(\mu,\gamma)}{\partial \mu \partial \gamma} > 0.$$

$$\frac{\partial}{\partial \mu}\left[l - c(\mu,l)\right] = -\frac{\partial c(\mu,\gamma)}{\partial \mu} < 0, \ \frac{\partial^2}{\partial \mu \partial \gamma}\left[l - c(\mu,l)\right] = -\frac{\partial^2 c(\mu,\gamma)}{\partial \mu \partial \gamma} > 0.$$

D.7. Theoretical Prediction on the Effectiveness of Monetary Policy When Productive Capacity Is Constrained

Next, we derive our theoretical prediction for the effectiveness of monetary policy in controlling inflation and output, depending on whether productive capacity of the economy is constrained or not. Similar to the scenario in which the supply chain is disrupted (as in Proposition 6), contractionary monetary policy is more effective at taming inflation and reducing the sensitivity of output when the productive capacity is constrained. The only difference, as we will elaborate below, is that the state-dependent effects of monetary policy are no longer conditional.

Referring to our theoretical model in Section 3, we describe a change in the stance of monetary policy through a change in μ. Whether productive capacity is constrained or not is represented by a change in the inelastic labor supply l. The comparative statics are summarized next.

Proposition 6′. *For any given threshold of reservation transportation cost $\tau > 0$ and parameter values relevant for monetary policy $\mu \in \mathbb{R}^+$ and productive capacity $l \in \mathbb{R}^+$, the responses of the endogenous variables to a change in monetary policy are described by the following partial derivatives:*

$$\frac{\partial c(\mu,l)}{\partial \mu} > 0, \ \frac{\partial p(\mu,l)}{\partial \mu} > 0, \ \frac{\partial \theta(\mu,l)}{\partial \mu} > 0, \ \frac{\partial r(\mu,l)}{\partial \mu} > 0,$$
$$\frac{\partial}{\partial \mu}\left[G(\tau)l - c(\mu,l)\right] < 0, \ \frac{\partial}{\partial \mu}\left[l - c(\mu,l)\right] < 0.$$

The cross derivatives that describe the variations in the responses of the endogenous variables

ascribed to the constrained productive capacity satisfy:

$$\frac{\partial^2 c(\mu,l)}{\partial\mu\partial l}>0,\ \frac{\partial^2 p(\mu,l)}{\partial\mu\partial l}<0,\ \frac{\partial^2\theta(\mu,l)}{\partial\mu\partial l}<0,\ \frac{\partial^2 r(\mu,l)}{\partial\mu\partial l}<0,$$
$$\frac{\partial^2}{\partial\mu\partial l}\left[G(\tau)l-c(\mu,l)\right]<0,\ \frac{\partial^2}{\partial\mu\partial l}\left[l-c(\mu,l)\right]<0,$$

where $c, p, \theta, r, G(\tau)l-c$, and $l-c$ represent consumption (or, equivalently, output), price, product market tightness, wholesale price, matching cost, and spare capacity (or, equivalently, unemployment), respectively.

Proof. Once again, we rely on the implicit function theorem, to derive the partial derivative $\partial p(\mu,l)/\partial\mu$. Consider the function $\mathbb{T}:[p^{min},+\infty)\times\mathbb{R}^+\times\mathbb{R}^+\to\mathbb{R}$:

$$\begin{aligned}\mathbb{T}(p,\mu,l)&=\chi^{\varepsilon}\frac{\mu}{G(\tau)l}-\frac{f(\theta)p}{1-G(\tau)+f(\theta)G(\tau)}\\&=\chi^{\varepsilon}\frac{\mu}{G(\tau)l}-\frac{\left\{1+\left[\frac{1-\eta}{\eta\rho}\left(p-\tau+\beta\int_0^\tau G(z')dz'\right)\right]^{-\xi}\right\}^{-\frac{1}{\xi}}p}{1-G(\tau)+\left\{1+\left[\frac{1-\eta}{\eta\rho}\left(p-\tau+\beta\int_0^\tau G(z')dz'\right)\right]^{-\xi}\right\}^{-\frac{1}{\xi}}G(\tau)}.\end{aligned}$$

Subsequently, assuming the existence of a tuple $(p_0,\mu_0,l_0)\in[p^{min},+\infty)\times\mathbb{R}^+\times\mathbb{R}^+$ such that $\mathbb{T}(p_0,\mu_0,l_0)=0$ and $\partial\mathbb{T}(p,\mu,l)/\partial p|_{p=p_0,\mu=\mu_0,l=l_0}\neq 0$, by the implicit function theorem, there is a neighborhood of (p_0,μ_0,l_0) such that whenever (μ,l) is sufficiently close to (μ_0,l_0), there is a unique p so that $\mathbb{T}(p,\mu,l)=0$. This assignment makes p a continuous function of μ and l. Applying implicit differentiation to $\mathbb{T}(p,\mu,l)$ around (p_0,μ_0,l_0) yields:

$$\frac{\partial p(\mu,l)}{\partial\mu}=-\frac{\partial\mathbb{T}(p,\mu,l)/\partial\mu}{\partial\mathbb{T}(p,\mu,l)/\partial p}.$$

The numerator can be written as:

$$\frac{\partial\mathbb{T}(p,\mu,l)}{\partial\mu}=\chi^{\varepsilon}\frac{1}{G(\tau)l}>0,$$

whereas the denominator is given by:

$$\frac{\partial\mathbb{T}(p,\mu,l)}{\partial p}=-\frac{\left(1-G(\tau)\right)\frac{1-\eta}{\eta\rho}q(\theta)^{1+\xi}p+f(\theta)\left(1-G(\tau)+f(\theta)G(\tau)\right)}{\left(1-G(\tau)+f(\theta)G(\tau)\right)^2}<0.$$

By combining $\partial\mathbb{T}(p,\mu,l)/\partial\mu$ with $\partial\mathbb{T}(p,\mu,l)/\partial p$, we get that:

$$\frac{\partial p(\mu,l)}{\partial\mu}=\frac{1}{\mu}\left[\frac{\left(1-G(\tau)\right)\frac{1-\eta}{\eta\rho}q(\theta)^{1+\xi}}{f(\theta)\left(1-G(\tau)+f(\theta)G(\tau)\right)}+\frac{1}{p}\right]^{-1}>0.$$

Using the expression for the aggregate demand in Equation (25), we can also derive the partial derivative of consumption (or, equivalently, output):

$$\frac{\partial c(\mu,\gamma)}{\partial \mu} = \chi^{\varepsilon}\left[p + \frac{f(\theta)\left(1-G(\tau)+f(\theta)G(\tau)\right)}{\left(1-G(\tau)\right)\frac{1-\eta}{\eta\rho}q(\theta)^{1+\xi}}\right]^{-1} > 0.$$

Next, we study the dependence of the partial derivatives on l by calculating the corresponding cross derivatives. For the price, it is written as:

$$\begin{aligned}\frac{\partial^2 p(\mu,l)}{\partial\mu\partial l} =& \Bigg[\frac{\left(1-G(\tau)\right)\frac{1-\eta}{\eta\rho}\theta^{\xi-1}(1+\xi)(1+\theta^{\xi})^{-\frac{1+\xi}{\xi}-1}}{f(\theta)\left(1-G(\tau)+f(\theta)G(\tau)\right)}\frac{\partial\theta(\mu,l)}{\partial l} \\ &+ \frac{\left(1-G(\tau)\right)\frac{1-\eta}{\eta\rho}q(\theta)^{2(1+\xi)}\left(1-G(\tau)+2f(\theta)G(\tau)\right)}{\left[f(\theta)\left(1-G(\tau)+f(\theta)G(\tau)\right)\right]^2}\frac{\partial\theta(\mu,l)}{\partial l} + \frac{1}{p^2}\frac{\partial p(\mu,l)}{\partial l}\Bigg] \\ &\cdot\left[\frac{\left(1-G(\tau)\right)\frac{1-\eta}{\eta\rho}q(\theta)^{1+\xi}}{f(\theta)\left(1-G(\tau)+f(\theta)G(\tau)\right)}+\frac{1}{p}\right]^{-2}\frac{1}{\mu} < 0,\end{aligned}$$

since the partial derivatives of product market tightness and price with respect to l are both negative, i.e., $\partial\theta(\mu,l)/\partial l < 0$ and $\partial p(\mu,l)/\partial l < 0$.[11] For consumption (or, equivalently, output), it is given by:

$$\begin{aligned}\frac{\partial^2 c(\mu,l)}{\partial\mu\partial l} =& -\Bigg\{\frac{\partial p(\mu,l)}{\partial l} + \Bigg[\frac{\left(1-G(\tau)\right)\frac{1-\eta}{\eta\rho}\theta^{\xi-1}(1+\xi)(1+\theta^{\xi})^{-\frac{1+\xi}{\xi}-1}}{f(\theta)\left(1-G(\tau)+f(\theta)G(\tau)\right)}\frac{\partial\theta(\mu,l)}{\partial l} \\ &+ \frac{\left(1-G(\tau)\right)\frac{1-\eta}{\eta\rho}q(\theta)^{2(1+\xi)}\left(1-G(\tau)+2f(\theta)G(\tau)\right)}{\left[f(\theta)\left(1-G(\tau)+f(\theta)G(\tau)\right)\right]^2}\frac{\partial\theta(\mu,l)}{\partial l}\Bigg]\left[\frac{\left(1-G(\tau)\right)\frac{1-\eta}{\eta\rho}q(\theta)^{1+\xi}}{f(\theta)\left(1-G(\tau)+f(\theta)G(\tau)\right)}\right]^{-2}\Bigg\} \\ &\cdot\left[p+\frac{f(\theta)\left(1-G(\tau)+f(\theta)G(\tau)\right)}{\left(1-G(\tau)\right)\frac{1-\eta}{\eta\rho}q(\theta)^{1+\xi}}\right]^{-2}\chi^{\varepsilon} > 0.\end{aligned}$$

With the derivatives of p and c determined, deriving the rest of the derivatives in Proposition 6′ becomes straightforward. First, concerning product market tightness, its partial and cross derivatives are given by:

$$\frac{\partial\theta(\mu,l)}{\partial\mu} = \frac{1-\eta}{\eta\rho}\frac{\partial p(\mu,l)}{\partial\mu} > 0,\quad \frac{\partial^2\theta(\mu,l)}{\partial\mu\partial l} = \frac{1-\eta}{\eta\rho}\frac{\partial^2 p(\mu,l)}{\partial\mu\partial l} < 0.$$

As for the wholesale price, the derivatives are written as follows:

$$\frac{\partial r(\mu,l)}{\partial\mu} = \frac{\partial p(\mu,l)}{\partial\mu} > 0,\quad \frac{\partial^2 r(\mu,l)}{\partial\mu\partial l} = \frac{\partial^2 p(\mu,l)}{\partial\mu\partial l} < 0.$$

[11] Recall our discussion in Section 3.4 and Appendix D.4, both product market tightness and price will increase following an adverse shock to productive capacity.

Lastly, regarding the matching cost and spare capacity (or, equivalently, unemployment), their derivatives are given by:

$$\frac{\partial}{\partial \mu}\left[G(\tau)l - c(\mu,l)\right] = -\frac{\partial c(\mu,l)}{\partial \mu} < 0,\ \frac{\partial^2}{\partial \mu \partial l}\left[G(\tau)l - c(\mu,l)\right] = -\frac{\partial^2 c(\mu,l)}{\partial \mu \partial l} < 0,$$

$$\frac{\partial}{\partial \mu}\left[l - c(\mu,l)\right] = -\frac{\partial c(\mu,l)}{\partial \mu} < 0,\ \frac{\partial^2}{\partial \mu \partial l}\left[l - c(\mu,l)\right] = -\frac{\partial^2 c(\mu,l)}{\partial \mu \partial l} < 0.$$

■

D.8. Fixed Price Aggregate Supply

In contrast to the flexible price aggregate supply discussed in the main text, we consider here an alternative pricing mechanism in which the price of goods is fixed, while the reservation transportation cost can vary. The fixed price aggregate supply is defined below, and its key analytical properties are summarized in Proposition 2′.

Definition 2″. *For an arbitrary price $\kappa \in (0,+\infty)$, the fixed price aggregate supply c_s^{fix} is the function of reservation transportation cost $\bar{z}$ defined by:*

$$c_s^{fix}(\bar{z}) = \frac{\left\{1+\left[\frac{1-\eta}{\eta\rho}\left(\kappa-\bar{z}+\beta\int_0^{\bar{z}}G(z')dz'\right)\right]^{-\xi}\right\}^{-\frac{1}{\xi}}G(\bar{z})l}{1-G(\bar{z})+\left\{1+\left[\frac{1-\eta}{\eta\rho}\left(\kappa-\bar{z}+\beta\int_0^{\bar{z}}G(z')dz'\right)\right]^{-\xi}\right\}^{-\frac{1}{\xi}}G(\bar{z})}, \tag{D.6}$$

for all $\bar{z} \in (0, \bar{z}^{max}]$, where $\bar{z}^{max}$ satisfies:

$$\kappa - \bar{z}^{max} + \beta\int_0^{\bar{z}^{max}} G(z')dz' = 0. \tag{D.7}$$

Proposition 2′. *The fixed price aggregate supply c_s^{fix} has the following properties:*

1. $\lim_{\bar{z}\to 0^+} c_s^{fix}(\bar{z}) = 0$;
2. $c_s^{fix}(\bar{z}^{max}) = 0$; *and*
3. *There exists at least one $\bar{z}^* \in (0, \bar{z}^{max}]$ such that $dc_s^{fix}(\bar{z})/d\bar{z}|_{\bar{z}=\bar{z}^*} = 0$.*

Proof. It is straightforward to prove the first property. When $\bar{z} \to 0^+$, $\lim_{\bar{z}\to 0^+}\theta(\bar{z}) = (1-\eta)\kappa/(\eta\rho)$, $\lim_{\bar{z}\to 0^+} f\left(\theta(\bar{z})\right) = \{1+[(1-\eta)\kappa/(\eta\rho)]^{-\xi}\}^{-1/\xi} > 0$. At the same time, when $\bar{z} \to 0^+$, $\lim_{\bar{z}\to 0^+} G(\bar{z}) = 0$. Therefore, $\lim_{\bar{z}\to 0^+} c_s^{fix}(\bar{z}) = 0$. In terms of the second property, it is obvious

from the definition of $\bar{z}^{max}$, together with $f(0) = 0$. Regarding the last property, the derivative of c_s^{fix} with respect to $\bar{z}$ can be expressed as follows:

$$\frac{dc_s^{fix}(\bar{z})}{d\bar{z}} = (1 - G(\bar{z}) + f(\theta)G(\bar{z}))^{-2} \cdot \Big[\underbrace{(1 - G(\bar{z}))\,\frac{1-\eta}{\eta\rho}\,(-1 + \beta G(\bar{z}))\,\theta^{-\xi-1} f(\theta)^{1+\xi} G(\bar{z}) l}_{\substack{\text{Product Market Tightness} \\ \text{Channel} < 0}} + \underbrace{f(\theta)\frac{1}{\bar{z}\sigma} g(\bar{z}) l}_{\substack{\text{Separation Margin} \\ \text{Channel} > 0}} \Big],$$

where $G(\bar{z}) \equiv \Phi[(\log \bar{z} - \gamma)/\sigma]$, $g(\bar{z}) \equiv \phi[(\log \bar{z} - \gamma)/\sigma]$, while $\Phi(.)$ and $\phi(.)$ are the standard normal cumulative density function and probability density function respectively. The product market tightness channel is negative, because a higher reservation transportation cost would reduce the total surplus to be shared between producers and retailers at the margin, hence dampening the incentives for retailers to visit producers, leading to a slack product market as well as a lower aggregate supply. On the other hand, the separation margin channel is positive, because a larger proportion of matches that would otherwise have been dismissed could now continue, hence contributing to a higher aggregate supply. The fixed price aggregate supply is determined jointly by these two channels, and the extent to which one channel dominates the other depends on both the parameter values and the reservation transportation cost itself.

When $\bar{z} \to 0^+$, we can show that the slope of the fixed price aggregate supply curve is positive:

$$\lim_{\bar{z}\to 0^+} \frac{dc_s^{fix}(\bar{z})}{d\bar{z}} = \Big\{1 + \left[\frac{(1-\eta)\kappa}{\eta\rho}\right]^{-\xi}\Big\}^{-\frac{1}{\xi}} \lim_{\bar{z}\to 0^+} \frac{1}{\bar{z}\sigma} g(\bar{z}) l > 0,$$

since the probability density function of a log-normal distribution is always positive. When $\bar{z} \to \bar{z}^{max}$, the slope becomes negative:

$$\lim_{\bar{z}\to \bar{z}^{max}} \frac{dc_s^{fix}(\bar{z})}{d\bar{z}} = \frac{1}{1 - G(\bar{z}^{max})} \frac{1-\eta}{\eta\rho}\,(-1 + \beta G(\bar{z}^{max}))\,G(\bar{z}^{max}) l < 0.$$

Consider $\varepsilon > 0$ such that $dc_s^{fix}(\bar{z})/d\bar{z}|_{\bar{z}=\varepsilon}$ and $\lim_{\bar{z}\to 0^+} dc_s^{fix}(\bar{z})/d\bar{z}$ have the same sign. By the intermediate value theorem, since $dc_s^{fix}(\bar{z})/d\bar{z}$ is continuous on $[\varepsilon, \bar{z}^{max}]$, there must exist at least one $\bar{z}^* \in [\varepsilon, \bar{z}^{max}]$ such that $dc_s^{fix}(\bar{z})/d\bar{z}|_{\bar{z}=\bar{z}^*} = 0$. Since $[\varepsilon, \bar{z}^{max}]$ is a sub-interval of $(0, \bar{z}^{max}]$, the last property thus holds. ■

To plot the fixed price aggregate supply, we also need to pin down its curvature. Since the value of the second derivative of c_s^{fix} cannot be determined analytically, we resort to numerical

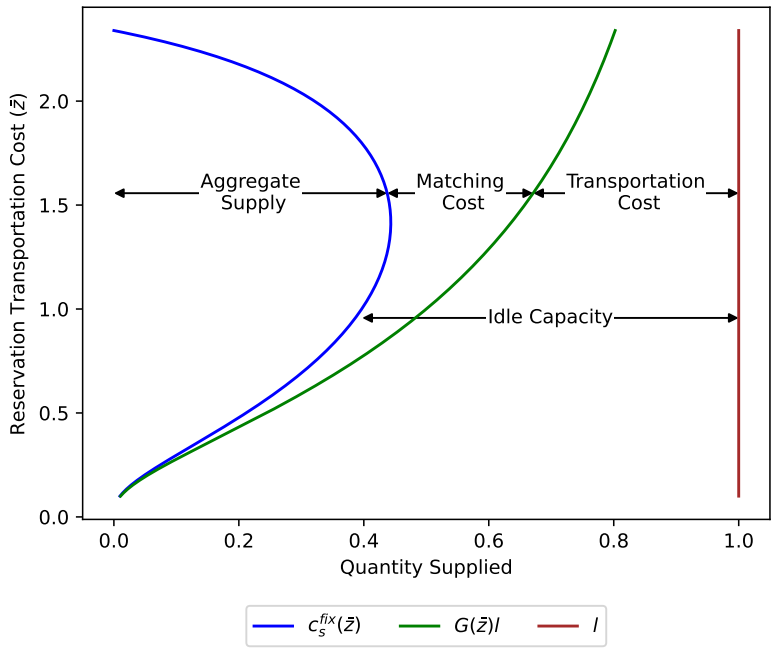

Figure D.2: Supply Side of the Economy When the Price of Goods Is Fixed

Notes. The figure plots the fixed price aggregate supply $c_s^{fix}(\bar{z})$, the maximum volume of goods supply if the matching frictions were absent $G(\bar{z})l$, and l for specific values of $\bar{z}$. The difference between $c_s^{fix}(\bar{z})$ and $G(\bar{z})l$ signifies the matching cost, while the difference between $G(\bar{z})l$ and l denotes the transportation cost (measured in units of goods). The gap between $c_s^{fix}(\bar{z})$ and l represents the spare capacity of producers, or, equivalently, unemployment. For the numerical approximation, the parameter values are set as follows: $\eta = 0.5, \rho = 0.5, \kappa = 1.2, \beta = 0.99, \xi = 2, l = 1, \gamma = 0$, and $\sigma = 1$. The value of $\bar{z}$ is derived from 1,000 evenly spaced numbers over the interval $[0.1, \bar{z}^{max}]$, where $\bar{z}^{max}$ is numerically determined based on its definition in Equation (D.7).

methods for an approximation. Figure D.2 plots the fixed price aggregate supply, along with the maximum volume of goods supply if the search and matching frictions were absent, and productive capacity. As observed, the non-monotonic behavior of the fixed price aggregate supply clearly illustrates the two aforementioned counteracting channels at play. Specifically, when the reservation transportation cost is relatively low, the separation margin channel dominates the product market tightness channel, and *vice versa*. Consequently, there exists a level of reservation transportation cost at which the aggregate supply is maximized. This behavior is akin to that considered in Michaillat and Saez (2015), where both the search and matching frictions in the product market and the matching cost per visit lead to the non-standard behavior of the aggregate supply curve.[12]

In terms of the other variables of interest, as the reservation transportation cost increases,

[12]In contrast to our fixed price aggregate supply curve, which is plotted in the $(c, \bar{z})$ plane, the aggregate supply curve in Michaillat and Saez (2015) is plotted in the (c, x) plane, where x refers to product market tightness. See Figure I of their paper for details.

the matching cost ($G(\bar{z})l - c$) rises, the transportation cost ($(1 - G(\bar{z}))l$) declines, and the spare capacity (or, equivalently, unemployment) represented by $l - c$ first decreases and then increases.

D.9. Supply Chain Disruptions and Reduced Matching Efficiency

Now, we extend our theoretical model by representing supply chain disruption as a reduction in matching efficiency when producers and retailers meet to form a match. This reduction in matching efficiency decreases the probability of retailers meeting producers, thus imposing larger costs on retailers to form a match. As we will elaborate below, modeling supply chain disturbances as a reduction in matching efficiency results in the same set of comparative statics on consumption, price, and spare capacity (or, equivalently, unemployment) as an increase in transportation cost (recall Table 1). Interestingly, while modeling the disruption as increased transportation costs does not allow for the specific determination of the effects on product market tightness and wholesale price, a reduced matching efficiency does provide this specificity. Lastly, the state-dependent effects of a contractionary monetary policy shock in controlling inflation and output are also maintained in this alternative setting. Specifically, at an equilibrium where the increase in product market tightness is sufficiently large during the supply chain disruption (as stated in Equation (D.10)), the disruption intensifies the decrease (or increase) in inflation while mitigating the decrease (or increase) in consumption (or, equivalently, output) associated with a contractionary (or expansionary) monetary policy shock.

Recall that the matching efficiency, denoted by $A \in (0, 1]$, enters the model via the matching function:

$$\mathscr{M} = A(x_U^{-\xi} + i_U^{-\xi})^{-\frac{1}{\xi}}.$$

Due to its presence, the probability for a producer to meet a retailer becomes:

$$f(\theta) = \frac{\mathscr{M}}{x_U} = A(1 + \theta^{-\xi})^{-\frac{1}{\xi}},$$

and the probability for a retailer to meet a producer changes to:

$$q(\theta) = \frac{\mathscr{M}}{i_U} = A(1 + \theta^{\xi})^{-\frac{1}{\xi}},$$

with product market tightness still defined as $\theta \equiv i_U/x_U$. The function $f(\theta)$ satisfies $f(0) = 0$, $\lim_{\theta \to +\infty} f(\theta) = A$, and $f'(\theta) = A^{-\xi} q(\theta)^{1+\xi} > 0$, whereas $q(\theta)$ satisfies $q(0) = A$, $\lim_{\theta \to +\infty} q(\theta) =$

0, and $q'(\theta) < 0$. $f(\theta)$ and $q(\theta)$ also satisfy $f(\theta)/q(\theta) = \theta$.

Since the model structure remains the same as in the baseline setup except for the matching function, we skip the model details and directly proceed to the comparative statics, focusing on the responses of the macro aggregates to adverse shocks to aggregate demand, productive capacity, and the supply chain at the flexible price steady state defined in Definition 4.

The derivation of the comparative statics for adverse demand and capacity shocks largely follows that in Appendix D.4, except for those related to the matching cost. Recall that the matching cost is measured by the difference between the flexible price aggregate supply and the maximum amount of goods that could be supplied in the absence of search frictions. In contrast to the baseline parameterization, the matching efficiency parameter A in this alternative setting ranges from zero to one, thereby allowing the matching cost to be expressed as follows:

$$\begin{aligned} \textit{matching cost} &= \frac{AG(\tau)}{1-(1-A)G(\tau)}l - c \\ &= \left[\frac{AG(\tau)}{1-(1-A)G(\tau)} - \frac{f(\theta)G(\tau)}{1-G(\tau)+f(\theta)G(\tau)}\right] l. \end{aligned} \tag{D.8}$$

Hence, it is straightforward to verify that the matching cost will increase in the case of an adverse demand shock, while it will decrease when there is a negative productive capacity shock.

Now, we consider the comparative statics for a supply chain disturbance. We first study the effect on price by re-visiting the function $\mathbb{T} : [p^{min}, +\infty) \times (0, 1] \to \mathbb{R}$:

$$\begin{aligned} \mathbb{T}(p, A) &= \chi^{\varepsilon}\frac{\mu}{G(\tau)l} - \frac{f(\theta)p}{1-G(\tau)+f(\theta)G(\tau)} \\ &= \chi^{\varepsilon}\frac{\mu}{G(\tau)l} - \frac{A\left\{1+\left[\frac{1-\eta}{\eta\rho}\left(p-\tau+\beta\int_0^{\tau}G(z')dz'\right)\right]^{-\xi}\right\}^{-\frac{1}{\xi}}p}{1-G(\tau)+A\left\{1+\left[\frac{1-\eta}{\eta\rho}\left(p-\tau+\beta\int_0^{\tau}G(z')dz'\right)\right]^{-\xi}\right\}^{-\frac{1}{\xi}}G(\tau)}. \end{aligned}$$

Assuming the existence of a tuple $(p_0, A_0) \in [p^{min}, +\infty) \times (0, 1]$ such that $\mathbb{T}(p_0, A_0) = 0$ and $\partial\mathbb{T}(p, A)/\partial p|_{p=p_0, A=A_0} \neq 0$, by the implicit function theorem, there is a neighborhood of (p_0, A_0) such that whenever A is sufficiently close to A_0, there is a unique p so that $\mathbb{T}(p, A) = 0$. This assignment makes p a continuous function of A. Applying implicit differentiation to $\mathbb{T}(p, A)$ around (p_0, A_0) yields:

$$\frac{dp(A)}{dA} = -\frac{\partial\mathbb{T}(p, A)/\partial A}{\partial\mathbb{T}(p, A)/\partial p}.$$

In terms of $\partial \mathbb{T}(p, A)/\partial A$, it is given by:

$$\frac{\partial \mathbb{T}(p, A)}{\partial A} = -\frac{(1 - G(\tau))\left(1 + \theta^{-\xi}\right)^{-\frac{1}{\xi}} p}{\left(1 - G(\tau) + f(\theta)G(\tau)\right)^2} < 0.$$

As for $\partial \mathbb{T}(p, A)/\partial p$, it can be written as follows:

$$\frac{\partial \mathbb{T}(p, A)}{\partial p} = -\frac{(1 - G(\tau))\frac{1-\eta}{\eta\rho} A^{-\xi} q(\theta)^{1+\xi} p + f(\theta)\left(1 - G(\tau) + f(\theta)G(\tau)\right)}{\left(1 - G(\tau) + f(\theta)G(\tau)\right)^2} < 0.$$

Substituting both terms into the equation for $dp(A)/dA$ yields:

$$\frac{dp(A)}{dA} = -\frac{(1 - G(\tau))\left(1 + \theta^{-\xi}\right)^{-\frac{1}{\xi}} p}{(1 - G(\tau))\frac{1-\eta}{\eta\rho} A^{-\xi} q(\theta)^{1+\xi} p + f(\theta)\left(1 - G(\tau) + f(\theta)G(\tau)\right)} < 0. \tag{D.9}$$

Consequently, the price p will increase following a reduction in A. Also, given that $dp(A)/dA < 0$, it is straightforward to derive the derivatives of the other endogenous variables with respect to A, except for the matching cost, since both the aggregate supply c and the maximum amount of goods that could be supplied in the absence of search frictions $AG(\tau)l/\left[1 - (1 - A)G(\tau)\right]$ will change following a change in A (see Equation (D.8)). Figure D.3 visualizes the results.

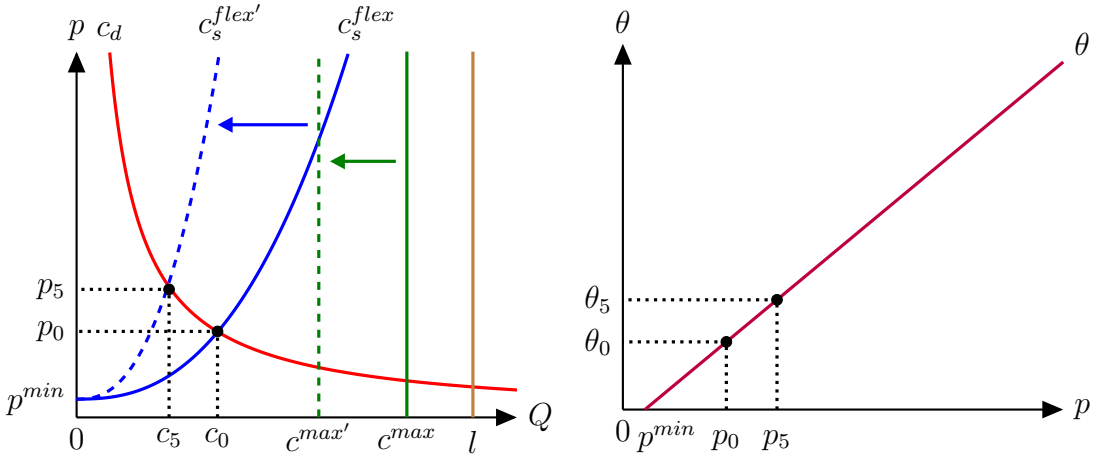

Figure D.3: An Adverse Shock to the Supply Chain, i.e., $A \downarrow$

Notes. c^{max} and $c^{max'}$ represent the maximum quantities of goods that could be supplied in the absence of search frictions, before and after a reduction in matching efficiency A, respectively.

In the last part, we study the state-dependent effects of a contractionary monetary policy shock when the supply chain disruption manifests as a reduction in matching efficiency. To do

so, we re-define the function $\mathbb{T}$ on the joint space of $p \in [p^{min}, +\infty), \mu \in \mathbb{R}^+$, and $A \in (0, 1]$:

$$\mathbb{T}(p, \mu, A) = \chi^{\varepsilon} \frac{\mu}{G(\tau) l} - \frac{A\left\{1 + \left[\frac{1-\eta}{\eta\rho}\left(p - \tau + \beta \int_0^\tau G(z')dz'\right)\right]^{-\xi}\right\}^{-\frac{1}{\xi}} p}{1 - G(\tau) + A\left\{1 + \left[\frac{1-\eta}{\eta\rho}\left(p - \tau + \beta \int_0^\tau G(z')dz'\right)\right]^{-\xi}\right\}^{-\frac{1}{\xi}} G(\tau)}.$$

Assuming the existence of a tuple $(p_0, \mu_0, A_0) \in [p^{min}, +\infty) \times \mathbb{R}^+ \times (0, 1]$ such that $\mathbb{T}(p_0, \mu_0, A_0) = 0$ and $\partial \mathbb{T}(p, \mu, A)/\partial p|_{p=p_0, \mu=\mu_0, A=A_0} \neq 0$, by the implicit function theorem, there is a neighborhood of (p_0, μ_0, A_0) such that whenever (μ, A) is sufficiently close to (μ_0, A_0), there is a unique p so that $\mathbb{T}(p, \mu, A) = 0$. This assignment makes p a continuous function of μ and A. Applying implicit differentiation to $\mathbb{T}(p, \mu, A)$ around (p_0, μ_0, A_0) yields:

$$\frac{\partial p(\mu, A)}{\partial \mu} = -\frac{\partial \mathbb{T}(p, \mu, A)/\partial \mu}{\partial \mathbb{T}(p, \mu, A)/\partial p}.$$

The numerator is written as follows:

$$\frac{\partial \mathbb{T}(p, \mu, A)}{\partial \mu} = \chi^{\varepsilon} \frac{1}{G(\tau) l} > 0,$$

whereas the denominator is given by:

$$\frac{\partial \mathbb{T}(p, \mu, A)}{\partial p} = -\frac{(1 - G(\tau)) \frac{1-\eta}{\eta\rho} A^{-\xi} q(\theta)^{1+\xi} p + f(\theta)\left(1 - G(\tau) + f(\theta) G(\tau)\right)}{\left(1 - G(\tau) + f(\theta) G(\tau)\right)^2} < 0.$$

Combining terms yields the partial derivative of p with respect to μ:

$$\frac{\partial p(\mu, A)}{\partial \mu} = \frac{1}{\mu}\left[\frac{(1 - G(\tau)) \frac{1-\eta}{\eta\rho} A^{-\xi} q(\theta)^{1+\xi}}{f(\theta)\left(1 - G(\tau) + f(\theta) G(\tau)\right)} + \frac{1}{p}\right]^{-1} > 0.$$

For the partial derivative of consumption (or, equivalently, output) with respect to μ, using the expression for the aggregate demand in Equation (25), we can derive that:

$$\frac{\partial c(\mu, A)}{\partial \mu} = \chi^{\varepsilon}\left[p + \frac{f(\theta)\left(1 - G(\tau) + f(\theta) G(\tau)\right)}{(1 - G(\tau)) \frac{1-\eta}{\eta\rho} A^{-\xi} q(\theta)^{1+\xi}}\right]^{-1} > 0.$$

Consequently, both the cross derivatives $\partial^2 p(\mu, A)/\partial \mu \partial A$ and $\partial^2 c(\mu, A)/\partial \mu \partial A$ depend on how the following fraction,

$$\frac{(1 - G(\tau)) \frac{1-\eta}{\eta\rho} A^{-\xi} q(\theta)^{1+\xi}}{f(\theta)\left(1 - G(\tau) + f(\theta) G(\tau)\right)},$$

responds to a decrease in A. Specifically, we show that the partial derivative of the fraction with

respect to A is proportional to the following expression:

$$\begin{aligned}
&\frac{\partial}{\partial A}\left[\frac{(1-G(\tau))^{\frac{1-\eta}{\eta\rho}}A^{-\xi}q(\theta)^{1+\xi}}{f(\theta)\left(1-G(\tau)+f(\theta)G(\tau)\right)}\right] \\
&\propto -(1+\theta^{-\xi})^{-\frac{1}{\xi}}\left(1-G(\tau)+A(1+\theta^{-\xi})^{-\frac{1}{\xi}}G(\tau)\right)\theta^{\xi-1}(1+\xi)(1+\theta^{\xi})^{-\frac{1+\xi}{\xi}-1}\frac{\partial\theta(\mu,A)}{\partial A} \\
&\quad -(1+\theta^{\xi})^{-\frac{1+\xi}{\xi}}\left(1-G(\tau)+A(1+\theta^{-\xi})^{-\frac{1}{\xi}}G(\tau)\right)\theta^{-(1+\xi)}(1+\theta^{-\xi})^{-\frac{1}{\xi}-1}\frac{\partial\theta(\mu,A)}{\partial A} \\
&\quad -(1+\theta^{\xi})^{-\frac{1+\xi}{\xi}}(1+\theta^{-\xi})^{-\frac{2}{\xi}}G(\tau) \\
&\quad -(1+\theta^{\xi})^{-\frac{1+\xi}{\xi}}A(1+\theta^{-\xi})^{-\frac{1}{\xi}}G(\tau)\theta^{-(1+\xi)}(1+\theta^{-\xi})^{-\frac{1}{\xi}-1}\frac{\partial\theta(\mu,A)}{\partial A}.
\end{aligned}$$

Now, suppose that the partial derivative $\partial\theta(\mu,A)/\partial A$ satisfies the condition defined below:

$$\frac{\partial\theta(\mu,A)}{\partial A} < -\frac{1+\theta^{\xi}}{A\theta^{\xi-1}}, \tag{D.10}$$

we can easily verify that the following inequality holds:

$$-(1+\theta^{-\xi})^{-\frac{1}{\xi}}A(1+\theta^{-\xi})^{-\frac{1}{\xi}}G(\tau)\theta^{\xi-1}(1+\theta^{\xi})^{-\frac{1+\xi}{\xi}-1}\frac{\partial\theta(\mu,A)}{\partial A}-(1+\theta^{\xi})^{-\frac{1+\xi}{\xi}}(1+\theta^{-\xi})^{-\frac{2}{\xi}}G(\tau)>0,$$

and subsequently,

$$\frac{\partial}{\partial A}\left[\frac{(1-G(\tau))^{\frac{1-\eta}{\eta\rho}}A^{-\xi}q(\theta)^{1+\xi}}{f(\theta)\left(1-G(\tau)+f(\theta)G(\tau)\right)}\right]>0.$$

Thus, the cross derivatives of p and c with respect to μ and A can be pinned down:

$$\begin{aligned}
\frac{\partial^2 p(\mu,A)}{\partial\mu\partial A} =& -\left\{\frac{\partial}{\partial A}\left[\frac{(1-G(\tau))^{\frac{1-\eta}{\eta\rho}}A^{-\xi}q(\theta)^{1+\xi}}{f(\theta)\left(1-G(\tau)+f(\theta)G(\tau)\right)}\right]-\frac{\partial p(\mu,A)}{\partial A}\frac{1}{p^2}\right\} \\
&\cdot\left[\frac{(1-G(\tau))^{\frac{1-\eta}{\eta\rho}}A^{-\xi}q(\theta)^{1+\xi}}{f(\theta)\left(1-G(\tau)+f(\theta)G(\tau)\right)}+\frac{1}{p}\right]^{-2}\frac{1}{\mu}<0,
\end{aligned}$$

$$\begin{aligned}
\frac{\partial^2 c(\mu,A)}{\partial\mu\partial A} =& -\left\{\frac{\partial p(\mu,A)}{\partial A}-\frac{\partial}{\partial A}\left[\frac{(1-G(\tau))^{\frac{1-\eta}{\eta\rho}}A^{-\xi}q(\theta)^{1+\xi}}{f(\theta)\left(1-G(\tau)+f(\theta)G(\tau)\right)}\right]\left[\frac{(1-G(\tau))^{\frac{1-\eta}{\eta\rho}}A^{-\xi}q(\theta)^{1+\xi}}{f(\theta)\left(1-G(\tau)+f(\theta)G(\tau)\right)}\right]^{-2}\right\} \\
&\cdot\left[p+\frac{f(\theta)\left(1-G(\tau)+f(\theta)G(\tau)\right)}{(1-G(\tau))^{\frac{1-\eta}{\eta\rho}}A^{-\xi}q(\theta)^{1+\xi}}\right]^{-2}\chi^{\varepsilon}>0,
\end{aligned}$$

where $\partial p(\mu,A)/\partial A < 0$ according to Equation (D.9). Coupled with the partial derivatives $\partial p(\mu,A)/\partial\mu > 0$ and $\partial c(\mu,A)/\partial\mu > 0$, they jointly imply that the supply chain disruption, represented by a reduction in matching efficiency, intensifies the decrease (or increase) in in-

flation while dampening the decrease (or increase) in consumption (or, equivalently, output) associated with a contractionary (or expansionary) monetary policy shock.

In terms of the other variables of interest, their behaviors can also be determined. The partial and cross derivatives for retail market tightness are given by:

$$\frac{\partial \theta(\mu, A)}{\partial \mu} = \frac{1-\eta}{\eta\rho}\frac{\partial p(\mu, A)}{\partial \mu} > 0, \ \frac{\partial^2 \theta(\mu, A)}{\partial \mu \partial A} = \frac{1-\eta}{\eta\rho}\frac{\partial^2 p(\mu, A)}{\partial \mu \partial A} < 0.$$

For the wholesale price, these derivatives are expressed as follows:

$$\frac{\partial r(\mu, A)}{\partial \mu} = \frac{\partial p(\mu, A)}{\partial \mu} > 0, \ \frac{\partial^2 r(\mu, A)}{\partial \mu \partial A} = \frac{\partial^2 p(\mu, A)}{\partial \mu \partial A} < 0.$$

Lastly, in terms of the matching cost, its partial and cross derivatives are given by:

$$\begin{aligned}
\frac{\partial}{\partial \mu}\left[\frac{AG(\tau)}{1-(1-A)G(\tau)}l - c(\mu, A)\right] &= -\frac{\partial c(\mu, A)}{\partial \mu} < 0, \\
\frac{\partial^2}{\partial \mu \partial A}\left[\frac{AG(\tau)}{1-(1-A)G(\tau)}l - c(\mu, A)\right] &= -\frac{\partial^2 c(\mu, A)}{\partial \mu \partial A} < 0,
\end{aligned}$$

and those corresponding to the spare capacity (or, equivalently, unemployment) are:

$$\begin{aligned}
\frac{\partial}{\partial \mu}\left[l - c(\mu, A)\right] &= -\frac{\partial c(\mu, A)}{\partial \mu} < 0, \\
\frac{\partial^2}{\partial \mu \partial A}\left[l - c(\mu, A)\right] &= -\frac{\partial^2 c(\mu, A)}{\partial \mu \partial A} < 0.
\end{aligned}$$

In summary, these derivatives suggest that during a supply chain disruption, the responses of product market tightness and wholesale price become more pronounced. In contrast, the responses of matching cost and spare capacity (or, equivalently, unemployment) are less pronounced.

D.10. Convergence Dynamics

In this appendix, we explore the convergence dynamics of our model from the initial steady state to the new steady state after an aggregate, unexpected, and permanent shock.

The model's dynamics involve the evolution of two key variables – the number of matched producers ($x_{M,t}$) and product market tightness (θ_t) – following each exogenous shock. Two transition equations govern these variables:

$$x_{M,t+1} = A(1+\theta_t^{-\xi})^{-\frac{1}{\xi}} G\left(\frac{\log\tau - \gamma}{\sigma}\right) + \left[1 - A(1+\theta_t^{-\xi})^{-\frac{1}{\xi}}\right] G\left(\frac{\log\tau - \gamma}{\sigma}\right) x_{M,t}, \qquad \text{(D.11)}$$

and

$$\theta_t = \frac{1-\eta}{\eta\rho}\left[\frac{\chi^{\varepsilon}\mu}{x_{M,t}l} - \tau + \beta\int_0^{\tau} G\left(\frac{\log z' - \gamma}{\sigma}\right) dz'\right], \tag{D.12}$$

where $G(\cdot)$ is the standard normal cumulative density function. The other variables of interest, as listed in Table 1, are essentially functions of $x_{M,t}$ and θ_t.

To examine the convergence dynamics, we first calculate the initial and new steady states of the model before and after the change in the respective parameter. This process involves setting $x_{M,t+1} = x_{M,t}$ and simultaneously solving Equations (D.11) and (D.12). Subsequently, assuming that the system starts at the initial steady state, we analyze the rate at which the system converges to the new steady state following each of the shocks of interest. Additionally, we investigate whether this convergence is monotonic.

Table D.1: Baseline Calibration

Parameter	**Description**	**Value**
η	Bargaining power of producer	0.5
ρ	Fixed search cost	0.5
χ	Taste for consumption	1
ε	Elasticity of substitution between c and m/p	2
μ	Nominal money supply	10
l	Labor supply	1
τ	Reservation transportation cost	9
β	Discount factor	0.99
γ	Scale parameter of $G(\cdot)$	1
σ	Shape parameter of $G(\cdot)$	1
A	Matching efficiency	1
ξ	Elasticity of substitution between x_U and i_U	2

We calibrate the model at a bi-weekly frequency using U.S. data (thus, two periods in our model correspond to one lag in our monthly SVAR). The baseline parameter values, which are standard in the literature, are summarized in Table D.1. In particular, we follow Fernández-Villaverde et al. (2024) by setting the bargaining share of the producer, η, to 0.5 to split the total surplus from matching evenly. Also, we set $\tau = 9$ to yield a steady-state value of spare capacity (or, equivalently, unemployment) equal to 12%, the average rate of idleness in the U.S., i.e., the share of time when employed workers are idle due to a lack of activity (Michaillat and Saez,

2015).[13] Lastly, the number of matched producers in the first iteration ($x_{M,1}$) is set to match its initial steady-state value.

D.10.1. An Adverse Shock to Aggregate Demand

We first consider an adverse shock to aggregate demand, represented either by a 10% decrease in the money supply μ from 10 to 9, or by a 10% decrease in the preference for consumption χ from 1 to 0.9. Tables D.2 and D.3 summarize the convergence dynamics of all variables of interest for these two cases, respectively. Meanwhile, Figures D.4 and D.5 plot the dynamics specific to consumption (or, equivalently, output) and price. In both scenarios, the system's convergence to the new steady state is almost instantaneous, requiring only one iteration (the model does not have a variable like capital that could generate persistence). Also, the convergence dynamics are monotonic.

Table D.2: Convergence Dynamics: An Adverse Shock to Aggregate Demand ($\mu = 10 \to 9$)

Iteration	# Matched Producers x_M	Product Market Tightness θ	Consumption (or Output) c	Price p	Wholesale Price r	Matching Cost $\frac{AG(\tau)}{1-(1-A)G(\tau)}l - c$	Spare Capacity (or Unemployment) $l - c$
Initial Steady State	0.884171	15.249329	0.884171	11.310030	13.967347	0.000220	0.115829
1	0.884171	12.987323	0.884171	10.179027	12.836344	0.000220	0.115829
New Steady State	0.884088	12.989230	0.884088	10.179980	12.837298	0.000302	0.115912

Notes. The values of the endogenous variables at the two steady states are calculated by setting $x_{M,t+1} = x_{M,t}$ and solving Equations (D.11) and (D.12) simultaneously. In this process, the parameter μ is set to 10 in the initial steady state and adjusted to 9 in the new steady state (i.e., a 10% decrease). For the first iteration, $x_{M,1}$ is set equal to its value in the initial steady state, and μ is decreased to 9.

[13] According to the Institute for Supply Management, the rate of idleness in the U.S. was approximately 12% before the Great Recession. In an alternative calibration, we target a steady-state value of spare capacity (or, equivalently, unemployment) equal to the average U.S. unemployment rate of 4% during 2017-2019. The convergence dynamics in this scenario are very similar to those when targeting the rate of idleness, and simulation results for this alternative calibration are available upon request.

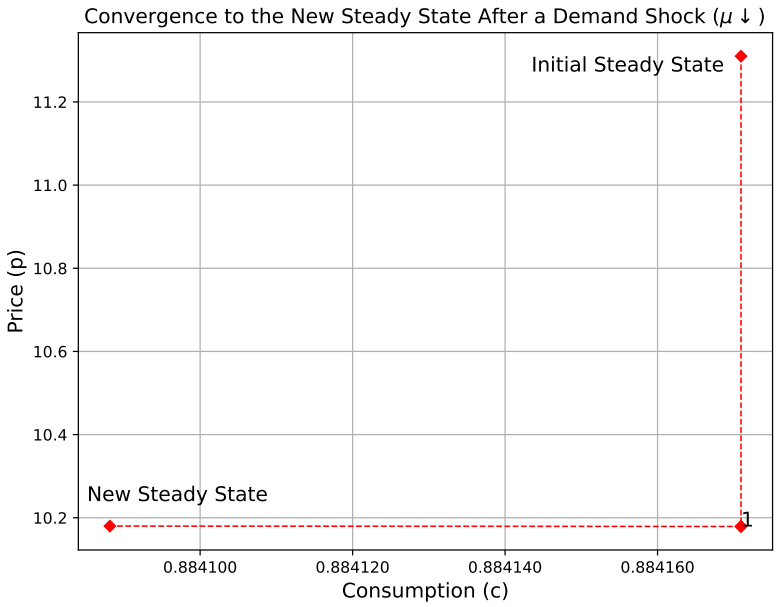

Figure D.4: Convergence Dynamics of Consumption and Price: An Adverse Shock to Aggregate Demand ($\mu = 10 \to 9$)

Notes. The figure plots the convergence dynamics of consumption (or, equivalently, output) and price from their initial steady-state values to their new steady-state values, following an adverse shock to aggregate demand (where μ decreases by 10% from 10 to 9). The iteration numbers are marked on the corresponding dots.

Table D.3: Convergence Dynamics: An Adverse Shock to Aggregate Demand ($\chi = 1 \to 0.9$)

Iteration	# Matched Producers x_M	Product Market Tightness θ	Consumption (or Output) c	Price p	Wholesale Price r	Matching Cost $\frac{AG(\tau)}{1-(1-A)G(\tau)}l - c$	Spare Capacity (or Unemployment) $l - c$
Initial Steady State	0.884171	15.249329	0.884171	11.310030	13.967347	0.000220	0.115829
1	0.884171	10.951518	0.884171	9.161124	11.818442	0.000220	0.115829
New Steady State	0.883966	10.955764	0.883966	9.163248	11.820565	0.000424	0.116034

Notes. The values of the endogenous variables at the two steady states are calculated by setting $x_{M,t+1} = x_{M,t}$ and solving Equations (D.11) and (D.12) simultaneously. In this process, the parameter χ is set to 1 in the initial steady state and adjusted to 0.9 in the new steady state (i.e., a 10% decrease). For the first iteration, $x_{M,1}$ is set equal to its value in the initial steady state, and χ is decreased to 0.9.

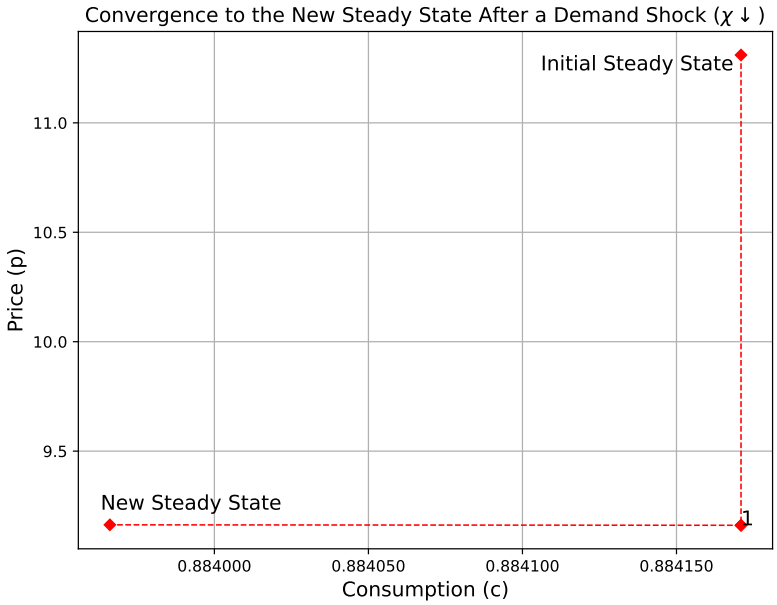

Figure D.5: Convergence Dynamics of Consumption and Price: An Adverse Shock to Aggregate Demand ($\chi = 1 \to 0.9$)

Notes. The figure plots the convergence dynamics of consumption (or, equivalently, output) and price from their initial steady-state values to their new steady-state values, following an adverse shock to aggregate demand (where χ decreases by 10% from 1 to 0.9). The iteration numbers are marked on the corresponding dots.

D.10.2. An Adverse Shock to Productive Capacity

Next, we consider an adverse shock to productive capacity, represented by a 10% decrease in the labor supply l from 1 to 0.9. The convergence dynamics, as observed in Table D.4 and Figure D.6, occur almost instantaneously, requiring only one iteration to reach the new steady state. Furthermore, the process is monotonic.

Table D.4: Convergence Dynamics: An Adverse Shock to Productive Capacity ($l = 1 \to 0.9$)

Iteration	# Matched Producers x_M	Product Market Tightness θ	Consumption (or Output) c	Price p	Wholesale Price r	Matching Cost $\frac{AG(\tau)}{1-(1-A)G(\tau)}l - c$	Spare Capacity (or Unemployment) $l - c$
Initial Steady State	0.884171	15.249329	0.884171	11.310030	13.967347	0.000220	0.115829
1	0.884171	17.762669	0.795754	12.566700	15.224017	0.000198	0.104246
New Steady State	0.884229	17.761033	0.795806	12.565882	15.223199	0.000146	0.104194

Notes. The values of the endogenous variables at the two steady states are calculated by setting $x_{M,t+1} = x_{M,t}$ and solving Equations (D.11) and (D.12) simultaneously. In this process, the parameter l is set to 1 in the initial steady state and adjusted to 0.9 in the new steady state (i.e., a 10% decrease). For the first iteration, $x_{M,1}$ is set equal to its value in the initial steady state, and l is decreased to 0.9.

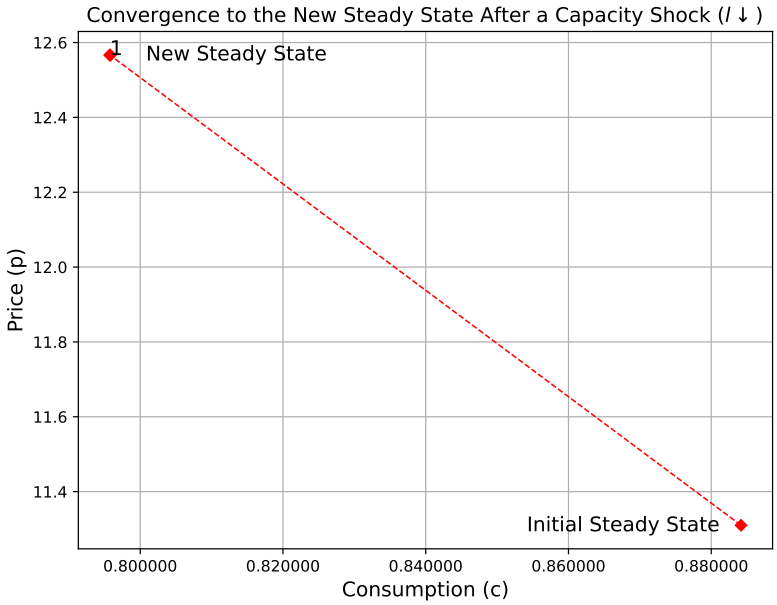

Figure D.6: Convergence Dynamics of Consumption and Price: An Adverse Shock to Productive Capacity ($l = 1 \to 0.9$)

Notes. The figure plots the convergence dynamics of consumption (or, equivalently, output) and price from their initial steady-state values to their new steady-state values, following an adverse shock to productive capacity (where l decreases by 10% from 1 to 0.9). The iteration numbers are marked on the corresponding dots.

D.10.3. An Adverse Shock to the Supply Chain

Lastly, we consider an adverse shock to the supply chain, represented either by a 10% increase in the scale parameter of the log-normal distribution of transportation costs, γ, from 1 to 1.1 (as illustrated in Table D.5 and Figure D.7), or by a 10% decrease in the matching efficiency A from 1 to 0.9 (as detailed in Table D.6 and Figure D.8). The convergence is achieved quickly, with the system requiring two iterations to reach the new steady state in the case of an increase in γ, and four iterations in the case of a decrease in A. Furthermore, as with the cases of adverse shocks to aggregate demand and productive capacity, the convergence dynamics are monotonic.

It is also noteworthy in Table D.5 that, in the scenario of a 10% increase in γ, the resulting price increase is sufficient to raise product market tightness in the new steady state. However, in an alternative scenario with only a 1% increase in γ, as shown in Table D.7, the resulting price increase does not lead to greater tightness in the product market. This observation corroborates our discussion in Section 3.4, which suggests that disturbances to the supply chain can either tighten or loosen product market tightness, depending on the relative magnitudes of the price rise and the decrease in expected profits due to higher transportation costs.

Table D.5: Convergence Dynamics: An Adverse Shock to the Supply Chain ($\gamma = 1 \to 1.1$)

Iteration	# Matched Producers x_M	Product Market Tightness θ	Consumption (or Output) c	Price p	Wholesale Price r	Matching Cost $\frac{AG(\tau)}{1-(1-A)G(\tau)}l - c$	Spare Capacity (or Unemployment) $l - c$
Initial Steady State	0.884171	15.249329	0.884171	11.310030	13.967347	0.000220	0.115829
1	0.884171	14.728412	0.884171	11.310030	13.837118	-0.020443	0.115829
2	0.863499	15.269942	0.863499	11.580795	14.107883	0.000230	0.136501
New Steady State	0.863476	15.270537	0.863476	11.581093	14.108181	0.000252	0.136524

Notes. The values of the endogenous variables at the two steady states are calculated by setting $x_{M,t+1} = x_{M,t}$ and solving Equations (D.11) and (D.12) simultaneously. In this process, the parameter γ is set to 1 in the initial steady state and adjusted to 1.1 in the new steady state (i.e., a 10% increase). For the first iteration, $x_{M,1}$ is set equal to its value in the initial steady state, and γ is increased to 1.1.

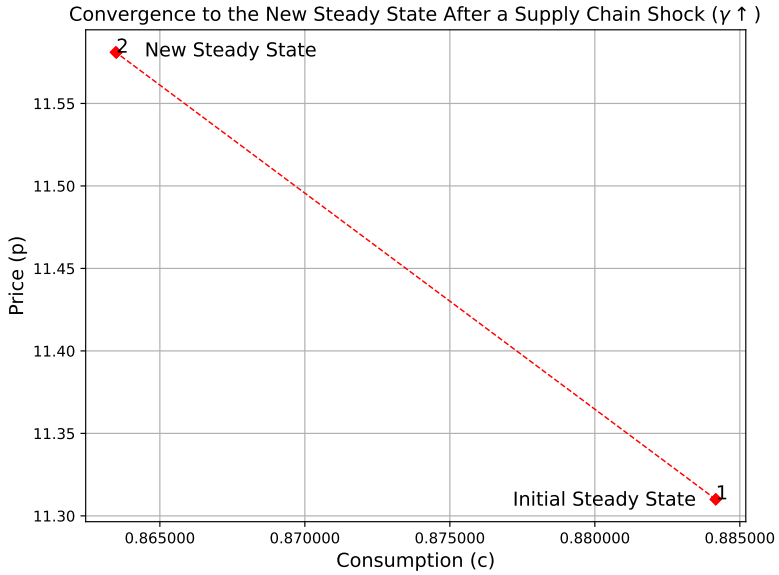

Figure D.7: Convergence Dynamics of Consumption and Price: An Adverse Shock to the Supply Chain ($\gamma = 1 \to 1.1$)

Notes. The figure plots the convergence dynamics of consumption (or, equivalently, output) and price from their initial steady-state values to their new steady-state values, following an adverse shock to the supply chain (where γ increases by 10% from 1 to 1.1). The iteration numbers are marked on the corresponding dots.

Table D.6: Convergence Dynamics: An Adverse Shock to the Supply Chain ($A = 1 \to 0.9$)

Iteration	# Matched Producers x_M	Product Market Tightness θ	Consumption (or Output) c	Price p	Wholesale Price r	Matching Cost $\frac{AG(\tau)}{1-(1-A)G(\tau)}l - c$	Spare Capacity (or Unemployment) $l - c$
Initial Steady State	0.884171	15.249329	0.884171	11.310030	13.967347	0.000220	0.115829
1	0.884171	15.249329	0.884171	11.310030	13.967347	-0.010997	0.115829
2	0.873949	15.513898	0.873949	11.442314	14.099632	-0.000775	0.126051
3	0.873035	15.537861	0.873035	11.454296	14.111613	0.000139	0.126965
4	0.872953	15.540006	0.872953	11.455368	14.112686	0.000221	0.127047
New Steady State	0.872946	15.540198	0.872946	11.455464	14.112781	0.000228	0.127054

Notes. The values of the endogenous variables at the two steady states are calculated by setting $x_{M,t+1} = x_{M,t}$ and solving Equations (D.11) and (D.12) simultaneously. In this process, the parameter A is set to 1 in the initial steady state and adjusted to 0.9 in the new steady state (i.e., a 10% decrease). For the first iteration, $x_{M,1}$ is set equal to its value in the initial steady state, and A is decreased to 0.9.

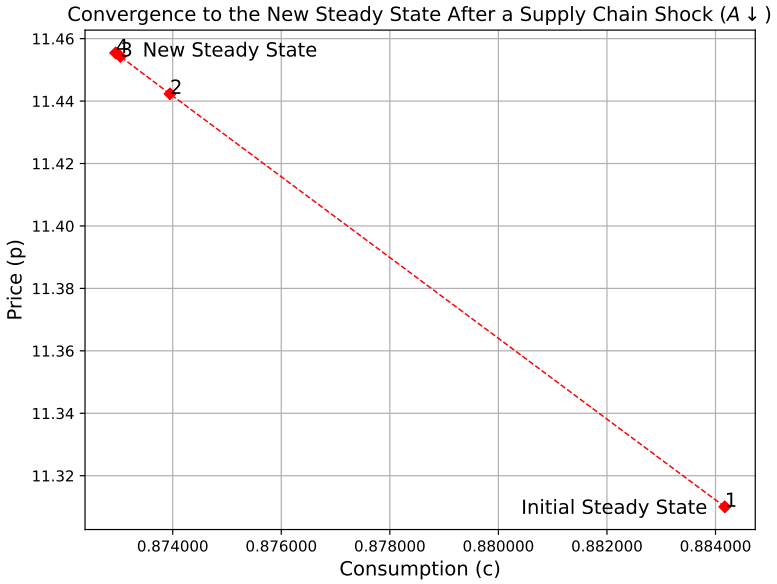

Figure D.8: Convergence Dynamics of Consumption and Price: An Adverse Shock to the Supply Chain ($A = 1 \to 0.9$)

Notes. The figure plots the convergence dynamics of consumption (or, equivalently, output) and price from their initial steady-state values to their new steady-state values, following an adverse shock to the supply chain (where A decreases by 10% from 1 to 0.9). The iteration numbers are marked on the corresponding dots.

Table D.7: Convergence Dynamics: An Adverse Shock to the Supply Chain ($\gamma = 1 \to 1.01$)

Iteration	# Matched Producers x_M	Product Market Tightness θ	Consumption (or Output) c	Price p	Wholesale Price r	Matching Cost $\frac{AG(\tau)}{1-(1-A)G(\tau)}l - c$	Spare Capacity (or Unemployment) $l - c$
Initial Steady State	0.884171	15.249329	0.884171	11.310030	13.967347	0.000220	0.115829
1	0.884171	15.197941	0.884171	11.310030	13.954500	-0.001740	0.115829
2	0.882210	15.248222	0.882210	11.335170	13.979641	0.000221	0.117790
New Steady State	0.882208	15.248280	0.882208	11.335200	13.979670	0.000223	0.117792

Notes. The values of the endogenous variables at the two steady states are calculated by setting $x_{M,t+1} = x_{M,t}$ and solving Equations (D.11) and (D.12) simultaneously. In this process, the parameter γ is set to 1 in the initial steady state and adjusted to 1.01 in the new steady state (i.e., a 1% increase). For the first iteration, $x_{M,1}$ is set equal to its value in the initial steady state, and γ is increased to 1.01.

E. Robustness of SVAR Results

E.1. Dropping the Zero Restrictions

In this appendix, we conduct a robustness check of our baseline results by relaxing the zero restrictions that are imposed on the on-impact responses of the ACR index to aggregate demand and productive capacity shocks in the SVAR estimation.[14] While we impose such zero restrictions in the baseline estimation to sharpen our identification of supply chain disturbances, removing them facilitates the comparison of our ACR index with other indices of supply chain disruptions found in the existing literature. As we will elaborate later in Appendix F, these indices often face potential endogeneity issues – such as higher demand for tradable goods translating into higher shipping prices – and large, time-varying measurement errors. For example, an increase in "delivery times" – the average duration that suppliers take to provide inputs to their customers' factories – reported in the PMI could stem from either a supply chain disruption or a reduction in productive capacity.

Specifically, without the zero restrictions, we re-write the identifying restrictions of the three shocks as follows:

Restriction 1′. ***An adverse shock to aggregate demand*** *leads to a negative response of real GDP, PCE goods price, retail market tightness, and import price, as well as to a positive response of unemployment at* $k = 1$.

Restriction 2′. ***An adverse shock to productive capacity*** *leads to a negative response of real GDP and unemployment, as well as to a positive response of PCE goods price, retail market tightness, and import price at* $k = 1$.

Restriction 3′. ***An adverse shock to the supply chain*** *leads to a negative response of real GDP, as well as to a positive response of PCE goods price, unemployment, and the ACR at* $k = 1$.

The estimation is still carried out using the Bayesian approach as in Arias et al. (2018, 2019, 2023). All the estimation specifications, except for the identifying restrictions, remain the same as those used in the baseline. As can be clearly seen in Figures E.1 through E.5, our main results still hold.

[14] We thank Frank Smets for suggesting this robustness check.

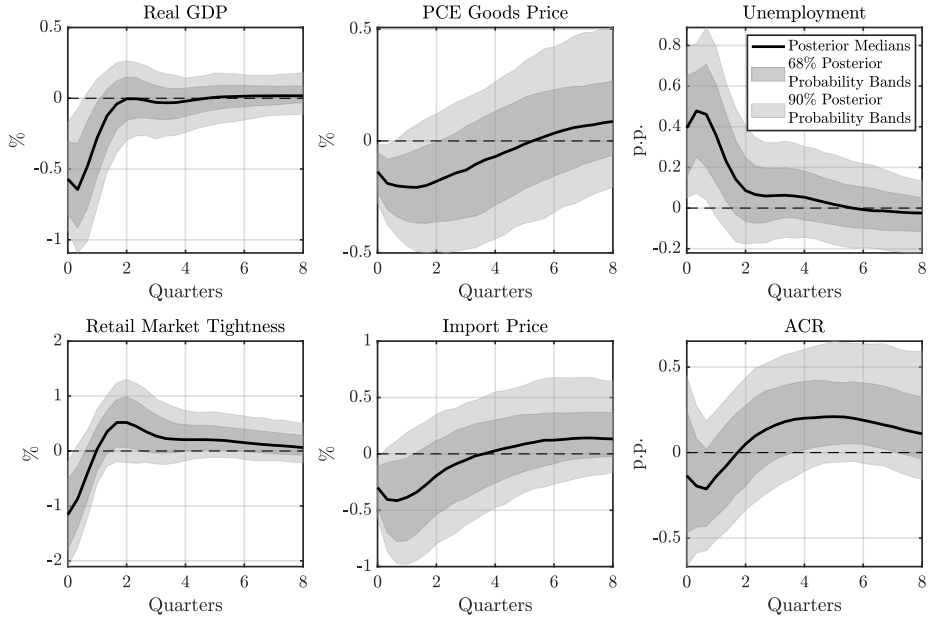

Figure E.1: IRFs to an Adverse Shock to Aggregate Demand: Dropping Zero Restrictions

Notes. The IRFs to a one standard deviation adverse shock to aggregate demand are identified using the ACR index and Restrictions 1′, 2′, and 3′. The solid line shows the point-wise posterior medians and the shaded bands show the 68% and 90% equal-tailed point-wise posterior probability bands. The figure is based on 100,000 independent importance sampling draws.

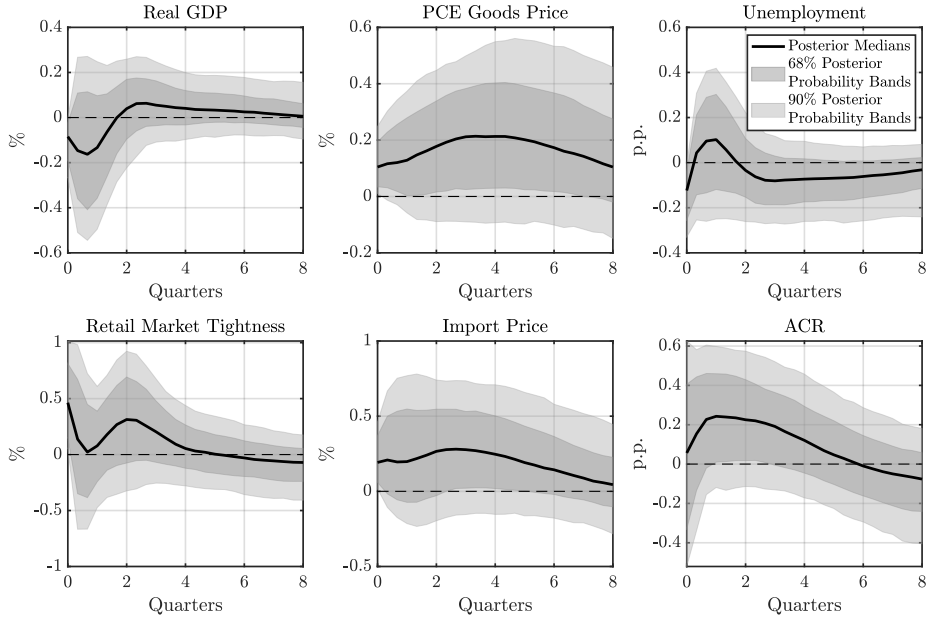

Figure E.2: IRFs to an Adverse Shock to Productive Capacity: Dropping Zero Restrictions

Notes. The IRFs to a one standard deviation adverse shock to productive capacity are identified using the ACR index and Restrictions 1′, 2′, and 3′. The solid line shows the point-wise posterior medians and the shaded bands show the 68% and 90% equal-tailed point-wise posterior probability bands. The figure is based on 100,000 independent importance sampling draws.

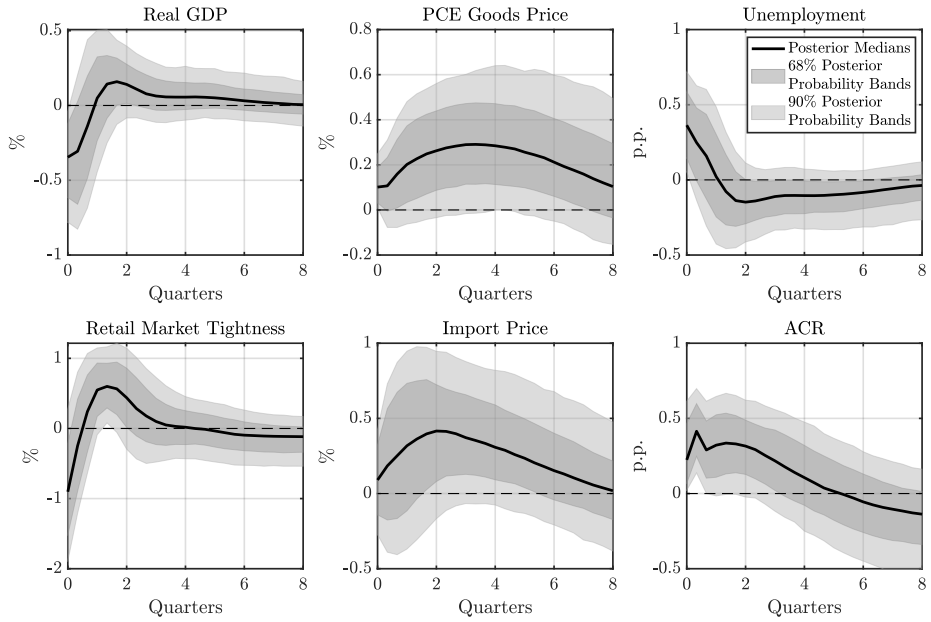

Figure E.3: IRFs to an Adverse Shock to the Supply Chain: Dropping Zero Restrictions

Notes. The IRFs to a one standard deviation adverse shock to the supply chain are identified using the ACR index and Restrictions 1′, 2′, and 3′. The solid line shows the point-wise posterior medians, and the shaded bands show the 68% and 90% equal-tailed point-wise posterior probability bands. The figure is based on 100,000 independent importance sampling draws.

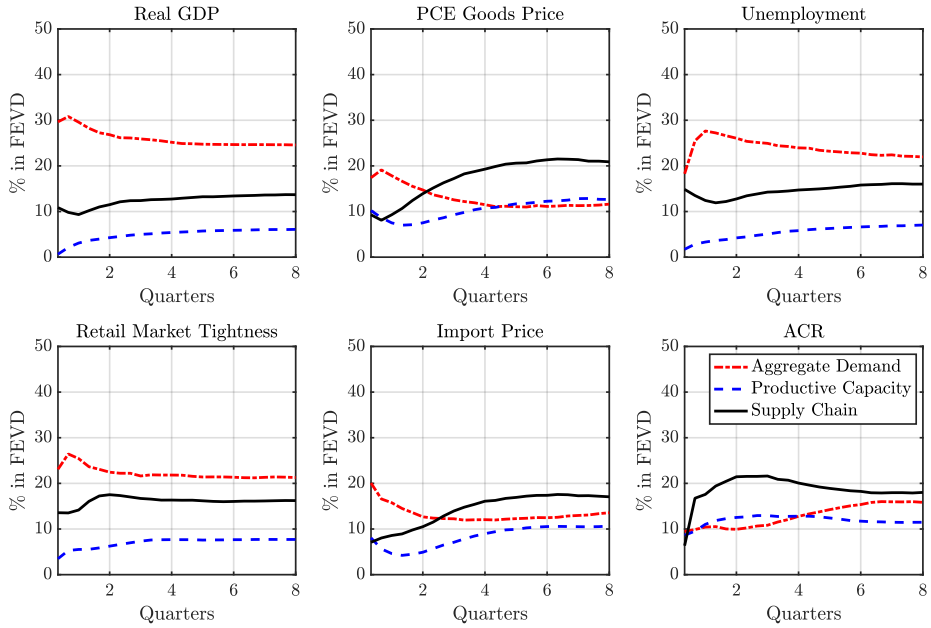

Figure E.4: FEVD from the SVAR: Dropping Zero Restrictions

Notes. Each line presents the median fraction of the forecast error variance for each endogenous variable, explained by each of the three identified structural shocks at various time horizons. The FEVD is estimated using the ACR index and Restrictions 1′, 2′, and 3′, and based on 100,000 independent importance sampling draws.

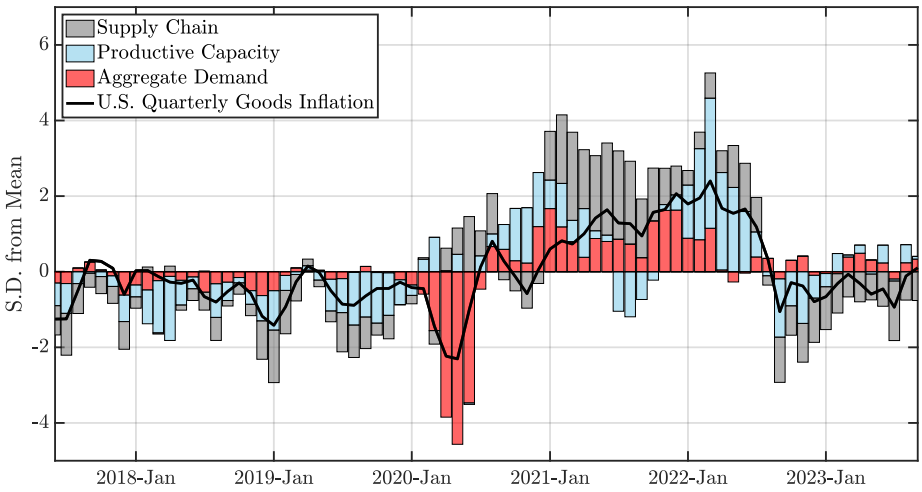

Figure E.5: HD of U.S. Quarter-on-Quarter Goods Inflation: Dropping Zero Restrictions

Notes. The solid line represents the standardized goods inflation rate in the U.S., i.e., the quarter-on-quarter growth of the PCE goods price index. The shaded bars represent the corresponding standardized cumulative historical contribution of shocks to aggregate demand, productive capacity, and the supply chain to goods inflation. The shocks are identified using the SVAR specification in Equation (28), with the ACR index included as the measure of global supply chain disruptions, and Restrictions 1′, 2′, and 3′ imposed on the IRFs of each endogenous variable. The figure is derived from the posterior medians, based on 100,000 independent importance sampling draws.

E.2. Different Lag Structures

In the SVAR estimation, the choice of lag structure critically influences the IRFs since too few lags might miss important dynamics, leading to incomplete IRF patterns. At the same time, too many lags can cause over-fitting and spurious results. Therefore, conducting robustness checks by varying lag lengths and assessing the consistency of IRFs is key.

In Figures E.6 through E.14, we show that the IRFs of adverse shocks to aggregate demand, productive capacity, and the supply chain are robust to considering different lag structures, i.e., one, three, or four lags. We do not consider higher lags due to parameter uncertainty resulting from our limited sample length.

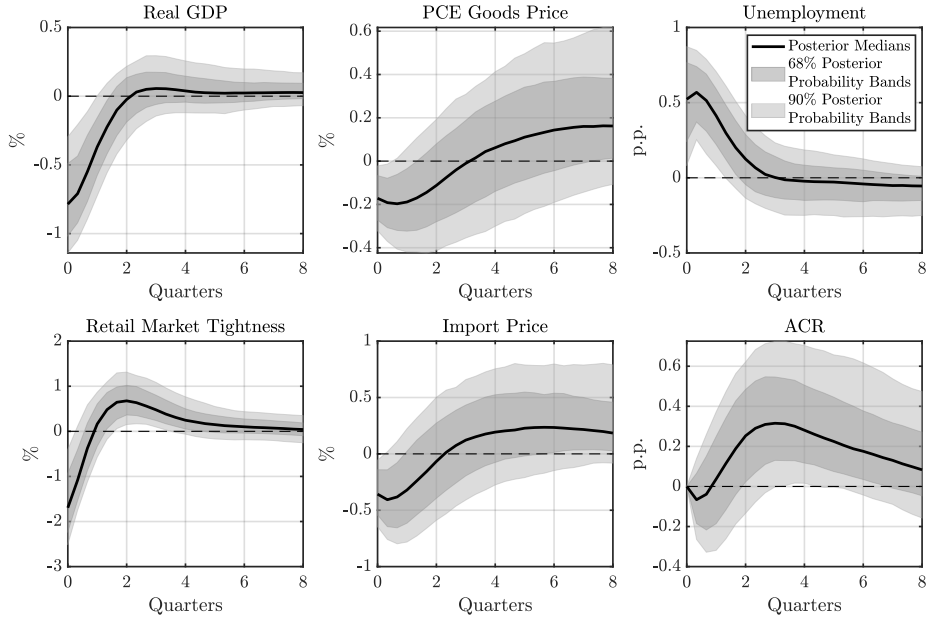

Figure E.6: IRFs to an Adverse Shock to Aggregate Demand: One Lag

Notes. The IRFs to a one standard deviation adverse shock to aggregate demand are identified using an SVAR specification in Equation (28) with one lag, with all other estimation specifications kept the same as in the baseline. The solid line shows the point-wise posterior medians and the shaded bands show the 68% and 90% equal-tailed point-wise posterior probability bands. The figure is based on 100,000 independent importance sampling draws.

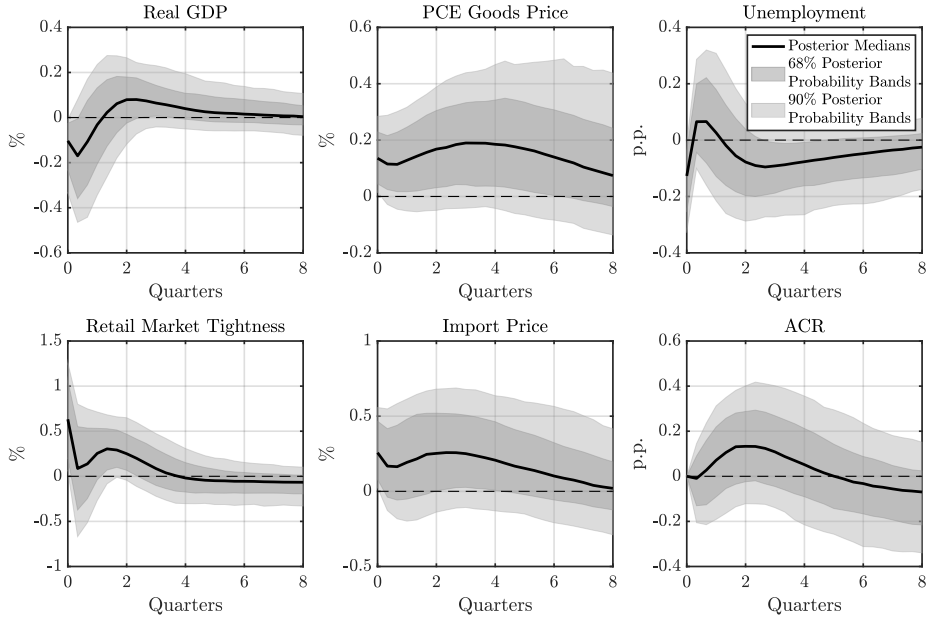

Figure E.7: IRFs to an Adverse Shock to Productive Capacity: One Lag

Notes. The IRFs to a one standard deviation adverse shock to productive capacity are identified using an SVAR specification in Equation (28) with one lag, with all other estimation specifications kept the same as in the baseline. The solid line shows the point-wise posterior medians and the shaded bands show the 68% and 90% equal-tailed point-wise posterior probability bands. The figure is based on 100,000 independent importance sampling draws.

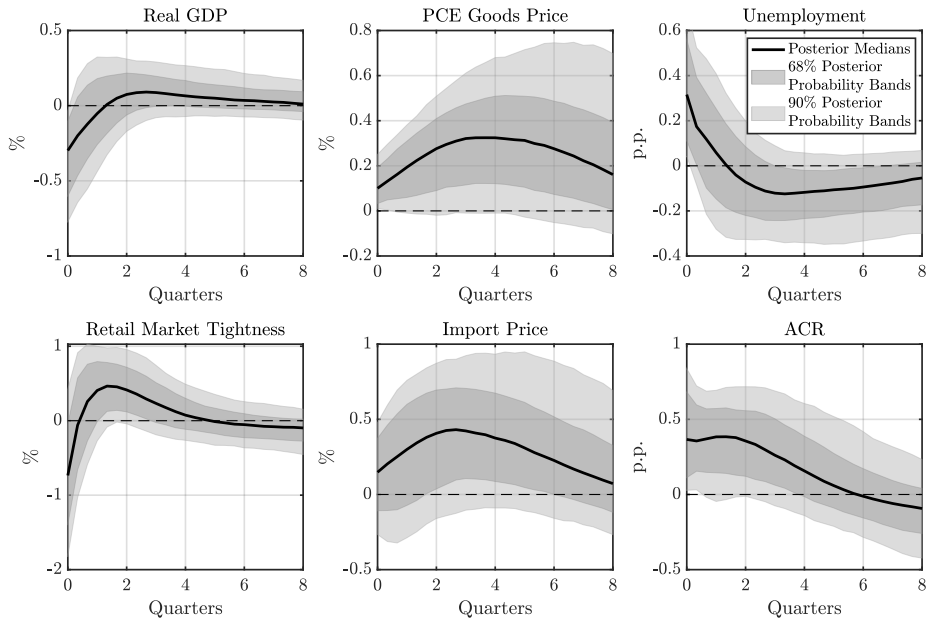

Figure E.8: IRFs to an Adverse Shock to the Supply Chain: One Lag

Notes. The IRFs to a one standard deviation adverse shock to the supply chain are identified using an SVAR specification in Equation (28) with one lag, with all other estimation specifications kept the same as in the baseline. The solid line shows the point-wise posterior medians and the shaded bands show the 68% and 90% equal-tailed point-wise posterior probability bands. The figure is based on 100,000 independent importance sampling draws.

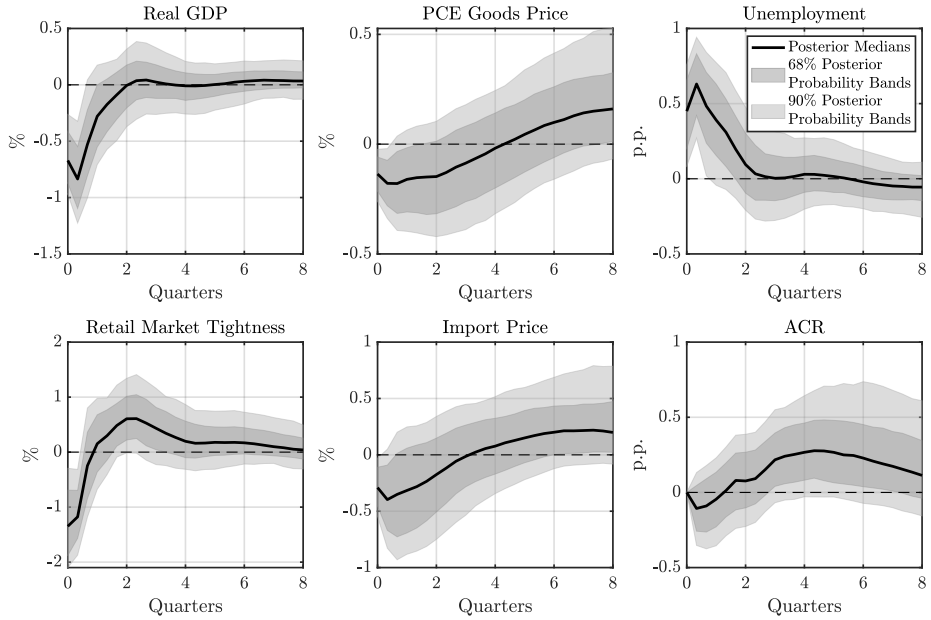

Figure E.9: IRFs to an Adverse Shock to Aggregate Demand: Three Lags

Notes. The IRFs to a one standard deviation adverse shock to aggregate demand are identified using an SVAR specification in Equation (28) with three lags, with all other estimation specifications kept the same as in the baseline. The solid line shows the point-wise posterior medians and the shaded bands show the 68% and 90% equal-tailed point-wise posterior probability bands. The figure is based on 100,000 independent importance sampling draws.

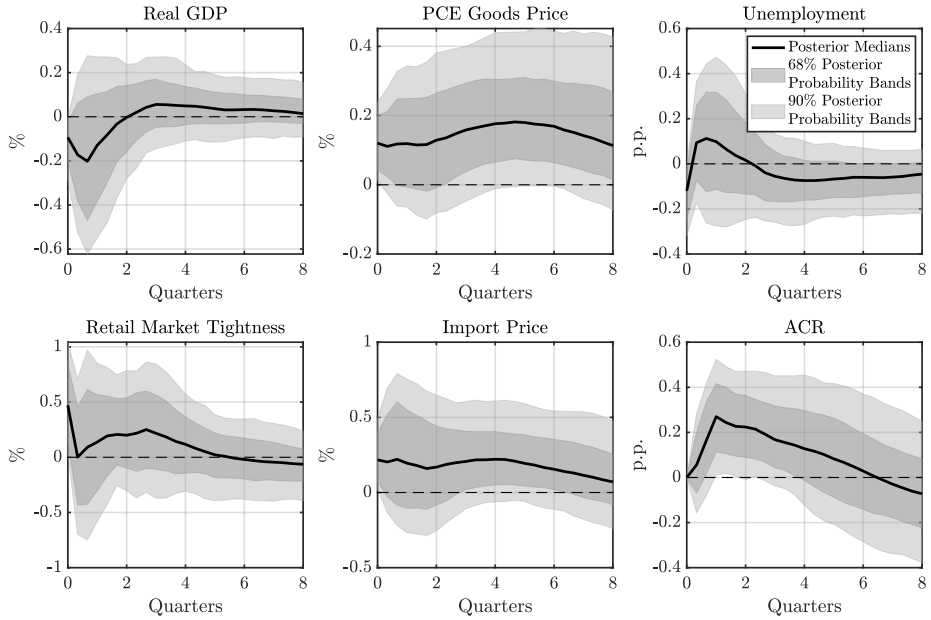

Figure E.10: IRFs to an Adverse Shock to Productive Capacity: Three Lags

Notes. The IRFs to a one standard deviation adverse shock to productive capacity are identified using an SVAR specification in Equation (28) with three lags, with all other estimation specifications kept the same as in the baseline. The solid line shows the point-wise posterior medians and the shaded bands show the 68% and 90% equal-tailed point-wise posterior probability bands. The figure is based on 100,000 independent importance sampling draws.

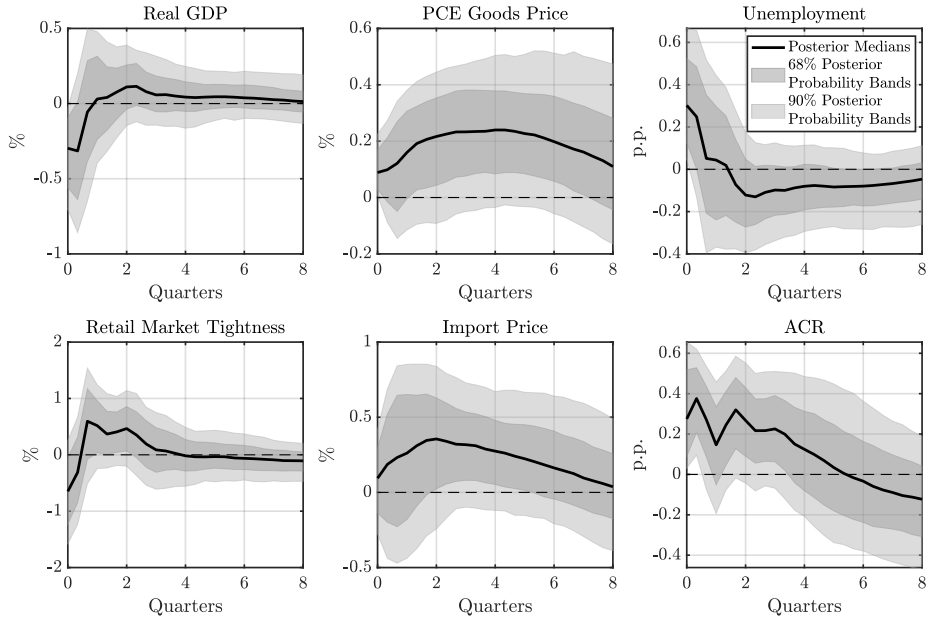

Figure E.11: IRFs to an Adverse Shock to the Supply Chain: Three Lags

Notes. The IRFs to a one standard deviation adverse shock to the supply chain are identified using an SVAR specification in Equation (28) with three lags, with all other estimation specifications kept the same as in the baseline. The solid line shows the point-wise posterior medians and the shaded bands show the 68% and 90% equal-tailed point-wise posterior probability bands. The figure is based on 100,000 independent importance sampling draws.

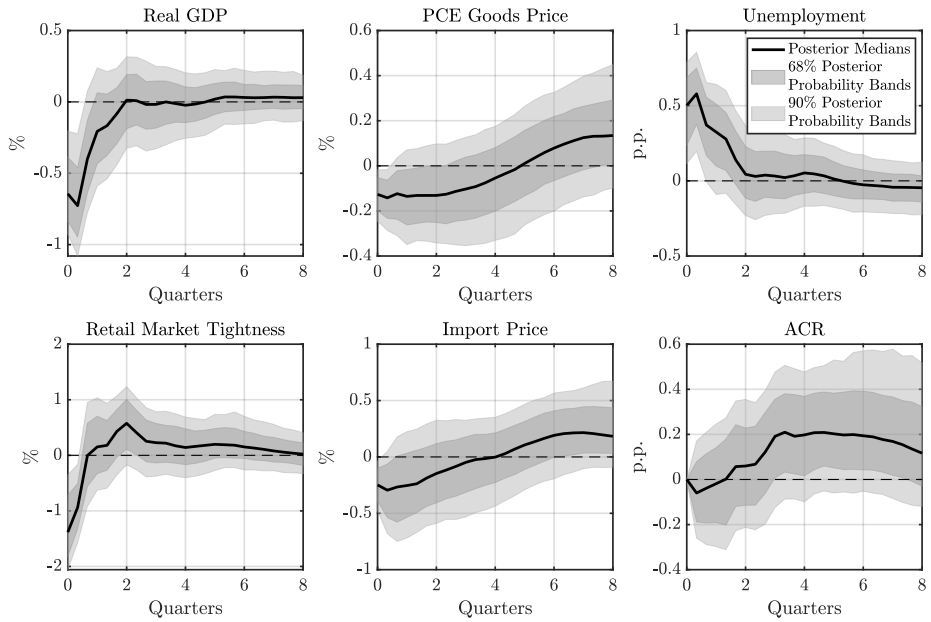

Figure E.12: IRFs to an Adverse Shock to Aggregate Demand: Four Lags

Notes. The IRFs to a one standard deviation adverse shock to aggregate demand are identified using an SVAR specification in Equation (28) with four lags, with all other estimation specifications kept the same as in the baseline. The solid line shows the point-wise posterior medians and the shaded bands show the 68% and 90% equal-tailed point-wise posterior probability bands. The figure is based on 100,000 independent importance sampling draws.

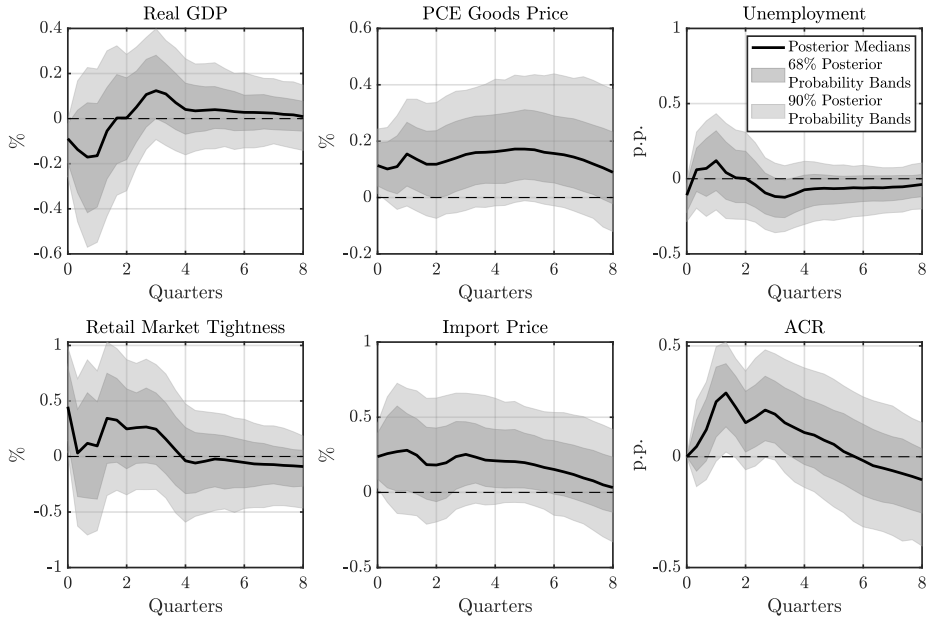

Figure E.13: IRFs to an Adverse Shock to Productive Capacity: Four Lags

Notes. The IRFs to a one standard deviation adverse shock to productive capacity are identified using an SVAR specification in Equation (28) with four lags, with all other estimation specifications kept the same as in the baseline. The solid line shows the point-wise posterior medians and the shaded bands show the 68% and 90% equal-tailed point-wise posterior probability bands. The figure is based on 100,000 independent importance sampling draws.

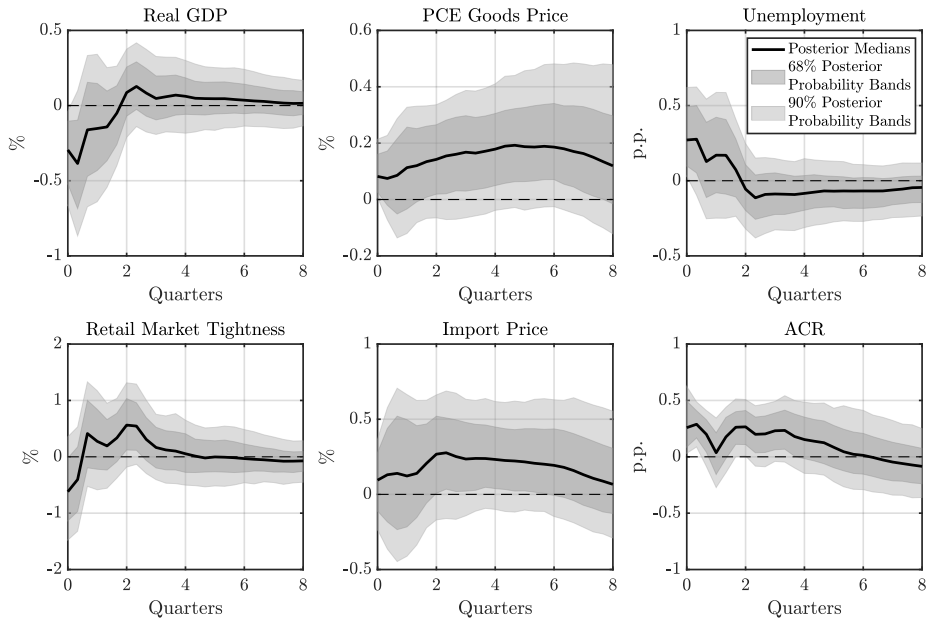

Figure E.14: IRFs to an Adverse Shock to the Supply Chain: Four Lags

Notes. The IRFs to a one standard deviation adverse shock to the supply chain are identified using an SVAR specification in Equation (28) with four lags, with all other estimation specifications kept the same as in the baseline. The solid line shows the point-wise posterior medians and the shaded bands show the 68% and 90% equal-tailed point-wise posterior probability bands. The figure is based on 100,000 independent importance sampling draws.

E.3. Alternative Proxies for Consumption, Prices, Spare Capacity, and Retail Market Tightness

In this appendix, we examine the robustness of our baseline results by replacing real GDP with the real PCE of goods, the PCE goods price with the GDP deflator, the import price with the producer price, and unemployment with spare capacity in the SVAR estimation, respectively. The monthly time series for the real PCE of goods is retrieved directly from FRED using the mnemonic `DGDSRX1`. The monthly time series for the GDP deflator is derived by interpolating the corresponding quarterly series using the Chow-Lin method, based on both the consumer price index and the producer price index. The mnemonics for these three series in the FRED database are `GDPDEF`, `CPIAUCSL`, and `WPSFD49207`. The monthly time series for the U.S. spare capacity is constructed by subtracting the capacity utilization rate, denoted by `TCU`, from 100. As indicated in Figures E.15 through E.26, the IRFs in each of these alternative scenarios remain consistent with those in the baseline estimation.

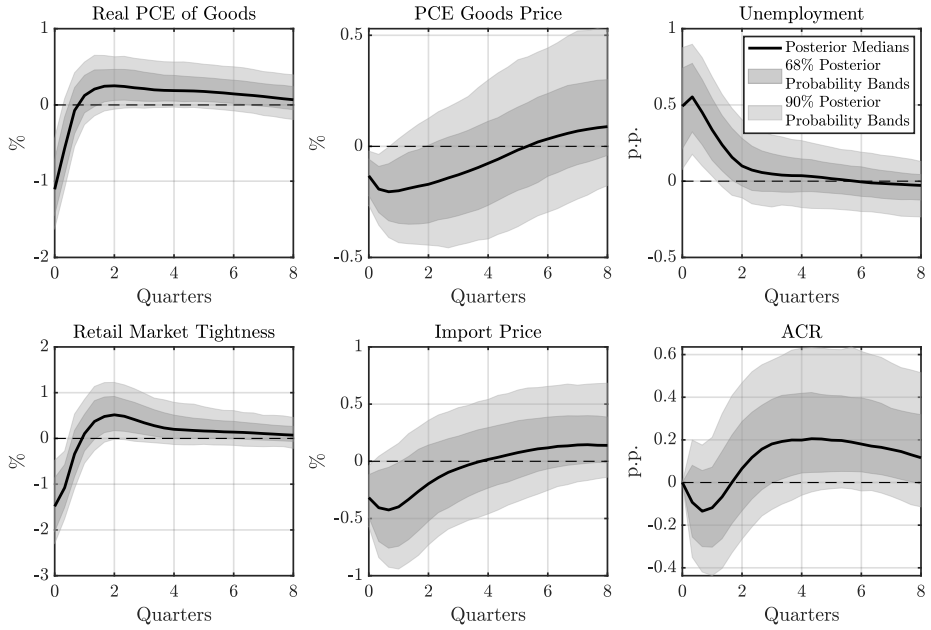

Figure E.15: IRFs to an Adverse Shock to Aggregate Demand: Real PCE of Goods

Notes. The IRFs to a one standard deviation adverse shock to aggregate demand are identified using an SVAR specification in Equation (28), with the real PCE of goods serving as the proxy for output. All other estimation specifications are kept the same as in the baseline. The solid line shows the point-wise posterior medians and the shaded bands show the 68% and 90% equal-tailed point-wise posterior probability bands. The figure is based on 100,000 independent importance sampling draws.

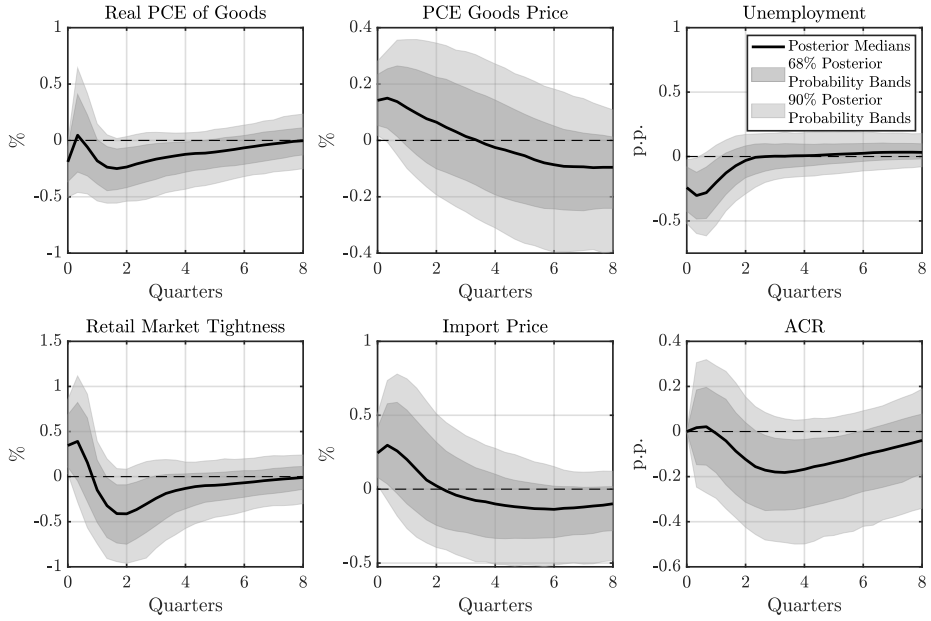

Figure E.16: IRFs to an Adverse Shock to Productive Capacity: Real PCE of Goods

Notes. The IRFs to a one standard deviation adverse shock to productive capacity are identified using an SVAR specification in Equation (28), with the real PCE of goods serving as the proxy for output. All other estimation specifications are kept the same as in the baseline. The solid line shows the point-wise posterior medians and the shaded bands show the 68% and 90% equal-tailed point-wise posterior probability bands. The figure is based on 100,000 independent importance sampling draws.

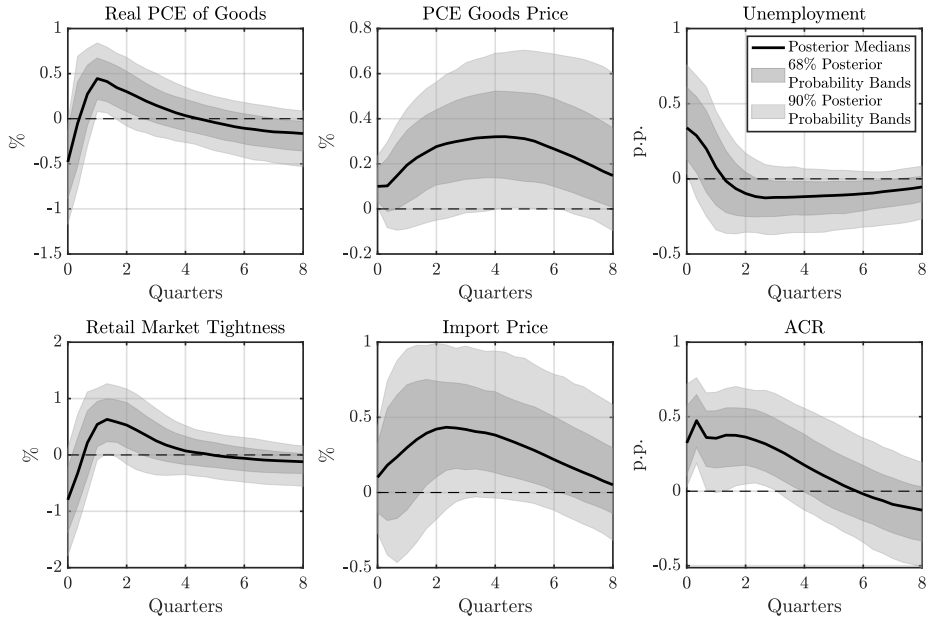

Figure E.17: IRFs to an Adverse Shock to the Supply Chain: Real PCE of Goods

Notes. The IRFs to a one standard deviation adverse shock to the supply chain are identified using an SVAR specification in Equation (28), with the real PCE of goods serving as the proxy for output. All other estimation specifications are kept the same as in the baseline. The solid line shows the point-wise posterior medians and the shaded bands show the 68% and 90% equal-tailed point-wise posterior probability bands. The figure is based on 100,000 independent importance sampling draws.

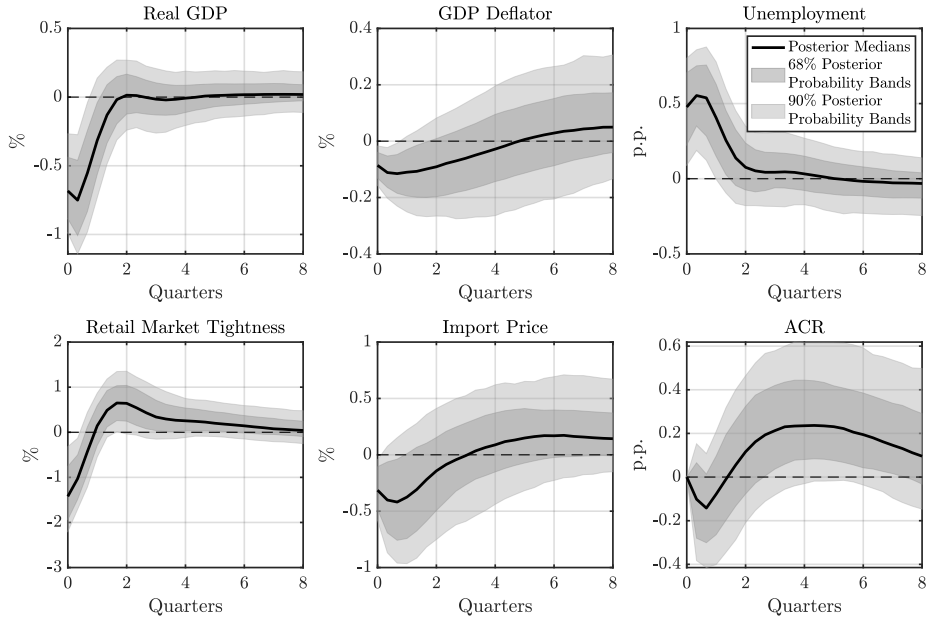

Figure E.18: IRFs to an Adverse Shock to Aggregate Demand: GDP Deflator

Notes. The IRFs to a one standard deviation adverse shock to aggregate demand are identified using an SVAR specification in Equation (28), with the GDP deflator serving as the proxy for price. All other estimation specifications are kept the same as in the baseline. The solid line shows the point-wise posterior medians and the shaded bands show the 68% and 90% equal-tailed point-wise posterior probability bands. The figure is based on 100,000 independent importance sampling draws.

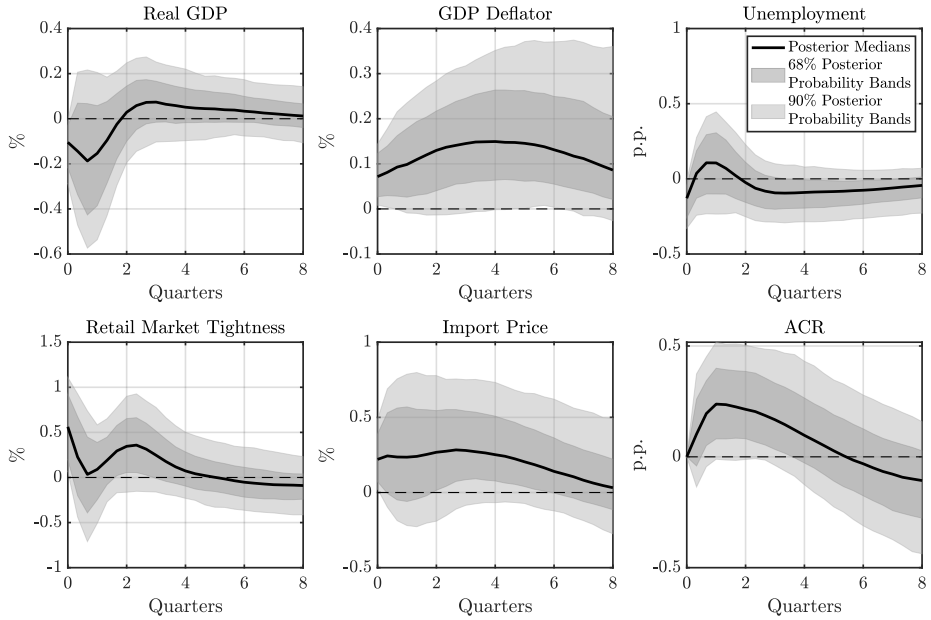

Figure E.19: IRFs to an Adverse Shock to Productive Capacity: GDP Deflator

Notes. The IRFs to a one standard deviation adverse shock to productive capacity are identified using an SVAR specification in Equation (28), with the GDP deflator serving as the proxy for price. All other estimation specifications are kept the same as in the baseline. The solid line shows the point-wise posterior medians and the shaded bands show the 68% and 90% equal-tailed point-wise posterior probability bands. The figure is based on 100,000 independent importance sampling draws.

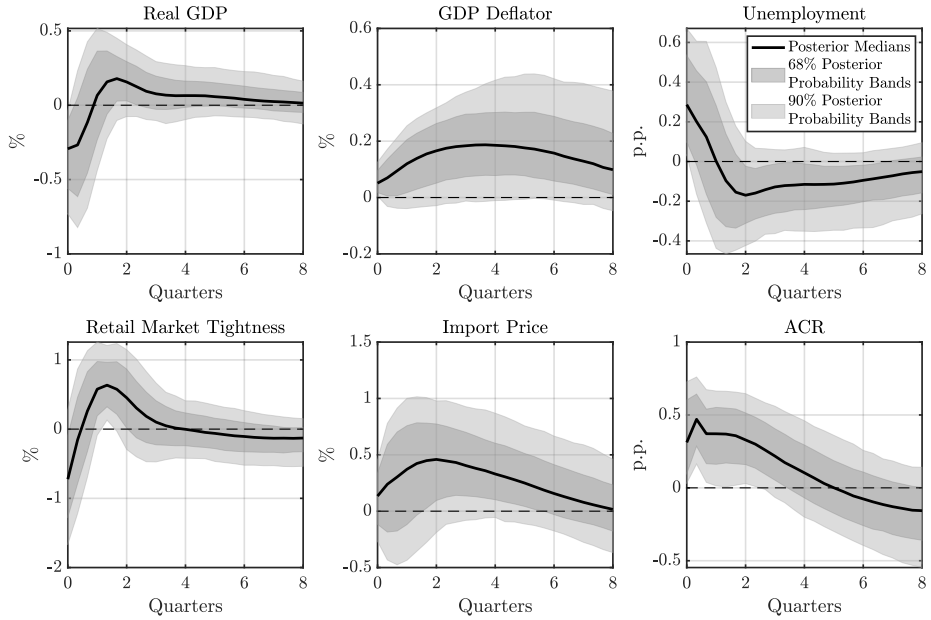

Figure E.20: IRFs to an Adverse Shock to the Supply Chain: GDP Deflator

Notes. The IRFs to a one standard deviation adverse shock to the supply chain are identified using an SVAR specification in Equation (28), with the GDP deflator serving as the proxy for price. All other estimation specifications are kept the same as in the baseline. The solid line shows the point-wise posterior medians and the shaded bands show the 68% and 90% equal-tailed point-wise posterior probability bands. The figure is based on 100,000 independent importance sampling draws.

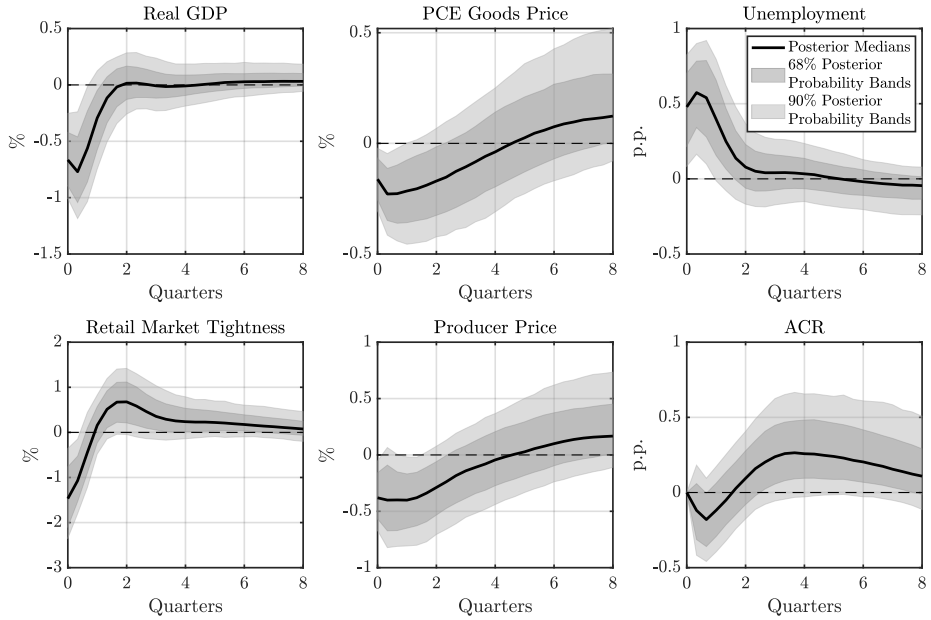

Figure E.21: IRFs to an Adverse Shock to Aggregate Demand: Producer Price

Notes. The IRFs to a one standard deviation adverse shock to aggregate demand are identified using an SVAR specification in Equation (28), with the producer price serving as the proxy for the wholesale price. All other estimation specifications are kept the same as in the baseline. The solid line shows the point-wise posterior medians and the shaded bands show the 68% and 90% equal-tailed point-wise posterior probability bands. The figure is based on 100,000 independent importance sampling draws.

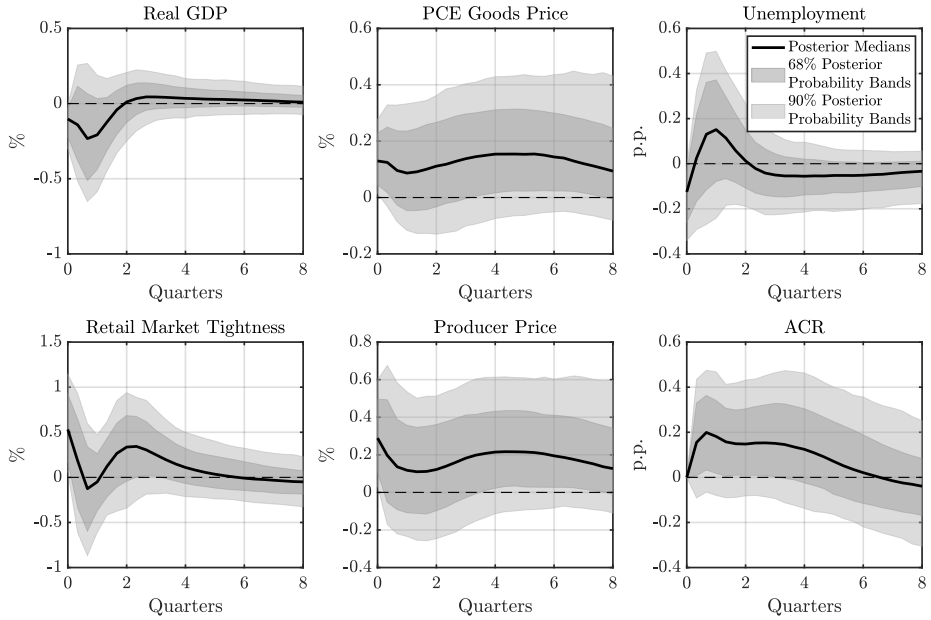

Figure E.22: IRFs to an Adverse Shock to Productive Capacity: Producer Price

Notes. The IRFs to a one standard deviation adverse shock to productive capacity are identified using an SVAR specification in Equation (28), with the producer price serving as the proxy for the wholesale price. All other estimation specifications are kept the same as in the baseline. The solid line shows the point-wise posterior medians and the shaded bands show the 68% and 90% equal-tailed point-wise posterior probability bands. The figure is based on 100,000 independent importance sampling draws.

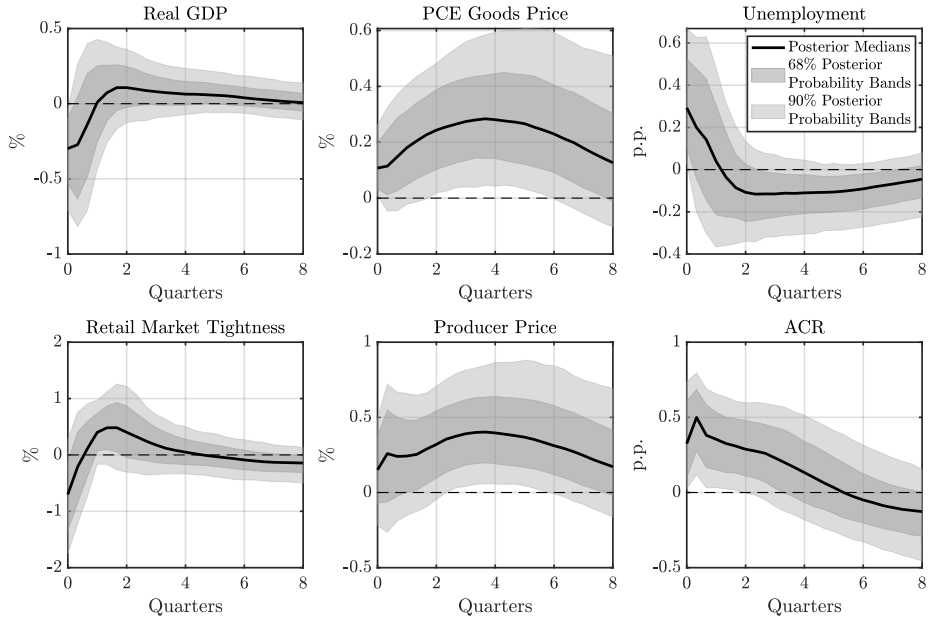

Figure E.23: IRFs to an Adverse Shock to the Supply Chain: Producer Price

Notes. The IRFs to a one standard deviation adverse shock to the supply chain are identified using an SVAR specification in Equation (28), with the producer price serving as the proxy for the wholesale price. All other estimation specifications are kept the same as in the baseline. The solid line shows the point-wise posterior medians and the shaded bands show the 68% and 90% equal-tailed point-wise posterior probability bands. The figure is based on 100,000 independent importance sampling draws.

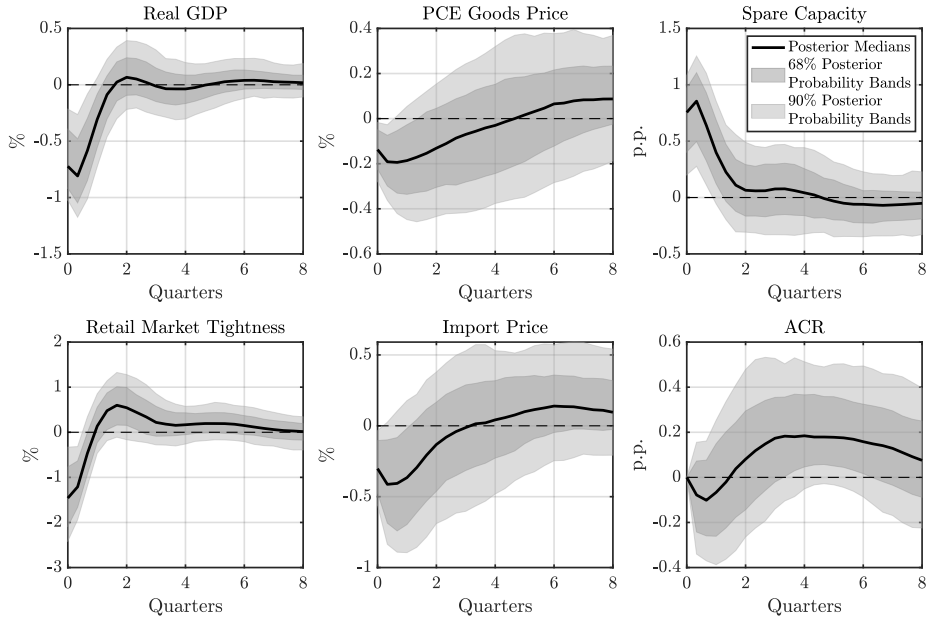

Figure E.24: IRFs to an Adverse Shock to Aggregate Demand: Spare Capacity

Notes. The IRFs to a one standard deviation adverse shock to aggregate demand are identified using an SVAR specification in Equation (28), with the U.S. spare capacity employed in the estimation. All other estimation specifications are kept the same as in the baseline. The solid line shows the point-wise posterior medians and the shaded bands show the 68% and 90% equal-tailed point-wise posterior probability bands. The figure is based on 100,000 independent importance sampling draws.

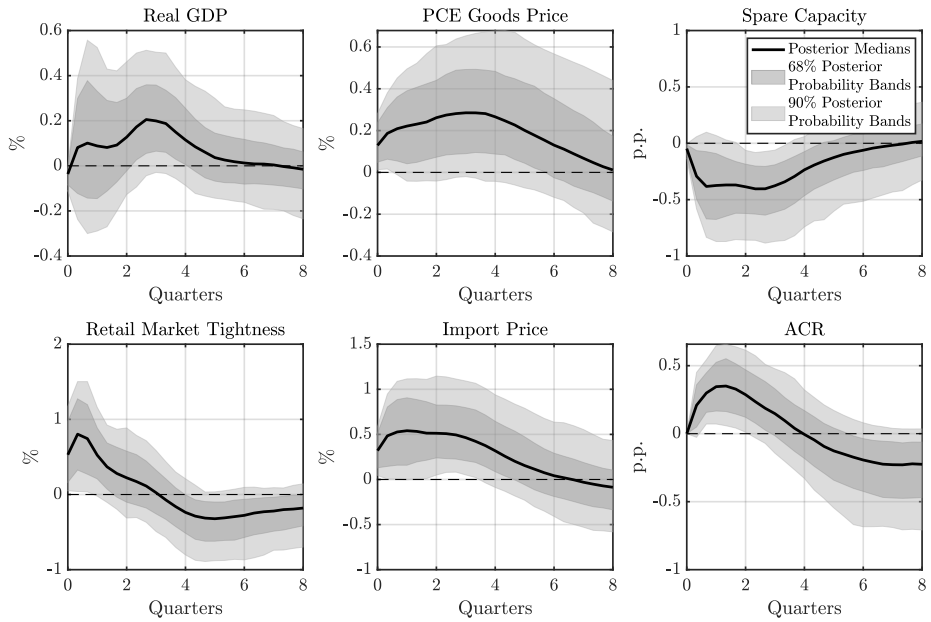

Figure E.25: IRFs to an Adverse Shock to Productive Capacity: Spare Capacity

Notes. The IRFs to a one standard deviation adverse shock to productive capacity are identified using an SVAR specification in Equation (28), with the U.S. spare capacity employed in the estimation. All other estimation specifications are kept the same as in the baseline. The solid line shows the point-wise posterior medians and the shaded bands show the 68% and 90% equal-tailed point-wise posterior probability bands. The figure is based on 100,000 independent importance sampling draws.

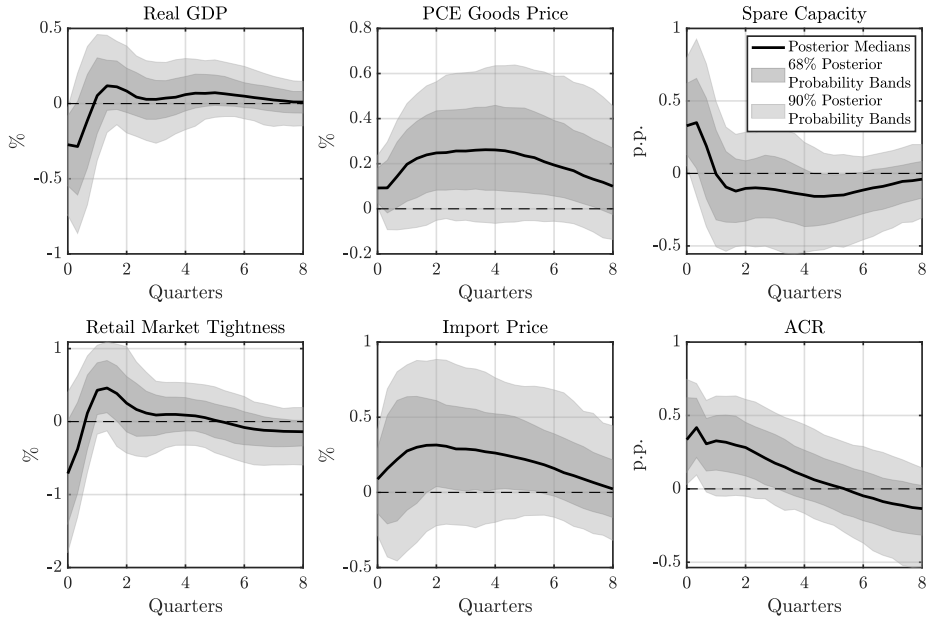

Figure E.26: IRFs to an Adverse Shock to the Supply Chain: Spare Capacity

Notes. The IRFs to a one standard deviation adverse shock to the supply chain are identified using an SVAR specification in Equation (28), with the U.S. spare capacity employed in the estimation. All other estimation specifications are kept the same as in the baseline. The solid line shows the point-wise posterior medians and the shaded bands show the 68% and 90% equal-tailed point-wise posterior probability bands. The figure is based on 100,000 independent importance sampling draws.

To further assess the robustness of our findings, we substitute manufacturers' inventories with merchant wholesalers' inventories, identified by the mnemonic `WHLSLRIMSA` in the FRED database, to construct the measure of retail market tightness. Specifically, we construct the monthly time series for retail market tightness by dividing the new orders placed by retailers against the inventories held by merchant wholesalers. We estimate the retailers' new orders ($Order_t$) using the following formula:

$$Order_t = (Inventory_t - Inventory_{t-1}) + Sale_t,$$

where $Inventory_t$ denotes the inventories of U.S. retailers and $Sale_t$ represents their sales in month t. The behaviors of the IRFs, as shown in Figures E.27 through E.29, are quantitatively similar to those observed in Figures 9, 10, and 11.

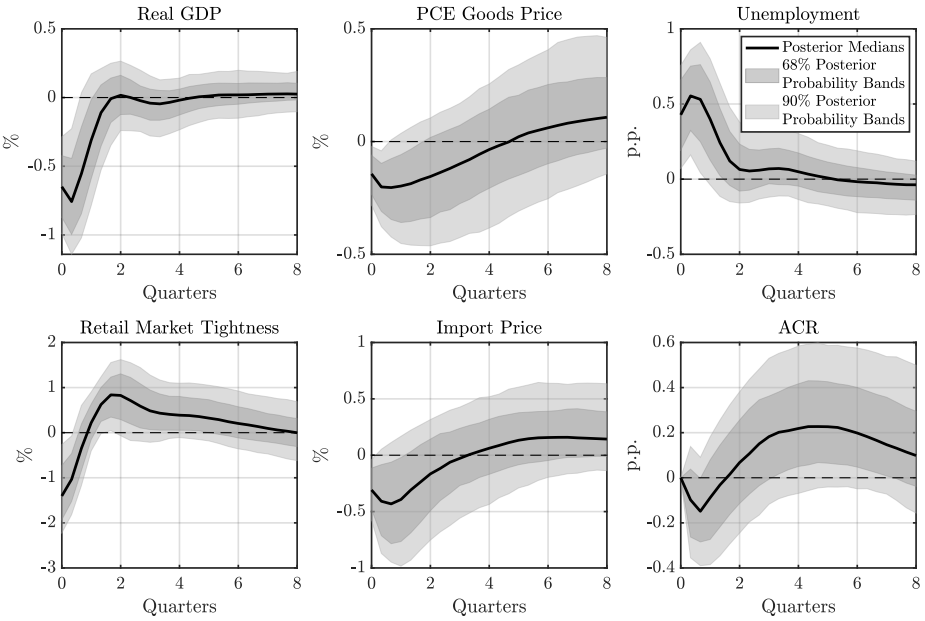

Figure E.27: IRFs to an Adverse Shock to Aggregate Demand: Wholesalers' Inventories

Notes. The IRFs to a one standard deviation adverse shock to aggregate demand are identified using an SVAR specification in Equation (28), with merchant wholesalers' inventories applied in the construction of retail market tightness. All other estimation specifications are kept the same as in the baseline. The solid line shows the point-wise posterior medians and the shaded bands show the 68% and 90% equal-tailed point-wise posterior probability bands. The figure is based on 100,000 independent importance sampling draws.

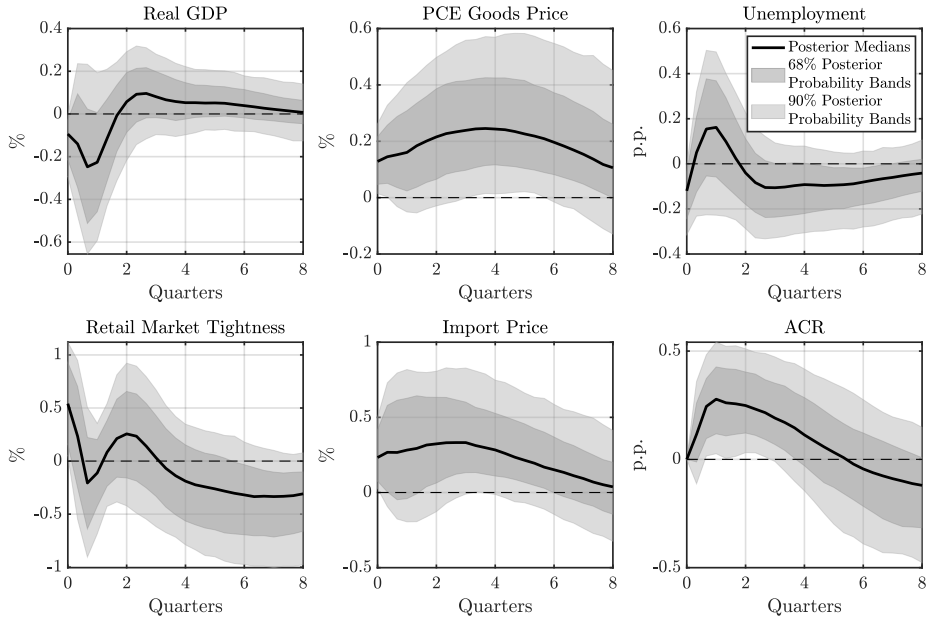

Figure E.28: IRFs to an Adverse Shock to Productive Capacity: Wholesalers' Inventories

Notes. The IRFs to a one standard deviation adverse shock to productive capacity are identified using an SVAR specification in Equation (28), with merchant wholesalers' inventories applied in the construction of retail market tightness. All other estimation specifications are kept the same as in the baseline. The solid line shows the point-wise posterior medians and the shaded bands show the 68% and 90% equal-tailed point-wise posterior probability bands. The figure is based on 100,000 independent importance sampling draws.

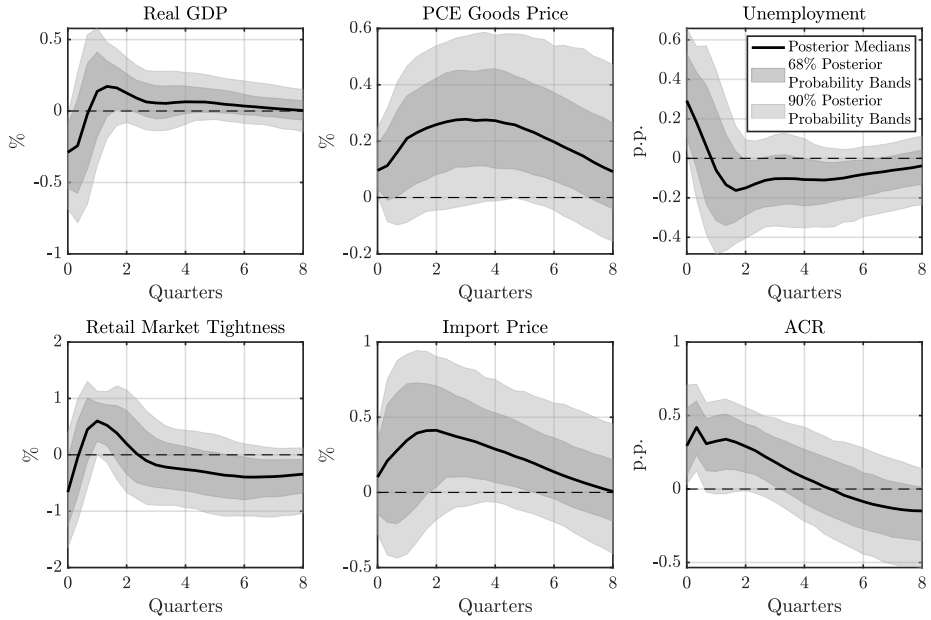

Figure E.29: IRFs to an Adverse Shock to the Supply Chain: Wholesalers' Inventories

Notes. The IRFs to a one standard deviation adverse shock to the supply chain are identified using an SVAR specification in Equation (28), with merchant wholesalers' inventories applied in the construction of retail market tightness. All other estimation specifications are kept the same as in the baseline. The solid line shows the point-wise posterior medians and the shaded bands show the 68% and 90% equal-tailed point-wise posterior probability bands. The figure is based on 100,000 independent importance sampling draws.

E.4. Fitted ACR

In this appendix, we conduct a robustness check of our baseline results by employing a fitted ACR index in our SVAR estimation after regressing the port-specific congestion rate on the Oxford Stringency (OS) Index (Mathieu et al., 2020) and extracting the fitted values.[15] This robustness check aims to mitigate potential endogeneity concerns with the ACR index. Such concerns may arise when significant changes in shipping capacity between routes, attributed to demand shifters, contribute to port congestion.

The OS Index primarily measures the severity of policies that restrict mobility. It aggregates data on the timing and nature of governmental actions taken to mitigate the spread of COVID-19. This involves averaging nine component indicators, which reflect the intensity of various measures: school closures, workplace shutdowns, public event cancellations, restrictions on public gatherings, public transport closures, stay-at-home orders, public information campaigns, internal movement limitations, and international travel controls. The OS Index is specifically designed to capture the strictness of government policies without being influenced by demand-side factors. Furthermore, stringent government policies, indicated by a high OS Index, are presumed to significantly exacerbate port congestion globally, thereby playing a central role in global supply chain disruptions.[16] Consequently, the OS Index is utilized as an instrument for the congestion rate. The resulting fitted ACR index, denoted as $\widehat{\text{ACR}}$, is employed to isolate the causal impact of global supply chain disruptions.

We calculate the monthly average OS Index for each country that hosts one of the top 50 container ports worldwide. Our sample is limited to the periods from January 2020 to December 2022, as the OS Index data are available only for these periods. Subsequently, we regress the port-specific congestion rate on the corresponding OS Index, extract the fitted values, and compute the weighted average, denoted as $\widehat{\text{ACR}}$. The relative number of ship visits to each port determines the weights. This fitted ACR index is then incorporated into our estimation. Consistent with our baseline approach, we apply Restrictions 1, 2, and 3 to the IRFs. Although we maintain the same specifications as in the baseline analysis, the shortened sample length necessitates limiting

[15] We thank Kun Wang for suggesting this robustness check.

[16] As highlighted in the main text, it is crucial to understand that personnel restrictions imposed by stringent government policies during the COVID-19 pandemic were not the cause of port congestion. This is because essential port workers were typically exempted from such restrictions as recorded in the OS Index. Rather, port delays were primarily triggered by upstream and downstream logistical issues.

the calculation of the IRFs to just one year post-impact to reduce parameter uncertainty.

Despite the increased uncertainty in our point estimates due to the reduced sample size, the IRFs to each structural shock, as illustrated in Figures E.30 to E.32, are quantitatively akin to those depicted in Figures 9 to 11, confirming the robustness of our baseline results.

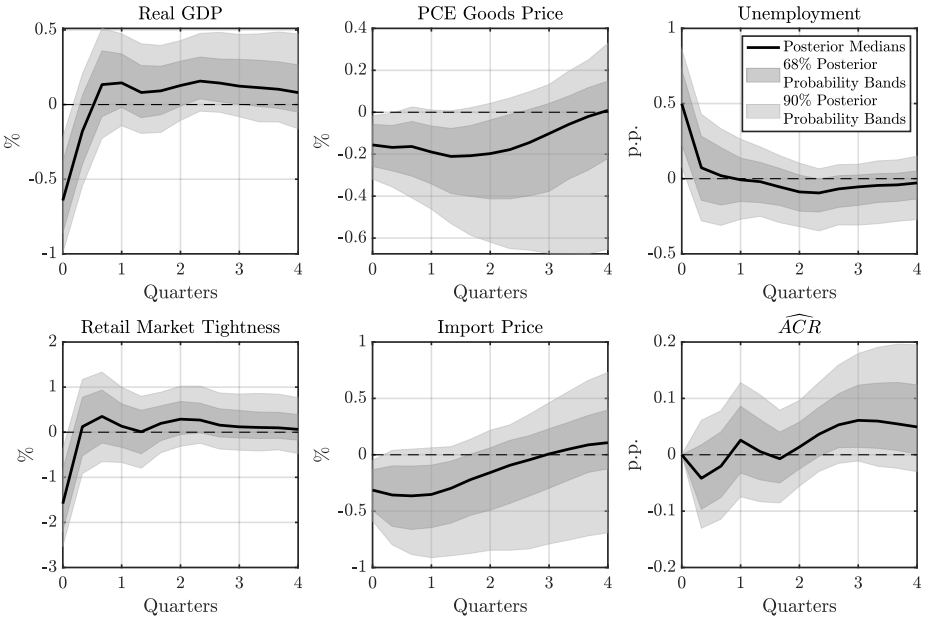

Figure E.30: IRFs to an Adverse Shock to Aggregate Demand: $\widehat{\text{ACR}}$

Notes. The IRFs to a one standard deviation adverse shock to aggregate demand are identified using the fitted ACR index ($\widehat{\text{ACR}}$) and Restrictions 1, 2, and 3. The solid line shows the point-wise posterior medians and the shaded bands show the 68% and 90% equal-tailed point-wise posterior probability bands. The figure is based on 100,000 independent importance sampling draws.

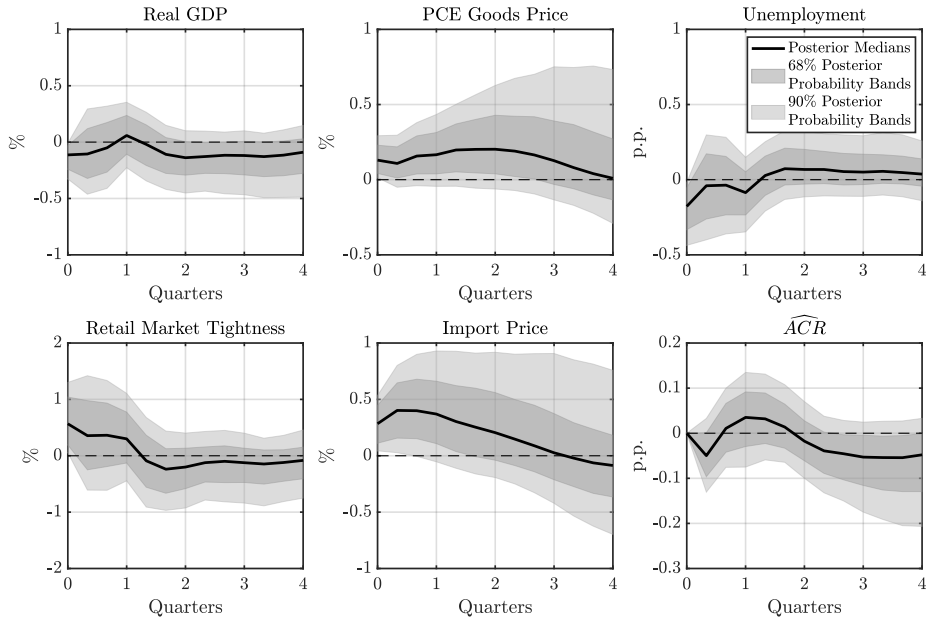

Figure E.31: IRFs to an Adverse Shock to Productive Capacity: $\widehat{\text{ACR}}$

Notes. The IRFs to a one standard deviation adverse shock to productive capacity are identified using the fitted ACR index ($\widehat{\text{ACR}}$) and Restrictions 1, 2, and 3. The solid line shows the point-wise posterior medians and the shaded bands show the 68% and 90% equal-tailed point-wise posterior probability bands. The figure is based on 100,000 independent importance sampling draws.

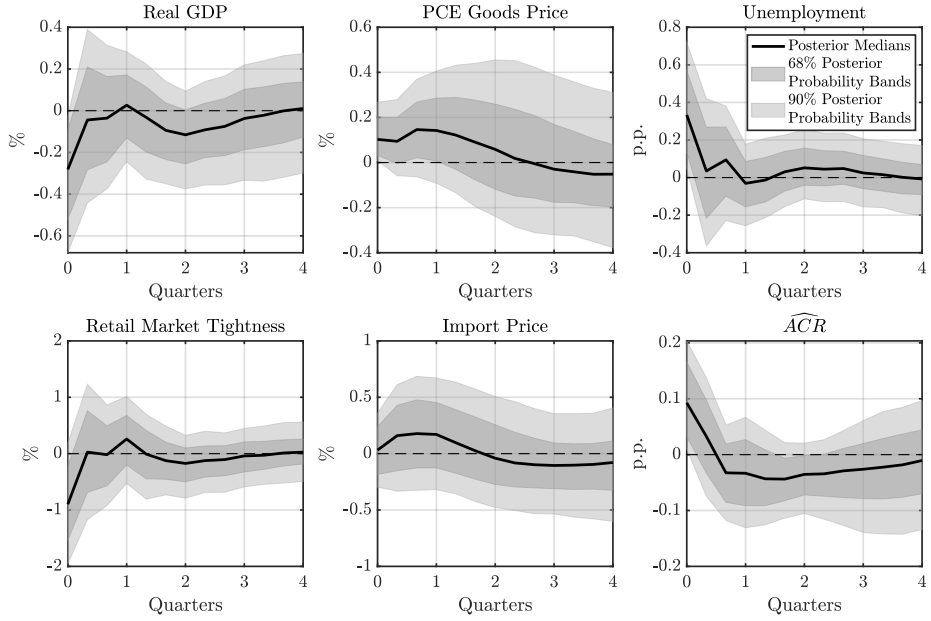

Figure E.32: IRFs to an Adverse Shock to the Supply Chain: $\widehat{\text{ACR}}$

Notes. The IRFs to a one standard deviation adverse shock to the supply chain are identified using the fitted ACR index ($\widehat{\text{ACR}}$) and Restrictions 1, 2, and 3. The solid line shows the point-wise posterior medians and the shaded bands show the 68% and 90% equal-tailed point-wise posterior probability bands. The figure is based on 100,000 independent importance sampling draws.

E.5. Prior Robustness

In this appendix, we demonstrate that the main conclusions from our baseline SVAR analysis remain robust when employing the prior robust approach for SVARs proposed by Giacomini and Kitagawa (2021). This approach eliminates the necessity of specifying a prior for the structural parameter based on the reduced-form parameter, which is primarily responsible for the asymptotic disagreement between Bayesian and frequentist inference. It is achieved by developing a class of priors that maintains a singular prior for the reduced-form parameter while permitting arbitrary conditional priors for the structural parameters, contingent upon the reduced-form parameter. This methodology enhances the robustness of our SVAR analysis, ensuring that our conclusions are not overly dependent on specific prior choices.

In practice, we apply their Algorithm 1 to numerically approximate the set of posterior means and the associated robust credible regions for the IRFs of selected endogenous variables in response to each structural shock. We make two modifications in the implementation of Algorithm 1. First, in Step 2 of Algorithm 1, to draw the orthonormal Q's subject to Restrictions 1, 2, and 3, we apply the QR decomposition method as in Arias et al. (2018) instead of the original linear projection approach. These two ways of drawing Q's are comparable in terms of both the resulting distribution of Q and the computational cost. Second, we replace Step 3 of Algorithm 1 with Step 3′ of Algorithm 2 to approximate the lower and upper bounds of the prior robust posterior means, as well as those associated with the robust credible regions. These modifications enhance the precision and applicability of the algorithm in our context, ensuring a more robust and accurate approximation of the posterior means and credible regions for the IRFs.

In Figures E.33, E.34, and E.35, the solid lines represent the point-wise posterior medians. At the same time, the shaded areas depict the 68% equal-tailed point-wise posterior probability bands. These are based on the baseline estimation data from Section 4. In addition, dotted curves are used to plot the set of prior robust posterior means, and the corresponding 68% robust credible regions are indicated with dashed-dotted curves. The underlying data for these plots are derived from 1,000 independent draws of the reduced-form parameters and 100,000 orthogonal matrix draws for each reduced-form parameter.

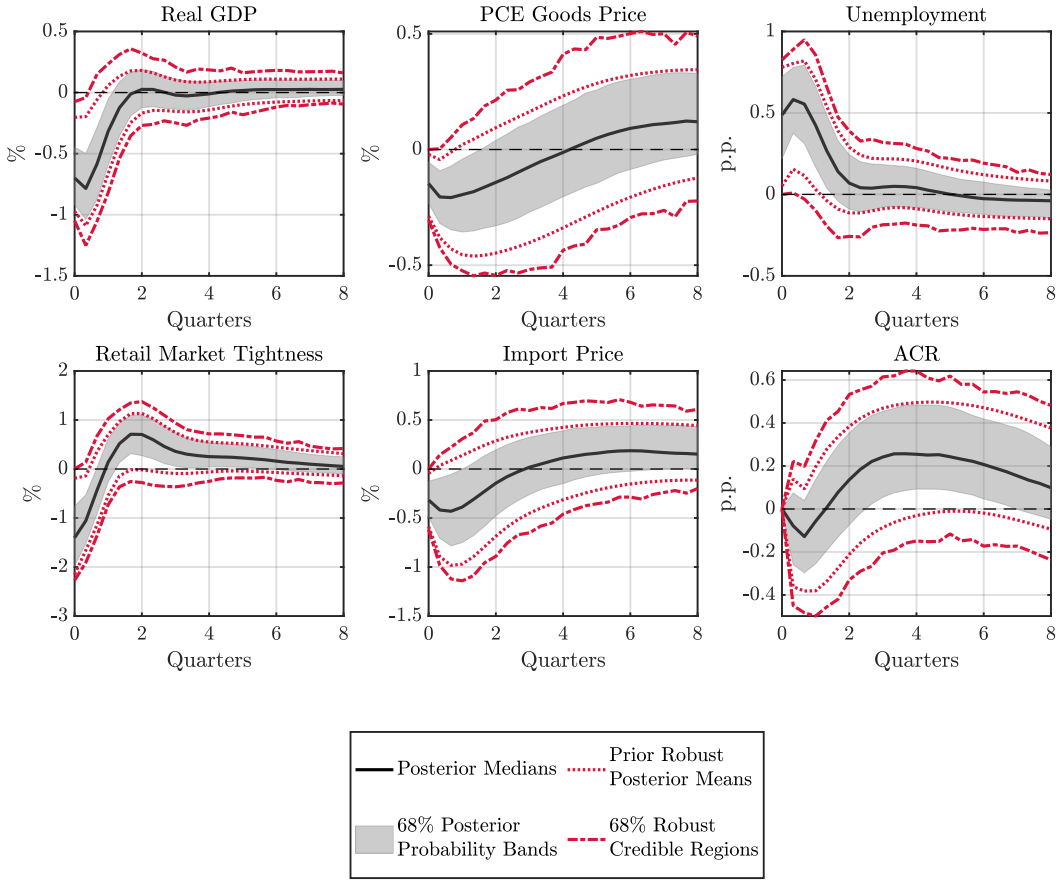

Figure E.33: IRFs to an Adverse Shock to Aggregate Demand: Prior Robustness

Notes. The IRFs to a one standard deviation adverse shock to aggregate demand are estimated using the prior robust approach for the SVARs proposed by Giacomini and Kitagawa (2021). The solid lines show the point-wise posterior medians and the shaded areas represent the 68% equal-tailed point-wise posterior probability bands, which are based on the data from our baseline estimation outlined in Section 4. The dotted curves illustrate the set of prior robust posterior means, and the dashed-dotted curves depict the 68% robust credible regions. These curves are obtained from 1,000 independent draws of the reduced-form parameters, and 100,000 orthogonal matrix draws for each reduced-form parameter.

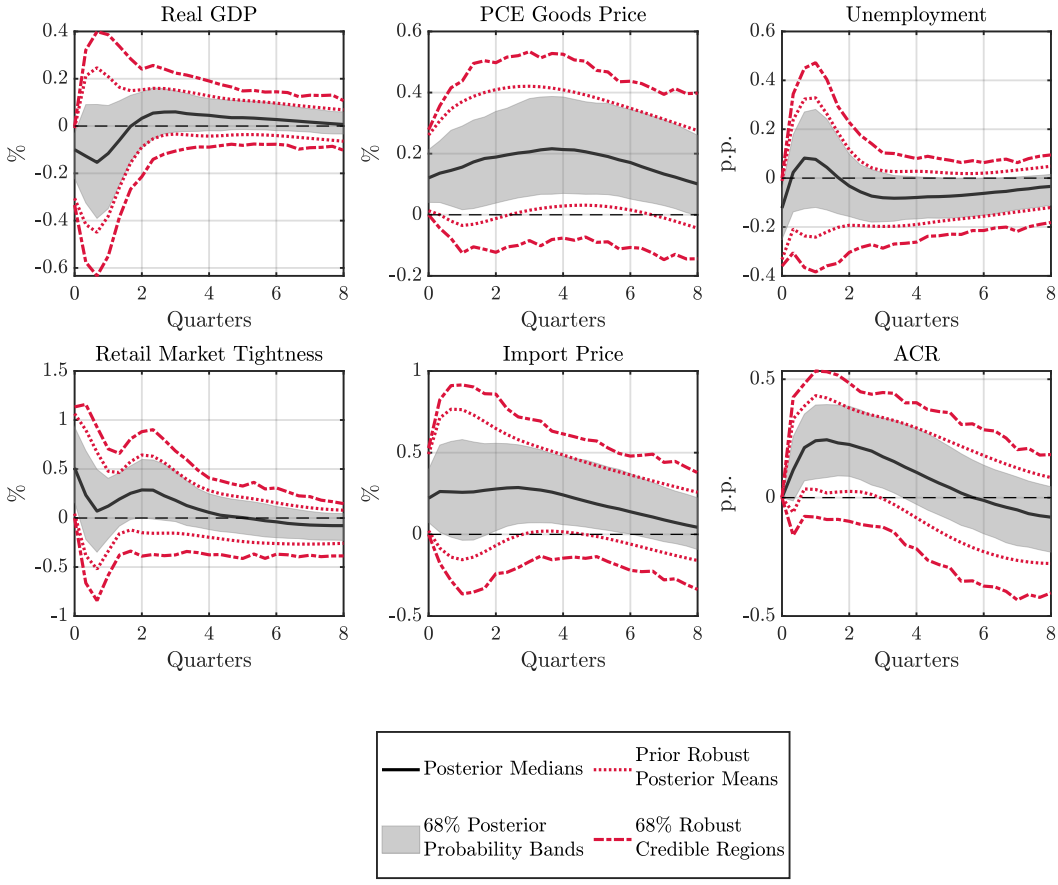

Figure E.34: IRFs to an Adverse Shock to Productive Capacity: Prior Robustness

Notes. The IRFs to a one standard deviation adverse shock to productive capacity are estimated using the prior robust approach for the SVARs proposed by Giacomini and Kitagawa (2021). The solid lines show the point-wise posterior medians and the shaded areas represent the 68% equal-tailed point-wise posterior probability bands, which are based on the data from our baseline estimation outlined in Section 4. The dotted curves illustrate the set of prior robust posterior means, and the dashed-dotted curves depict the 68% robust credible regions. These curves are obtained from 1,000 independent draws of the reduced-form parameters, and 100,000 orthogonal matrix draws for each reduced-form parameter.

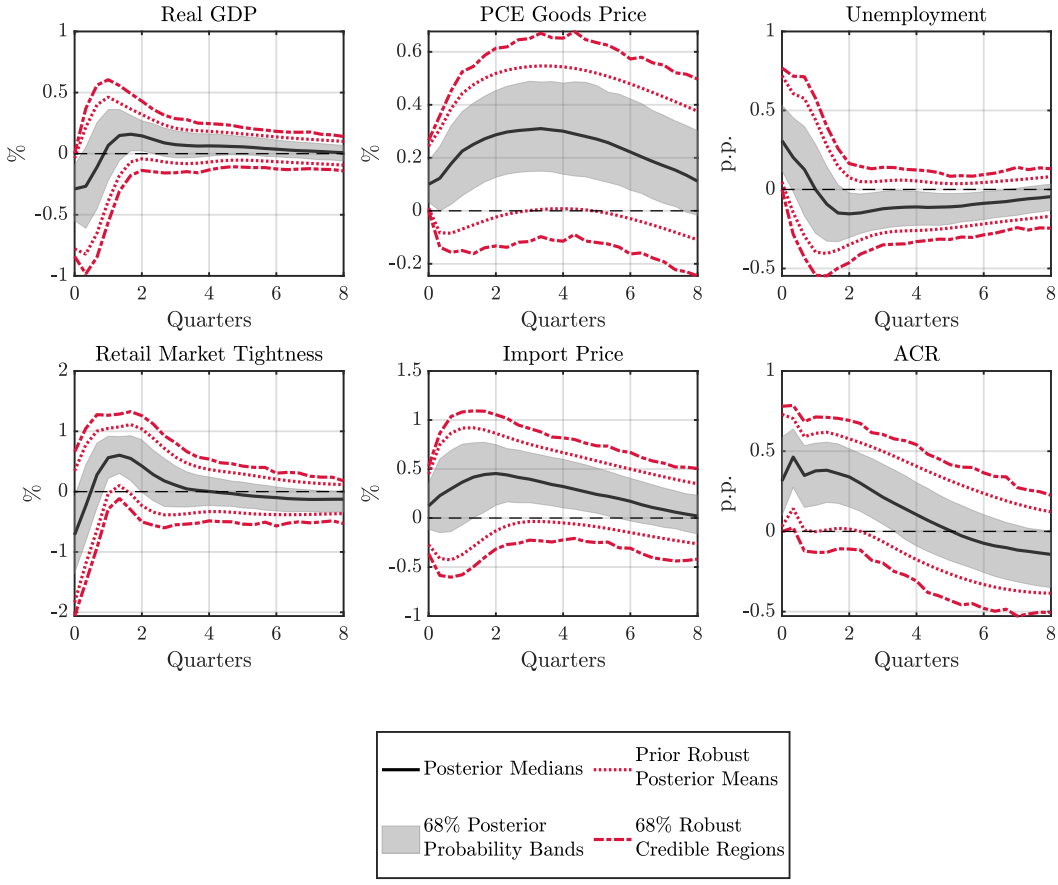

Figure E.35: IRFs to an Adverse Shock to the Supply Chain: Prior Robustness

Notes. The IRFs to a one standard deviation adverse shock to the supply chain are estimated using the prior robust approach for the SVARs proposed by Giacomini and Kitagawa (2021). The solid lines show the point-wise posterior medians and the shaded areas represent the 68% equal-tailed point-wise posterior probability bands, which are based on the data from our baseline estimation outlined in Section 4. The dotted curves illustrate the set of prior robust posterior means, and the dashed-dotted curves depict the 68% robust credible regions. These curves are obtained from 1,000 independent draws of the reduced-form parameters, and 100,000 orthogonal matrix draws for each reduced-form parameter.

E.6. Additional Sign Restrictions on Retail Market Tightness and Import Price

In an alternative SVAR estimation, together with Restrictions 1, 2, and 3, we apply additional positive sign restrictions on the contemporary responses of retail market tightness and import price in response to an adverse supply chain shock. This robustness check aligns with our theoretical prediction in Proposition 5 for a supply chain disturbance represented by a reduction in matching efficiency. As illustrated in Figures E.36 through E.40, the results are quantitatively similar to those obtained without these additional sign restrictions.

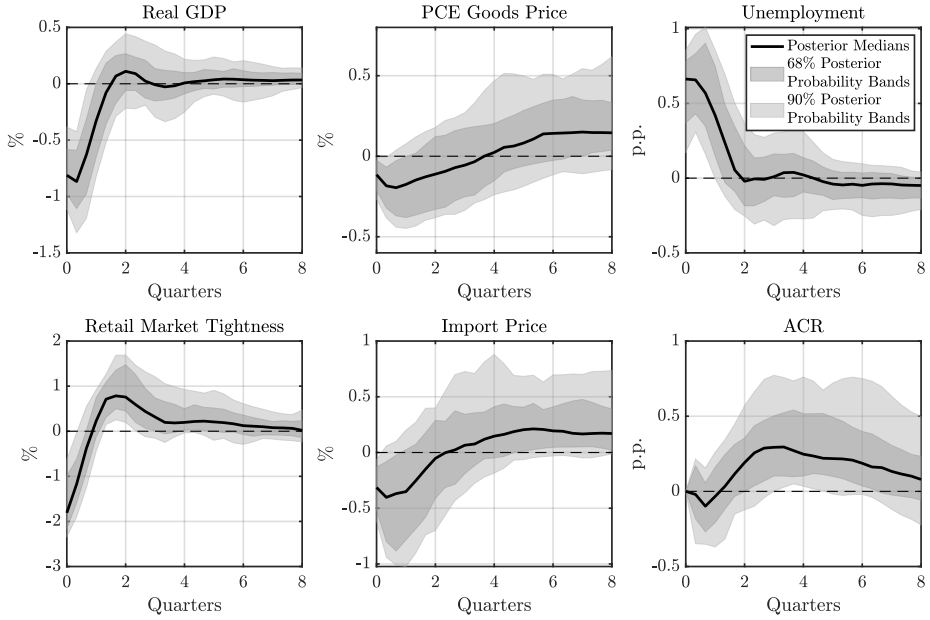

Figure E.36: IRFs to an Adverse Shock to Aggregate Demand: Additional Sign Restrictions

Notes. The IRFs to a one standard deviation adverse shock to aggregate demand are identified by imposing additional positive sign restrictions on the contemporary responses of retail market tightness and import price in the case of a supply chain disturbance. These restrictions are applied in conjunction with Restrictions 1, 2, and 3. The solid line shows the point-wise posterior medians and the shaded bands show the 68% and 90% equal-tailed point-wise posterior probability bands. The figure is based on 100,000 independent importance sampling draws.

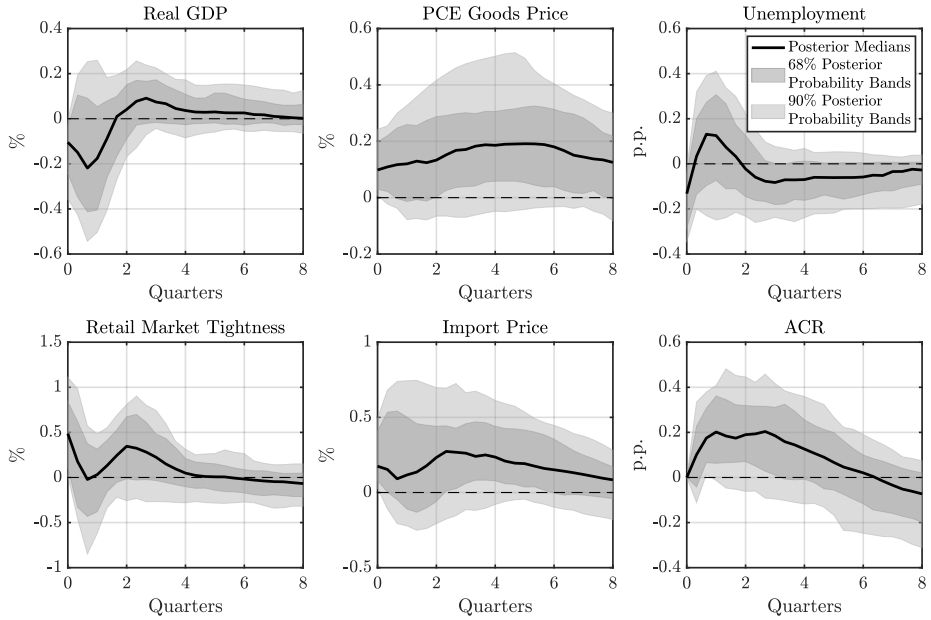

Figure E.37: IRFs to an Adverse Shock to Productive Capacity: Additional Sign Restrictions

Notes. The IRFs to a one standard deviation adverse shock to productive capacity are identified by imposing additional positive sign restrictions on the contemporary responses of retail market tightness and import price in the case of a supply chain disturbance. These restrictions are applied in conjunction with Restrictions 1, 2, and 3. The solid line shows the point-wise posterior medians and the shaded bands show the 68% and 90% equal-tailed point-wise posterior probability bands. The figure is based on 100,000 independent importance sampling draws.

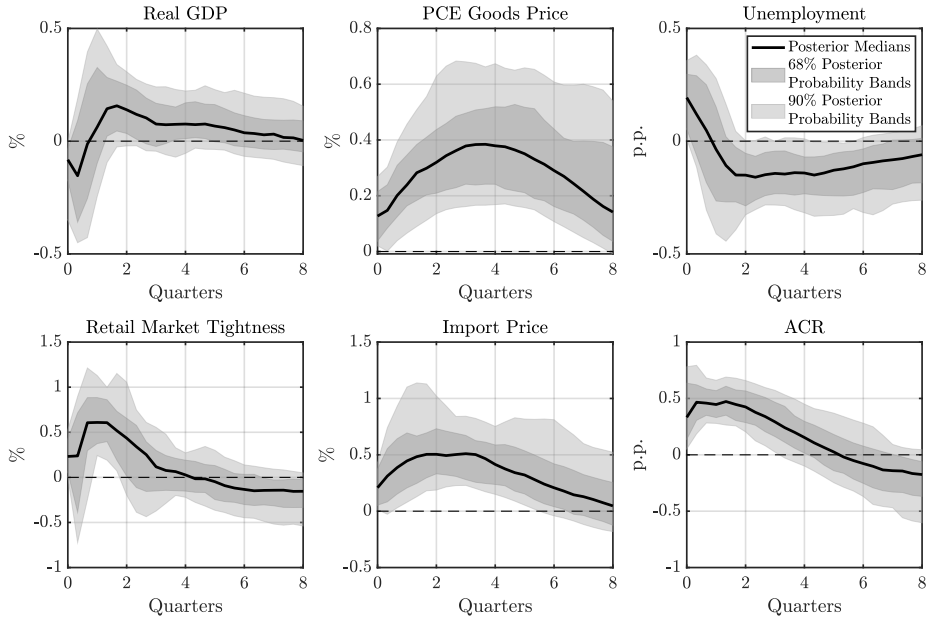

Figure E.38: IRFs to an Adverse Shock to the Supply Chain: Additional Sign Restrictions

Notes. The IRFs to a one standard deviation adverse shock to the supply chain are identified by imposing additional positive sign restrictions on the contemporary responses of retail market tightness and import price in the case of a supply chain disturbance. These restrictions are applied in conjunction with Restrictions 1, 2, and 3. The solid line shows the point-wise posterior medians and the shaded bands show the 68% and 90% equal-tailed point-wise posterior probability bands. The figure is based on 100,000 independent importance sampling draws.

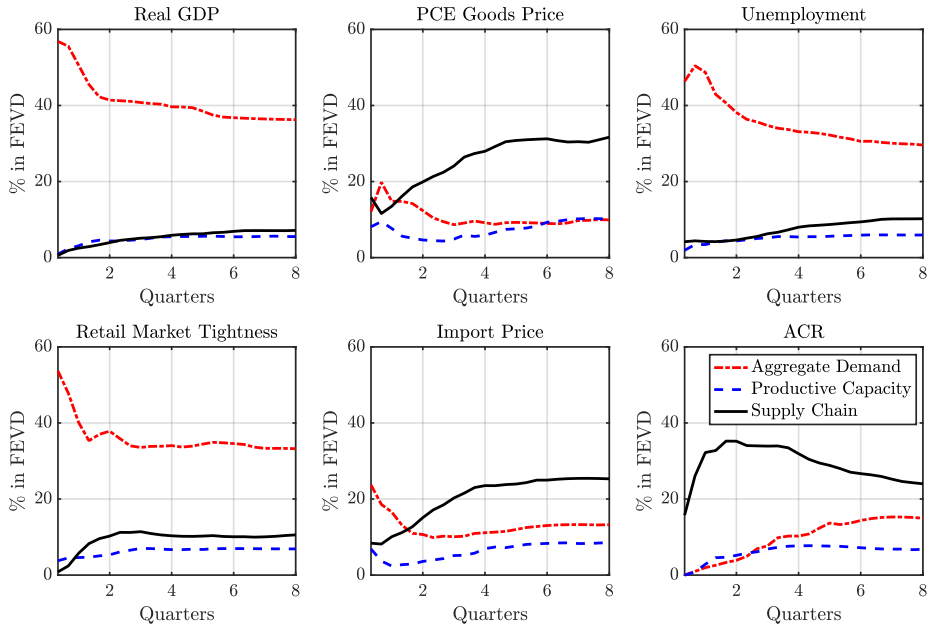

Figure E.39: FEVD from the SVAR: Additional Sign Restrictions

Notes. Each line presents the median fraction of the forecast error variance for each endogenous variable, explained by each of the three identified structural shocks at various time horizons. The FEVD is estimated by applying additional positive sign restrictions on the contemporary responses of retail market tightness and import price to a supply chain disturbance, in conjunction with Restrictions 1, 2, and 3. The figure is based on 100,000 independent importance sampling draws.

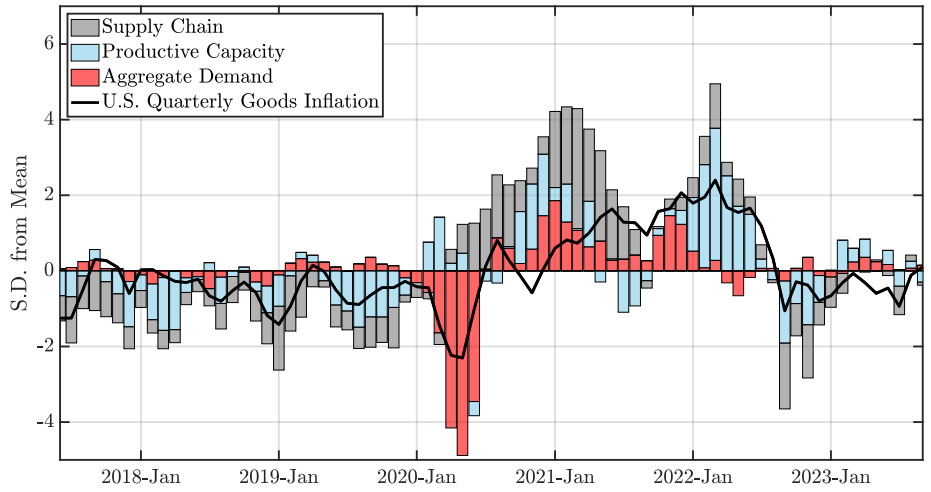

Figure E.40: HD of U.S. Quarter-on-Quarter Goods Inflation: Additional Sign Restrictions

Notes. The solid line represents the standardized goods inflation rate in the U.S., i.e., the quarter-on-quarter growth of the PCE goods price index. The shaded bars represent the corresponding standardized cumulative historical contribution of shocks to aggregate demand, productive capacity, and the supply chain to goods inflation. The shocks are identified using the SVAR specification in Equation (28), with the ACR index included as the measure of global supply chain disruptions, and additional positive sign restrictions imposed on the contemporary responses of retail market tightness and import price to a supply chain disturbance, in conjunction with Restrictions 1, 2, and 3. The figure is derived from the posterior medians, based on 100,000 independent importance sampling draws.

F. Alternative Indices of Supply Chain Disruptions

In this appendix, we compare our ACR index to other popular indices of supply chain disruptions in the existing literature: namely, the Harper Peterson Time Charter Rates Index (HARPEX), the Global Supply Chain Pressure Index (GSCPI) from the Federal Reserve Bank of New York (Benigno et al., 2022), and the Supply Disruptions Index (SDI) constructed by Smirnyagin and Tsyvinski (2022). Our analysis reveals significant disparities between these indices, which affect the impact of supply chain disruptions on key macroeconomic indicators. In addition, we show that using the ACT index, as developed in Appendix B.3, in the causality assessment delivers quantitatively similar results to those obtained with the ACR index.

F.1. HARPEX

Shipping costs serve as a natural proxy for supply chain disruptions (Benigno et al., 2022). However, as in the classical identification problem with simultaneous equations, shipping costs are influenced by both supply- and demand-side factors. For instance, an increase in the demand for tradable goods can lead to higher shipping costs, even if the global supply chain is working without problems.

Figure F.1 illustrates the relationship between the ACR index and the HARPEX. The HARPEX is a widely recognized composite indicator of container shipping rates in the time charter market across eight different classes of container ships (Attinasi et al., 2021; Benigno et al., 2022; Finck and Tillmann, 2022). It is also integral to the construction of the New York Fed's GSCPI as a measure of cross-border transportation costs. As expected, we observe a parallel movement between the HARPEX and our ACR index since the onset of the pandemic. This correlation is particularly evident as delays in container processing became more frequent and port congestion intensified globally, causing ships to be tied up at ports. This scenario led to a marked shortage in the supply of shipping services, thereby driving up shipping prices. However, there are instances in which the two series did not closely align. This divergence, as previously discussed, can be attributed to the influence of both demand- and supply-side factors on their fluctuations.

Figures F.2, F.3, and F.4 present the estimation results with the HARPEX included in the SVAR as the measure of supply chain disruptions. In this analysis, we have removed the zero restrictions while retaining the sign restrictions to discipline the IRFs. By examining the IRFs

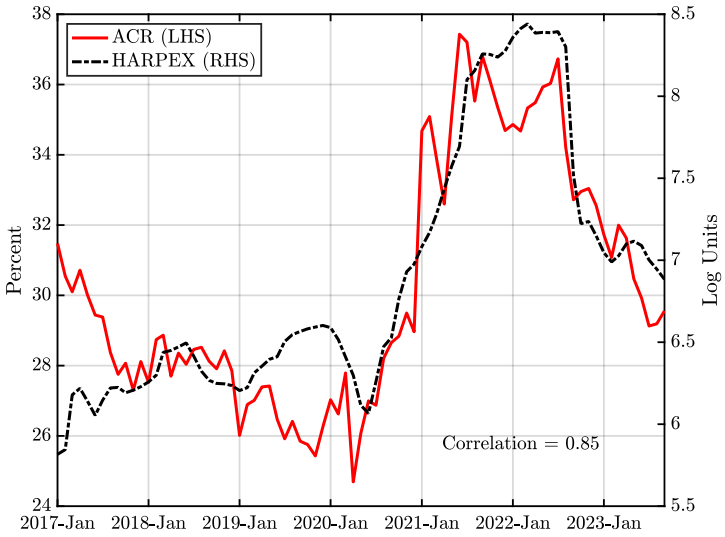

Figure F.1: ACR vs. HARPEX

Notes. Figure F.1 plots the ACR index (solid red line) against the HARPEX (dashed-dotted black line) for the sample period from January 2017 to September 2023. The ACR index is computed using the AIS data of container ships and our IMA-DBSCAN algorithm, as detailed in Appendix B. The HARPEX series is published by Harper Peterson and retrieved from the Refinitiv data platform. The ACR index and HARPEX are presented in percentage terms and log units, respectively. Both series have been seasonally adjusted.

to a supply chain disturbance, we find that the shock of supply chain disruption is estimated to be stagflationary. Similar to the results obtained when using the ACR index, supply chain disturbances still account for the largest fraction of the unexpected fluctuations in PCE goods and import prices over longer horizons. In terms of the historical decomposition of U.S. goods inflation, the HARPEX also yields results that are quantitatively similar to those obtained using the ACR index.

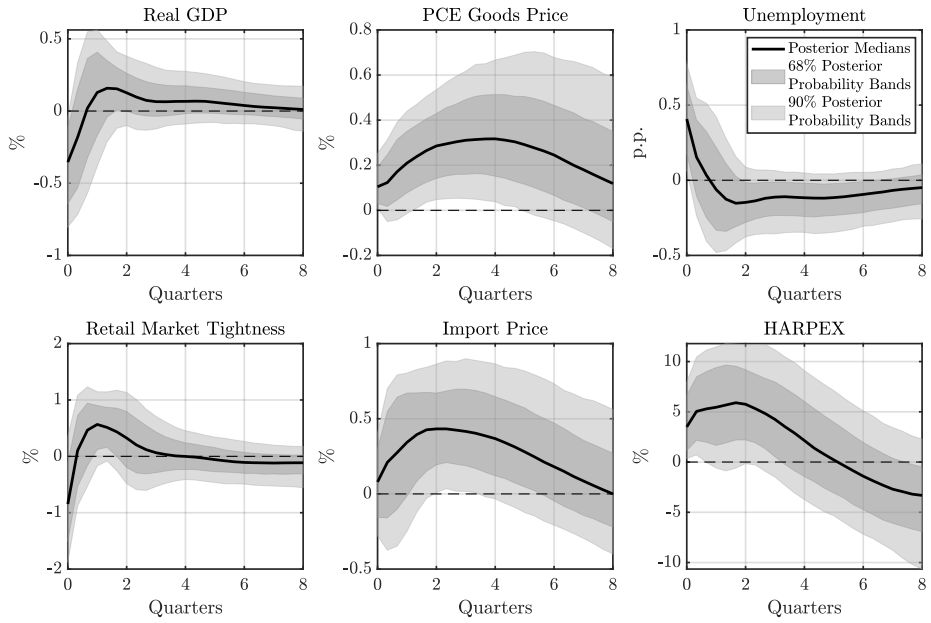

Figure F.2: IRFs to an Adverse Shock to the Supply Chain: The HARPEX and Restrictions 1′, 2′, and 3′

Notes. The IRFs to a one standard deviation adverse shock to the supply chain are identified using the HARPEX and Restrictions 1′, 2′, and 3′. The solid line shows the point-wise posterior medians, and the shaded bands represent the 68% and 90% equal-tailed point-wise posterior probability bands. The figure is based on 100,000 independent importance sampling draws.

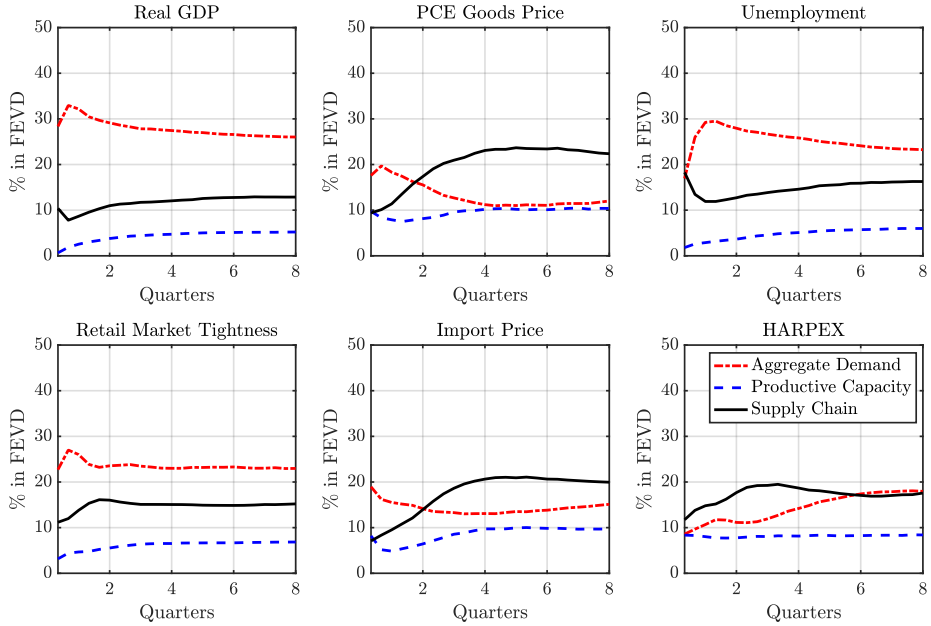

Figure F.3: FEVD from the SVAR: The HARPEX and Restrictions 1′, 2′, and 3′

Notes. Each line presents the median fraction of the forecast error variance for each endogenous variable, explained by each of the three identified structural shocks at various time horizons. The FEVD is estimated using the HARPEX and Restrictions 1′, 2′, and 3′, and based on 100,000 independent importance sampling draws.

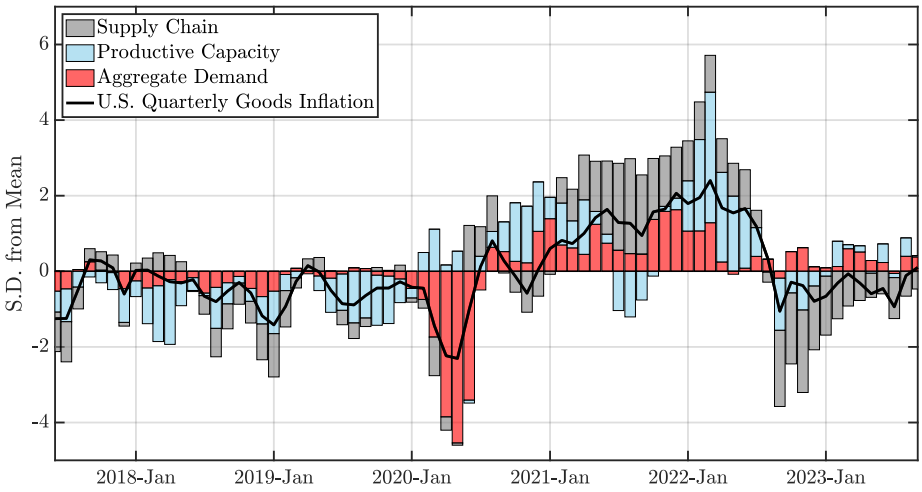

Figure F.4: HD of U.S. Quarter-on-Quarter Goods Inflation: The HARPEX and Restrictions 1′, 2′, and 3′

Notes. The solid line represents the standardized goods inflation rate in the U.S., i.e., the quarter-on-quarter growth of the PCE goods price index. The shaded bars represent the corresponding standardized cumulative historical contribution of shocks to aggregate demand, productive capacity, and the supply chain to goods inflation. The shocks are identified using the SVAR specification in Equation (28), with the HARPEX included as the measure of supply chain disruptions, and Restrictions 1′, 2′, and 3′ imposed on the IRFs of each endogenous variable. The figure is derived from the posterior medians, based on 100,000 independent importance sampling draws.

F.2. GSCPI

Next, we compare our ACR index with the New York Fed's GSCPI to highlight the differences in the measurement of supply chain disruptions. The GSCPI uses information on cross-border transportation costs and the sub-components of the country-specific manufacturing PMI (e.g., "delivery times" as in Kamali and Wang 2021 and Benigno et al. 2022) to infer supply chain disruptions.[17] As discussed in the main text, the GSCPI is potentially problematic because it (i) relies on transportation costs that are subject to variations in the supply and the demand for tradable goods, (ii) depends on information gathered from purchasing managers that might reflect subjective views rather than actual disturbances to the supply chain, and (iii) uses the PMI, which does not specify whether an increase in delivery times results from a disruption to the supply chain or from issues within the actual production process.

In contrast, our ACR index utilizes maritime satellite data to estimate congestion at seaports globally. Our approach effectively sidesteps the main shortcomings of the GSCPI. As extensively documented in Stopford (2008), Song and Dong (2012), Wang et al. (2019), and Brancaccio et al. (2020, 2023), container ships typically operate on fixed itineraries and predetermined routes.[18] Consequently, our index is minimally affected by the strategic decisions of shipping companies and prevailing economic conditions. Table F.1 demonstrates that the port-specific congestion rate, as defined in Equation (1) in the main text, is statistically uncorrelated with the number of ship visits (Column 1). In contrast, the HARPEX, which captures shipping prices, is significantly correlated with the number of ship visits (Column 2).[19] Additionally, any infrequent adjustments in shipping capacity across routes to accommodate demand fluctuations, and the consequent changes in congestion at different ports, are canceled out when aggregating the congestion rates to construct the ACR index. This enhances its exogeneity in measuring global supply chain disruptions. Moreover, by tracking congestion at seaports in real time, we avoid the issue of biased managerial perceptions. Collectively, our ACR index offers an exogenous and precise

[17] IHS Markit (Williamson, 2021) calculates the suppliers' delivery times using the survey responses in the PMI. Specifically, participating purchasing managers are asked if it takes their suppliers more or less time to provide inputs to their factories on average. The percentages of companies reporting an improvement, deterioration, or no change in delivery times are then weighted to derive the index.

[18] Routes are rarely altered because diversions in shipping routes typically incur substantial transition costs. Furthermore, changes in routes could severely affect the stability of shipping operations and customer loyalty (Wang et al., 2019).

[19] It is important to note that the correlation between the HARPEX and the number of ship visits is estimated at an aggregate level, as disaggregated data on shipping prices at the port level are not available.

measure of global supply chain disruptions.

Table F.1: Congestion Rate, the HARPEX, and Ship Visits

	(1) Congestion Rate	(2) HARPEX
# Ship Visits	0.0153923	−0.0002396***
	(0.0157181)	(0.0000473)
Port FE	Yes	N/A
Year & Month FE	Yes	N/A
Obs	3,807	81
R^2	0.0016	0.2449

Notes. Column (1) shows the estimated coefficient and clustered standard error (countries hosting the top 50 container ports as clusters) for regressing the port-specific congestion rate on the number of ship visits, controlling for port, year, and month fixed effects (FE). Column (2) shows the estimated coefficient and standard error for the regression of the HARPEX on the total number of ship visits across these ports. Both the congestion rate and the number of ship visits are computed using the AIS data of container ships and our IMA-DBSCAN algorithm, as detailed in Appendix B, whereas the HARPEX series is published by Harper Peterson and retrieved from the Refinitiv data platform. The ACR index is in percentage terms, and the HARPEX is in log units. *** signifies $p < 0.01$.

Figure F.5 plots the ACR and the GSCPI indices from January 2017 to September 2023. Prior to 2020, the dynamics of these two indices were aligned. However, at the onset of the COVID-19 pandemic in early 2020, the GSCPI saw a substantial increase and remained high in the first half of the year. From late 2020 onward, both series exhibited a parallel rise until January 2022. In an influential paper, di Giovanni et al. (2022) link the early 2020 surge in the GSCPI to the beginning of the lockdown in China and the subsequent decline in the second half of 2020 to the partial reopening of China and Europe.

Our port congestion index suggests that the initial lockdown in China did not cause congestion to a degree that would lead to significant global supply chain disruptions. Similarly, the reopening of China and Europe did not notably alleviate port congestion. Thus, the fluctuations in the GSCPI are likely influenced by abrupt shifts in demand and managerial misperceptions of supply chain issues, as indicated by PMI surveys, not a surprise given the high levels of uncertainty about COVID-19 during the first weeks of the pandemic. Notably, the two series diverged again in early 2022; the ACR index remained high, while the GSCPI started to decrease. We argue that the elevated levels of the ACR index during the first half of 2022 were largely due to the stringent containment measures in China, which remained in effect during this period and exerted

significant pressure on the global supply chain.

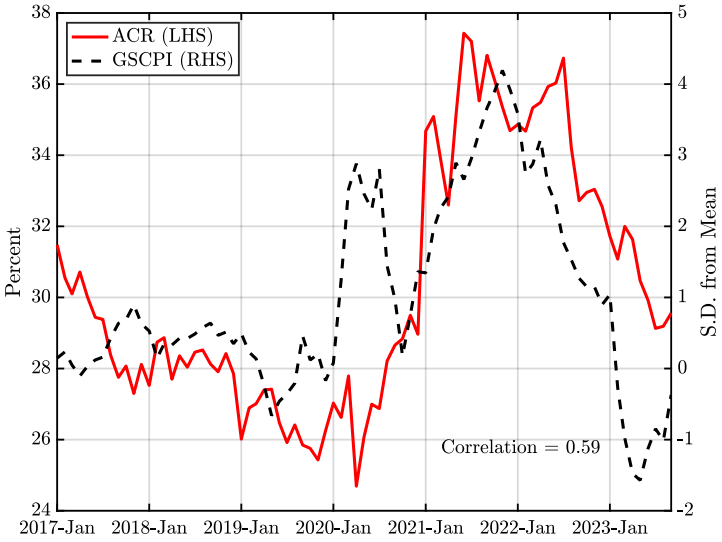

Figure F.5: ACR vs. GSCPI

Notes. Figure F.5 plots the ACR index (solid red line) against the GSCPI (dashed black line) for the sample period from January 2017 to September 2023. The ACR index is computed using the AIS data of container ships and our IMA-DBSCAN algorithm, as detailed in Appendix B. The GSCPI is retrieved from the website of the Federal Reserve Bank of New York. The ACR index is measured in percentage terms, while the GSCPI is in standard deviations from the mean. Both series have been seasonally adjusted.

Now, we examine the implications of the discrepancies between the ACR and GSCPI indices for the inferences drawn by the SVAR model regarding the causal effects of supply chain disruptions. Figure F.6 plots the IRFs in response to an adverse supply chain disturbance, with the GSCPI incorporated in the SVAR as the measure of supply chain disruptions. While the median responses of the endogenous variables are akin to the baseline responses obtained using the ACR index, the probability bands are clearly wider, suggesting less precision in the estimates. Notably, the lower bounds of the 68% posterior probability bands for the PCE goods and import prices are close to zero. In contrast, the baseline estimates, as depicted in Figure 11, consistently show these responses well above the zero line.

Figure F.7 presents the proportion of forecast error variance explained by each of the three structural shocks, as identified using the GSCPI along with Restrictions 1′, 2′, and 3′. Consistent with the decomposition observed using the ACR index (as depicted in Figure 12), shocks to aggregate demand continue to be the primary source of unexpected fluctuations in real GDP, unemployment, and retail market tightness, even when the GSCPI is included in the estimation. However, there is a notable difference in the impact of supply chain shocks. While these

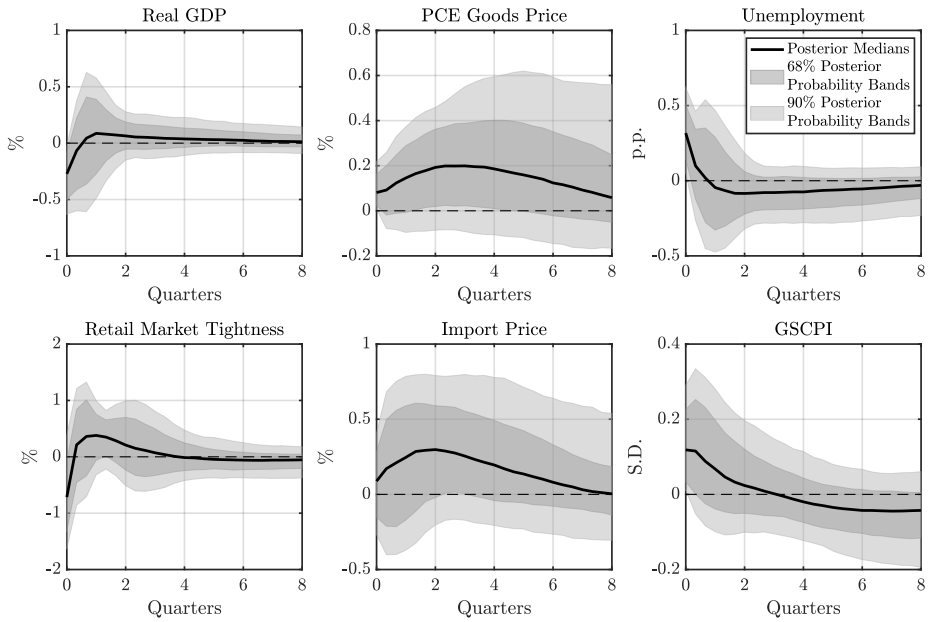

Figure F.6: IRFs to an Adverse Shock to the Supply Chain: The GSCPI and Restrictions 1′, 2′, and 3′

Notes. The IRFs to a one standard deviation adverse shock to the supply chain are identified using the GSCPI and Restrictions 1′, 2′, and 3′. The solid line shows the point-wise posterior medians and the shaded bands represent the 68% and 90% equal-tailed point-wise posterior probability bands. The figure is based on 100,000 independent importance sampling draws.

shocks account for a considerable portion of the unforeseen variations in PCE goods and import prices over extended periods in analyses using the ACR index, their influence is markedly less pronounced when the GSCPI is employed.

Finally, Figure F.8 displays the cumulative historical contribution of each of the three identified shocks to U.S. goods inflation when the GSCPI is incorporated into the estimation. Unlike the results based on the ACR index, those using the GSCPI attribute the sudden decline in inflation at the onset of the COVID-19 pandemic to both adverse demand shocks and supply chain disruptions. Meanwhile, the sustained increase in inflation from late 2020 onward is primarily explained by positive demand shocks, with supply chain disturbances no longer playing a dominant role in driving inflation dynamics in subsequent sampling periods.

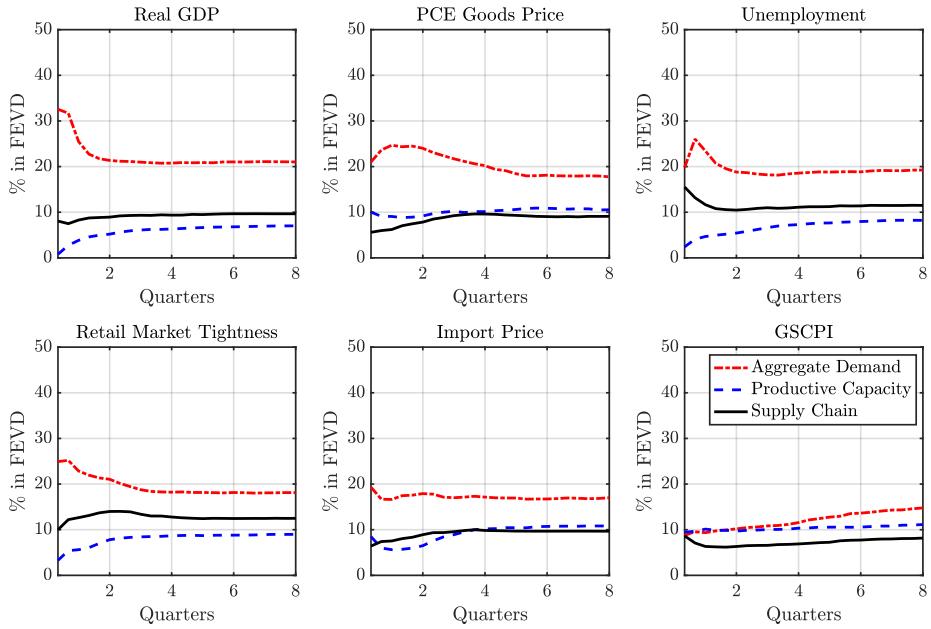

Figure F.7: FEVD from the SVAR: The GSCPI and Restrictions 1′, 2′, and 3′

Notes. Each line presents the median fraction of the forecast error variance for each endogenous variable, explained by each of the three identified structural shocks at various time horizons. The FEVD is estimated using the GSCPI and Restrictions 1′, 2′, and 3′, and based on 100,000 independent importance sampling draws.

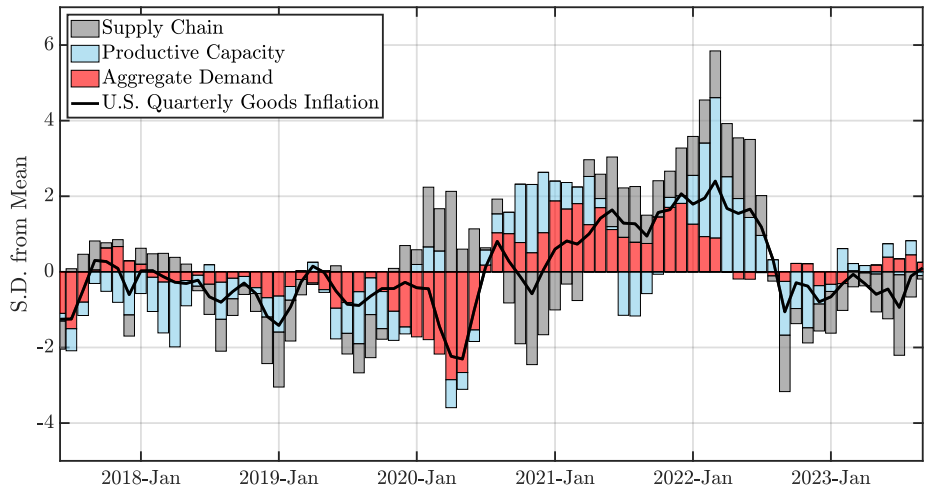

Figure F.8: HD of U.S. Quarter-on-Quarter Goods Inflation: The GSCPI and Restrictions 1′, 2′, and 3′

Notes. The solid line represents the standardized goods inflation rate in the U.S., i.e., the quarter-on-quarter growth of the PCE goods price index. The shaded bars represent the corresponding standardized cumulative historical contribution of shocks to aggregate demand, productive capacity, and the supply chain to goods inflation. The shocks are identified using the SVAR specification in Equation (28), with the GSCPI included as the measure of supply chain disruptions, and Restrictions 1′, 2′, and 3′ imposed on the IRFs of each endogenous variable. The figure is derived from the posterior medians, based on 100,000 independent importance sampling draws.

F.3. SDI

In addition to the HARPEX and GSCPI, several other indices of supply chain disruptions utilize either more advanced techniques (e.g., machine learning) or more granular data (e.g., import transactions). For instance, Smirnyagin and Tsyvinski (2022) leverage the S&P Global Panjiva dataset, a comprehensive repository of U.S. seaborne import records, to derive the U.S. Supply Disruptions Index (SDI). They identify supply chain disruptions by observing regular and active consignee-shipper relationships over quarterly periods; a disruption is marked when a consistently active relationship becomes inactive for a quarter before resuming. Although this identification strategy zeroes in on disruptions within established trading relationships, potential endogeneity concerns may arise. For example, a consignee might temporarily cease orders due to diminished demand rather than a genuine supply chain disruption. Parsing out these scenarios based solely on the activity of consignee-shipper relationships can be intricate. Furthermore, while the SDI provides invaluable insights into U.S. imports and excels in generating asset pricing predictions, the ACR index is more aligned with our primary objective of pinpointing *global* supply chain disruptions.

Figure F.9 plots both the ACR and the SDI indices. The SDI was observed to remain low prior to 2020 and experienced a significant but brief spike in 2020, followed by a moderate and sustained increase throughout 2021 before it began to decline in 2022. The estimation results, incorporating the SDI in the SVAR as the measure of supply chain disruptions, are depicted in Figures F.10, F.11, and F.12. Echoing the findings using the GSCPI, the responses of PCE goods and import prices to a supply chain shock, as estimated with the SDI, are less precise. Furthermore, only a small fraction of the unexpected fluctuations in these prices is attributed to supply chain disturbances. Regarding the historical decomposition of U.S. goods inflation, the SDI suggests that the initial drop in inflation at the onset of the pandemic was due to a combination of a collapse in demand and favorable supply chain shocks. It also indicates that a mix of demand and supply shocks drove the subsequent increase in inflation from late 2020 onward.

In addition to the SDI, another notable measure is the text-based index of supply disruptions developed by Burriel et al. (2023) using newspaper data, following the methodology of Baker et al. (2016). While this index effectively addresses the endogeneity issue by focusing exclusively

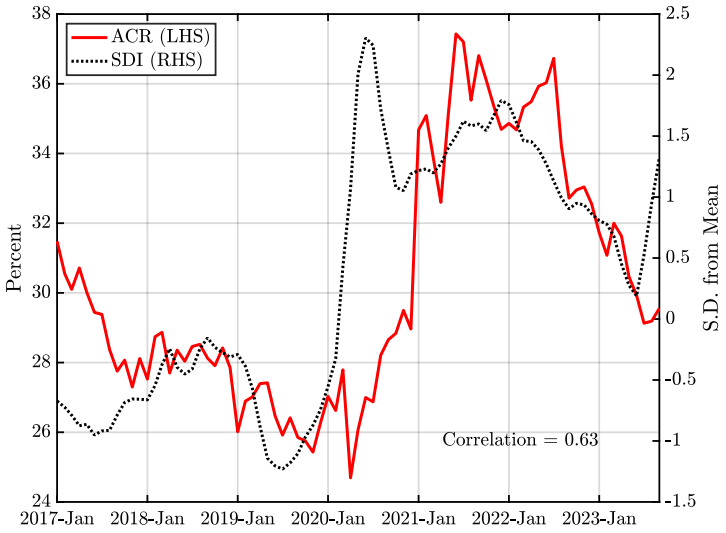

Figure F.9: ACR vs. SDI

Notes. Figure F.9 plots the ACR index (solid red line) against the SDI (black dotted line) for the sample period from January 2017 to September 2023. The ACR index is computed using the AIS data of container ships and our IMA-DBSCAN algorithm, as detailed in Appendix B. The SDI is retrieved from the author's website. The ACR index is measured in percentage terms, while the SDI is measured in standard deviations from the mean. Both series have been seasonally adjusted.

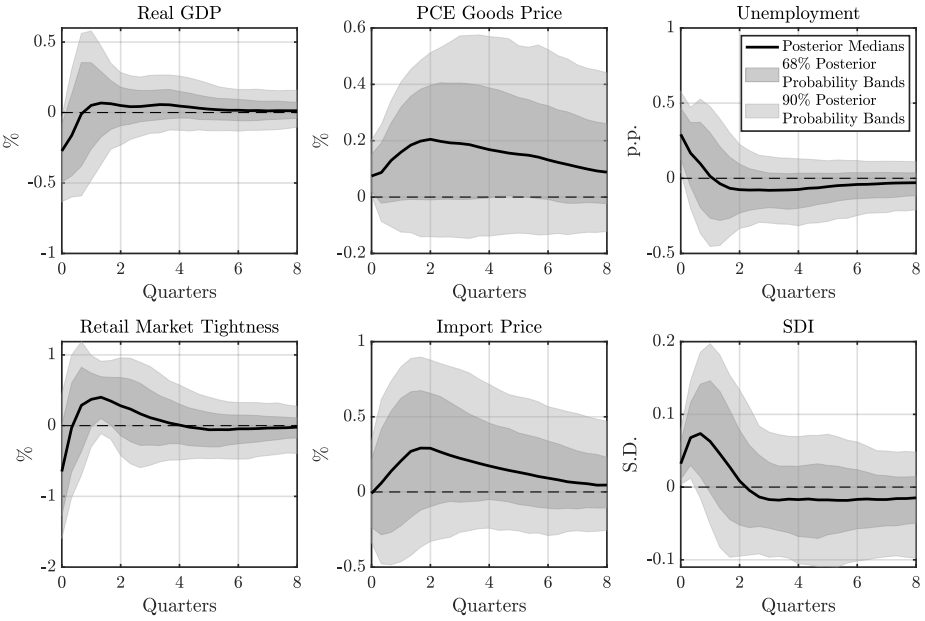

Figure F.10: IRFs to an Adverse Shock to the Supply Chain: The SDI and Restrictions 1′, 2′, and 3′

Notes. The IRFs to a one standard deviation adverse shock to the supply chain are identified using the SDI and Restrictions 1′, 2′, and 3′. The solid line shows the point-wise posterior medians, and the shaded bands represent the 68% and 90% equal-tailed point-wise posterior probability bands. The figure is based on 100,000 independent importance sampling draws.

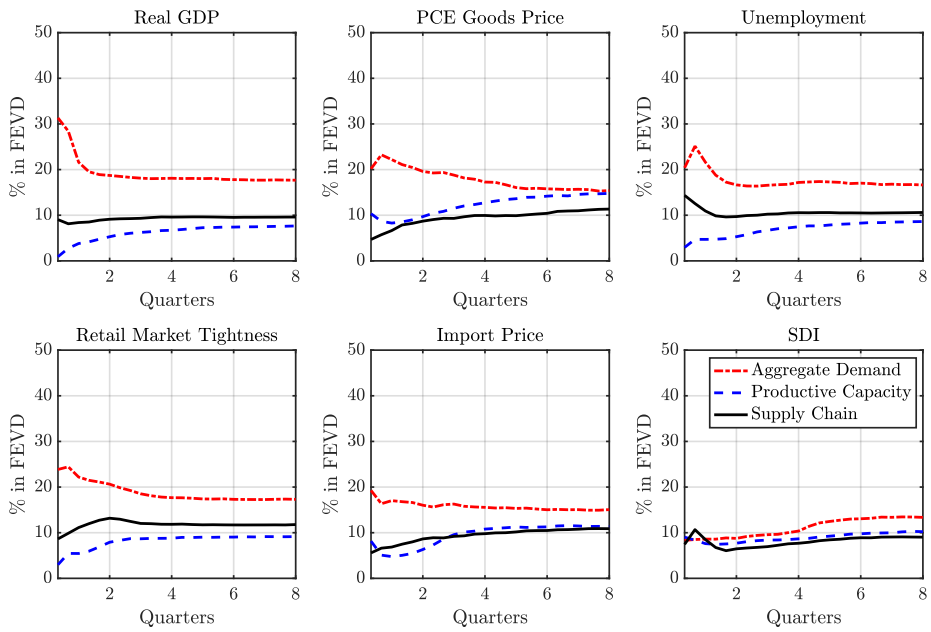

Figure F.11: FEVD from the SVAR: The SDI and Restrictions 1′, 2′, and 3′

Notes. Each line presents the median fraction of the forecast error variance for each endogenous variable, explained by each of the three identified structural shocks at various time horizons. The FEVD is estimated using the SDI and Restrictions 1′, 2′, and 3′, and based on 100,000 independent importance sampling draws.

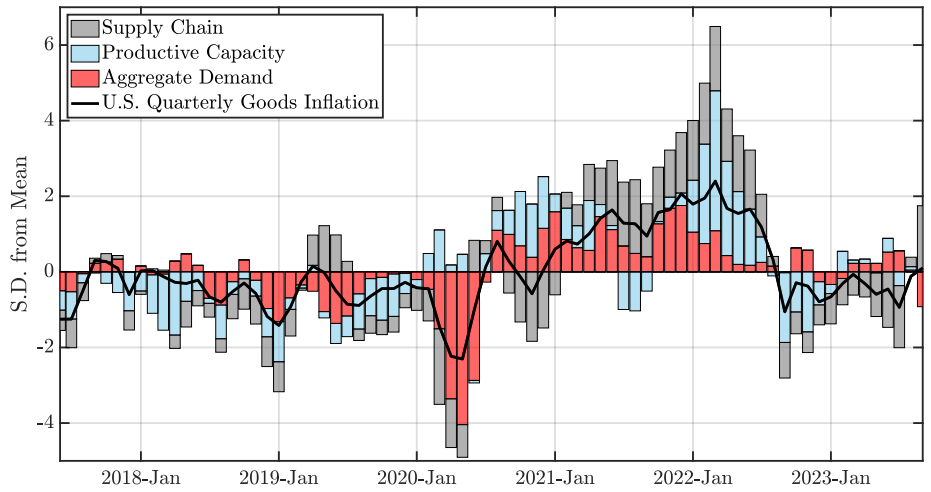

Figure F.12: HD of U.S. Quarter-on-Quarter Goods Inflation: The SDI and Restrictions 1′, 2′, and 3′

Notes. The solid line represents the standardized goods inflation rate in the U.S., i.e., the quarter-on-quarter growth of the PCE goods price index. The shaded bars represent the corresponding standardized cumulative historical contribution of shocks to aggregate demand, productive capacity, and the supply chain to goods inflation. The shocks are identified using the SVAR specification in Equation (28), with the SDI included as the measure of supply chain disruptions, and Restrictions 1′, 2′, and 3′ imposed on the IRFs of each endogenous variable. The figure is derived from the posterior medians, based on 100,000 independent importance sampling draws.

on supply-side events, it is not immune to measurement errors inherent in word definitions. For instance, a disruption in "supply" is distinct from one in the "supply chain," as the former may result from factors such as a labor supply shortage.

Lastly, the Kiel Trade Indicator (Stamer, 2021), which utilizes the same AIS data as our ACR index, offers an alternative perspective on the global supply chain strain by estimating imports and exports and tracking the movement of container ships at major ports, as well as freight on stationary ships. However, this indicator faces several challenges. First, the calculation of TEUs is problematic because the draft of a container ship does not reliably indicate its loading status, given that loading and unloading operations can occur simultaneously. Second, variations in imports and exports are influenced by demand-side factors, which introduces endogeneity concerns similar to those of indices based on transportation costs. Third, the methodology for estimating cargo capacity tied up at ports does not distinguish between the mooring positions of container ships (i.e., berth or anchorage), potentially leading to an overestimation of port congestion, as argued in Talley and Ng (2016).

F.4. ACT

As introduced in Appendix B.3, we define an alternative congestion metric for ports, namely the Average Congestion Time (ACT). This metric measures the average number of hours a container ship waits in an anchorage area of a port before docking at a berth, with the measurement weighted by the relative number of ship visits to each port. Figure F.13 plots the ACT index alongside the ACR index at a monthly frequency.

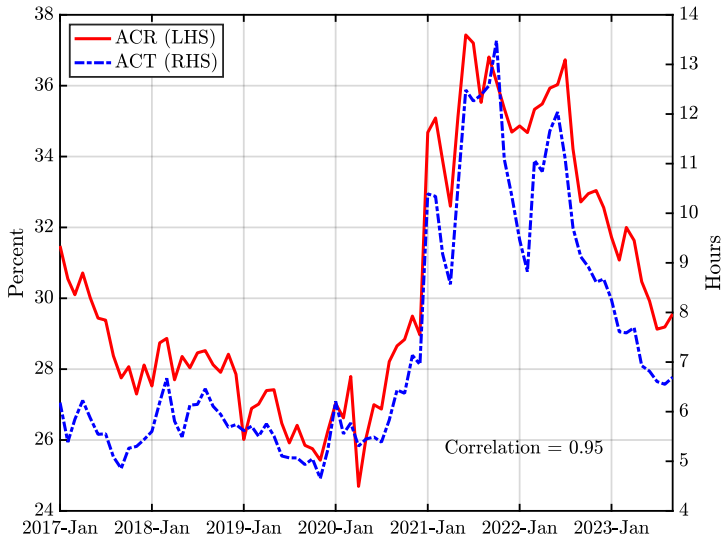

Figure F.13: ACR vs. ACT

Notes. Figure F.13 plots the ACR index (solid red line) against the ACT index (dashed-dotted blue line) for the sample period from January 2017 to September 2023. Both the ACR and ACT indices are computed using the AIS data of container ships and our IMA-DBSCAN algorithm, as detailed in Appendix B. The ACR index is measured in percentage terms, while the ACT index is measured in hours. Both series have been seasonally adjusted.

As shown in Figure F.13, the two congestion indices closely co-move with each other, exhibiting a correlation of 0.95. Not surprisingly, as illustrated in Figures F.14, F.15, and F.16, using the ACT index in the causality assessment delivers results quantitatively similar to those obtained with the ACR index.

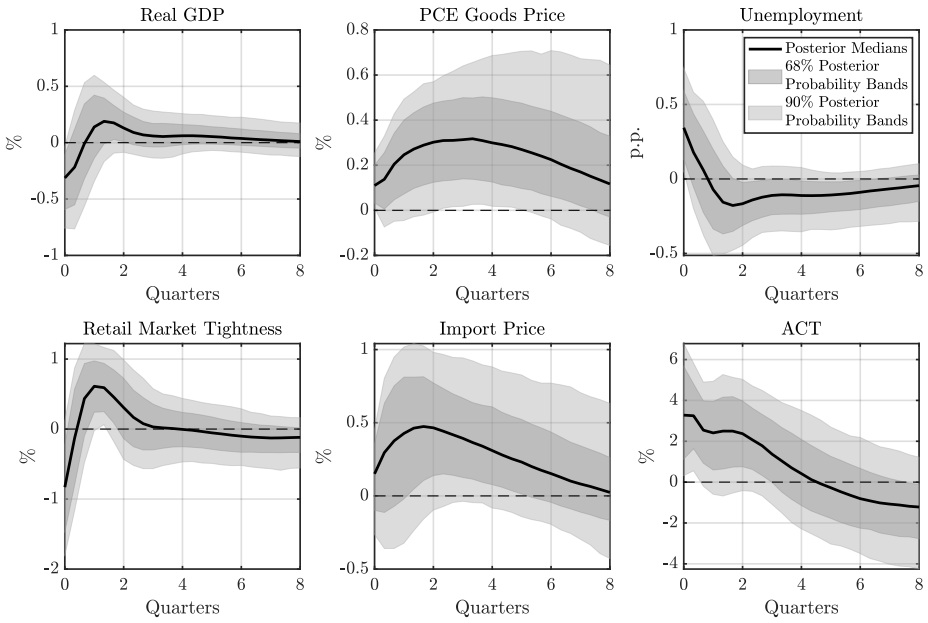

Figure F.14: IRFs to an Adverse Shock to the Supply Chain: The ACT Index and Restrictions 1, 2, and 3

Notes. The IRFs to a one standard deviation adverse shock to the supply chain are identified using the ACT index and Restrictions 1, 2, and 3. The solid line shows the point-wise posterior medians, and the shaded bands represent the 68% and 90% equal-tailed point-wise posterior probability bands. The figure is based on 100,000 independent importance sampling draws.

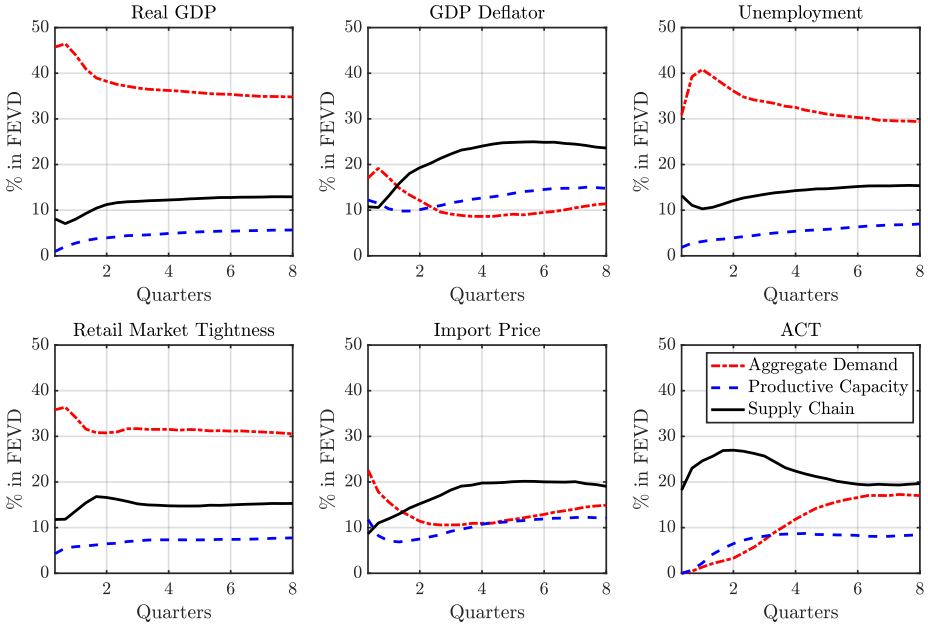

Figure F.15: FEVD from the SVAR: The ACT Index and Restrictions 1, 2, and 3

Notes. Each line presents the median fraction of the forecast error variance for each endogenous variable, explained by each of the three identified structural shocks at various time horizons. The FEVD is estimated using the ACT index and Restrictions 1, 2, and 3, and based on 100,000 independent importance sampling draws.

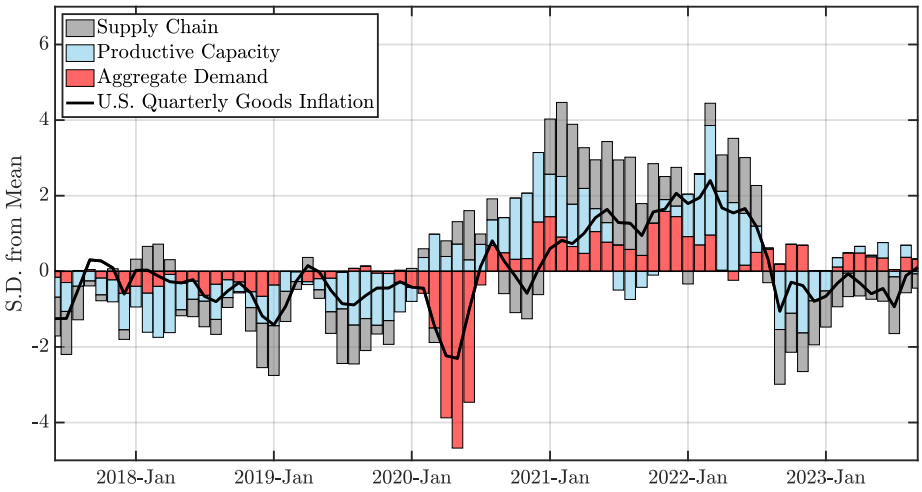

Figure F.16: HD of U.S. Quarter-on-Quarter Goods Inflation: The ACT Index and Restrictions 1, 2, and 3

Notes. The solid line represents the standardized goods inflation rate in the U.S., i.e., the quarter-on-quarter growth of the PCE goods price index. The shaded bars represent the corresponding standardized cumulative historical contribution of shocks to aggregate demand, productive capacity, and the supply chain to goods inflation. The shocks are identified using the SVAR specification in Equation (28), with the ACT index included as the measure of global supply chain disruptions, and Restrictions 1, 2, and 3 imposed on the IRFs of each endogenous variable. The figure is derived from the posterior medians, based on 100,000 independent importance sampling draws.

G. Priors and Identification in the TVAR

G.1. Priors

Our formulation of the prior in the TVAR model follows Bańbura et al. (2010), Mumtaz and Zanetti (2012), and Pizzinelli et al. (2020), and the same prior has been applied to the parameters in both the supply chain disrupted ($\mathbb{D}$) and undisrupted ($\mathbb{U}$) regimes. Specifically, we write the TVAR model in Equation (31) compactly as a system of multivariate regressions:

$$\boldsymbol{y} = (\boldsymbol{M}_{\mathbb{D}}\boldsymbol{x}_{\mathbb{D}} + \boldsymbol{u}_{\mathbb{D}})\boldsymbol{I} + (\boldsymbol{M}_{\mathbb{U}}\boldsymbol{x}_{\mathbb{U}} + \boldsymbol{u}_{\mathbb{U}})(\boldsymbol{1}_{T\times T} - \boldsymbol{I}), \tag{G.1}$$

where $\boldsymbol{y} = [\boldsymbol{y}_1 \ \dots \ \boldsymbol{y}_T]$ is an $n \times T$ matrix, $\boldsymbol{x}_{\mathbb{D}} = [\boldsymbol{x}_{\mathbb{D},1} \ \dots \ \boldsymbol{x}_{\mathbb{D},T}]$ is an $m \times T$ matrix with $\boldsymbol{x}_{\mathbb{D},t} = [\boldsymbol{y}'_{t-1} \ \dots \ \boldsymbol{y}'_{t-L} \ \boldsymbol{\omega}'_t]'$, $\boldsymbol{x}_{\mathbb{U}} = [\boldsymbol{x}_{\mathbb{U},1} \ \dots \ \boldsymbol{x}_{\mathbb{U},T}]$ is an $m \times T$ matrix with $\boldsymbol{x}_{\mathbb{U},t} = [\boldsymbol{y}'_{t-1} \ \dots \ \boldsymbol{y}'_{t-L} \ \boldsymbol{\omega}'_t]'$, $\boldsymbol{\omega}_t = [1, t]'$ is a 2×1 vector of a constant and a linear trend, $\boldsymbol{u}_{\mathbb{D}} = [\boldsymbol{\Sigma}_{\mathbb{D}}^{1/2}\boldsymbol{\varepsilon}_1 \ \dots \ \boldsymbol{\Sigma}_{\mathbb{D}}^{1/2}\boldsymbol{\varepsilon}_T]$ is an $n \times T$ matrix, $\boldsymbol{u}_{\mathbb{U}} = [\boldsymbol{\Sigma}_{\mathbb{U}}^{1/2}\boldsymbol{\varepsilon}_1 \ \dots \ \boldsymbol{\Sigma}_{\mathbb{U}}^{1/2}\boldsymbol{\varepsilon}_T]$ is an $n \times T$ matrix, $\boldsymbol{\Sigma}_{\mathbb{D}}$ and $\boldsymbol{\Sigma}_{\mathbb{U}}$ are the covariance matrices, $\boldsymbol{I} = diag[I_1 \ \dots \ I_T]$ is a $T \times T$ diagonal matrix, $\boldsymbol{M}_{\mathbb{D}} = [\boldsymbol{B}'_{\mathbb{D},1} \ \dots \ \boldsymbol{B}'_{\mathbb{D},L} \ \boldsymbol{C}'_{\mathbb{D}}]$ and $\boldsymbol{M}_{\mathbb{U}} = [\boldsymbol{B}'_{\mathbb{U},1} \ \dots \ \boldsymbol{B}'_{\mathbb{U},L} \ \boldsymbol{C}'_{\mathbb{U}}]$ are two $n \times m$ matrices containing the TVAR coefficients associated with each regime, and $m = nL + 2$. Given Equation (G.1), for each regime $r \in \{\mathbb{D}, \mathbb{U}\}$, we assume that the prior distribution of the parameter vector, $vec(\boldsymbol{M}_r)$, has a Normal-Inverse-Wishart (NIW) conjugate form.[20] Such a form can be written as:

$$\begin{aligned} vec(\boldsymbol{M}_r)|\boldsymbol{\Sigma}_r &\sim N\left(vec(\boldsymbol{M}_r^0), \boldsymbol{\Sigma}_r \otimes \boldsymbol{\Omega}_r^0\right), \\ \boldsymbol{\Sigma}_r &\sim IW\left(\boldsymbol{S}_r^0, \alpha_r^0\right), \end{aligned} \tag{G.2}$$

where $vec(\boldsymbol{M}_r^0)$ is the prior mean of the parameter vector, $\boldsymbol{\Omega}_r^0$ controls the tightness around this prior, $\boldsymbol{S}_r^0$ is the prior scale matrix of the Inverse-Wishart (IW) distribution, and α_r^0 denotes the prior degrees of freedom. Essentially, the prior in Equation (G.2) is a generalization of the Minnesota prior discussed in Litterman (1986) and assumes that the endogenous variables follow a random walk or an AR(1) process. This is based on the idea that recent lags provide more reliable information on the dynamics of the system and therefore the estimation should assign them a higher weighting. Unlike the original formulation in Litterman (1986), however, the prior in Equation (G.2) does not assume a diagonal, fixed, and known covariance matrix, making it

[20] $vec(\cdot)$ denotes the operator that stacks the columns of a matrix into a vector.

more suitable for our structural analysis.

The Normal-Inverse-Wishart prior implies that, while the prior expectations and variances of the coefficient matrices for the constant and linear trend, $\boldsymbol{C}_r$, are diffuse, those associated with the autoregressive matrices, $\boldsymbol{B}_{r,l}$, can be written as follows:

$$\begin{aligned}\mathbb{E}[(\boldsymbol{B}_{r,l})_{i,j}] &= \begin{cases}\beta^0_{r,i}, & \text{if } i=j,\ l=1;\\ 0, & \text{otherwise;}\end{cases}\\ \mathbb{V}[(\boldsymbol{B}_{r,l})_{i,j}] &= \lambda\sigma_i^2/\sigma_j^2,\end{aligned} \tag{G.3}$$

where $\beta^0_{r,1},\ldots,\beta^0_{r,n}$ are the prior means of the autoregressive coefficients, $\sigma_1,\ldots,\sigma_n$ are the prior error standard deviations, and the hyper-parameter λ controls the overall tightness of the prior distribution such that a larger λ corresponds to a looser prior. As described in Bańbura et al. (2010) and commonly used in the literature of Bayesian SVARs, the prior moments in Equation (G.3) can be implemented by adding $T_{r,d}$ dummy observations $\boldsymbol{y}_{r,d}$ and $\boldsymbol{x}_{r,d}$ to the system of regressions in Equation (G.1) that correspond to each regime, with $\boldsymbol{y}_{r,d}$ and $\boldsymbol{x}_{r,d}$ satisfying the following structures:

$$\boldsymbol{y}_{r,d} = \begin{bmatrix} diag[\beta^0_{r,1}\sigma_1 \ \ldots \ \beta^0_{r,n}\sigma_n]/\lambda \\ \mathbf{0}_{n(L-1)\times n} \\ diag[\sigma_1 \ \ldots \ \sigma_n] \\ \mathbf{0}_{2\times n}\end{bmatrix},\ \boldsymbol{x}_{r,d} = \begin{bmatrix} J_L \otimes diag[\sigma_1 \ \ldots \ \sigma_n]/\lambda & \mathbf{0}_{nL\times 1} & \mathbf{0}_{nL\times 1} \\ \mathbf{0}_{n\times nL} & \mathbf{0}_{n\times 1} & \mathbf{0}_{n\times 1} \\ \mathbf{0}_{1\times nL} & \xi & 0 \\ \mathbf{0}_{1\times nL} & 0 & \xi\end{bmatrix},$$

where $J_L = diag[1 \ \ldots \ L]$ and the hyper-parameter ξ controls the prior on the constant and the linear trend such that a small number makes the prior uninformative. Subsequently, the prior moments in Equation (G.2) are simply functions of $\boldsymbol{y}_{r,d}$ and $\boldsymbol{x}_{r,d}$, which are given by:

$$\begin{aligned}\boldsymbol{M}^0_r &= \boldsymbol{y}_{r,d}\boldsymbol{x}'_{r,d}(\boldsymbol{x}_{r,d}\boldsymbol{x}'_{r,d})^{-1},\\ \boldsymbol{\Omega}^0_r &= (\boldsymbol{x}_{r,d}\boldsymbol{x}'_{r,d})^{-1},\\ \boldsymbol{S}^0_r &= (\boldsymbol{y}_{r,d}-\boldsymbol{M}^0_r\boldsymbol{x}_{r,d})(\boldsymbol{y}_{r,d}-\boldsymbol{M}^0_r\boldsymbol{x}_{r,d})',\\ \alpha^0_r &= T_{r,d}-m.\end{aligned}$$

With the Normal-Inverse-Wishart prior being conjugate, the conditional posterior distribution of the parameter vector is also Normal-Inverse-Wishart (Bańbura et al., 2010; Mumtaz and

Zanetti, 2012):

$$vec(\boldsymbol{M}_r)|\boldsymbol{\Sigma}_r, \boldsymbol{y} \sim N\left(vec(\tilde{\boldsymbol{M}}_r), \boldsymbol{\Sigma}_r \otimes (\tilde{\boldsymbol{x}}_r \tilde{\boldsymbol{x}}_r')^{-1}\right),$$
$$\boldsymbol{\Sigma}_r|\boldsymbol{y} \sim IW\left(\tilde{\boldsymbol{S}}_r, T_{r,d} + 2 + T - m\right),$$

where the parameters associated with the posterior are given by:

$$\tilde{\boldsymbol{M}}_r = \tilde{\boldsymbol{y}}_r \tilde{\boldsymbol{x}}_r' (\tilde{\boldsymbol{x}}_r \tilde{\boldsymbol{x}}_r')^{-1},$$
$$\tilde{\boldsymbol{S}}_r^0 = (\tilde{\boldsymbol{y}}_r - \tilde{\boldsymbol{M}}_r \tilde{\boldsymbol{x}}_r)(\tilde{\boldsymbol{y}}_r - \tilde{\boldsymbol{M}}_r \tilde{\boldsymbol{x}}_r)',$$

in which the terms $\tilde{\boldsymbol{y}}_r$ and $\tilde{\boldsymbol{x}}_r$ are the matrices of $\boldsymbol{y}_r$ and $\boldsymbol{x}_r$ augmented with the dummy observations $\boldsymbol{y}_{r,d}$ and $\boldsymbol{x}_{r,d}$ respectively.[21]

Following Mumtaz and Zanetti (2012) and Pizzinelli et al. (2020), we obtain the values of the prior mean of each autoregressive coefficient, $\beta_{r,i}^0$, as well as the prior error standard deviation, σ_i, from the OLS estimation of a univariate AR(1) model for each endogenous variable. In addition, we set $\lambda = 0.25$ to ensure fast lag decay toward zero. Finally, in terms of the prior distribution of $\overline{ACR}$, we assume that it is normally distributed, with the mean set at the median of the ACR series and the standard deviation calibrated to deliver a Markov chain Monte Carlo acceptance rate of approximately 70% to 80%.

G.2. Identification Using the PFA

Following Uhlig (2005) and Mountford and Uhlig (2009), the identification scheme we employ in the study of the state-dependent effects of a contractionary monetary policy shock amounts to finding an impulse vector a that minimizes a given criterion function $f(\cdot)$ on the space of all impulse vectors. This function penalizes positive impulse responses of real GDP, PCE goods price, retail market tightness, and import price as well as negative impulse responses of the federal funds rate and unemployment at horizons $k = 1, \ldots, K$, while satisfying the zero restriction imposed on the impulse response of the ACR index at horizon $k = 1$.[22] The scheme is applied separately for the observations in each regime. Hence, for simplicity, we drop the regime-specific notation $r \in \{\mathbb{D}, \mathbb{U}\}$ in the following description.

[21] $\boldsymbol{y}_r$ is the part of $\boldsymbol{y}$ that is associated with regime $r \in \{\mathbb{D}, \mathbb{U}\}$.

[22] Our identification results using the PFA are also robust to removing the zero restriction imposed on the impulse response of the ACR index at horizon $k = 1$.

The PFA is implemented numerically as follows. Define the penalty function as:

$$f(x) = \begin{cases} x, & \text{if } x \leq 0; \\ 100x, & \text{if } x > 0, \end{cases} \tag{G.4}$$

which penalizes positive responses in linear proportion and rewards negative responses in linear proportion, albeit at a slope one hundred times smaller than the slope for penalties on the positive side. For the true VAR coefficients, let $r_{j,a}(k),\ k = 1, \ldots, K$ be the impulse response of variable j and let σ_j be the standard deviation of the series for variable j. Let $\iota_j = -1$ if j is the index of the federal funds rate or unemployment in the data vector, and $\iota_j = 1$ if j is the index of real GDP, PCE goods price, retail market tightness, or import price in the data vector. Define the contractionary monetary policy impulse vector as that impulse vector a, which minimizes the total penalty $\varphi(a)$ subject to the zero restriction imposed on the impulse response of the ACR index at horizon $k = 1$:

$$\varphi(a) = \sum_{j \in \left\{ \begin{array}{c} \text{“federal funds rate,”} \\ \text{“real GDP,”} \\ \text{“PCE goods price,”} \\ \text{“unemployment,”} \\ \text{“retail market tightness,”} \\ \text{“import price”} \end{array} \right\}} \left[\sum_{k=1}^{K} f\left(\iota_j \frac{r_{j,a}(k)}{\sigma_j} \right) \right].$$

The re-scaling by σ_j is necessary to make the deviations across different impulse responses comparable to each other. Notice that the sign of the penalty direction is flipped for the federal funds rate and unemployment. Since the true VAR is unknown, we find the contractionary monetary policy vector for each draw from the posterior. Such a step involves numerical minimization, and we keep all the draws and accordingly calculate all the corresponding impulse vectors. As a result, the IRFs in the main text are calculated based on these.

G.3. Posterior and Identified Regimes

The posterior distribution of the threshold $\overline{ACR}$ is plotted in Figure G.1, while the time series of the identified regimes using the median of such a posterior is plotted in Figure G.2.

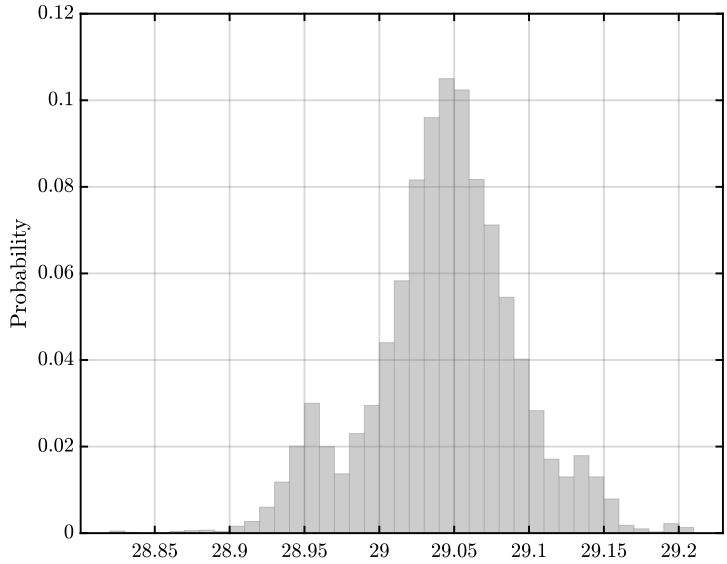

Figure G.1: Posterior Distribution of the Threshold $\overline{ACR}$

Notes. The figure plots the posterior distribution of the ACR threshold value, i.e., $\overline{ACR}$, based on 10,000 independent draws.

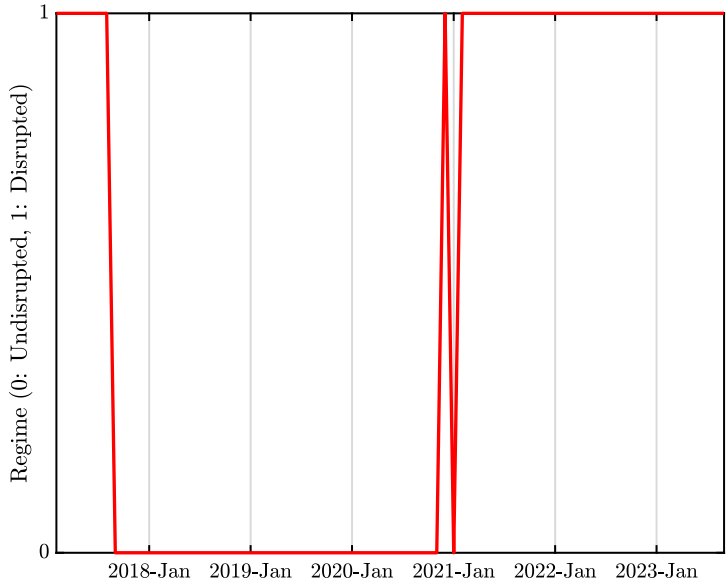

Figure G.2: Regimes Based on the Median of the Posterior $\overline{ACR}$

Notes. The solid red line, switching from zero to one, represents the current regime as identified by the median of the posterior distribution of the ACR threshold, i.e., $median(\overline{ACR}) = 29.05\%$. The value of one corresponds to the supply chain disrupted ($\mathbb{D}$) regime, while the value of zero corresponds to the supply chain undisrupted ($\mathbb{U}$) regime.

H. Robustness of TVAR Results

In this appendix, we conduct several robustness checks of our identification results presented in Section 5 regarding the state-dependent effects of monetary policy. In Figure H.1, we first show that our state-dependence results are robust to using the Wu-Xia shadow federal funds rate (Wu and Xia, 2016). This series provides an estimated federal funds rate during periods when the zero lower bound constrains it and, therefore, reflecting the effects of unconventional monetary policy.

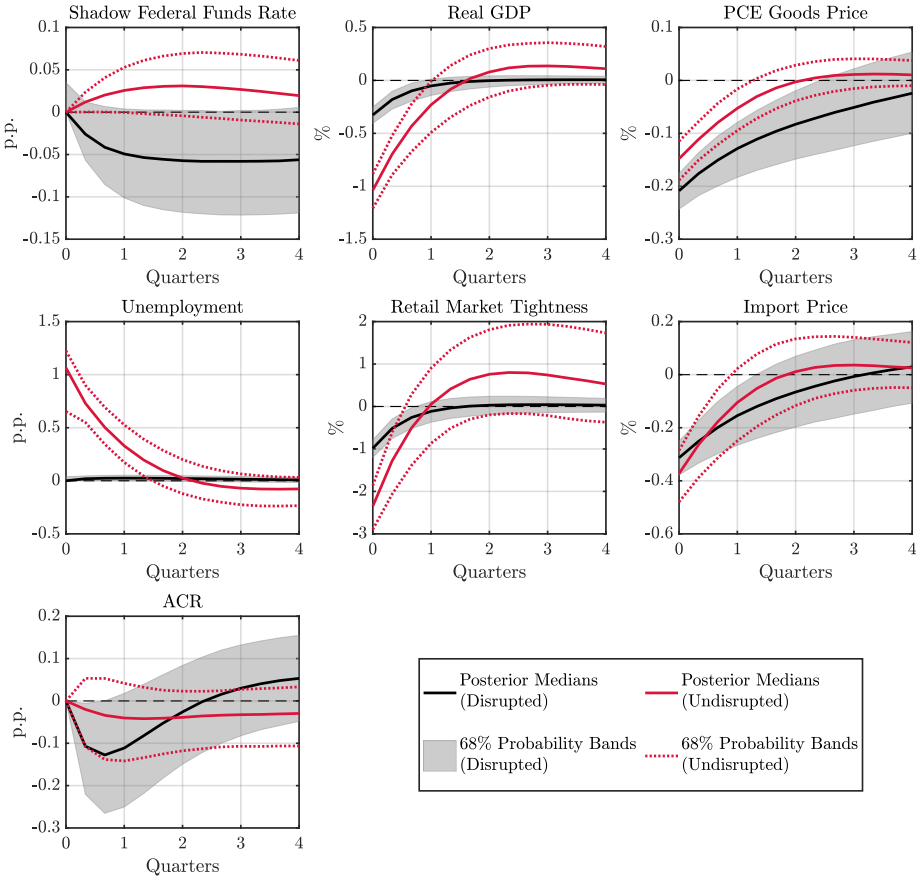

Figure H.1: State-Dependent Effects of a Contractionary Monetary Policy Shock: Wu-Xia shadow federal funds rate

Notes. The figure shows the IRFs to a one standard deviation contractionary monetary policy shock identified using a TVAR specification as in Equation (31), with the Wu-Xia shadow federal funds rate (Wu and Xia, 2016) included to reflect the stance of U.S. monetary policy, as well as Restriction 4 imposed on the IRFs of each endogenous variable, for both the supply chain disrupted and undisrupted regimes. The solid black (solid red) line shows the point-wise posterior medians, and the shaded black area (dotted red lines) depicts the 68% equal-tailed point-wise posterior probability bands for the supply chain disrupted (undisrupted) regime. The figure is based on 10,000 independent draws from the posterior.

In Figure H.2, we show that our state-dependence results are robust to dropping the zero restriction imposed on the on-impact response of the ACR index to the contractionary monetary

policy shock.

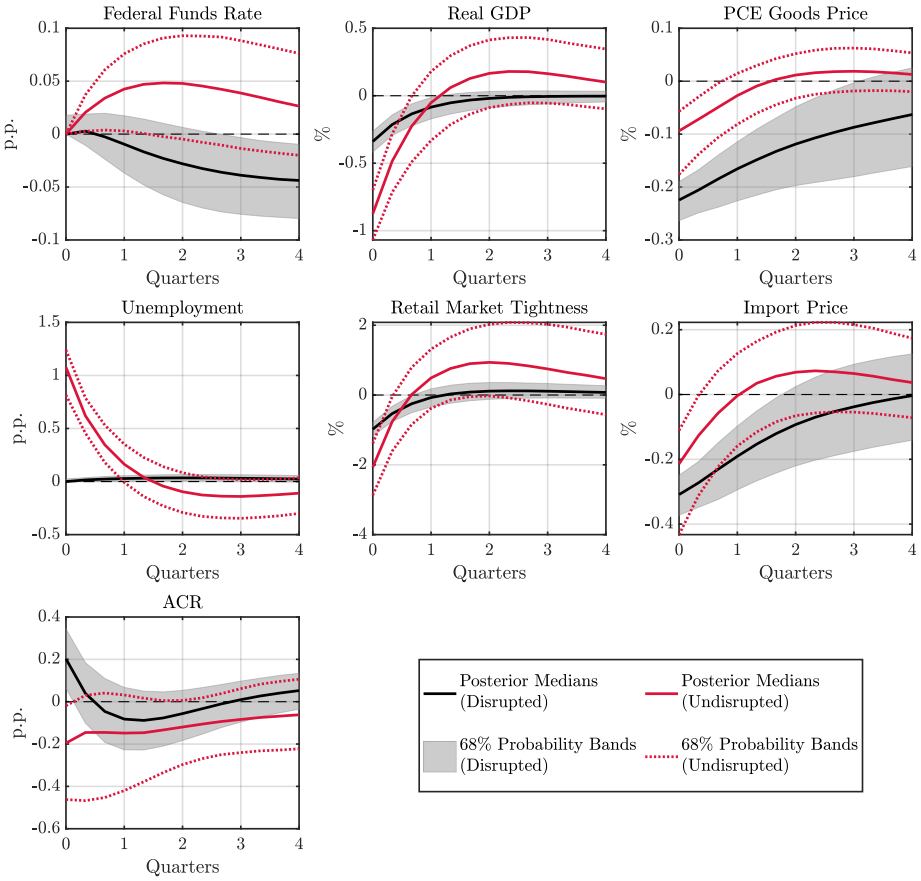

Figure H.2: State-Dependent Effects of a Contractionary Monetary Policy Shock: No Zero Restriction on the ACR Index

Notes. The figure shows the IRFs to a one standard deviation contractionary monetary policy shock, identified using a TVAR specification as in Equation (31), but without the zero restriction imposed on the on-impact response of the ACR index, for both the supply chain disrupted and undisrupted regimes. The solid black (solid red) line shows the point-wise posterior medians, and the shaded black area (dotted red lines) depicts the 68% equal-tailed point-wise posterior probability bands for the supply chain disrupted (undisrupted) regime. The figure is based on 10,000 independent draws from the posterior.

Also, in Figures H.3 and H.4, we show that our state-dependence results are robust to considering different lag structures, i.e., two or three lags. We do not consider four lags or beyond due to parameter uncertainty resulting from our limited sample length. We also show in Figure H.5 that the results are robust when a looser prior is undertaken in the estimation, i.e., $\lambda = 0.5$.

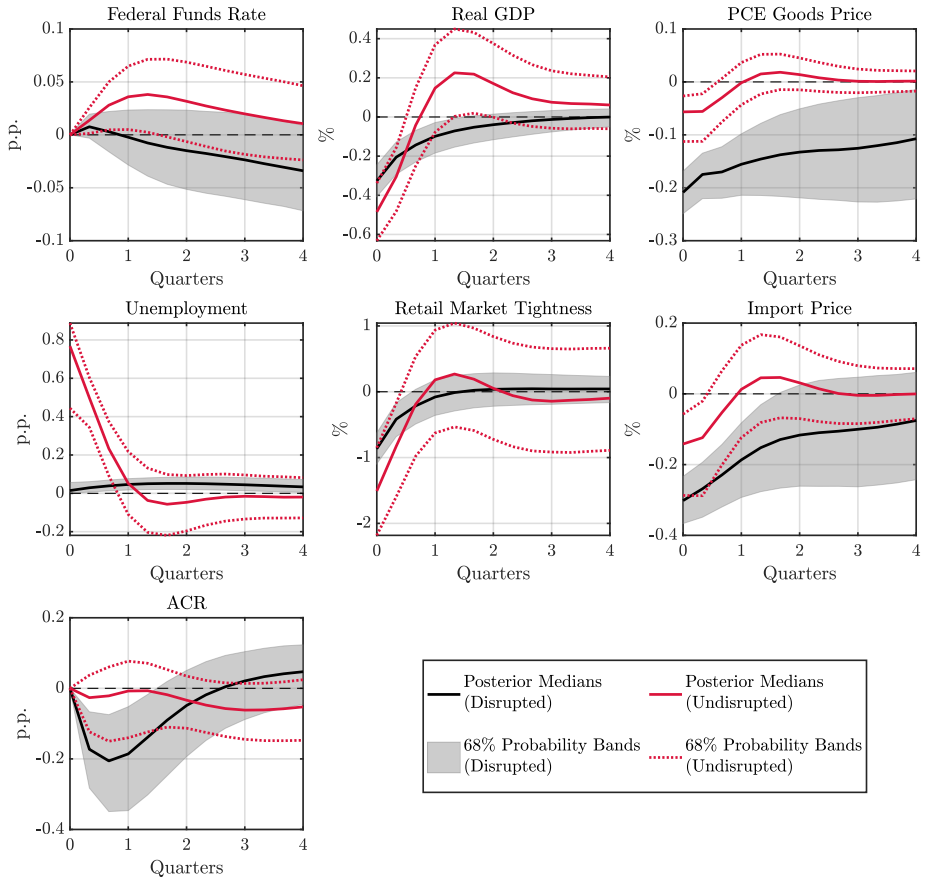

Figure H.3: State-Dependent Effects of a Contractionary Monetary Policy Shock: Two Lags

Notes. The figure shows the IRFs to a one standard deviation contractionary monetary policy shock identified using a TVAR specification as in Equation (31) with two lags, as well as Restriction 4 imposed on the IRFs of each endogenous variable, for both the supply chain disrupted and undisrupted regimes. The solid black (solid red) line shows the point-wise posterior medians, and the shaded black area (dotted red lines) depicts the 68% equal-tailed point-wise posterior probability bands for the supply chain disrupted (undisrupted) regime. The figure is based on 10,000 independent draws from the posterior.

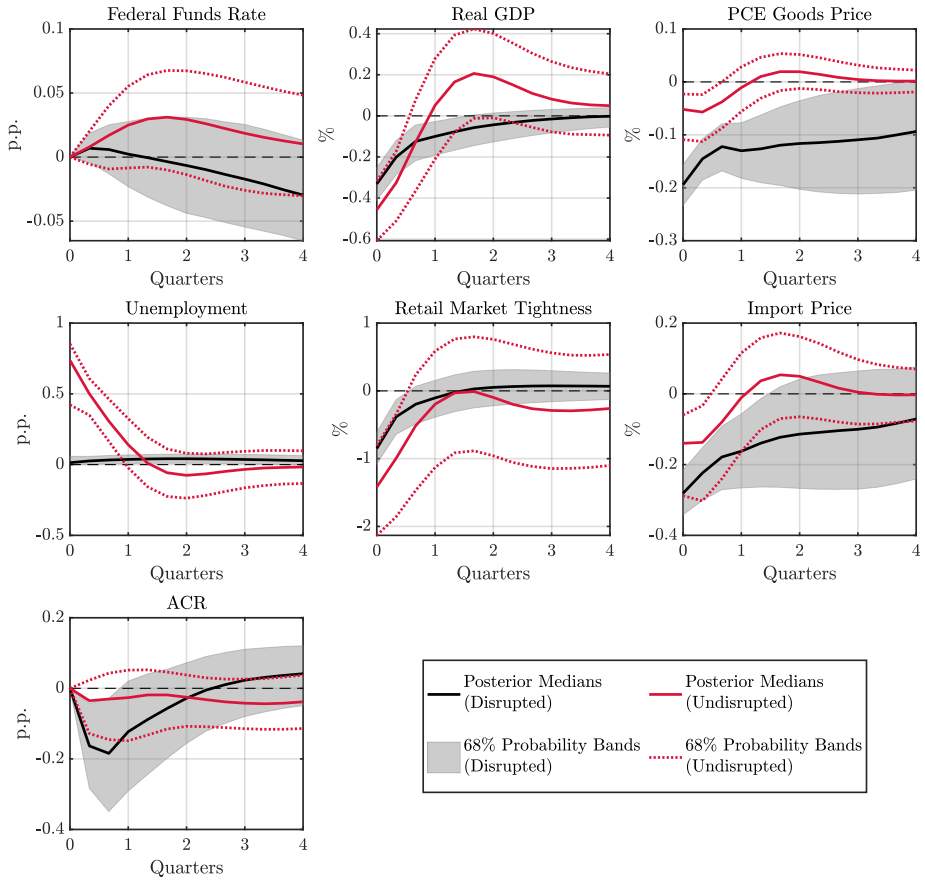

Figure H.4: State-Dependent Effects of a Contractionary Monetary Policy Shock: Three Lags

Notes. The figure shows the IRFs to a one standard deviation contractionary monetary policy shock identified using a TVAR specification as in Equation (31) with three lags, as well as Restriction 4 imposed on the IRFs of each endogenous variable, for both the supply chain disrupted and undisrupted regimes. The solid black (solid red) line shows the point-wise posterior medians, and the shaded black area (dotted red lines) depicts the 68% equal-tailed point-wise posterior probability bands for the supply chain disrupted (undisrupted) regime. The figure is based on 10,000 independent draws from the posterior.

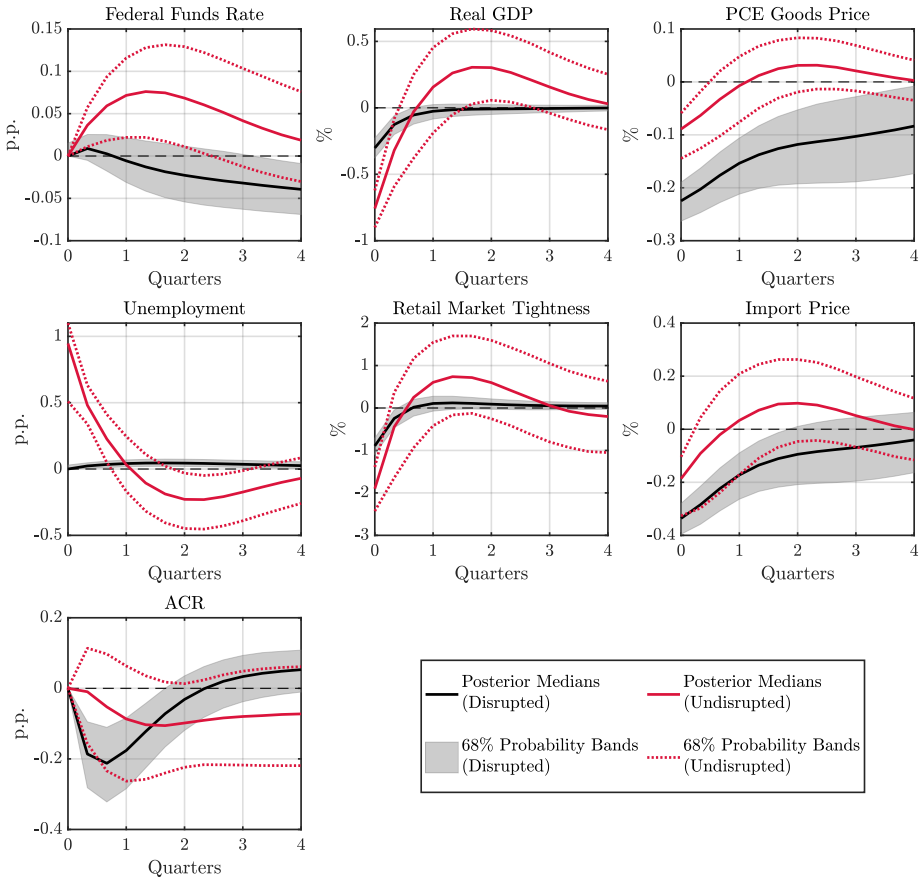

Figure H.5: State-Dependent Effects of a Contractionary Monetary Policy Shock: Looser Prior

Notes. The figure shows the IRFs to a one standard deviation contractionary monetary policy shock identified using a TVAR specification as in Equation (31) with $\lambda = 0.5$, as well as Restriction 4 imposed on the IRFs of each endogenous variable, for both the supply chain disrupted and undisrupted regimes. The solid black (solid red) line shows the point-wise posterior medians, and the shaded black area (dotted red lines) depicts the 68% equal-tailed point-wise posterior probability bands for the supply chain disrupted (undisrupted) regime. The figure is based on 10,000 independent draws from the posterior.

I. State-Dependence Results Using Local Projections

As a robustness check to our state-dependence results obtained using the TVAR model, we work with the local projections (LPs) to identify a contractionary monetary policy shock and analyze how it affects the macro aggregates for the U.S. economy depending on the level of global supply chain disruptions. LPs are a flexible approach that allows us to address the state-dependent effects of monetary policy without making strong parametric assumptions. Specifically, we use the LPs with interaction terms as in Ramey and Zubairy (2018), Ghassibe and Zanetti (2022), and Arias et al. (2023), and our identification scheme consists of sign restrictions implemented as described in Plagborg-Møller and Wolf (2021). Consider the following $n \times (K+1)$ projections:

$$\begin{aligned} y_{i,t+k} =& I_t \left[\boldsymbol{\beta}'_{\mathbb{D},i,k,0} \boldsymbol{y}_t + \sum_{l=1}^{L} \boldsymbol{\beta}'_{\mathbb{D},i,k,l} \boldsymbol{y}_{t-l} + \boldsymbol{C}'_{\mathbb{D},i,k} \boldsymbol{\omega}_t \right] \\ &+ (1 - I_t) \left[\boldsymbol{\beta}'_{\mathbb{U},i,k,0} \boldsymbol{y}_t + \sum_{l=1}^{L} \boldsymbol{\beta}'_{\mathbb{U},i,k,l} \boldsymbol{y}_{t-l} + \boldsymbol{C}'_{\mathbb{U},i,k} \boldsymbol{\omega}_t \right] + u_{i,k,t}, \end{aligned} \tag{I.1}$$

where $1 \leq i \leq n$, $0 \leq k \leq K$, $\boldsymbol{y}_t$ is an $n \times 1$ vector of the same endogenous variables as in Section 5.2 save for the ACR index (since it is the variable we use to split the sample), $y_{i,t+k}$ is the value of the i-th variable in $\boldsymbol{y}_{t+k}$, $\boldsymbol{\omega}_t = [1, t]'$ is a 2×1 vector of a constant and a linear trend, and $u_{i,k,t}$ is the reduced-form error corresponding to the i-th variable. The vector of the reduced-form errors for $k = 1$, $\boldsymbol{u}_{1,t} = [u_{1,1,t} \ \ \ldots \ \ u_{n,1,t}]'$, is assumed to have mean zero and covariance matrix equal to $\mathbb{E}(\boldsymbol{u}_{1,t}\boldsymbol{u}'_{1,t}) = \boldsymbol{\Sigma}$.

Similar to the approach in the TVAR model, I_t serves as a dummy variable indicating whether the supply chain is disrupted. The regime of supply chain disruption is defined based on whether the one-month lag of the ACR index exceeds its median level over the sample period. Figure I.1 illustrates the time series of the ACR index alongside its sample median. It is observed that, prior to mid-2017, the ACR index was consistently above its sample median, signifying the presence of the supply chain disrupted regime. However, from the second half of 2017 until the end of 2020, the ACR index remained below its sample median. This pattern reversed from early 2021 onward, with the ACR index rising above the median, indicating that the U.S. economy entered the disrupted regime. It is noteworthy that the transitions between the two regimes, as depicted in Figure I.1, closely align with those shown in Figure G.2, where the threshold $\overline{ACR}$ is determined endogenously in the TVAR estimation.

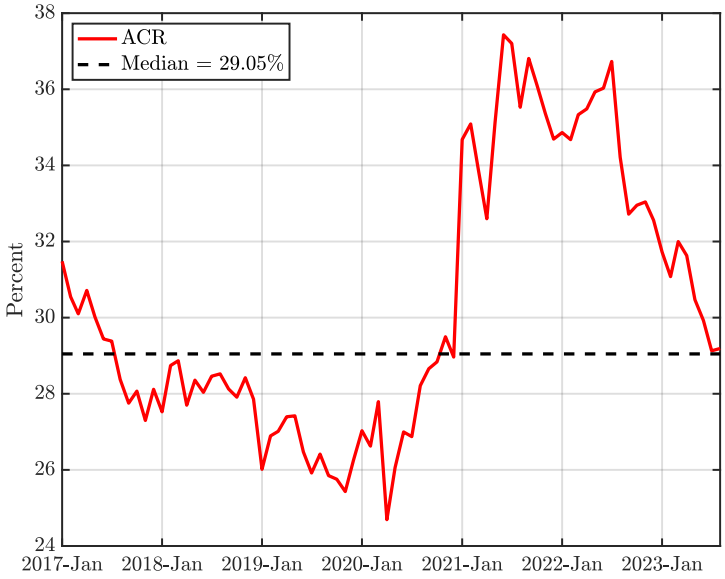

Figure I.1: ACR and Its Sample Median

Notes. The figure plots the ACR index as well as its sample median during the sample period from January 2017 to September 2023. The ACR index is computed using the AIS data of container ships and our IMA-DBSCAN algorithm, as detailed in Appendix B. The ACR index is measured in percentage terms and has been seasonally adjusted.

With the two regimes defined, the parameters $\boldsymbol{\beta}_{\mathbb{D},i,k,0}, \boldsymbol{\beta}_{\mathbb{D},i,k,l}$, and $\boldsymbol{C}_{\mathbb{D},i,k}$ correspond to the supply chain disrupted regime ($\mathbb{D}$), whereas the parameters $\boldsymbol{\beta}_{\mathbb{U},i,k,0}, \boldsymbol{\beta}_{\mathbb{U},i,k,l}$, and $\boldsymbol{C}_{\mathbb{U},i,k}$ correspond to the supply chain undisrupted regime ($\mathbb{U}$). As in our choice of the lag structure in the TVAR model, we include only one lag in the estimation of the LPs so as to reduce parameter uncertainty.[23]

In order to identify a contractionary monetary policy shock, we follow our theoretical prediction in Proposition 6 and come up with an identification scheme similar to that in Section 5.2. Yet, since the ACR index is not included in the estimation, we drop the zero restriction in Restriction 4 and re-write it as the following:

Restriction 4′. ***A contractionary monetary policy shock*** *leads to a negative response of real GDP, PCE goods price, retail market tightness, and import price, as well as to a positive response of unemployment and the federal funds rate at* $k = 1, 2, 3$. *In addition, the on-impact response of unemployment in p.p. is bounded to be smaller than ten times that of the federal funds rate in p.p.*

Restriction 4′ is similar to Restriction 4, except that we impose restrictions on the subsequent

[23] We have also tried two lags in the estimation and derived similar results.

horizons to sharpen our identification, and an elasticity bound is imposed to discipline the identified set of IRFs corresponding to unemployment. The latter variation is critical to ensure that our estimation is plausible, since in the absence of such a bound, the identified set of IRFs would include an increase in the unemployment rate of 100 p.p. as being equally likely as an increase in the unemployment rate of 1 p.p., following an unexpected increase in the federal funds rate of 0.05 p.p. Hence, we use the elasticity bound to rule out dubious IRFs following Kilian and Murphy (2012) and Arias et al. (2019, 2023).

With Restriction 4′, we determine the identified set of IRFs for each regime by numerically solving the quadratic program outlined in the supplement to Plagborg-Møller and Wolf (2021), using Algorithm 2 from Giacomini and Kitagawa (2021). Without loss of generality, we normalize the first shock to be the shock of interest. Let $\boldsymbol{S}_1$ denote a $12 \times n$ matrix that selects the IRFs that we restrict to be negative, and let $\boldsymbol{S}_2$ denote a $6 \times n$ matrix that selects the IRFs that we restrict to be positive (there are a of total 18 sign restrictions in Restriction 4′). Then, for each regime, we draw $D = 100,000$ orthogonal matrices $\boldsymbol{Q}_{r,d}$ (i.e., $\boldsymbol{Q}'_{r,d}\boldsymbol{Q}_{r,d} = \boldsymbol{Q}_{r,d}\boldsymbol{Q}'_{r,d} = \mathbf{1}_{n\times n}$) that satisfy the following:

$$\begin{aligned} \boldsymbol{S}_1 \hat{\boldsymbol{B}}_{r,0:2} \hat{\boldsymbol{\Omega}} \boldsymbol{Q}_{r,d} \boldsymbol{e}_1 &\leq 0, \\ \boldsymbol{S}_2 \hat{\boldsymbol{B}}_{r,0:2} \hat{\boldsymbol{\Omega}} \boldsymbol{Q}_{r,d} \boldsymbol{e}_1 &\geq 0, \\ \frac{\boldsymbol{e}_4' \hat{\boldsymbol{B}}_{r,0} \hat{\boldsymbol{\Omega}} \boldsymbol{Q}_{r,d} \boldsymbol{e}_1}{\boldsymbol{e}_1' \hat{\boldsymbol{B}}_{r,0} \hat{\boldsymbol{\Omega}} \boldsymbol{Q}_{r,d} \boldsymbol{e}_1} - 10 &\leq 0, \end{aligned} \tag{I.2}$$

where $r \in \{\mathbb{D}, \mathbb{U}\}$, $1 \leq d \leq D$, $\hat{\boldsymbol{B}}_{r,0:2} = [\hat{\boldsymbol{B}}'_{r,0} \;\; \hat{\boldsymbol{B}}'_{r,1} \;\; \hat{\boldsymbol{B}}'_{r,2}]'$, $\hat{\boldsymbol{B}}_{r,k} = [\hat{\boldsymbol{\beta}}_{r,1,k,0} \;\; \dots \;\; \hat{\boldsymbol{\beta}}_{r,n,k,0}]'$, $\hat{\boldsymbol{\beta}}_{r,i,k,0}$ is the OLS estimate of $\boldsymbol{\beta}_{r,i,k,0}$, $\hat{\boldsymbol{\Omega}} = chol(\hat{\boldsymbol{\Sigma}})'$, $chol$ is the upper triangular Cholesky decomposition of $\hat{\boldsymbol{\Sigma}}$, and $\hat{\boldsymbol{\Sigma}}$ is the OLS estimate of $\boldsymbol{\Sigma}$.[24] Given that the entry (i, j) in $\hat{\boldsymbol{B}}_{r,k}\hat{\boldsymbol{\Omega}}\boldsymbol{Q}_{r,d}$ gives the response of the i-th endogenous variable to the j-th shock at horizon k, the first two inequality conditions in Equation (I.2) summarize all the sign restrictions imposed on IRFs, while the last inequality condition contains the elasticity bound, as $(\boldsymbol{e}_4'\hat{\boldsymbol{B}}_{r,0}\hat{\boldsymbol{\Omega}}\boldsymbol{Q}_{r,d}\boldsymbol{e}_1)/(\boldsymbol{e}_1'\hat{\boldsymbol{B}}_{r,0}\hat{\boldsymbol{\Omega}}\boldsymbol{Q}_{r,d}\boldsymbol{e}_1)$ denotes the ratio between the on-impact responses of unemployment and the federal funds rate, where e_i is the i-th column of the n-dimensional identity matrix.

Given $\hat{\boldsymbol{B}}_{r,k}$ and $\hat{\boldsymbol{\Omega}}$, let $\{\boldsymbol{Q}_{r,d}\}_{d=1,\dots,D}$ be the draws of orthogonal matrices that satisfy the restrictions in Equation (I.2). The identified set of IRFs of the i-th endogenous variable at

[24] Vector inequalities are to be understood element-wise.

horizon k is thus given by:

$$\left[\min_{d}\left\{0.05\frac{\boldsymbol{e}_i'\hat{\boldsymbol{B}}_{r,k}\hat{\boldsymbol{\Omega}}\boldsymbol{Q}_{r,d}\boldsymbol{e}_1}{\boldsymbol{e}_1'\hat{\boldsymbol{B}}_{r,0}\hat{\boldsymbol{\Omega}}\boldsymbol{Q}_{r,d}\boldsymbol{e}_1}\right\}_{d=1,\ldots,D},\ \max_{d}\left\{0.05\frac{\boldsymbol{e}_i'\hat{\boldsymbol{B}}_{r,k}\hat{\boldsymbol{\Omega}}\boldsymbol{Q}_{r,d}\boldsymbol{e}_1}{\boldsymbol{e}_1'\hat{\boldsymbol{B}}_{r,0}\hat{\boldsymbol{\Omega}}\boldsymbol{Q}_{r,d}\boldsymbol{e}_1}\right\}_{d=1,\ldots,D}\right], \tag{I.3}$$

where the factor $0.05/(\boldsymbol{e}_1'\hat{\boldsymbol{B}}_{r,0}\hat{\boldsymbol{\Omega}}\boldsymbol{Q}_{r,d}\boldsymbol{e}_1)$ is a normalization imposed so that in both regimes, the contractionary monetary policy shock raises the federal funds rate by 0.05 percentage point on impact.

Figure I.2 presents the point-wise medians and the 68% equal-tailed point-wise probability bands for the identified set of IRFs in each regime following a contractionary monetary policy shock. In line with the TVAR model, the IRFs are shown from horizon $k = 0$ to horizon $k = 12$, which equates to four quarters. As depicted in Figure I.2, the state-dependent effects of a contractionary monetary policy shock are still evident. More specifically, the responses of real GDP and unemployment are more subdued. At the same time, those of the PCE goods price and import price are more pronounced during periods of global supply chain disruption. However, the differences in the responses to retail market tightness between the two regimes are not distinctly discernible.

We have also explored alternative thresholds at the 40th and 60th percentiles of the ACR index to differentiate between the supply chain disrupted and undisrupted regimes. The findings, as illustrated in Figures I.3 and I.4, demonstrate that our main results remain robust under these varying thresholds.

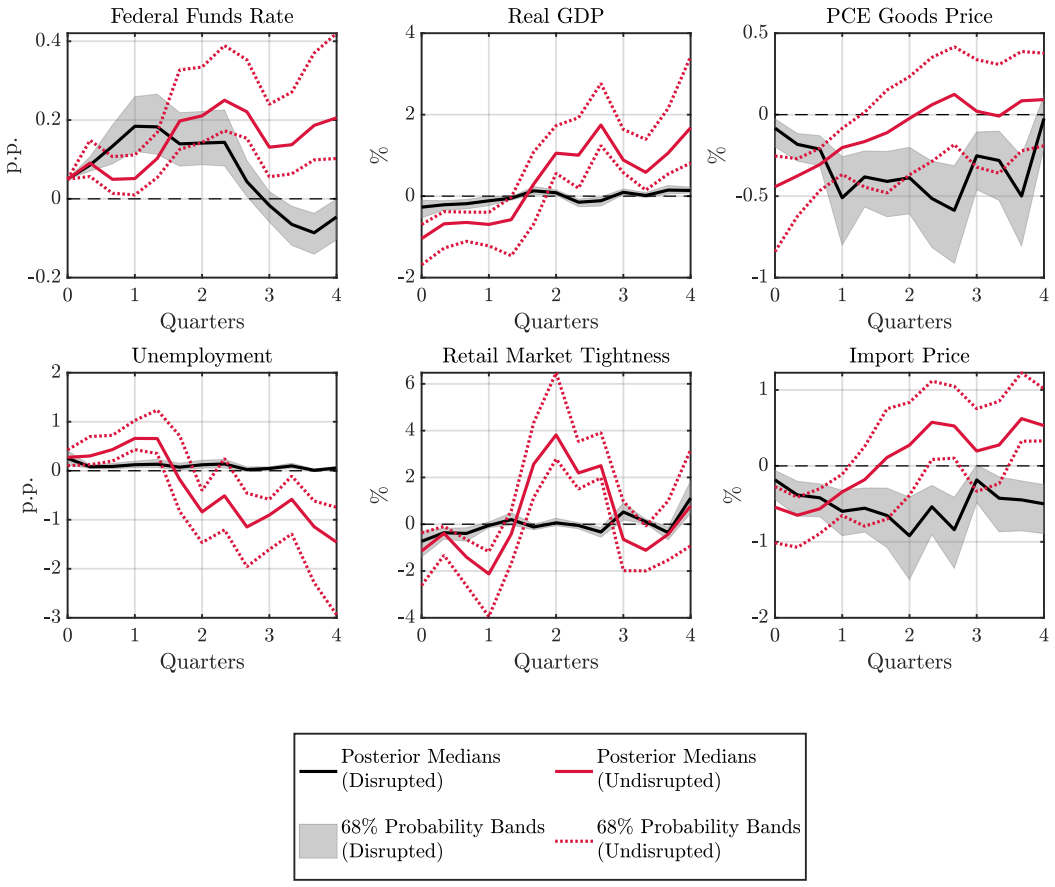

Figure I.2: State-Dependent Effects of a Contractionary Monetary Policy Shock: Using the LPs With Interaction Terms and a Threshold at the Median of the ACR Index

Notes. The figure shows the IRFs to a contractionary monetary policy shock identified using the LPs with interaction terms as in Ramey and Zubairy (2018), Ghassibe and Zanetti (2022), and Arias et al. (2023), along with Restriction 4′ imposed on the IRFs of each endogenous variable, for both the supply chain disrupted and undisrupted regimes. A threshold at the sample median of the ACR index is applied to distinguish between the two regimes. The solid black (solid red) line shows the point-wise medians and the shaded black area (dotted red lines) shows the 68% equal-tailed point-wise probability bands for the supply chain disrupted (undisrupted) regime. The figure is based on 100,000 draws of orthogonal matrices.

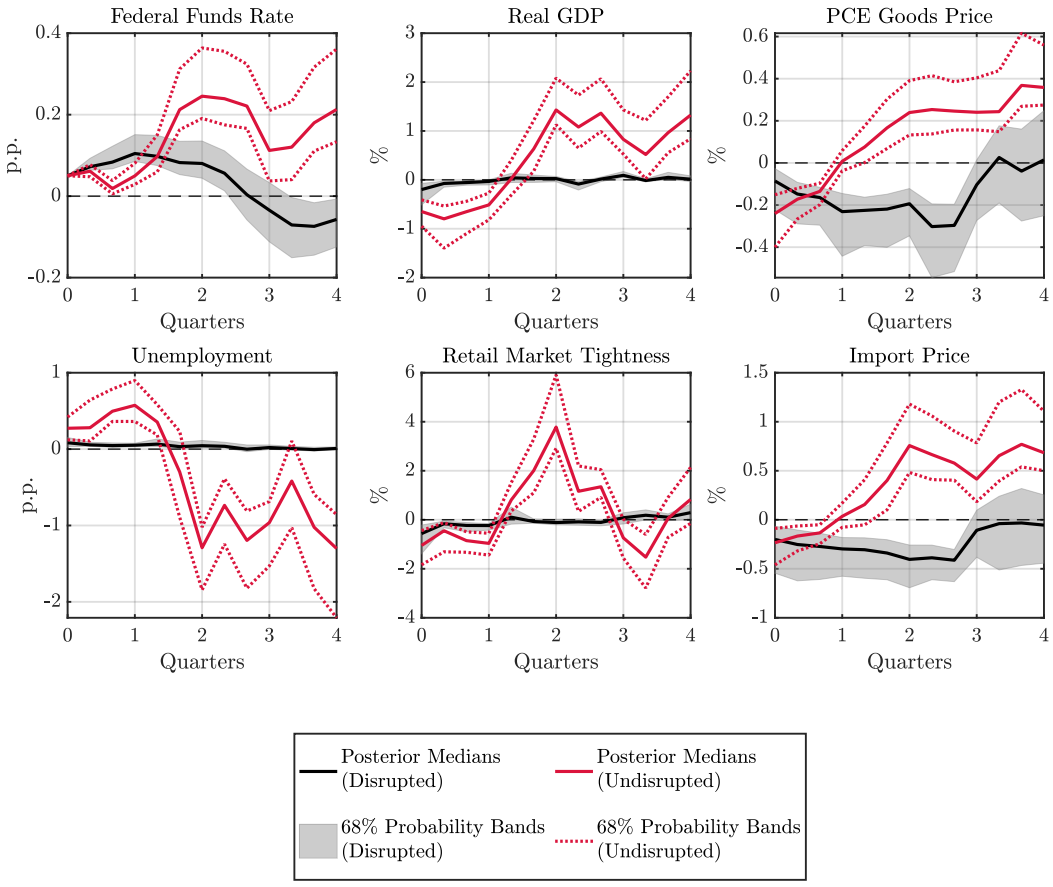

Figure I.3: State-Dependent Effects of a Contractionary Monetary Policy Shock: Using the LPs With Interaction Terms and a Threshold at the 40th Percentile of the ACR Index

Notes. The figure shows the IRFs to a contractionary monetary policy shock identified using the LPs with interaction terms as in Ramey and Zubairy (2018), Ghassibe and Zanetti (2022), and Arias et al. (2023), along with Restriction 4′ imposed on the IRFs of each endogenous variable, for both the supply chain disrupted and undisrupted regimes. A threshold at the 40th percentile of the ACR index is applied to distinguish between the two regimes. The solid black (solid red) line shows the point-wise medians and the shaded black area (dotted red lines) shows the 68% equal-tailed point-wise probability bands for the supply chain disrupted (undisrupted) regime. The figure is based on 100,000 draws of orthogonal matrices.

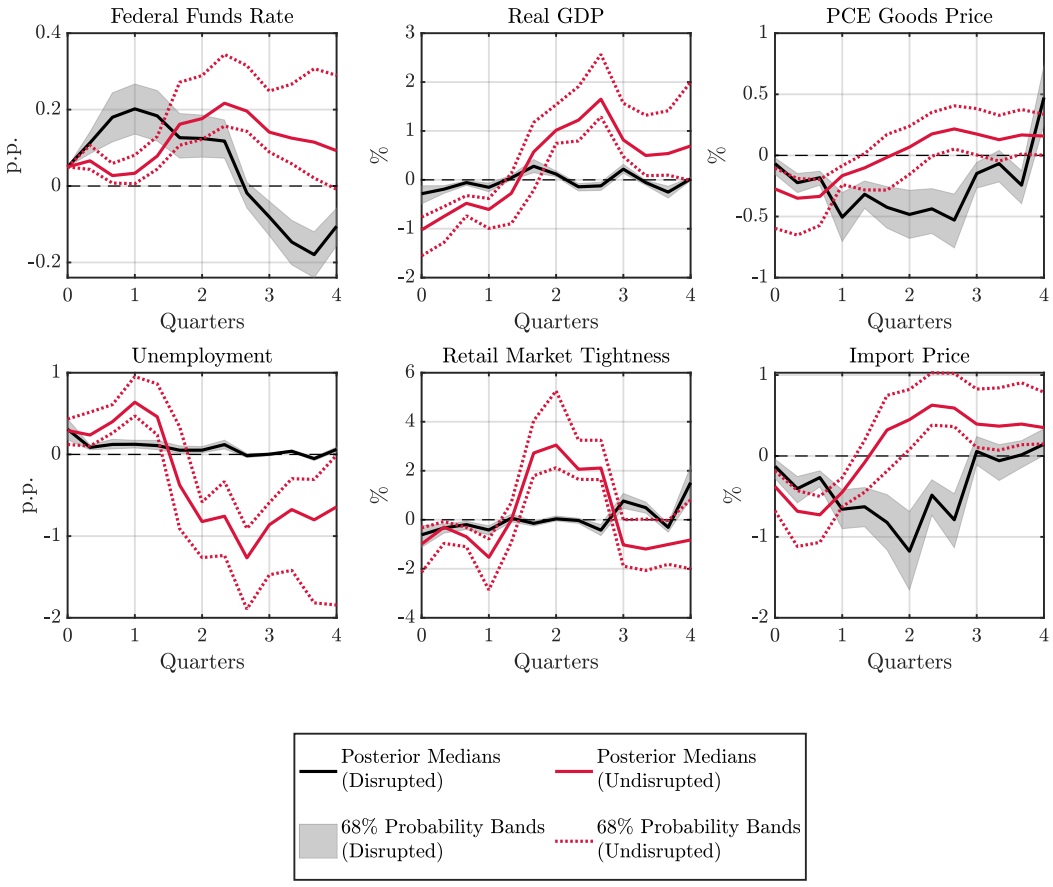

Figure I.4: State-Dependent Effects of a Contractionary Monetary Policy Shock: Using the LPs With Interaction Terms and a Threshold at the 60th Percentile of the ACR Index

Notes. The figure shows the IRFs to a contractionary monetary policy shock identified using the LPs with interaction terms as in Ramey and Zubairy (2018), Ghassibe and Zanetti (2022), and Arias et al. (2023), along with Restriction 4′ imposed on the IRFs of each endogenous variable, for both the supply chain disrupted and undisrupted regimes. A threshold at the 60th percentile of the ACR index is applied to distinguish between the two regimes. The solid black (solid red) line shows the point-wise medians and the shaded black area (dotted red lines) shows the 68% equal-tailed point-wise probability bands for the supply chain disrupted (undisrupted) regime. The figure is based on 100,000 draws of orthogonal matrices.

References for Appendices

Adland, R. and Jia, H. (2016). Dynamic Speed Choice in Bulk Shipping. *Maritime Economics & Logistics*, 20(3):253–266.

Allen, T. (2014). Information Frictions in Trade. *Econometrica*, 82:2041–2083.

Arias, J. E., Caldara, D., and Rubio-Ramírez, J. F. (2019). The Systematic Component of Monetary Policy in SVARs: An Agnostic Identification Procedure. *Journal of Monetary Economics*, 101:1–13.

Arias, J. E., Fernández-Villaverde, J., Rubio-Ramírez, J. F., and Shin, M. (2023). The Causal Effects of Lockdown Policies on Health and Macroeconomic Outcomes. *American Economic Journal: Macroeconomics*, 15(3):287–319.

Arias, J. E., Rubio-Ramírez, J. F., and Waggoner, D. F. (2018). Inference Based on Structural Vector Autoregressions Identified With Sign and Zero Restrictions: Theory and Applications. *Econometrica*, 86:685–720.

Attinasi, M. G., Balatti, M., Mancini, M., and Metelli, L. (2021). Supply Chain Disruptions and the Effects on the Global Economy. *ECB Economic Bulletin Issue 8*.

Bai, X. and Li, Y. (2022). The Congestion Effect of Oil Transportation and Its Trade Implications. *Working Paper*.

Bai, X., Ma, Z., Hou, Y., Li, Y., and Yang, D. (2023). A Data-Driven Iterative Multi-Attribute Clustering Algorithm and Its Application in Port Congestion Estimation. *IEEE Transactions on Intelligent Transportation Systems*, 24:12026–12037.

Baker, S. R., Bloom, N., and Davis, S. J. (2016). Measuring Economic Policy Uncertainty. *Quarterly Journal of Economics*, 131:1593–1636.

Bańbura, M., Giannone, D., and Reichlin, L. (2010). Large Bayesian Vector Auto Regressions. *Journal of Applied Econometrics*, 25:71–92.

Benguria, F. (2021). The Matching and Sorting of Exporting and Importing Firms: Theory and Evidence. *Journal of International Economics*, 131:103430.

Benigno, G., di Giovanni, J., Groen, J. J., and Noble, A. I. (2022). The GSCPI: A New Barometer of Global Supply Chain Pressures. *Federal Reserve Bank of New York Staff Reports 1017*.

Bils, M., Chang, Y., and Kim, S.-B. (2011). Worker Heterogeneity and Endogenous Separations in a Matching Model of Unemployment Fluctuations. *American Economic Journal: Macroeconomics*, 3:128–154.

Birant, D. and Kut, A. (2007). ST-DBSCAN: An Algorithm for Clustering Spatial–Temporal Data. *Data & Knowledge Engineering*, 60:208–221.

Brancaccio, G., Kalouptsidi, M., and Papageorgiou, T. (2020). Geography, Transportation, and Endogenous Trade Costs. *Econometrica*, 88(2):657–691.

Brancaccio, G., Kalouptsidi, M., Papageorgiou, T., and Rosaia, N. (2023). Search Frictions and Efficiency in Decentralized Transport Markets. *Quarterly Journal of Economics*, 138:2451–2503.

Brown, J., Englert, D., and Hoffmann, J. (2021). International Transport Costs: Why and How to Measure Them? World Bank Blogs – Transport. Available at: https://blogs.worldbank.org/transport/international-transport-costs-why-and-how-measure-them (Accessed: March 6, 2022).

Burriel, P., Kataryniuk, I., Pérez, C. M., and Viani, F. (2023). A New Supply Bottlenecks Index Based on Newspaper Data. *Banco de España Working Paper 2304*.

Chaney, T. (2014). The Network Structure of International Trade. *American Economic Review*, 104(11):3600–3634.

di Giovanni, J., Şebnem Kalemli-Özcan, Silva, A., and Yildirim, M. A. (2022). Global Supply Chain Pressures, International Trade, and Inflation. *NBER Working Paper 30240*.

Du, Y., Chen, Q., Lam, J. S. L., Xu, Y., and Cao, J. X. (2015). Modeling the Impacts of Tides and the Virtual Arrival Policy in Berth Allocation. *Transportation Science*, 49(4):939–956.

Dunn, J. and Leibovici, F. (2023). Navigating the Waves of Global Shipping: Drivers and Aggregate Implications. *Federal Reserve Bank of St. Louis Working Paper 2023-002*.

Eaton, J. and Kortum, S. (2002). Technology, Geography, and Trade. *Econometrica*, 70:1741–1779.

Ester, M., Kriegel, H.-P., Sander, J., and Xu, X. (1996). A Density-Based Algorithm for Discovering Clusters in Large Spatial Databases With Noise. *KDD-96 Proceedings*.

Fernández-Villaverde, J., Mandelman, F., Yu, Y., and Zanetti, F. (2024). Search Complementarities, Aggregate Fluctuations, and Fiscal Policy. *Review of Economic Studies*. forthcoming.

Finck, D. and Tillmann, P. (2022). The Macroeconomic Effects of Global Supply Chain Disruptions. *BOFIT Discussion Paper 14/2022*.

Fujita, S. and Ramey, G. (2012). Exogenous Versus Endogenous Separation. *American Economic Journal: Macroeconomics*, 4:68–93.

Ghassibe, M. and Zanetti, F. (2022). State Dependence of Fiscal Multipliers: The Source of Fluctuations Matters. *Journal of Monetary Economics*, 132:1–23.

Giacomini, R. and Kitagawa, T. (2021). Robust Bayesian Inference for Set-Identified Models. *Econometrica*, 89:1519–1556.

Kamali, P. and Wang, A. (2021). Longer Delivery Times Reflect Supply Chain Disruptions. IMF Blog. Available at: https://www.imf.org/en/Blogs/Articles/2021/10/25/longer-delivery-times-reflect-supply-chain-disruptions (Accessed: October 25, 2021).

Kasahara, H. and Lapham, B. (2013). Productivity and the Decision to Import and Export: Theory and Evidence. *Journal of International Economics*, 89:297–316.

Kilian, L. and Murphy, D. P. (2012). Why Agnostic Sign Restrictions Are Not Enough: Understanding the Dynamics of Oil Market VAR Models. *Journal of the European Economic Association*, 10:1166–1188.

Krolikowski, P. M. and McCallum, A. H. (2021). Goods-Market Frictions and International Trade. *Journal of International Economics*, 129:103411.

Lenoir, C., Martin, J., and Mejean, I. (2022). Search Frictions in International Goods Markets. *Journal of the European Economic Association*, 21(1):326–366.

Li, C., Qi, X., and Song, D. (2016). Real-Time Schedule Recovery in Liner Shipping Service With Regular Uncertainties and Disruption Events. *Transportation Research Part B: Methodological*, 93:762–788.

Litterman, R. B. (1986). Forecasting With Bayesian Vector Autoregressions: Five Years of Experience. *Journal of Business & Economic Statistics*, 4:25–38.

Mathieu, E., Ritchie, H., Rodés-Guirao, L., Appel, C., Giattino, C., Hasell, J., Macdonald, B., Dattani, S., Beltekian, D., Ortiz-Ospina, E., and Roser, M. (2020). Coronavirus Pandemic (COVID-19). Our World in Data. Available at: https://ourworldindata.org/coronavirus (Accessed: August 17, 2022).

Melitz, J. and Toubal, F. (2014). Native Language, Spoken Language, Translation and Trade. *Journal of International Economics*, 93:351–363.

Melitz, M. J. (2003). The Impact of Trade on Intra-Industry Reallocations and Aggregate Industry Productivity. *Econometrica*, 71:1695–1725.

Menzio, G. and Shi, S. (2011). Efficient Search on the Job and the Business Cycle. *Journal of Political Economy*, 119:468–510.

Michaillat, P. and Saez, E. (2015). Aggregate Demand, Idle Time, and Unemployment. *Quarterly Journal of Economics*, 130:507–569.

Mountford, A. and Uhlig, H. (2009). What Are the Effects of Fiscal Policy Shocks? *Journal of Applied Econometrics*, 24:960–992.

Mumtaz, H. and Zanetti, F. (2012). Neutral Technology Shocks and the Dynamics of Labor Input: Results From an Agnostic Identification. *International Economic Review*, 53:235–254.

Naudé, W. and Matthee, M. (2011). The Impact of Transport Costs on New Venture Internationalisation. *Journal of International Entrepreneurship*, 9:62–89.

Notteboom, T. E. (2006). The Time Factor in Liner Shipping Services. *Maritime Economics & Logistics*, 8:19–39.

Pizzinelli, C., Theodoridis, K., and Zanetti, F. (2020). State Dependence in Labor Market Fluctuations. *International Economic Review*, 61:1027–1072.

Plagborg-Møller, M. and Wolf, C. K. (2021). Local Projections and VARs Estimate the Same Impulse Responses. *Econometrica*, 89:955–980.

Ramey, V. A. and Zubairy, S. (2018). Government Spending Multipliers in Good Times and in Bad: Evidence From US Historical Data. *Journal of Political Economy*, 126:850–901.

Rodrigue, J.-P. (2020). *The Geography of Transport Systems*. Routledge, 5 edition.

Samuelson, P. A. (1954). The Transfer Problem and Transport Costs, II: Analysis of Effects of Trade Impediments. *The Economic Journal*, 64(254):264–289.

Smirnyagin, V. and Tsyvinski, A. (2022). Macroeconomic and Asset Pricing Effects of Supply Chain Disasters. *NBER Working Paper 30503*.

Song, D.-P. and Dong, J.-X. (2012). Cargo Routing and Empty Container Repositioning in Multiple Shipping Service Routes. *Transportation Research Part B: Methodological*, 46(10):1556–1575.

Stamer, V. (2021). Thinking Outside the Container: A Sparse Partial Least Squares Approach to Forecasting Trade Flows. *Kiel Working Papers 2179*.

Stopford, M. (2008). *Maritime Economics*. Routledge, London, 3 edition.

Talley, W. K. and Ng, M. W. (2016). Port Multi-Service Congestion. *Transportation Research Part E: Logistics and Transportation Review*, 94:66–70.

Uhlig, H. (2005). What Are the Effects of Monetary Policy on Output? Results From an Agnostic Identification Procedure. *Journal of Monetary Economics*, 52:381–419.

Wang, Y., Meng, Q., and Jia, P. (2019). Optimal Port Call Adjustment for Liner Container Shipping Routes. *Transportation Research Part B: Methodological*, 128:107–128.

Williamson, C. (2021). Understanding … PMI Suppliers' Delivery Times: A Widely Used Indicator of Supply Delays, Capacity Constraints and Price Pressures. S&P Global Market Intelligence Economics Commentary. Available at: https://ihsmarkit.com/research-analysis/understanding--pmi-suppliers-delivery-times-a-widely-used-indicator-of-supply-delays-capacity-constraints-and-price-pressures-Jul21.html (Accessed: May 2, 2022).

Wong, W. F. (2022). The Round Trip Effect: Endogenous Transport Costs and International Trade. *American Economic Journal: Applied Economics*, 14:127–166.

Wu, J. C. and Xia, F. D. (2016). Measuring the Macroeconomic Impact of Monetary Policy at the Zero Lower Bound. *Journal of Money, Credit and Banking*, 48(2-3):253–291.